Engineering biointerfaces to reveal collagen IV disease mechanisms

Elie Ngandu Mpoyi
(BSc (Hons), MRes^2)

Submitted in fulfilment of the requirements for the Degree of Doctor of Philosophy

Biomedical Engineering
School of Engineering
University of Glasgow

August 2017

Abstract

Basement Membranes (BMs) are specialised extracellular matrix (ECM) structures that underlie all endothelial and epithelial cells, and provide structural support to tissues as well as influence cell behaviour and signalling. Mutations in the BMs major component collagen IV cause eye, kidney and cerebrovascular disease including intracerebral haemorrhaging (ICH). Haemorrhagic stroke accounts for 15% adult stroke and 50% paediatric stroke, and carries the worst prognosis and there are no therapeutic strategies. Mutations in the genes *COL4A1/COL4A2* (collagen IV alpha chain 1 and 2) cause BM defects due to mutant protein incorporation in the BM or its absence by ER retention, and ER-stress due to intracellular accumulation of collagen IV. Despite this, the mechanism(s) of collagen IV mutations disease remain poorly characterised.

To provide novel insights into mechanisms of collagen diseases, this study investigates the effect of defined engineered biointerfaces on cell behaviour/signalling, collagen secretion in *COL4A2* mutant and wild-type cells. Atomic force microscopy and spectroscopy were employed together with confocal and biochemical analyses of cells cultured on engineered synthetic polymers, poly(ethyl acrylate) and poly(methyl acrylate), coated with ECM proteins, namely laminin, collagen IV and fibronectin. This enabled us to address the hypothesis that biomaterials may alter the behaviour of $COL4A2^{+/G702D}$ mutant cells by overcoming some of the defects caused by the mutation and rescuing the downstream effect of the ER stress.

Of the ECM proteins that were used, only fibronectin was observed to undergo a drastic structural change depending on the substrate chemistry. On poly(ethyl acrylate), fibronectin was assembled into fibrillary networks upon adsorption, and these nanonetworks induced increased secretion of Col4a2 in $COL4A2^{+/G702D}$ cells than on poly(methyl acrylate) or control glass. The behaviour of the mutant cells appeared to be influenced by the underlying biointerface, increased levels of molecular chaperones and reduced ER area suggested an increased collagen IV folding capacity when the cells were cultured on the FN nanonetworks compared to the other surfaces. $COL4A2^{+/G702D}$ cells interacted with the adsorbed proteins and were able to mechanically translocate them. Enhanced formation of focal adhesions was also seen on FN-coated polymers, where ligand density and actin-myosin contractility accounted for the observed increase in cell adhesion strength. The stiffness of the mutant fibroblasts and of their ECMs was found to be 10 times lower than that of the wild-type cells; interestingly, mutant cells cultured on FN nanonetworks on poly(ethyl acrylate) were able

to deposit a protein matrix with significantly higher Young modulus than on glass or poly(methyl acrylate). These findings suggest that biomaterials are able to influence the behaviour of these mutant cells through changes in the interfacial layer of adsorbed proteins presented to them.

Collectively, these data provide an understanding of the effect of mutations on cell characteristic and a basis of concept that material may be employed to modulate effects of mutations of collagen/ECM molecules. Understanding the mechanisms through which these surfaces trigger a change in cell response will prove valuable for the development of new therapeutic approaches to address pathologies due to collagen IV mutations. In this respect, further investigation is needed to dissect the signalling pathways involved.

Table of Contents

Chapter 4 Interaction of Wild Type Cells with Biointerfaces

Chapter 5 Interaction of *COL4A2*$^{+/G702D}$ Mutant Fibroblast Cells with Biointerfaces

Chapter 6 Cell Adhesion and Signalling

Chapter 7 Overall discussions and conclusions

List of Tables

List of Figures

Acknowledgement

I would like to designate my deepest gratitude to my supervisors, Prof Manuel Salmeron-Sanchez, Dr Tom Van Agtmael and Dr Marco Cantini, for giving me the opportunity to work in their labs and for providing me with continuing support and trust throughout. I praise them for their devotion to help and support me unconditionally and providing inspirational discussions and thoughtful criticism.

My warmest and special thanks to Dr Marco Cantini for his spectacular knowledge in science that inspired me and still continues to motivate me. I am extremely fortunate to have had him advising me and guiding me in the right direction when I was lost. He was unreplaceable throughout my PhD. His personal guidance, support and advice were absolutely essential; he has witnessed and tolerated the best and worst of me with understanding. Going to see him was like consulting a Roman, Caesar; knowledge strategies and ideas that he reformed were all I needed. You are Italian, we got the same blood!

Thanks to all work colleagues in the Mime lab (Microenvironment for medicine) and Tom's lab (Cardiovascular and Medical Sciences), University of Glasgow, for their support, advice and putting up with me all the period of time.

I also thank my funders for the financial support without which I would have been able to foot the bill for living.

Dedications

This thesis is dedicated to my most lovely family who have supported me during this period and since I was born; Pierrot Tshibuyi, Francine Masengu, Henoc Bananga, Rachel Miandabu, Pierrette Kabisa, Joel Mukanya, Nathan Lukusa and particularly to my aunt Regine Kabisa for calling me on a regular base to know how I was doing down in Glasgow, maternal love. I also would like to dedicate this to my cherished grandmother Jeanne Masengu mua Mpoyi in Canada. Their love, generosity and everlasting support was more of a fuel to keep me going. I am grateful to them for emotional, moral and financial support. Thank you to my entire family, friends and relatives for accepting me in their world.

Special to my wife Jemima Mbombo

A man can inherit a house and money from his parents, but only the Lord can give him a sensible wife (Proverbs 19:14).

Lastly by not least and most importantly, I dedicate this piece of work to you Jemima Mbombo, I can not have enough words to thank you my dear darling. Thanks for your advices, continuous prayers and support during this study. You are truly an intelligent woman, you live up to my desired wife status, one in 6 billion, and I am happy to have you in my life. Thanks God for your blessing.

Author Declaration

I declare that the work presented in this thesis represents the original work carried out by the author in the laboratory of Prof. Manuel Salmeron-Sanchez and Dr. Tom Van Agtmael, University of Glasgow, and has not been submitted in any form to another University. Where use has been made of materials provided by others, due acknowledgments have been made. This thesis is being submitted for the degree of Doctor of Philosophy at the University of Glasgow.

August 2017

Elie Ngandu Mpoyi

University of Glasgow

Presentations and Publications

Oral presentations

International Nanoscience Student Conference (INASCON 2017), Bristol, UK. 21-24 August 2017. Fibronectin Adsorption as a Key Mediator in the Nanotopographical Control of Cell Behaviour.

Biomaterials Seminars; University of Glasgow, UK. 21 March 2017. Engineering biointerfaces to reveal collagen IV disease mechanisms. Presentation of first year results.

Biomaterials Seminars; University of Glasgow, UK. 23 February 2016. Engineering biointerfaces to reveal collagen IV disease mechanisms. Presentation of second year results.

Biomaterials Seminars; University of Glasgow, UK. 14 May 2015. Engineering biointerfaces to reveal collagen IV disease mechanisms. Presentation of third year results.

Doctoral Training Centre (DTC) exams, University of Glasgow, UK. 31 July 2014 Protein interfaces between nanoscale materials and cells.

DTC exams, University of Glasgow, UK. 30 July 2014. Raman spectroscopic study for the future of malaria diagnosis.

Poster presentations

European Society for Biomaterials (ESB), 28th Annual Conference of the. 4-8 September 2017, Athens, Greece. Engineering biointerfaces to reveal collagen IV disease mechanisms. E., Ngandu Mpoyi, M., Cantini, T., Van Agtmael ; M., Salmerón-Sánchez.

Bone Research Society and British Society for Matrix Biology, 3rd joint meeting, Edinburgh, UK. 1-3 September 2015. Engineering biointerfaces to reveal collagen IV disease mechanisms. E., Ngandu Mpoyi, M., Cantini, T., Van Agtmael & M., Salmeron-Sanchez.

DTC Symposium, University of Glasgow, UK. 27th March 2015. Engineering biointerfaces to reveal collagen IV disease mechanisms. E., Ngandu Mpoyi.

DTC exams, University of Glasgow, UK. 30 July 2014. Raman spectroscopic study for the future of malaria diagnosis. E., Ngandu Mpoyi.

Internship

Visiting scholar: Petit Institute for Bioengineering and Bioscience, Georgia Institute of Technology. Andrés J. García laboratory.

Publications

Protein Adsorption as a Key Mediator in the Nanotopographical Control of Cell Behaviour. *ACS Nano2016*. Ngandu-Mpoyi, E.; Cantini, M.; Gadegaard, N.; Dalby, M. J.; Salmerón-Sánchez, M.

A material characterisation for fibroblast cells. In progress. Ngandu Mpoyi E, Cantini M, Salmeron-Sanchez M. 2017.

FN engineered biointerfaces revealing *COL4A2* mutation cellular behaviour. In progress. Ngandu Mpoyi E, Cantini M, Van Agtmael T, Salmeron-Sanchez M.

Definitions / Abbreviations

%	Per cent
°C	Degrees centigrade
2D	Two dimensional
3D	Three dimensional
α1(IV)	Collagen IV alpha chain 1
α2(IV)	Collagen IV alpha chain 2
α3(IV)	Collagen IV alpha chain 3
α4(IV)	Collagen IV alpha chain 4
α5(IV)	Collagen IV alpha chain 5
α6(IV)	Collagen IV alpha chain 6
Abs	Absorbance
Asc-2-P	L-ascorbic acid 2-phosphate
AFM	Atomic force microscopy
ANOVA	Analysis of variance
AU	Arbitrary units
BIP	Binding immunoglobulin protein
BM	Basement membrane
BSA	Bovine serum albumin
bp	Base pair
Col4	Type IV collagen
Cy3	Cyanine dye three
DAPI	Diamidino-2-phenylindole dye
ddH20	Double distilled hydrogen dioxide
dNTP	Deoxyribonucleotide triphosphate
DMEM	Dulbecco’s modified eagle medium
DMSO	Dimethyl sulfoxide
DNA	Deoxyribonucleic acid
DPBS	Dulbecco's phosphate buffered saline
DTT	Dithiothreitol
ECM	Extracellular matrix

EDTA	Ethylenediaminetetraacetic acid
ELISA	Enzyme-linked immunosorbent assay
EM	Electron microscopy
ER	Endoplasmic reticulum
ERK	Extracellular regulated kinase
FA	Focal adhesion
FAK	Focal adhesion kinase
FBS	Fetal bovine serum
FD	Fractal dimension
FDA	Food and drug administration
FITC	Fluorescein isothiocyanate
FN	Fibronectin
Gly	Glycine
g	Grams
GBM	Glomerular basement membrane
gDNA	Genomic DNA
Gly	Glycine
h	Hour
HANAC	Hereditary angiopathy with nephropathy, aneurysms, and muscle cramps
HRP	Horseradish peroxidase
Hsp47	Heat shock protein forty seven
ICC	Immunocytochemistry
ICH	Intracerebral haemorrhage
IgG	Immunoglobulin G protein
IHC	Immunohistochemistry
LM	Laminin
min	Minutes
mL	Millilitres
mm	Millimeters
mM	Millimoles
mol	Moles

NC-1	Non-collagenous
ng	Nanograms
nm	Nanometer
nM	Nanomoles
PEA	Poly(ethyl acrylate)
PDI	Protein disulphide isomerase
PFA	Paraformaldehyde
PMA	Poly(methyl acrylate)
RIPA	Radioimmunoprecipitation assay buffer
RNA	Ribonucleic acid
qPCR	Quantitative real-time polymerase chain reaction
RIPA	Radioimmunoprecipitation assay buffer
rpm	Rotations per minute
RT	Room temperature
sec	Second
SEM	Scanning electron microscopy
SD	Standard deviation
SDS	Sodium dodecyl sulphate
TBS	Tris buffered saline
TBST	Tris buffered saline with tween-20
TE	Tris ethylenediaminetetraacetic acid
µg	Micrograms
µl	Microlitres
µm	Micrometers
µM	Micromoles
UV	Ultraviolet
V	Volts
VEGF	Vascular endothelial growth factor
WB	Western blot
WT	Wild type
WTB	Western transfer buffer

Chapter 1

General Introduction

Contents

It is important to have knowledge of the native structure and chemical properties of the basement membrane (BM) and type IV collagen (Col4) to understand the characteristics of the mutation of Col4 affecting the BM. Therefore, this chapter introduces the structure and components of the BM and the use of biomaterials in this study.

1. 1 Extracellular Matrix

Mammals are not made up of cells alone. A substantial part of their volume, approximately half of mass excluding fat, is extracellular space, which is largely filled by an intricate network of macromolecules constituting the extracellular matrix (ECM) (Avram et al. 2010). The ECM includes the interstitial matrix (IM) and the basement membranes (BMs) (Hynes 2009). The IM consists mainly of the fibrous collagen type I, which, together with fibronectin, confers mechanical strength to tissues. The BMs, unlike the IM, are specialized form of sheet-like depositions of ECM to which epithelial cells can anchor and which interact directly with the epithelium and endothelium (Cox and Erler 2011, Erler and Weaver 2009).

Though fundamentally the ECM is made of water, proteins and polysaccharides, each tissue has an ECM with a unique composition and topology that is generated during tissue development through a biochemical and biophysical dialogue between the various cellular components (e.g. adipocyte, endothelial, epithelial, fibroblast elements) and the evolving cellular and protein microenvironment. This matrix is composed of a variety of proteins, polysaccharides and a host of regulatory molecules such as cytokines and proteolytic enzymes that are secreted locally and assembled into an organized meshwork in close association with the surface of the cell that produced them. The major fibrous proteins in the ECM are collagens, nidogens, fibronectins and laminins, which all have important structural roles (Alberts et al. 2007).

ECM's components' design, distribution and architecture are tissue specific and are due to the different cell types that secrete them and result in the varied morphology of resultant tissue types. The structure and composition of the ECM are designed to withstand the stressful demands of the microenvironment, resulting in constant remodelling and reorganisation at various stages in cell and tissue development; therefore, the characteristic nature of the ECM is not only tissue specific but has a degree of heterogeneity within tissues themselves to facilitate proper functionality (Hunziker et al. 2002). The elasticity and stiffness of the matrix is also important for determining cell behaviours such as

differentiation (Engler et al. 2008), migration (Hadjipanayi et al. 2009), and proliferation (Provenzano et al. 2009).

The ECM is the non-cellular component present within all tissues and organs, and provides not only essential physical scaffolding for the cellular constituents but also initiates crucial biochemical and biomechanical cues that are required for tissue morphogenesis, differentiation and homeostasis (Järveläinen et al. 2009). It plays an important role in protecting cells by acting as a compression buffer against the stress placed on the ECM (Cox and Erler 2011, Erler and Weaver 2009). ECM function is influenced by both its composition and environment. The matrix regulates a cell's dynamic behaviour providing support, segregating tissues from one another, and regulating intercellular communication. It is essential for a multitude of biological processes; *i.e.* cell proliferation, growth, survival, shape, migration, tissue development, regeneration, and stem cell differentiation (Frantz et al. 2010). Genetic mutations that affect ECM composition or regulation (Bateman et al. 2009) can cause many different diseases (Jarvelainen et al. 2009); *e.g.* bone and vascular and connective tissue diseases. The ECM play a role in common diseases such as cancer (Kalluri 2003) and fibrosis (Bissell and Radisky 2001, Cox and Erler 2011).

1. 2 Fibronectin

Fibronectin (FN) is a large multidomain protein of the ECM that regulates cell adhesion, migration and differentiation (Schwarzbauer and DeSimone 2011). It is secreted as a large ECM glycoprotein and assembles via a cell-mediated process into fibrillary structures around cells (Singh et al. 2010). FN subunit sizes ranges from 230 to 270 kDa, as determined by the difference splice isoforms of the mRNA, and forms dimers through two disulphide bonds at the C-terminus of the protein. Each FN subunit is folded into a series of functionally distinct domains separated by regions of flexible polypeptide chain type I, type II and type III structure repeats (Figure 1.3B) (Schwarzbauer and DeSimone 2011, Singh et al. 2010).

Intramolecular disulphide bonds between the modules stabilize the folded tertiary structure of the FN subunit, and FN dimers form via antiparallel disulphide bonds at the C terminus. FN RGD or Arg-Gly-Asp (a specific tripeptide sequence in one of the type III repeats) is a central binding domain for binding cell surface receptors such as integrins (Schwarzbauer and DeSimone 2011, Singh et al. 2010).

There are multiple isoforms of FN, and the major different forms are, plasma or soluble FN (pFN), all other forms assemble on the surface of cells and are deposited in the ECM as

highly insoluble FN fibrils, generally called cellular FN (cFN) (Mouw et al. 2014). cFN is secreted by cell types, including fibroblasts, endothelial cells, chondrocytes, synovial cells and myocytes as a dimer in a compact globular structure and is then assembled into an insoluble, fibrillar form in a cell-dependent process. pFN is produced by hepatocytes and secreted into the blood plasma, where it circulates at 300-400 μg/mL in a soluble, compact, inactive form (To and Midwood 2011).

FN is important for cell adhesion to the matrix as well as for guiding cell migration in vertebrate embryos (Mouw et al. 2014). Many of the ECM proteins described below interact with cells through crucial connections with the multidomain protein FN to regulate cell adhesion, migration and differentiation. FN therefore affects cell signalling by being recognized by the integrins $\alpha_5\beta_1$ and $\alpha V\beta_3$. FN also contains various binding sites for ECM proteins such as FN, type I and III collagen, and LM. FN is found to be important for cell migration during development and has been implicated in cardiovascular disease and tumour metastasis (Rozario and DeSimone 2010, Tsang et al. 2010).

1. 3 Basement Membranes

Identified first in skeletal muscle 177 years ago (Bowman 1840), the elucidation of basement membranes (BMs) constituents, functions, genetics and structure has required advances in multiple fields over many years including biochemistry, biophysics, cell biology, genetics, bioengineering. These approaches have led to our current understanding of BMs, yet more is to be undertaken to understand the mechanical properties of the BMs.

BMs are delicate, nanoscale and pliable sheets of specialized ECM protein complex that are 50 to 100 nm thick. They are found basolateral to all cell monolayers (epithelium and endothelium) in the body (Figure 1.1) (Kalluri 2003, LeBleu et al. 2007). The BMs are the fusion of two laminae, the basal lamina and an adjacent reticular lamina of connective tissue; the two layers are attached to each other with Col7 anchoring fibrils and fibrillin microfibrils (Paulsson 1992). The basal lamina layer is further divided into two layers. The lamina lucida which is a clear layer closer to the epithelium, and the lamina densa, a dense layer closer to the connective tissue. The latter is an electron-dense membrane of about 30-70 nm thick, consisting of an underlying network of reticular collagen IV fibrils averaging 30 nm (Noonan et al. 1991).

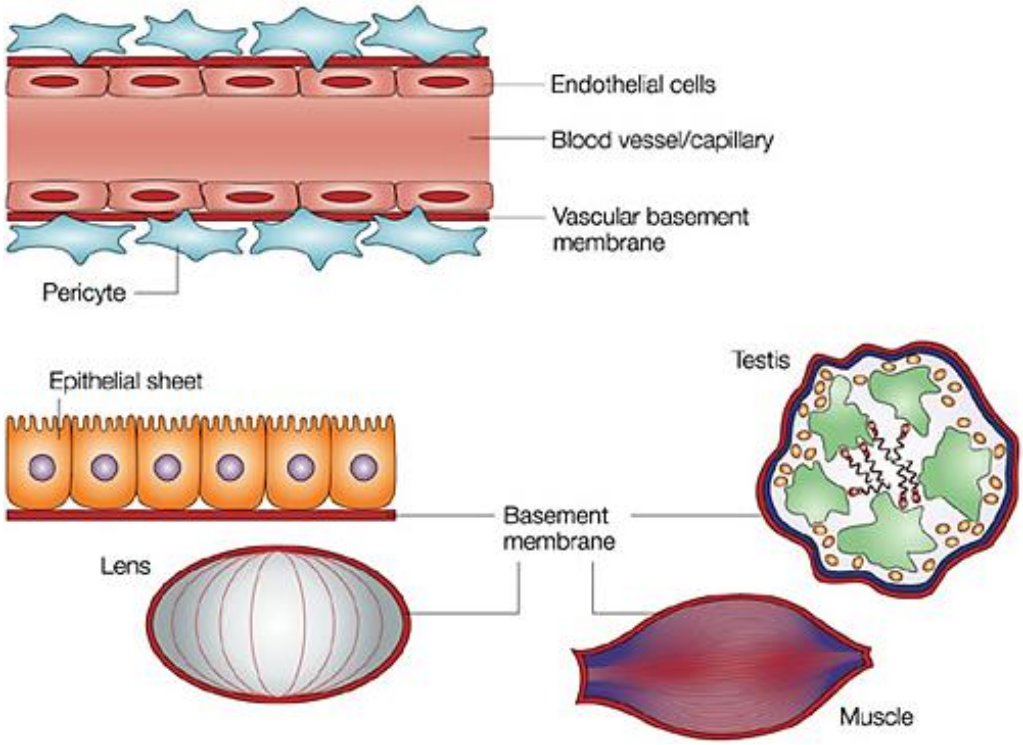

Figure 1.1 Representation of the basement membrane (BM) in a selection of tissues. BM location including in the blood vessels, epithelial cell layers, the lens of the eye, the testis and in muscle. The red line signifies the BM. Adapted from (Kalluri, 2003).

1. 3. 1 Function of the BM

The BMs act as linings or partitions in organisms, and an anchor for the attachment of epithelium, endothelium, and the underlying tissue (reviewed in (Van Agtmael and Bruckner-Tuderman 2010)), to guide development and differentiation and to function as a mechanical barrier to cells (preventing malignant cells from invading the deeper tissues) and macromolecules (Mouw et al. 2014). BMs do not only provide mechanical support and divide tissues into compartments, but also influence and modify cellular behaviour via outside-in signalling, acting as complex signalling platforms (Paulsson 1992), via different cell surface receptors including integrins (Sun et al. 2016). BMs play various roles amongst which, blood filtration, muscle homeostasis, growth factors and cytokines storing, control of angiogenesis and tumour growth, maintenance of skin integrity, neuromuscular structure and affecting adipogenesis and fibrosis (Kalluri 2003, Yurchenco and O'Rear 1994). Though considerable work has been undertaken to elucidate the BM role, our understanding of its functions and interactions is by no means complete. For example, many questions remain regarding the regulatory processes for the production of various components of the BM, and the mechanisms by which BMs influence cell behaviour. Nonetheless, our understanding of

the composition, structure and function of the BM is continuously evolving, aided by the combined use of cell biology, novel approaches in synthetic chemistry and glycobiology, and cutting-edge imaging techniques to visualize large-scale structures.

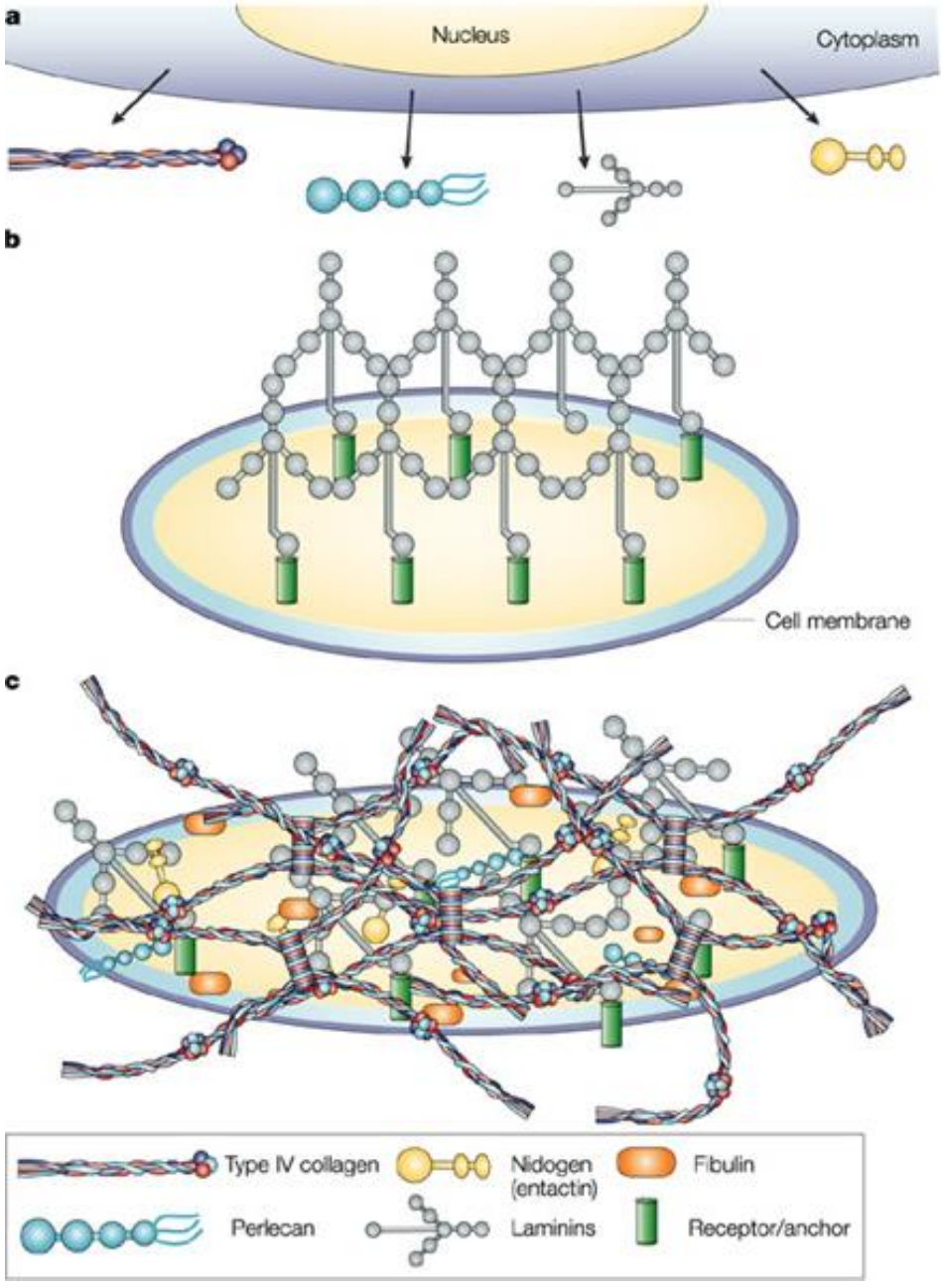

Figure 1.2 BM formation. A representation of how the major BM components interact to form the extracellular BM. **A)** Intracellular production of BM components, **B)** initial laminin network, **C)** BM components interacting in the ECM to form a network. Adapted from (Kalluri, 2003). Laminins are central organizers of BMs and binds to several integrins, nidogens (Nd) and polymerizes via its LN domains. Type IV Collagen (three isoforms) and perlecan bind to nidogen, completing the core basement membrane scaffold.

1. 3. 2 Composition, structure and assembly of BMs

BMs are biochemically and morphologically distinct from the IM; which is less compact and more porous than BM (Linsenmayer et al. 1991), they surround muscle and fat cells, line up around the lens in the eye, enfold testes and are present at neuromuscular junctions (Figure 1.1) (Kalluri 2003, Timpl and Aumailley 1989)). BMs differ in their composition in different tissue types, leading to an abundance of diverse interacting partners and added complexity, yet, all have common components. About 50 proteins are known to make up the BMs, amongst which LMs, Col4, perlecan (a heparan sulphate proteoglycan (HSPG)), and nidogens/entacin (linker proteins) are the main components (Kalluri 2003).

Most BMs components have the ability to self-assemble into sheet-like structures (Kalluri 2002, Yurchenco and Schittny 1990, Yurchenco and O'Rear 1994, Yurchenco et al. 2002). Col4 and LM contain essential information within their primary sequence allowing the initiation of intermolecular self-assembly and formation of independent (Col4 and LM) sheet-like structures, whose interaction with each other is facilitated by nidogen/entactin (Aumailley M. et al. 1989, Aumailley M. et al. 1993, Kalluri 2002, Timpl and Brown 1996, Yurchenco and Schittny 1990, Yurchenco and O'Rear 1994, Yurchenco et al. 2002). However, other BM components, nidogen and perlecan, are not able to self-assemble (Timpl and Brown 1996).

Recent studies on BM assembly have shown that, while LM is the centrepiece of the network and initiates BM formation, Col4 provides the scaffold and is required for maintaining its structural integrity (Poschl et al. 2004). Concisely, the initial deposition of LM polymers is facilitated by cell-surface proteins such as integrins (especially β_1 integrins) and dystroglycan via site-specific interactions, and then Col4 polymers form a network which then associates with the LM networks and with the cell via integrin and DDR receptors (Figure 1.2) (Aumailley M. et al. 2000, Charonis et al. 1985, Willem et al. 2002).

In addition to mutations in genes encoding BM components (more further down), changes in the composition of the BMs can also lead to pathological conditions, indicating that the type of BM component is a key regulator of tissue function (Kalluri 2003). BM components are also involved in auto-immune diseases and tumorigenesis. For example, epitopes on collagens and laminins are targeted by auto-antibodies and lymphocytes in Goodpasture's disease, rheumatoid arthritis, post-lung transplant bronchiolitis obliterans syndrome, and multiple autoimmune dermatoses (Foster 2017).

The most common defect of BMs is seen in longstanding diabetes mellitus, causing almost pathognomonic thickening of microvascular BMs in the retina, peripheral nerve and kidney glomerulus with associated blindness, neuropathy and proteinuria/chronic renal failure. The basis for the BM thickening, which precedes proteinuria, is not well understood or studied, but may involve changes in synthesis, degradation/remodelling (Pozzi et al. 2016).

1. 3. 2. 1 Laminin

Laminins (LMs) are a family of large, mosaic high-molecular weight (~400 to ~900 kDa) glycoproteins. They are heterotrimers consisting of α-, β- and γ-chain combinations based on sequence identity and protein domain organization. All laminin chains share a common domain structure with a number of globular and rod-like domains. The three chains combine *via* the triple-helical coiled-coil domain in the centre of each chain to form structures with either a cruciform (cross-shaped, three short arms and one long coiled-coil arm; e.g. LM111, LM211, LM511), Y shaped (three arms, due to absence of the α-short arm; e.g., LM411) or rod-shaped (single arm; truncated short arms; LM3A32) structure (Figure 1.3A) (Timpl and Brown 1994). The end of the long arm of the α chain are five laminin G-like (LG) domains that contain the major cell-adhesive sites of laminin. The homologous short arms are composed of a distal laminin N-terminal (LN) domain that is followed by tandem repeats of laminin-type epidermal growth factor-like (LE) domains, interspersed with globular domains of unknown structure. As discussed below, the LN domains are essential for laminin polymerization and BM assembly (Hohenester and Yurchenco 2013).

The α-chain averages 400 kDa in size and 160 nm in length. The 1000 C-terminal amino acids (AA) residues contribute to five homologous 150–180 AA LG domains (globular motifs), collectively known as the G domain which is the major site for cell adhesion of laminin. Both the β- and the γ-chains average 200 kDa, both with short arms of ~50 nm in length, and lacking the G domain (LeBleu et al. 2007). The C-terminal laminin-type globular (LG) domains are the major receptor-binding domains, located at the C-terminal moiety of the α-subunit; these can interact with laminin-class integrins ($\alpha_3\beta_1$, $\alpha_6\beta_1$, $\alpha_7\beta_1$, $\alpha_6\beta_4$), α-dystroglycan, sulfated glycolipids and heparin. Laminin also binds to several integrins, nidogens (Nd) and polymerizes via its LN domains. 15 different LMs are expressed in vertebrates, of which $\alpha_1\beta_1\gamma_1$ is the major isoform in embryonic BMs (Durbeej 2010). The current nomenclature of laminin is based on chain composition, for instance laminin-511 contains α_5, β_1, and γ_1 chains (Aumailley Monique et al. 2005).

Similar to all secreted protein, laminin heterotrimers are assembled inside the endoplasmic reticulum of the cell, but further extracellular proteolytic processing may occur in various chains before the laminins reach their final form. This is particularly evident in laminin-332, which undergoes extensive and specific proteolysis (Tzu and Marinkovich 2008). LMs are primarily located in the basal lamina (part of the BM) and some mesenchymal compartments. LM mutations in humans can affect tissues such as skin (Aumailley M. et al. 2006), smooth muscle (Helbling-Leclerc et al. 1995) and kidney (Zenker et al. 2004). Defects of LMγ_1 chain, which is essential for embryogenesis, is presumed to result in embryonic death, LM being central in initial BMs composition (Pozzi et al. 2016).

LM is used extensively in cell culture to provide a biologically relevant environment that mimics the ECM cells. It enhances a multitude of biological processes including cell adhesion, growth, proliferation, and stem cell differentiation (Baur et al. 1995, Domogatskaya et al. 2008, Hall et al. 2008, Miyazaki et al. 2008, Rodin et al. 2010).

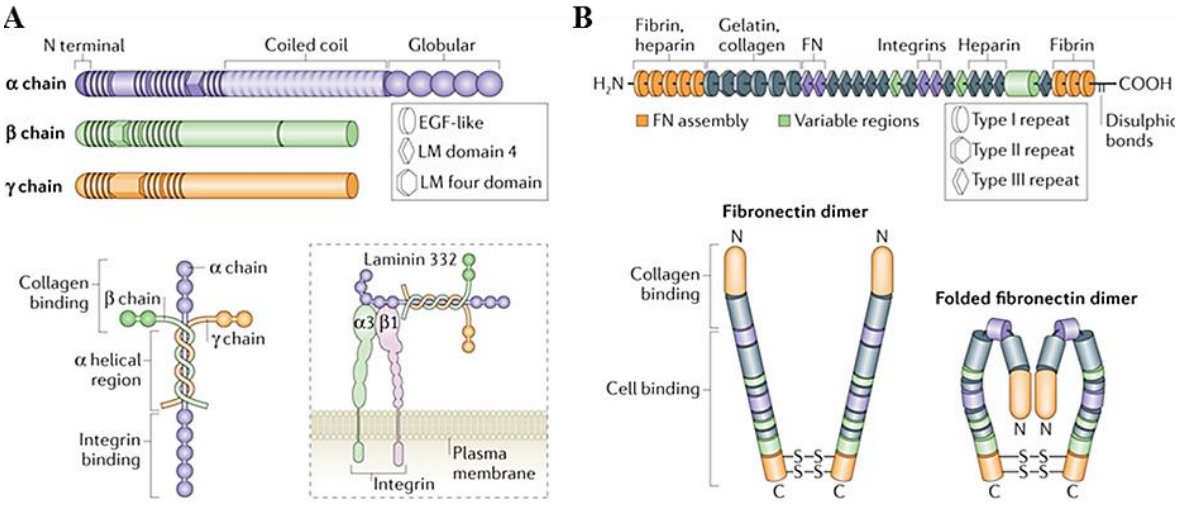

Figure 1.3 BM fibrous components. A) Laminins, formed by the combination of α, β and γ chains into a cruciform, Y shaped or rod-like structure. The chains are characterized by different domains, as shown. The domain structures depicted represent only one isoform for each chain type; the β and γ chains are shown without the globular regions. LMs interact with collagen and also with cell surface receptors, such as integrins. **B)** Fibronectin domain structure and the domains to which extracellular matrix (ECM) molecules and cell surface receptors bind are indicated. Adapted from (Mouw et al., 2014)

1. 3. 2. 2 Perlecan

Perlecan is the major heparan sulfate proteoglycans (HSPG) in BM expressed by many different cell types, including endothelial cells. It is a multidomain proteoglycan, with five domains labelled I-V, that binds to and cross-links many ECMs components and cell-surface

molecules (Iozzo 1994). Endorepellin, the C-terminal domain of perlecan, plays an anti-angiogenic role by interacting with VEGFR2 and is pro-autophagic by promoting the formation of LC3-positive autophagosomes independently of nutrition deprivation (Gubbiotti and Iozzo 2015, Pozzi et al. 2016). HSPGs in the BM serve as a reservoir for HS-binding growth factors, and facilitate the interaction between these growth factors and their receptors. Hence, HSPGs orchestrate growth factor activity and availability; these are two key important factors in organogenesis and branching morphogenesis (Pozzi et al. 2016).

Perlecan is encoded by the *HSPG2* gene. *HSPG2*$^{-/-}$ deficient mice are viable, yet, they demonstrate severe BM deterioration at sites of mechanical stress, and developing blood vessels in the brain (Costell et al. 1999). *HSPG2* mutations in human and mice have been shown to cause two allelic disorders, Schwartz-Jampel syndrome (SJS) and dyssegmental dysplasia Silverman-Handmaker type (DDSH). The later displays chondrodysplasia characterized by severe disorganization of chondrocytes and reduced ECM deposition (Arikawa-Hirasawa et al. 1999, Rodgers et al. 2007, Van Agtmael and Bruckner-Tuderman 2010). Jones and colleagues have shown that *Col4a1* mutations not only affect BM structure but also alter BM composition, including a ∼40% reduction in perlecan incorporation, indicating α1α1α2(IV) is required for perlecan deposition in the BM (Jones et al. 2016, Pastor-Pareja and Xu 2011).

1. 3. 2. 3 Nidogen

Nidogen, previously known as entactin, is another component of BMs, and the vertebrate genome encodes two types of nidogen: NID1, nidogen-1 and NID2, nidogen-2. Both these glycoproteins are dumbbell-shaped and are essential components of the BM that interact with several other BMs components acting as a central link. Like perlecan, nidogen connects the networks formed by collagens and LMs to each other (Yurchenco and Patton 2009). Nidogen-1 knockout mice causes seizure-like behaviour, indicating that it is essential for normal neuronal network excitability and plasticity (Vasudevan et al. 2010). However, this has been challenged by results showing that a loss of function mutation of nidogen in *Caenorhabditis elegans* does not affect BM assembly (Kang and Kramer 2000) and that Nid1-/- mice have a normal BM structure and no pathological features (Murshed et al. 2000)

1. 3. 2. 4 Collagen

Collagens (Cols) are the major structural component of the ECM and make up to ~30% of total protein mass in mammals (Rozario and DeSimone 2010). Therefore, process that results in degradation, damage or loss of integrity of this protein has significant health implications (Watanabe, 2004). The vertebrate genome encodes 29 different types of collagen (Mouw et al. 2014, Myllyharju and Kivirikko 2004, Soderhall et al. 2007) which are divided into eight sub-families based on their supramolecular and protein domain structure: fibril forming, BM forming, microfibrillar, anchoring fibrillar, hexagonal network forming, fibril associated Cols with interrupted triple helices (FACIT), transmembrane, and multiplexins (Table 1.1).

The classification of collagens into these different types is largely based on their supramolecular structure, but each type of collagen molecule is characterised by the presence of a collagen triple helical repeat. This triple helical repeat can be interrupted, for example in collagen IV and FACIT type collagen, or be continuous as is the case in the classical fibrillar collagens such as type I and III. Collagen molecules are secreted by cells as a trimer of alpha chains. These different alpha chains then interact in a variety of way of to give rise to the particular supramolecular structure, for example collagen IV (see further below for more details) will form a lattice style of network in the BM while in the case of fibrillar collagens, the different alpha chains called pro-collagen molecules are cleaved by enzymes to remove the C and N-terminal pro-peptide. The mature collagen molecules then from fibrils which themselves are crosslinked together to form collagen fibres. However, collagen fibrils often contain different types of collagen, for example collagen I fibrils often contain small levels of collagen V, III and XII. Some collagen molecules are inserted in the plasma membrane by virtue of their transmembrane domains and this class of molecules are called “collagens with transmembrane domains” (e.g. collagen XIII and XVII) (Mouw et al. 2014, Myllyharju and Kivirikko 2004, Soderhall et al. 2007).

It is thanks to this variety in collagen network structure that collagen plays such a crucial and varied role in biology that is not limited to structural function in the ECM. They are also important for tissue architecture, organization and cellular processes such as adhesion and migration (Hanein and Horwitz 2012, Mouw et al. 2014, Van Agtmael and Bruckner-Tuderman 2010). They have a dominant role in maintaining the biologic and structural integrity of ECM. Their interactions with ECM proteins and cell surface receptors are important during processes such as development, growth, tissue remodelling and disease

pathologies (LeBleu et al. 2007, Mouw et al. 2014, Van Agtmael and Bruckner-Tuderman 2010). For instance, they associate with the integrins $\alpha_1\beta_1$ and $\alpha_2\beta_1$ to affect cell signalling.

Each collagen molecule consists of three alpha chains which form homo- or hetero-trimers. The structural hallmark of every collagen is the presence of a triple helical collagen domain(s), which form tight right-handed helix of three α-chains, each of which consists of the highly conserved repeating amino acid (AA) Gly-X-Y triplet motifs, in which every third amino acid is a glycine residue. X and Y residues can be anything but is often proline and hydroxyproline, and are not as highly conserved as glycine (LeBleu et al. 2007, Prockop 1992). Although highly conserved and in contrast to fibrillar collagens, the Gly-X-Y motif is not present as an uninterrupted motif in any non-fibrillar collagens, such as collagen IV (Table 1.1). All non-fibrillar collagen alpha chains contain interruptions to this helical region (Myllyharju and Kivirikko 2004). Selectivity of Col trimer formation is controlled by the non-collagenous (NC)-1 domain, that indeed enables only specific alpha chain combinations to interact (LeBleu et al. 2007).

Type	**Molecular species**	**Class**	**Pathology**	**Diseases**
I	α12α2(I), α1(I)3	Fibrillar	Heart, bone, dermis, tendon, ligament, cornea	Osteogenesis Imperfecta, Ehlers-Danlos syndrome, osteoporosis
II	α1(II)3	Fibrillar	Cartilage,	Chondrodysplasias
III	$\alpha1(III)_3$	Fibrillar	Heart, skin, vasculature, reticular fibres throughout body	Ehlers-Danlos syndrome, arterial aneurysm
IV	$\alpha1_2\alpha2(IV)$ α3α4(IV), α5(IV), $\alpha5(IV)_2$, α6(IV)	Network	BMs	Alport syndrome, Goodpasture syndrome, HANAC syndrome
V[a]	$\alpha1_2\alpha2(V)$, $\alpha1(V)_3$, $\alpha1_2\alpha4(V)$, α1(XIα1(V)α3(XI)	Fibrillar	Heart, lung, cornea, bone, foetus	Ehlers-Danlos syndrome

Type	Molecular species	Class	Pathology	Diseases
VI[b c]	α1α2α3(VI), α1α2α4(VI), α1α2α5(VI), α1α2α6(VI)	Microfibillar	Widespread throughout body	Bethlem Myopathy, Ullrich muscular dystrophy Keloid scarring Keratosis pilaris
VII	$\alpha1(VII)_3$	Anchoring fibrils	Skin, dermis	Dystrophic Eppidermolysis bullosa
VIII	$\alpha1_2\alpha2\alpha1(VIII)$, $\alpha2_2\alpha1_3\alpha2(VIII)_3$	Network	Endothelium	Fuchs endothelial corneal dystrophy
IX[e]	α1α2α3(IX)	FACIT	Cartilage, eye	Epiphysial dysplasia
X	$\alpha1(X)_3$	Network	Cartilage	Schmid metaphysical dyschondroplasia
XI[d]	α1α2α3(XI) α1α1α3(XI)	Fibrillar	Cartilage, eye	Chondrodysplasias
XII[e]	$\alpha1(XII)_3$	FACIT	Ligaments, tendons	None
XIII[f]	$\alpha1(XIII)_3$	MACIT	Epidermis, chondrocytes, lungs, liver, hair follicles	None
XIV[e]	$\alpha1(XIV)_3$	FACIT	Demis, tendon, vasculature, placenta, lungs, liver	None
XV[g]	$\alpha1(XV)_3$	Multiplexin	Endothelium, heart, muscle, nerves, kidney, pancreas, fibroblasts	None
XVI[e]	$\alpha1(XVI)_3$	FACIT	Dermis, kidney	Eppidermolysis bullosa
XVII[f]	$\alpha1(XVII)_3$	MACIT	Dermis	Eppidermolysis bullosa
XVIII[g]	$\alpha1(XVIII)_3$	Multiplexin	Epithelium, lungs, liver, kidney, muscle, eye, fibroblasts	Knobloch syndrome

Type	Molecular species	Class	Pathology	Diseases
XIX[e]	α1(XIX)$_3$	FACIT	Muscle, spleen, prostate, kidney, liver, placenta, colon, skin	None
XX[e]	α1(XX)$_3$	FACIT	Not human	None
XXI[e]	α1(XXI)$_3$	FACIT	Vasculature	None
XXII[e]	α1(XXII)$_3$	FACIT	Cartilage, hair follicles, muscle	None
XXIII[f]	α1(XXIII)$_3$	MACIT	Lung, kidney	None
XXIV	α1(XXIV)$_3$	Fibrillar	Embryonic eye and skeleton	None
XXV[f]	α1(XXV)$_3$	MACIT	Neurons, brain, heart, testis	Amyloid formation*
XXVI	α1(XXVI)$_3$	FACIT	Testis, ovaries	None
XXVII	α1(XXVII)$_3$	Fibrillar	Cartilage, eye, colon, lung	None
XXVIII	α1(XXVIII)$_3$	possibly FACIT	Dorsal root, peripheral nerves, dermis	Neurodegenerative disease*
XXIX	α1(XXIX)$_3$	Uncharacterised, possibly microfibrillar	Skin, lung, small intestine, colon, testis.	None

Table 1.1 The collagen family. Summary of collagen family based on their alpha chains, the tissues in which they have been detected, and examples of diseases caused by mutations in the collagen types. Adapted from (Gordon and Hahn 2010, Koch et al. 2004, Myllyharju and Kivirikko 2004, Ricard-Blum 2011, Soderhall et al. 2007, Tong et al. 2010).

Individual α chains, molecular species, and supramolecular assemblies of collagen types.

[a]The α4(V) chain is solely synthesized by Schwann cells.

[b]The α4(VI) chain does not exist in humans.

[c]The α5(VI) has been designated as α1(XXIX).

[d]The α3(XI) chain has the same sequence as the α1(II) chain but differs in its posttranslational processing and cross-linking.

[e]FACIT, Fibril-Associated Collagens with Interrupted Triple helices.

[f]MACIT, Membrane-Associated Collagen with Interrupted Triple helices.

[g]Multiplexin, multiple triple helix domains and interruptions.

*Predictions, not yet experimentally confirmed.

1. 3. 2. 5 Collagen IV

Col4 is specific to and is the major structural component of the BM, making up about 50% of all BM proteins, and although not the most abundant collagen, it is the most widely distributed in organs (Kalluri 2003, LeBleu et al. 2007, Timpl and Aumailley 1989, Van Agtmael and Bruckner-Tuderman 2010). It is a "network-forming collagen" due to its capacity to self-assemble into organized lattice type structure (Kalluri 2003, LeBleu et al. 2007). The ability to form these networks is mediated by the presence of its NC1 and 7S domain that are retained within the mature molecule, in contrast to fibrillar collagen where the pro-peptides are proteolytically cleaved. Six different Col4 α-chains are identified in vertebrates, and encoded by the genes COL4A1-COL4A6, which are genomically organized into pairs in a head-to-head style (COL4A1 with COL4A2, COL4A3 with COL4A4, and COl4A5 with COL4A6) (Figure 1.4). Col4 self-assembles into a network-like polymer through N-terminal (7S), lateral, and C-terminal (NC1) domain interactions that become covalently stabilized through the 7S and NC1 domains (Van Agtmael and Bruckner-Tuderman 2010).

Col4 networks are diversely expressed, the α1.α1.α2(IV) being the most widely expressed throughout embryonic development and adulthood (Figure 1.4) (Poschl et al. 2004). The α3.α4.α5(IV) and α5.α5.α6(IV) networks have a more discrete expression pattern and in renal and testicular BMs α3.α4.α5(IV) replaces α1.α1.α2(IV) during development (Harvey et al. 2006). Col4, unlike LM which is required for the initial BM formation, is found to be required for BM maintenance rather than initial formation (Poschl et al. 2004). Col4 is normally found only in the BM, however, during pathogenesis, it is associated with organ or tumour fibrosis, and accumulates in the tumour interstitium (Kalluri 2003). Tumours studies have shown that Col4 network formation is vital for BM stability and assembly (Kalluri 2003).

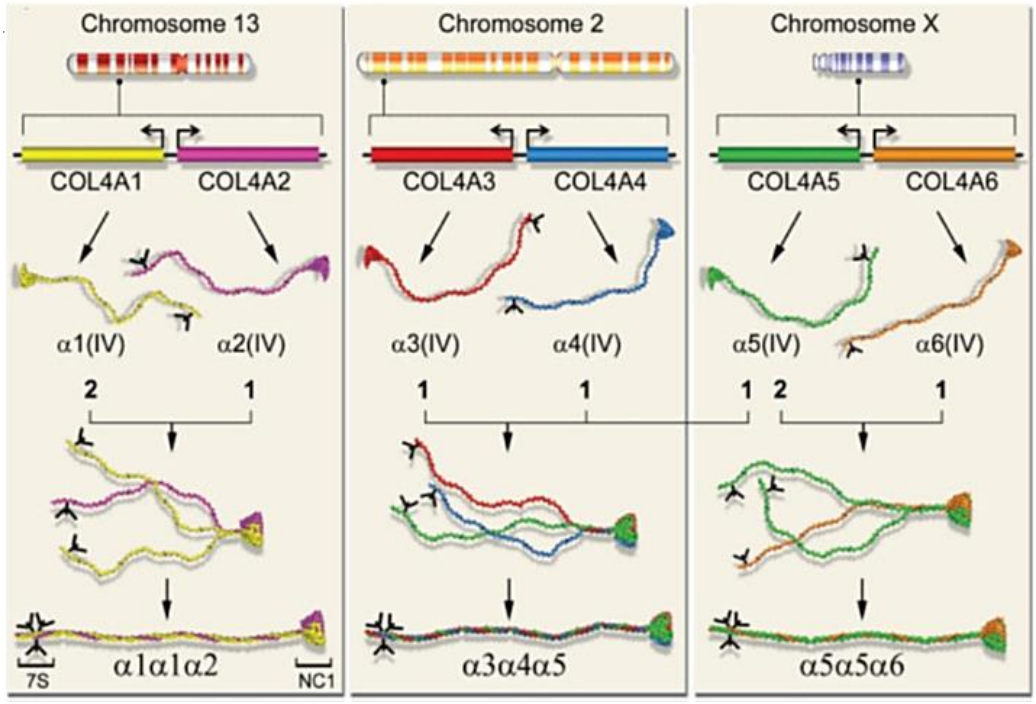

Figure 1.4 Collagen type IV genes. Representation of how collagen IV alpha chains are encoded by 6 genes arranged in head to head formations across three chromosomes. These alpha chains then interact at their N termini and fold into three kinds of trimer. Adapted from (Khoshnoodi et al. 2008).

Similar to all secreted and membrane proteins, Col4 mRNA is translated by ribosomes on the surface of the endoplasmic reticulum (ER), and as AAs are added, the nascent polypeptide is fed into the ER lumen. In the ER, these nascent polypeptides are folded and into the secretory pathway. The highly conserved protein structure of the six alpha chains consists of a collagenous central domain of ~1400 amino acids, a 230 residue non-collagenous domain (NC1) at the carboxyl terminus, and a 25- residue 7S domain at the amino terminus (Boutaud et al. 2000). Within the ER lumen, NC1 domains of alpha chains come together by forming 12 covalent bonds via cysteine residues (LeBleu et al. 2007). NC1 domains are cross-linked by protein disulfide isomerase ((PDI) forms disulphide bonds), which allows trimerisation to occur. Being highly selective, the trimerisation process only produces three alpha chain combinations (α1.α1.α2(IV), α3.α4.α5(IV), and α5(IV)2α6(IV)) despite the 76 theoretically possible (Figure 1.4) (Borza et al. 2001, Boutaud et al. 2000).

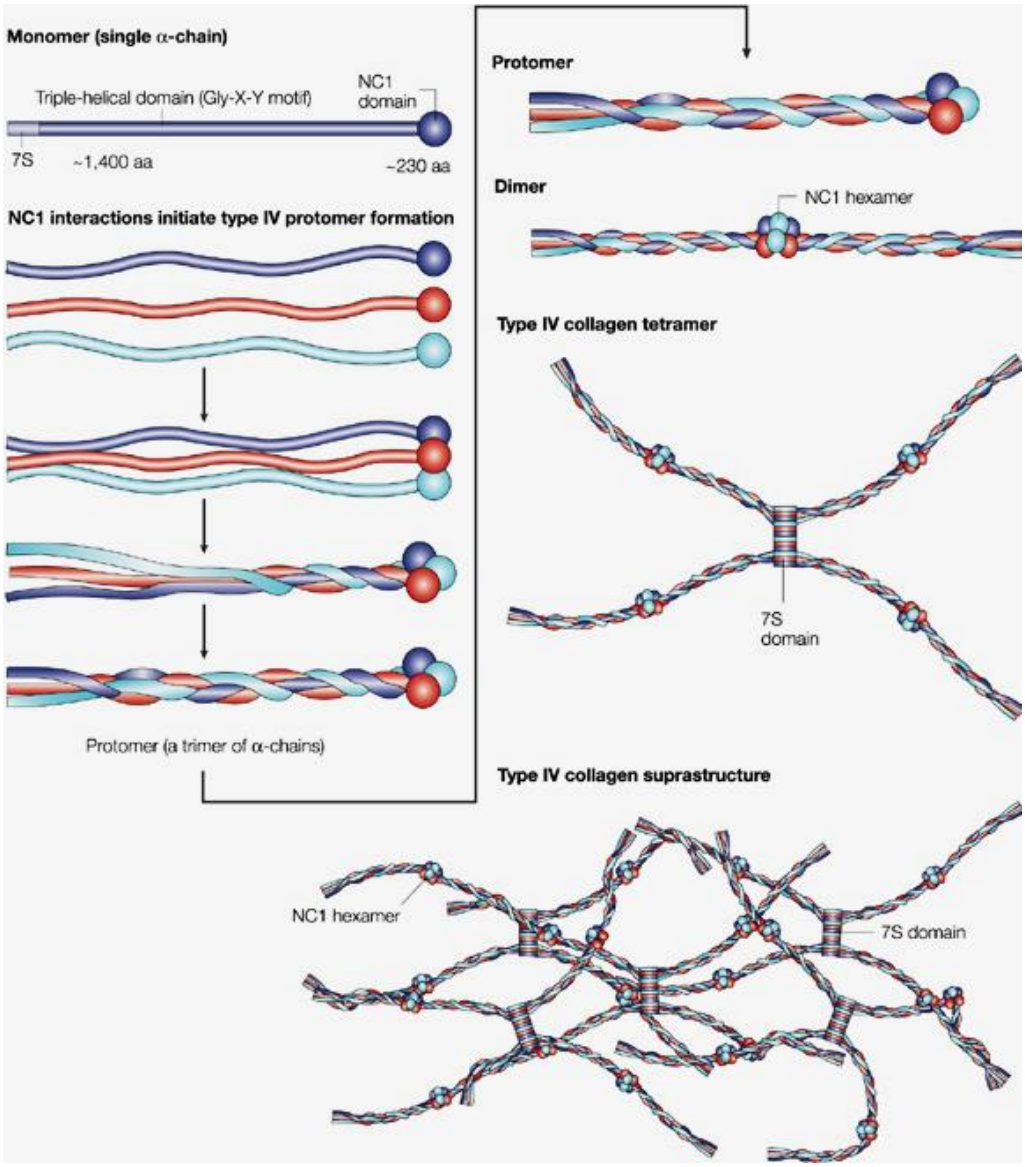

Figure 1.5 Type IV collagen folding and network formation. Type IV collagens in mammals have six genetically distinct α-chain polypeptides (α1(IV)– α6(IV)), and have similar domain structures and share between 50–70% homology at the amino-acid (AA) level. They have three domains: an amino-terminal 7S domain, a middle triple-helical domain, and a carboxy-terminal globular non-collagenous (NC)-1 domain. The triple-helical part is the longest domain 1,400 AA in length; the NC1 domain of each alpha-chain is about 230 AA in length. A trimer is assembled when three NC1 domains initiate interaction between three α-chains. Two Col4 protomers associate to form an NC1 hexamer via their carboxy-terminal NC1 trimers. Four protomers interact at the glycosylated amino-terminal 7S region to form tetramers becoming the nucleus for a Col4 scaffold. The scaffold evolves into Col4 suprastructure. Adapted from (Kalluri, 2003).

This trimerization leads to the typical collagen triple helix which is formed in a zipper-like fashion from the C to N terminal. The Gly-X-Y repeats are essential for this triple helical folding of the collagenous domain whereby glycine residues are located at the centre of the helix. As each third amino acid of the Gly-X-Y repeat is located within the centre of the

helix this has to be a neutral amino acid. Furthermore, the size constrains dictates that only glycine, the smallest amino acid, can be accommodated at this position. Thus, these glycine residues, and the triple helix are very sensitive to any amino acid substitutions. This can be clearly seen by the fact that the vast majority of collagen mutations (e.g. >85% of col4a1/4a2 mutations) affect these glycine residues (Mouw et al. 2014, Myllyharju and Kivirikko 2004). In general, it can be postulated that any substitution is thought likely to affect the folding of the triple helix causing many Col diseases (Table 1.1).

Several chaperone proteins such as glucose regulatory protein/immunoglobulin heavy chain binding immunoglobulin protein (BIP), and heat shock protein 47 (HSP47) make it energetically favourable for alpha chains to twist into triple helices, in a C to N-terminal direction, in a zipper like fashion, resulting in collagen IV trimers (Khoshnoodi et al. 2008). HSP47, a collagen specific heat shock protein, will bind to the collagen molecules in the ER and will effectively "coat" the collagen molecules to prevent intracellular aggregation of collagen. Very recently, a role for HSP47 in the secretion of collagen has also been proposed whereby it is important for loading of collagen into the secretory vesicles (Ishikawa et al. 2016). HSP47 dissociates from collagen molecules in the Golgi due to a change in pH change and is then recycled to the ER (Dafforn et al. 2001). Thus a large number of proteins are required for collagen folding, and transportation between organelles, ER to the Golgi body and then to the plasma membrane for secretion (Dafforn et al. 2001, Polishchuk et al. 2000).

After Col4 trimers have been secreted, NC1 domains of the same network type cross-link, via sulfilimine bonds (Vanacore et al. 2009), between Met-Lys interactions, to form Col4 dimers. The cysteine rich 7S domains of four collagen IV trimers interact via covalent bonds to form collagen IV tetramers, producing a network structure (Figure 1.5) (Boutaud et al. 2000). The interactions at both N and C termini of the trimers result in a collagen IV lattice network within the BM.

In addition to interactions between Col4 trimers, Col4 similarly binds to other BM components: LM, HSPG, nidogen (Laurie et al. 1986) and to other cell surface proteins: integrins (Kern et al. 1993), discoidin domain receptor 1 (DDR1) (Gross et al. 2004) and also to bone morphogenetic proteins (BMPs) (Paralkar et al. 1992).

1. 3. 2. 6 Diseases to collagen IV mutations

The description of Alport Syndrome and the identification that it was due to mutations in collagen IV paved the way for the analysis of basement membrane diseases and the role of collagen IV therein. It has now become clear that many mutations are found in COL4A genes and (Table 1. 2) lists them with their diseases. As this thesis focuses on Col4a1 and Col4a2, this introduction will be limited to diseases caused by mutations in these genes and will not cover pathologies associated with the other collagen IV networks. Absence of Col4 leads to embryonic lethality in mice (Poschl et al. 2004) and in *C. elegans* mutations lead to embryonic lethality (Gupta et al. 1997).

Mutations in Col4a1 and Col4a2 cause a wide variety of clinical phenotypes that affect multiple different organs (Table 1.2), reflecting the expression of these alpha chains in almost every BM. Furthermore, a feature of the COL4A1 and COL4A2 mutations is that they are pleiotropic and causing a broad spectrum of disorders with abnormalities in multiple organs, including the brain, eyes, kidneys and muscles, both in humans and in mice (Gould et al. 2006, Jeanne Marion and Gould 2012, 2016, Van Agtmael and Bruckner-Tuderman 2010). In addition, the same mutation may cause different pathologies and some mutations may even appear to be non-pathogenic in some individuals while causing a severe phenotype in other members of the same family (Gould et al. 2007, Murray et al. 2014).

The identification of the human disease was based on the identification and analysis of the different mouse models (Favor et al. 2007, Gould et al. 2005, Van Agtmael et al. 2005). Mutations in Col4a1/Col4a2 lead to eye, kidney, muscle and vascular defects (Favor et al. 2007, Gould et al. 2007, Gould et al. 2006, Van Agtmael et al. 2005). The eye defects are characterised by a complex phenotype consisting of anterior segment dysgenesis, which affects the anterior structures including the lens, cornea, iris etc (Alavi et al. 2016, Favor et al. 2007, Gould et al. 2007). In the kidney in mice glomerular defects, mainly affecting Bowmans Capsule and tubular defects which increase in severity with age and lead to the proteinuria (protein in urine), polyuria (increased urine production), cyst formation (Favor et al. 2007, Jones et al. 2016, Van Agtmael et al. 2010). The muscle defects lead to forms of congenital muscular dystrophy, such as Walker-Warburg syndrome and Muscle-eye-brain disease (Labelle-Dumais et al. 2011). However, most attention has focused on the vascular defects of these mutations, which may also play a significant part in the aforementioned pathologies.

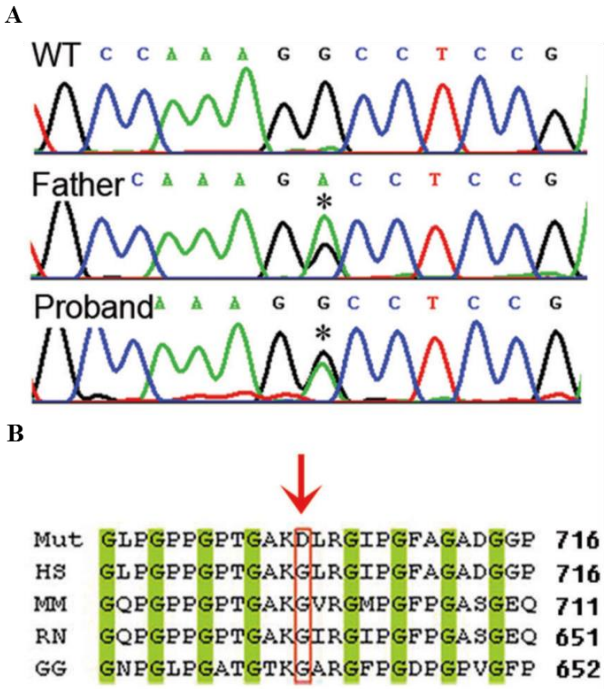

Figure 1.6 Identification of the *COL4A2*$^{+/G702D}$ mutation. A) The spectrogram sequence of the cDNA from the control (WT), father and proband *COL4A2* transcripts. * indicates the affected nucleotide. **B**) The amino acid alignment, displays the level of conservation between species of the affected amino acid. Mut: proband and father with *COL4A2* mutation, HS: control human, MM: mus musculous, RN: rattus norvegicus, GG: gallus gallus. Green boxes indicate highly conserved glycines. Red arrow indicates the amino acid affected by the mutation. Note: the father is not affected by the disease phenotype. Adapted from (Murray et al. 2014).

Col4a1 mutations cause cerebrovascular disease affecting the small vessels of the brain. It can thus be classed as small vessel disease and leads to ICH, which can lead to porencephaly(which is the formation of cerebral cavity due to intracerebral haemorrhage (ICH)), white matter hyperintensities and haemorrhagic stroke (Breedveld et al. 2006, Gould et al. 2005, Murray et al. 2014, Vahedi and Alamowitch 2011). To date about 100 different mutations have been described, the vast majority of which affect glycine residues and lead to amino acid substitutions. In rare cases, mutations have been described that appear to affect collagen IV protein levels rather than protein composition but the effects of these nonsense and extremely rare mutations remains even more unclear than those for the missense mutations (Gunda et al. 2014, Jeanne M. and Gould 2017, Verbeek et al. 2012). While mutations lead to rare Mendelian forms of cerebrovascular disease, recent evidence has confirmed a role for these proteins in common forms of these disease. For example, common variants in *COL4A2* are a risk factor for deep ICH in the general population, which leads to haemorrhagic stroke, the stroke subtype with the worst prognosis (Rannikmae et al. 2015,

Traylor et al. 2016). In addition, genetic association has also been documented for myocardial infarct in Japanese men, coronary artery disease and vascular stiffness (Yamada et al. 2007). Thus, collagen IV is emerging as a major component for vascular diseases for which there is an urgent need for treatment as there are no specific treatment for ICH or for collagen IV pathologies.

Gene	**Mutation type and effects**	**Human diseases and pathologies**	**Mouse model phenotypes**
COL4A1	Frameshift: Disruption of the C-terminal NC1 domain (Gale et al. 2016) G1236R, G749S G1769A: Amino acid change in the triple-helical domain (Jeanne Marion et al. 2012)	Haemorrhagic stroke HANAC syndrome, Familial porencephaly, Familial eye defects, Heart defects, Kidney defects including urinary retention and atrophy of medulla, Muscle-eye brain disease, Walker-Warburg Syndrome Small vessel disease	Eye defects, renal disease, hypotension, lung defects, haemorrhaging, porencephaly, reduced viability, tendon defects (Jeanne Marion and Gould 2016)
COL4A2	Amino acid change in the triple-helical domain (Jeanne Marion et al. 2012)	Haemorrhagic stroke, Familial porencephaly Small vessel disease	Eye defects, Haemorrhaging (Favor et al. 2007)
COL4A3	Splicing variants, missense mutations (Gould et al. 2006)	Alport's syndrome Thin basement membrane nephropathy	(Cosgrove and Liu 2016)
COL4A4	Splicing variants, missense mutations: altered chain expression	Cataract (Alavi et al. 2016) Alport's syndrome Thin basement membrane nephropathy (Hudson et al. 2003)	
COL4A5	Splicing variants, missense mutations	X-linked Alport's syndrome	(Cosgrove and Liu 2016)
COL4A6	Splicing variants, missense mutations: altered chain expression	X-linked Alport's syndrome Leiomyomatosis	(Cosgrove and Liu 2016)

Table 1.2 Genetic diseases associated with mutations in *COL4A* genes. Data are collected from (Vahedi and Alamowitch 2011) and inserted references.

1. 3. 2. 7 Mechanisms of collagen IV mutations

Despite the increasing research into collagen IV mutations, their contribution to disease pathogenesis and their pathomolecular mechanism remain poorly understood. As described, collagen type IV is folded within the ER and secreted into the matrix. While traditionally it had been considered that diseases due to mutations in matrix components are due to their effects on the matrix, recent evidence has emerged that is challenging this notion, with an increasing role of intracellular consequences and responses to the expression of the mutations (Bateman et al. 2009). In particular this has been the notion of ER stress due to the retention of misfolded protein. Intracellular accumulation of mis-folded proteins causes ER stress resulting in ER swelling, at the expense of their secretion; and in turn switches on the unfolded protein response (UPR) (Gould et al. 2007, Jeanne Marion et al. 2012, Murray et al. 2014). UPR is an ER mechanism to prevent incomplete or incorrectly folded proteins being released from the ER. It achieves this by effectively reprogramming gene expression of the cell via a general reduction in mRNA translation while upregulating the expression of chaperone proteins. In addition, the ER stress response also activates by promoting protein degradation pathways (Tabas and Ron 2011). While this ER stress is a homeostatic response, when it becomes chronic, ER stress and the UPR induces apoptosis of cells and has been shown to be causative factor for disorders such as achondroplasia due to mutations in type X collagen (Bateman et al. 2009).

For the case of mutations in collagen IV, mouse models with Col4a1 mutations were shown to display extensive structural BM defects in all affected tissues (Van Agtmael 2005, Gould 2005). This also affected the attachment of endothelial cells to the underlying BM and smooth muscle cells within the aorta of mice (Van Agtmael et al 2010). While thee defects may be related to the incorporation of the mutant protein, they may also be due to reduced levels or absence of collagen IV. This is supported by data from mouse models that showed intracellular retention of mutant protein (Gould et al. 2005) and activation of the ER stress response (Gould et al. 2006, Van Agtmael et al. 2010). This has also been observed in patient cells whereby a marked accumulation of Col4a1 and Col4a2 was observed (Murray et al. 2014). It has been postulated this retention is due to accumulation of misfolded protein, although it should be pointed out that this has not been directly tested. No structural or

biochemical analysis has been performed on mutant collagen IV to confirm the effects of these mutations on the collagen molecule.

Thus in general, it is assumed that the mutation in α1.α1.α2(IV) trimer causes its mis-folding, and subsequent intracellular accumulation and ER retention (Bateman et al. 2009, Murray et al. 2014). As mentioned, this retention can reduce the amount of collagen IV that is secreted, which may cause BM defects and/or ER-stress. If mutant protein is secreted, it may cause BM defects by affecting its interactions with other proteins such as matrix components, cell receptors etc (Bateman et al. 2009, Murray et al. 2014). These mechanisms are not mutually exclusive and given the pleiotropy of the effects of different mutations, the possibility that this can vary between mutations can not be excluded (Jeanne et al. 2012, Jones et al. 2016, Murray et al. 2014, Van Agtmael et al. 2005, Verbeek et al. 2012).

The BM defects are associated with cerebrovascular disease including ICH, and eye and kidney disease (Jeanne Marion et al. 2012, Murray et al. 2014, Rannikmae et al. 2015, Van Agtmael et al. 2010, Van Agtmael et al. 2005). However accumulating data support a role for ER stress in the disease pathogenesis. Previous analysis in the Van Agtmael laboratory of cell of patients of a family with porencephaly identified that the disease is associated with ER stress and ER retention of collagen IV protein due to the COL4A2+G702D mutation rather than BM defects (Murray et al. 2014). This was confirmed by analysis of an allelic series of mouse models with Col4a1 mutations that showed that severity of intracerebral haemorrhage correlated with ER stress levels and ER retention of collagen IV (Jeanne et al. 2015). Intriguingly, recent data suggested that these mutations may have cell dependent mechanisms as evidence supported that in kidney phenotype of a mouse model the glomerular disease are associated with BM defects and the tubular phenotypes with ER stress (Jones et al. 2016). However, the relative contribution of these mechanisms remains to be directly disentangled.

This thesis will focus on a particular COL4A2 mutation, *COL4A2*$^{+/G702D}$ which was identified previously in the laboratory of Dr. Tom Van Agtmael (Murray et al. 2014). This mutation causes familial porencephaly (Murray et al. 2014). The mutations result in a single nucleotide change that changes a highly conserved glycine residue of a Gly-X-Y repeat for an aspartic acid (Figure 1.6A & B). Analysis of the *COL4A2*$^{+/G702D}$ mutation revealed the presence of BM defects in the skin of individuals carrying this mutation. In addition, based on analysis of cells from patients the mutations is likely interfere with the triple helix 3D structure of the α1.α1.α2(IV) trimer and/or affect the trimers. The mutation in cells from a

patient leads to ER retention of collagen IV and ER-stress (due to protein retention). Therefore, the BM defects may be due to mutant protein incorporation and/or reduced incorporation due to ER retention (Jeanne Marion et al. 2012, Murray et al. 2014, Van Agtmael et al. 2010, Van Agtmael et al. 2005). While the actual mechanisms remain poorly defined, as mentioned the intracellular retention rather than BM defects were associated with disease development.

1. 4. Biointerfaces

A biomaterial has been defined widely as "any substance (other than drug) or combination of substances, synthetic or natural in origin, which can be used for any period of time, as a whole or part of system, which treats, augments, or replaces any tissue, organs, or function of the body" (Dee et al. 2003); or "a material intended to interface with biological systems to evaluate, treat, augment, or replace any tissue, organ, or function in the body" (Black 2006). Traditionally referred to as materials used in medical devices, biomaterials have been used since antiquity, but recently their degree of sophistication has significantly increased. Biomaterials have been widely used for many applications including, cardiovascular, orthopaedics implant devices, wound healing, and others. They also provide information rich data that enables the study of cellular behaviour. Biomaterials include metallic, ceramic, polymeric, composite, biodegradable polymeric and biologic. These are widely used in different field of medical industries, and continuing research on them focuses on biocompatibility, bioinerty, bioactivity, biodegradabilty, sterilizability, adequate mechanical and physical properties, manufacturability etc.

Biomaterial surfaces, including synthetic polymers combined with ECM proteins, are powerful tools to control cell fate and study a myriad of biological processes (Cantini 2012, Llopis-Hernandez et al. 2011). They provide cells with well-defined microenvironments and, as a consequence, constitute a tool to interrogate them and provide further insights into pathological and physiological cell behaviour. Many studies have been undertaken to investigate the interaction of different ECM proteins with various material surfaces, in combination with their effect on cell behaviour (Baetscher et al. 1986, Cantini 2012, Coelho et al. 2011a-b, Cortiella et al. 2010, Dupont-Gillain et al. 2004, Llopis-Hernández et al. 2013, Rodriguez Hernandez et al. 2007, Salmeron-Sanchez et al. 2011, Vanterpool et al. 2014). Interfacial protein layer constitutes biointerface together with the material surface, these will be used to culture cells in order to investigate their responses. Biointerfaces can modulate

cell behaviour and thus this may open avenue of modulating cell to collagen mutations or of overcoming cell defects by altering matrix.

1. 4. 1 Cell interaction with biomaterials

To ascertain the intricacies of cell behaviour and capabilities in tissue engineering, an understanding of cell interactions with the ECM is of fundamental importance. With the intention of replicating innate cell behaviour *ex vivo*, a number of naturally occurring and synthetic substrates have been developed for use in tissue engineering. These aim to cater for a range of demands from being able to support adherence and viability to the more intricately tailored designs geared towards researching a particular hypothesis.

Protein remodelling (after adsorption) at the cell–material interface is an important factor to direct cell behaviour on biomaterials for tissue engineering. It is known that cell adhesion onto a synthetic surface involves different phenomena in which different biological molecules participate: ECM proteins, cell membrane proteins, and cytoskeleton proteins that interact to convey information, transcribe factors, and regulate gene expression (Cantini 2012, Vanterpool et al. 2014). ECM proteins are adsorbed onto the material, either from the physiological fluids *in vivo* or intentionally deposited through adsorption of ECM proteins (FN, Cols, LM… etc.), or *via* chemical attachment to the substrate. The concentration, distribution and mobility of ECM proteins adsorbed on a surface hence play a fundamental role in the biofunctionality of a synthetic material, and are key factors for the biological response of a substrate.

Protein adsorption on solid surfaces is a phenomenon observed in various fields. The changes in proteins structures and functions upon adsorption as well as the adsorbed amounts have a very important consequence (Nakanishi et al. 2001). Despite considerable progress in this field, there are still widely differing and even contradictive opinions on how to explain the frequently observed phenomena. Protein adsorption on a surface is affected by various factors such as properties of proteins and the solid substrate surface, and environmental conditions. With respect to properties of proteins, the charge, size, stability of the structure, amino acid composition, and steric conformation may affect the adsorbed protein. Moreover, external parameters such as temperature, pH, ionic strength, and buffer composition are to be considered. For solid substrate surfaces, surface energy, polarity, charge, morphology and wettability) are some of the properties that may affect the adsorbed protein (reviewed by (Rabe et al. 2011)). Surface-induced denaturation is one factor that has important

implications for the development of materials that are resistant and/or innocuous to biomolecules. Experimental results that unequivocally explain the underlying principles of the surface-induced denaturation of proteins are difficult to find in the literature. This is due to the limited availability of methods to resolve protein structure at the solution–solid interface.

As mentioned above, the properties of solid substrate surface influence protein the adsorption of proteins. The effect of surface chemistry and wettability on LM morphologies was investigated by AFM using a series of different copolymers based on ethyl acrylate and hydroxyethyl acrylate. LM molecules showed globular to completely extended morphologies on the hydrophilic polymer as the amount of −OH groups diminished (Rodriguez Hernandez et al. 2007). Collagen is shown to form a fine network on hydrophilic glass and a prominent polygonal network on hydrophobic octadecylsilane that alters significantly Col IV activity (Baetscher et al. 1986, Cortiella et al. 2010). Coelho and coworkers have described the arrangement behaviour of LM and Col4 using AFM on substrates with controlled density of –OH groups (Coelho et al. 2011b). They also showed the arrangement behaviour of Col4 using AFM on NH2 and COOH functionalized surfaces (Coelho et al. 2011a), and on model OH, CH3, NH2 and COOH surfaces (Coelho et al. 2013) and on hydrophilic and hydrophobic substrata (Coelho et al. 2010). The layer of the adsorbed ECM proteins (LM or Col4) was displaying structures mostly resembling a network.

Dupont-Gillain and colleagues have demonstrated that it was possible to control the supramolecular organisation of adsorbed collagen layers on polymer surfaces as a function of properties of the substrates (chemical nature, roughness) and of characteristics of the collagen solution (concentration, state of aggregation) as well as details of the preparation procedure (adsorption time, drying rate) (Dupont-Gillain et al. 2004). They also showed, using a combination of X-ray photoelectron spectroscopy (XPS), AFM and water contact angle (WCA), the nano-organised layers of collagen on a series of polystyrene (PS)/poly(methyl methacrylate) (PMMA) (Zuyderhoff and Dupont-Gillain 2011).

Many studies have been dedicated to the adsorption of FN. For example, Emch and coworkers imaged FN with scanning tunnelling microscopy (STM) on mica shadowed with a thin platinum carbide conductive film observing that is well adsorbed on Ti and V substrates, but is not biologically active on V (Emch R et al. 1990). Likewise, using scanning force microscopy (SFM) of FN sprayed on mica and PMMA, protein morphology was found to be influenced by substrate surface properties (Emch Roger et al. 1992). MacDonald and

colleagues also imaged FN adsorbed onto polished commercially pure titanium (cpTi) by using AFM and electron spectroscopy for chemical analysis (ESCA) (MacDonald et al. 1998). Furthermore, using AFM it has been demonstrated that when FN is adsorbed onto biomaterials, it may undergo a conformational change depending on surface properties such as surface charge, hydrophilicity, hydrophobicity, and plays a critical role in mediating cell responses. For example it changes from a globular structure on PMA to extended structure, a physiological-like fibrillary (nano) networks on PEA (Llopis-Hernandez et al. 2016, Llopis-Hernández et al. 2013, Salmeron-Sanchez et al. 2011, Soria et al. 2007, Vanterpool et al. 2014).

Non-(bio)chemical factors such as roughness, texture and surface patterns have an undeniable influence on protein adsorption and cells on all materials. Dynamic interactions between nanoscale surface topographies and proteins are complex due to the combination of attractive and repulsive forces that are governed by local changes in surface properties, including chemistry, which may lead to spatial changes in the quantity, density and orientation of adsorbed proteins (Wilson et al. 2005). For instance, Deligianni and colleagues have shown that the adhesion of scaffold proteins and osteoblasts has been demonstrated to be encouraged by surface roughness resulting in an increase in surface mineralization (Deligianni et al. 2001). The use of ECMs coated surfaces have found widespread use in research applications; nonetheless, they are not without their idiosyncrasies. While ECM proteins are able to support cell adhesion and activity on synthetic surfaces, protein interaction with biomaterial polymers can develop in its own interactions which in turn can lead to changes in protein conformational state and adsorption properties resulting in differential cellular interactions both between biomaterial types and from that observed *in vivo* (Cantini 2012, Coelho et al. 2011b, Dupont-Gillain et al. 2004, Llopis-Hernández et al. 2013).

The differential behaviour of protein types used to coat synthetic polymers has prompted to the characterisation studies in which binding kinetics demonstrated that there is an optimal concentration at which cells interact with ECM proteins to enable cell adhesion and spreading (Coelho et al. 2011a, Vanterpool et al. 2014). ECM protein/polymer composition has been shown to have the tendency to affect the type of proteolytic cleavage that occurs during adsorption (Coelho et al. 2013). Furthermore, this effect may also elucidate the varied expression of cellular integrins when cells are seeded onto ECM coated polymers (Rezania and Healy 1999).

The density of adsorbed protein on the surfaces has been found to influence cell behaviour. FA plaques are found to develop better on surfaces coated with higher FN concentration (Llopis-Hernández et al. 2013, Vanterpool et al. 2014), and enhanced signalling by FAK and pFAK is observed when cells are cultured on highest FN concentration (Llopis-Hernández et al. 2013). Moreover, myogenic differentiation is considerably more robust on higher FN density compared to the lower density (Salmeron-Sanchez et al. 2011). Apart from the density and spatial orientation of surface ligands, the topography of the substrates is known to be a recognisable instructional cue to elicit specific cell responses. For example, Dalby and colleagues have shown the use of nanoscale disorder to stimulate human mesenchymal stem cells (MSCs) to produce bone mineral in vitro (Dalby et al. 2007). Cells respond to nanopits coated FN by forming larger FAs and by mimicking the pit patterns within their cytoskeleton, nanoimprinting, ultimately achieving higher levels of myogenic differentiation compared to a flat control (Ngandu Mpoyi et al. 2016). Tissues possess structures with varied topologies, from smooth or striated muscle to the roughened surface of trabecular bone. It is possible therefore that mimicking these patterns *in vitro* can lead to behavioural changes to closely match that which occurs *in vivo*.

Cell adhesion to ECM or surface-grafted proteins occurs via receptor protein including integrins (Figure 1.7). Integrins are major cell surface receptors and form a large family of α/β heterodimers typically in the size range of 9–12 nm in length. Integrins recognize specific sequences of ECM proteins such as the arginine-glycine-aspartic acid tripeptide (RGD), present on fibronectin and vitronectin, VPGVG on elastin, IKVAV on laminin and GFOGER on collagen; providing a trans-membrane link between the ECM and actin cytoskeleton (Huang et al. 2009, Knight et al. 2000, Mecham et al. 1989, Nomizu et al. 1995). Although constitutively expressed, most integrins on the cell surface are in an inactive state, neither ligand binding nor signalling. Integrins can be activated by ligand binding or by intracellular signalling, due to effects in its cytoplasmic domains, resulting in conformational changes which expose epitopes for specific activation antibodies. Integrins play a dual role when activated through ligand binding: mediating cell attachment and triggering several intracellular signalling pathways, which can in turn influence growth, migration, differentiation or proliferation (Berrier and Yamada 2007).

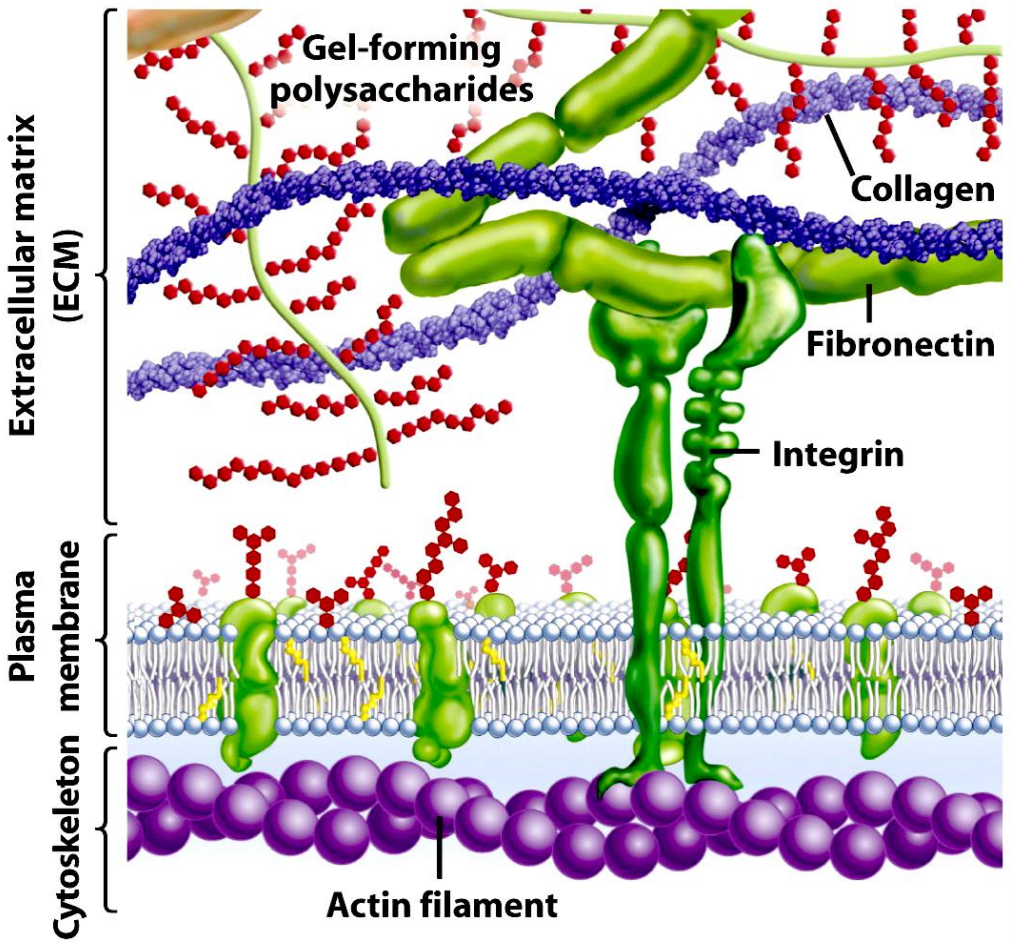

Figure 1.7 Integrins mediate cells-ECMs interactions. Cells-ECMs interaction takes place via integrins, membrane-bound receptors that trigger several signalling pathways and influences cell behaviour. Adapted from (Freeman 2014).

Integrins cluster and develop focal adhesions (FAs) once bound to their substrate. The anchored cells spread displaying a developed actin cytoskeleton, providing mechanical stability and transmitting forces to the intracellular regions. FAs are discrete supramolecular complexes that contain important structural proteins and signalling molecules, anchoring the cell to the substrate. They are flat, small and elongated structures several square microns in size and are mostly located near the cell periphery (Sastry and Burridge 2000). They mediate strong adhesion to the substrate linking bundles of actin microfilaments through a plaque formed by many different proteins amongst others vinculin, paxillin, talin and tyrosine phosphorylated proteins.

FAs are believed to act as mechanosensors, allowing cells to sense physical properties of the substrate such as stiffness and transform them into specific biological signals (Sun et al. 2016). FAs not only play the role of mechanical anchors between the ECMs and the actin cytoskeleton; but after integrin clustering, various signalling molecules such as the focal

adhesion kinase (FAK) and the integrin-linked kinase (ILK) are recruited by adapter proteins. These, becoming activated trigger several intracellular signalling pathways (Han et al. 2001). FAK is an important mechanotransducer triggering the majority of those signalling pathways (Hanks et al. 1992, Rubin et al. 2006). FAK is important in the regulation of actin cytoskeleton and FAs formation on FN-coated substrates (Parsons 2003). In the absence of FAK, actin cables lined cell boundaries, in contrast with organized actin networks converging at peripheral FAK-positive FAKs. Additionally, in the absence of FAK, the small central FAs diminished dramatically in number and are replaced by large focal contacts (Ilic et al. 2004).

Several authors have studied the effect of substrate properties in protein adsorption and cell responses. In particular, different studies have focused on investigating the influence of these surface parameters in intracellular signalling pathways (reviewed by (Aiyelabegan and Sadroddiny 2017, Burridge 2017, Jansen et al. 2017, Weinberg et al. 2017)). Mechanical properties, surface chemistry, and topography of the ECM regulate cell behaviour including cell adhesion, spreading, proliferation, and differentiation, through activation of different signalling pathways. In this study, the surface chemistry will be manipulated to control the fate of *COL4A2* mutant cells.

1. 5 Work leading to project

Recent analysis by Murray and colleagues has revealed that haemorrhagic stroke was associated with collagen IV ER-retention and ER-stress in a patient carrying a *COL4A2* mutation (glycine to aspartic acid (*COL4A2*$^{+/G702D}$)) (Murray et al. 2014). Their analysis of primary patient cells showed that missense mutations in the *COL4A1/COL4A2* genes can lead to mis-folding and intracellular accumulation, resulting in ER and cell stress, UPR activation, reduced cell proliferation and increased apoptosis (Murray et al. 2014). Importantly, they found that treatment of cells carrying Col4 mutations with a food and drug administration (FDA) approved chemical chaperone (phenyl butyric acid, PBA) decreased intracellular *COL4A2* levels, ER stress and apoptosis, demonstrating that reducing intracellular accumulation can ameliorate the cellular phenotype of *COL4A2* mutations. This suggests that targeting this intracellular accumulation can modify disease development (Figure 1.8) (Murray et al. 2014).

However, the effects of *COL4A2* mutations on BM function (e.g. influence cell behaviour/signalling) and characteristics (*e.g*. rigidity, stiffness), which also contribute to

disease development (Jones et al. 2016) have not been investigated in detail. Thus, there is a need to study more closely the mechanism that affect the BMs and how *COL4A2* mutant cells respond to the extracellular milieu to provide novel insights into collagen disease mechanisms. Important questions remain including but not limited to (1) what is the secretion state of ECM proteins that make up the BM? (2) What is the physiological structural integrity of the BMs? (3) What influence has each ECM protein on the formation of the BM? Hence, can biomaterials be employed to get an understanding to these questions?

Cells behaviour and protein conformation can be influenced by the manipulation of surface substrates chemistry and topography (Baetscher et al. 1986, Soria et al. 2007, Wilson et al. 2005). For this work, poly(ethyl-acrylate) (PEA) and poly(methyl-acrylate) (PMA) polymer substrates were employed. These substrates have similar chemical structure, consisting of a vinyl backbone chain with either –COOCH2CH3 or –COOCH3 side groups respectively (Figure 1.9). The difference of only one single methyl group in the lateral chain yielded substrates with similar physicochemical properties (Gonzalez-Garcia et al. 2012). They have a thickness of ~1 µm (Vanterpool et al. 2014). Moreover, AFM nano-indentation of a coated layer on glass coverslips determined distinct elastic moduli: PEA's is lower than that of PMA, yet the Young's moduli of both surfaces were ≥1 MPa, greater than the 40-kPa stiffness threshold that cells can detect (Balaban et al. 2001, Bathawab et al. 2016).

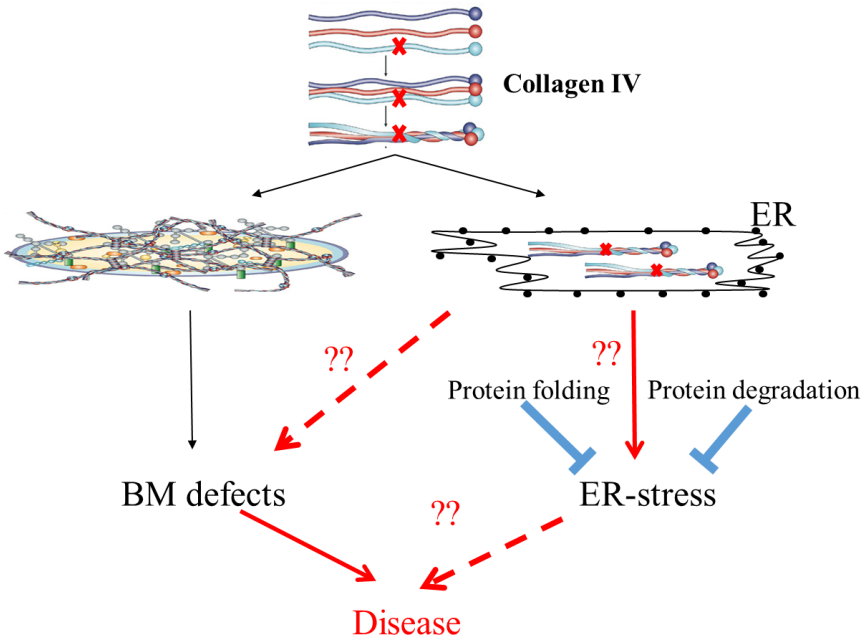

Figure 1.8 Collagen IV disease mechanism hypothesis. A representation of how BM defects and UPR could be caused by a collagen IV mutation.

These substrates have been shown to modulate the adsorption, conformation and distribution of coated proteins. The adsorption of ECM proteins onto different substrates has been widely investigated in literature using a number of different methods, which include atomic force microscopy (AFM) and scanning electron microscopy (SEM). For example, the fractal nature of polymerised LM on glass was analysed using confocal fluorescence microscopy (CFM), SEM and AFM on glass by Hochman-Mendez and colleagues (Hochman-Mendez et al. 2014).

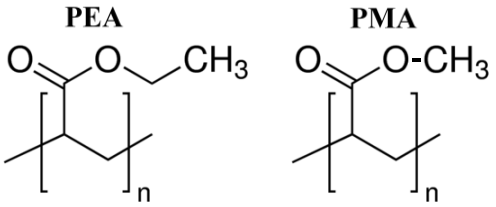

Figure 1.9 Chemical structure of polymers. PEA, poly(ethyl-acrylate); PMA, poly(methyl-acrylate).

In our group (Microenvironment for Medicine (MiMe) Research Group), methodologies have been developed to engineer biomaterial surfaces with controlled properties (*e.g.* chemistry, stiffness, topography) that determine the conformation and distribution of ECM proteins upon adsorption. In turn, these control cell adhesion on these interfaces triggering signalling pathways and directing key cellular processes, including the secretion of the ECM (Llopis-Hernandez et al. 2011, Salmeron-Sanchez et al. 2011). To enable us to address the hypothesis, biomaterials including PEA and PMA synthetic polymers (Figure 1.9) combined with ECM proteins (such as FN, LM, COL4) will be used; these have been demonstrated to provide microenvironments greatly influencing cells behaviour.

Although for most of these genetic BM linked diseases there are limited treatment options, cell-based therapeutic approaches based on delivering pluripotent and/or differentiated cells are emerging as a plausible and promising treatment for these devastating pathologies (Nystrom et al. 2017). Yet, to use cell-based therapy, the disease mechanisms must first be understood.

1. 6 Project Aims

The molecular and cellular consequences of *COL4A1/COL4A2* mutations remain poorly understood. Hence, this study proposes to employ engineered biointerfaces to provide novel insights into Col4 diseases mechanisms. The hypothesis is that biointerfaces can be used to investigate the effect of *Col4* mutations on cell function and that biomaterials can be used to

modulate and perhaps overcome some of the cellular defects caused by the expression of these mutant proteins. This project will use *COL4A2*$^{+/G702D}$ cells (mutations affecting α1.α1.α2(IV)) to address the effect of defined engineered biointerfaces on cell behaviour/signalling and Col4 secretion (Figure 1.10). Can engineered biointerfaces influence mutant cells and lead to a more functional BM and rescue downstream effect of ER-stress altering disease development, thereby informing on the disease mechanism.

In order to probe this hypothesis, the aims of this project are:

(1) Characterise the biointerfaces: analyse the state of ECMs adsorbed on the polymeric substrates.
(2) Investigate whether these biointerfaces can ameliorate/alleviate the cellular disease phenotypes, if so explore signalling pathways.
(3) Investigate the effects of mutant Col4 network on the BM structure and biomechanics using AFM as a tool.

Combined, these aims will assist in understanding how mutation in *COL4A2* affects the BM composition and structure; and how each ECM protein affects the formation of the BM. The results of this work will elucidate whether biomaterials can alter collagen mutant cells behaviour by overcoming some of the defects caused and rescuing downstream effect of ER stress. Deepening our understanding of how these mutations affect cell function/behaviour will increase our knowledge of Col4 disease mechanisms. This can in the long-term lead to the development of new therapeutic approaches for ICH and pathologies due to collagen IV mutations.

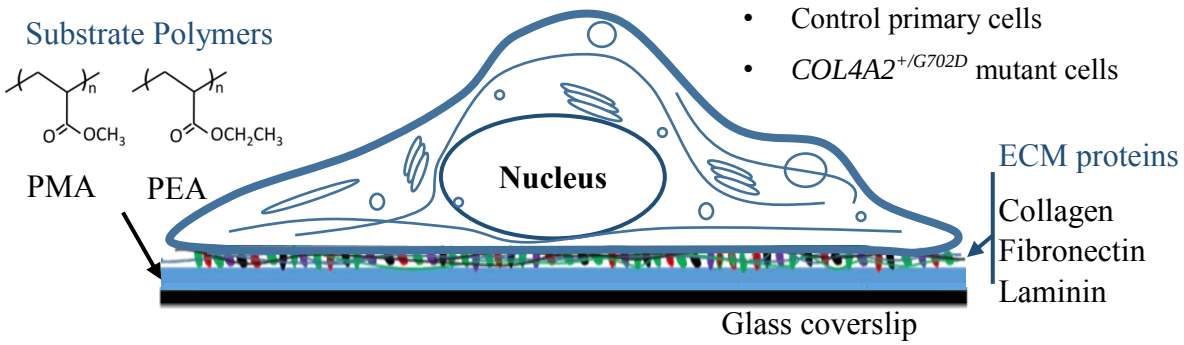

Figure 1.10 Biointerfaces concept model. The chemistry of the surface substrate will be manipulated to modulate protein adsorption, conformation and distribution in order to influence cells (mutated *COL4A2*$^{+/G702D}$) behaviour and study whether it can ameliorate/alleviate some effects of the mutation effects. PEA: Poly(Ethyl) Acrylate; PMA: Poly(methyl) Acrylate, consisting of similar chemistry. These synthetic polymers have similar physicochemical properties.

Chapter 2

Materials and Methods

Contents

2. 1 Reagents and Solutions

All other reagents were from Sigma-Aldrich Company Ltd. (Gillingham, Dorset SP8 4XT, U.K.), except where otherwise specified, and buffer compositions are provided in (Table 2.3). All solutions were warmed in a water bath at 37^{o}C before use, unless otherwise stated.

2. 2 Surface preparation

Polymers were synthesized by radical polymerization of ethyl acrylate (EA) and methyl acrylate (MA) (Sigma, St. Louis, MO), initiated by benzoin at 1 wt%. The reaction was carried out in ultraviolet light for 24 h. After polymerization, low molecular weight substances were extracted from the material by drying in vacuum to constant weight, and polyacrylate solutions prepared by dissolving bulk polymers in toluene, with a 4% w/v solution for PMA and a 6% w/v for PEA. 12 or 25 mm diameter glass coverslips (VWR) were cleaned by immersing in ethanol then placed in an ultrasonic bath for 20 min before drying at 60 °C in an oven for up to 30 min. Thin layers of PEA and PMA were prepared using a spin-coater (Brewer Science). Spin-casting was performed by adding ~100 μL of polymer solution to the surface on glass coverslips and spun at 3000 rpm, 3000 rpm/sec acceleration for 30 sec. To remove residual solvent, the spun samples were placed and dried in a desiccator within a 60 °C oven under vacuum for 2 h, then kept in vacuum before further characterization. The obtained films were not porous and had approximately 1 μm of thickness.

2. 3 Protein adsorption

Polymer surfaces on 12 mm glass coverslips were coated with either human type IV collagen (Col4) (Millipore), or natural mouse LM (Invitrogen) or human plasma FN (Sigma) solutions, in Dulbecco's phosphate buffered saline (DPBS) at concentrations 2, 10, 20, 50, and 100 μg/mL (specific concentrations in figure captions) for 10 min or 1h.

2. 4 Quantification of adsorbed protein

The biochemical assay based on the bicinchoninic acid assay (BCA protein assay, Thermo Fisher Scientific, Waltham, MA) was used following manufacturer instructions to determine the total amount of protein adsorbed on PEA and PMA substrate surfaces. The latter were coated with either Col4, FN or LM for 1h at different solution concentrations and the density of adsorbed protein was determined by measuring the amount of non-adsorbed proteins. A

stock solution of protein was diluted at 2, 10, 20, 50, and 100 μg/mL (specific concentrations for each protein shown in figure captions) to determine the exact concentration of the stock solution and the amount of deposited protein onto the surfaces. After coating for 1 h, the supernatant was collected and transferred to a 96-well plate followed by the addition of the bicinchoninic acid working reagent (Thermo Fisher Scientific, Waltham, MA). The plate was then placed in an incubator for 2h at 37°C. Then the absorbance was read on a Tecan NanoQuant Infinite M200 Pro plate reader (Männedorf, Switzerland) at 562 nm. The total protein adsorbed on the substrates was calculated subtracting the amount of protein remaining in the supernatant from the total amount of protein in the initial solution.

2. 5 Immunostaining of adsorbed protein

To visualise protein adsorbed on PEA and PMA, Col4, FN and LM coated for 1h at the indicated concentration were fixed with 3.7% paraformaldehyde (PFA), incubated with blocking buffer (BB) DPBS/BSA 1% w/v for 30 min, then stained with primary monoclonal mouse anti-Collagen 4α2(IV) 1:300 (Milllipore, Cat. No. MAB1910), polyclonal rabbit anti-LM 1:200 (Sigma, Cat. No. L9393) or polyclonal rabbit anti-FN 1:400 (Millipore, Darmstadt, Germany) antibodies in BB for 1h at room temperature (RT). Coverslips were then incubated with secondary Cy™3 AffiniPure goat anti-mouse/rabbit 1:200 (Cat. No. 115-165-062) (Jackson ImmunoResearch Laboratories inc) in BB for 1h at RT and finally mounted on microscopic slides with mounting medium (VectaShield, Vector Laboratories, Inc., Peterborough, UK) and images acquired with an inverted Zeiss Axio Observer.Z1 epifluorescence microscope (Jena, Germany) (fully motorised fitted with an Andor Luca R EMCCD camera for fluorescence) fitted with x5, x10 and x40 LD objectives and Zeiss set 43 for Cy3. All the samples were in triplicates.

2. 6 Water contact angle

The surface wettability was investigated by water contact angle (WCA^{o}) measurements both statically and dynamically, the latter providing the hysteresis angle of the surface. Measurements were carried out on bare and protein coated PEA and PMA substrates using the sessile drop method with a Theta optical tensiometer (Biolin Scientific, Stockholm, Sweden). For each condition, the static contact angle (SCA) of the drop was determined by placing a drop of 3 μl of water on the surface using a needle and stabilization allowed (∼10 s) and recording the images at 12 frames/sec for 30 sec while measuring the angle of the drop with the substrate surfaces. Also advancing contact angle (ACA), and receding contact

angle (RCA) were determined, the needle was placed in the original static volume previously deposited and water is added or removed at a rate of 0.1 µL/s in order to observe an increase or decrease in the length of the baseline. Hysteresis is the difference between the ACA and RCA. All these measurements were performed at RT and average values were obtained from 3 measurements of at least three different samples (n=9).

2. 7 Atomic force microscopy

Atomic force microscopy (AFM) experiments were performed with a JPK Nanowizard® 3 BioScience (JPK Instruments, Berlin, Germany). AFM was used to analyse protein organization on material surfaces. Polymers were adsorbed with a solution concentration of 2, 10, 20, 50, and 100 µg/mL of Col IV, FN and LM (specific concentration shown in figure captions) for 10 min and 1h in DPBS. After adsorption, the samples were rinsed with DPBS and Milli-Q water and dried with N2. The difference in time is to aid in the imaging of the network via AFM, which can reduce in clarity at higher time points due to adsorption of more protein. The images were acquired in tapping mode in air using silicon cantilevers (MPP-21120 Bruker AFM Probes, Billerica, MA) with a pyramidal shape, a force constant of 3 N/m, a resonance frequency of ~75 kHz, a radius of curvature below 10 nm. The AFM images were scanned at 1×1 μm^2 (1 Hz) (area sizes and line rates unless specified). The surface height, lock-in phase, and lock-in amplitude magnitudes were recorded simultaneously for each image. Acquired images were analysed using JPK data processing software (v4.3.21) to observe the initial topography of non-coated surfaces, as well as, the distribution and confirmation of protein on the different polymers.

2. 8 Calculus of the fractal dimension

ImageJ fractal analysis plugins FracLac (Abràmoff et al. 2004, Karperien 2013) or Fractal Box Counting (Russell et al. 1980) were used to determine fractal dimension (FD) of adsorbed Col4, FN and LM proteins and also of secreted Col4 on the polymer surfaces obtained by immunofluorescence. The "capacity" fractal dimension algorithm called, in fractal parlance, the "box counting" method was used. The box-counting dimension is an estimate of the Hausdorff dimension based on covering the investigated set with a fixed grid of size (Soille and Rivest 1996, Theiler 1990) using the formula, $DH = \frac{-\Delta[\log k(r)]}{\Delta \log r}$, where *k(r)* is a number of grid boxes that contain any part of the investigated set. D_H is known as the Hausdorff dimension, the Minkowski-Bouligand dimension, the Kolmogorov capacity

or dimension, or simply the box-counting dimension. In short, the routine counts the number of boxes of a given size needed to cover a one pixel wide, binary (black on white) border.

The procedure is repeated for boxes that are 2,3,4,6,8,12,16,32,64 pixels wide on a black background. The output consists of two columns labelled "size" and "count". A plot is generated with the log of size on the x-axis and the log of count on the y-axis and the data is fitted with a straight line, (Smith et al. 1996). Before applying the box-counting algorithm, the original image was equalized and the resulting image was binarized (Figure 2.1). Finally, the box-counting estimate was calculated on this image; a graph plot is produced showing the measurement. All this process was performed on four different images of the same size (256 pixels 256 pixels, 8-bit).

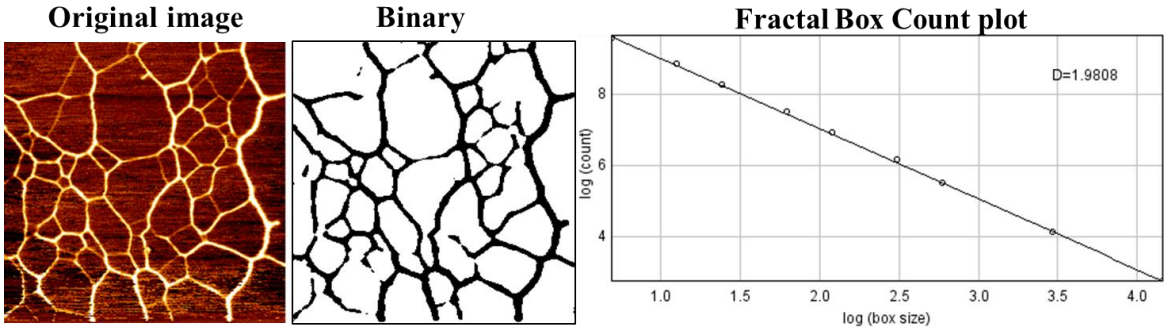

Figure 2.1 Image processing in order to prepare the image for the fractalboxcounting.

2. 9 Cell Culture

COL4A2^{G702D} primary dermal fibroblast cell cultures from an affected patient were established from skin biopsies collected from the upper inner arm. This was performed by the Medical Genetics Department of the Hopital Erasme at the Université Libre de Bruxelles (Belgium). For control cells, age, sex, and ethnicity matched cells were purchased from Tissue Culture Solutions Cell Works (UK). Cells were cultured in DMEM supplemented with 1% Glutamax (Invitrogen™), 1% penicillin and streptomycin solution (Gibco®) (final concentrations of 100 µg/mL), and 10% FBS (Invitrogen™) and kept in an incubator at 37ºC with 5% CO_2. L-ascorbic acid 2-phosphate sesquimagnesium salt hydrate (0.25 mM; Sigma) was administered for 72h to standardise collagen expression and post-translational modifications.

Cell counting, preservation and thawing. Cells were counted using a haemocytometer and preserved in freezing media (10% DMSO, 45% DMEM and 45% FBS) at 2x10^6 cells/mL in cryovials and placed in isopropanol chambers containers (Mr. Frosty™, Thermo Scientific)

and placed in -80º C freezer overnight for 24h, then transferred to liquid nitrogen for long-term storage. To defrost, frozen vial of cells was placed in 37ºC water bath for ~1 min until completely thawed then contents transferred to pre-warmed media into flask and cells incubated at 37ºC with 5% CO_2.

2. 10 Cell proliferation analysis

To measure the proliferation rates of cell cultures, cells were seeded at 5,000 cells/cm^2 density on glass and PEA and PMA (sterilised under UV for 20 min into 24 well plates) coated for 1h with 20 μg/mL FN and left to adhere for 24h, 3 and 7 days. DMEM was changed after every 2 days to discard non-adherent cells. For each time point, adherent cells were washed and fixed with 3.7% PFA for 20 min at 4°C. Cells were stained with DAPI and nucleus of each sample were counted using or ImageJ (1.47v) and then averaged for each time point.

2. 11 Cell attachment assay

This was done according to the protocol by Humphries (Humphries 2009). UV-sterilized glass, PEA and PMA samples were coated with Col IV 50 μg/mL, FN 20 μg/mL or LM 20 μg/mL for 1h and washed twice with DPBS. Samples were then blocked with heat-denatured BSA 1% w/v (Roche, Basel, Switzerland) for 30 min at RT. During this period, cells were harvested, trypsinized, and re-suspended in complete medium (containing 10% FBS). The cells suspension was then incubated for 10 min at 37°C. Cells were seeded onto the surfaces at a seeding density of 8.5×10^4 cells/cm^2 for 20 min at 37°C. Surfaces were washed twice with DPBS to remove cells that were not firmly attached, fixed with PFA 3.7% for 20 min at 4°C, and washed again. Samples mounted with vectashield with DAPI to stain the nuclei. Images were taken using an inverted epifluorescence microscope (Zeiss AXIO Observer Z1) and the number of cells attached was determined using CellC total cell count analysis (Selinummi et al. 2005) or ImageJ (1.47v).

2. 12 Early Adhesion Assay

Cells were seeded at 5,000 cells/cm^2 density on the substrates (sterilised under UV for 20 min in 24 well plate) coated for 1h with either 50, 100 μg/mL Col4, or 2, 20 μg/mL FN, or 2, 20, 50, 100 μg/mL LM. Samples were fixed with 3.7% PFA for 20 min at 4°C after incubation for 3h without FBS, permeabilised for 5 min using a Triton X-100 based

permeabilisation buffer (0.5% v/v Triton X-100, 10.3 w/v% saccharose, 0.292% w/v NaCl, 0.06% w/v MgCl2, and 0.476%w/v HEPES adjusted to pH 7.2), and blocked with 1% v/v DPBS/BSA for 30 min. Then samples were stained for 1h at room temperature (RT) with primary antibodies against mouse vinculin hVIN-1 1:400 (Sigma-Aldrich, St. Louis, MO) or polyclonal rabbit paxillin 1:400 (Thermo Fisher Scientific, Waltham, MA) in BB, which stains the focal adhesions. Afterwards, the samples were washed 3 times with DPBS/tween20 0.5% w/v, then incubated for a further 1h in the dark at RT with a Cy™3 AffiniPure anti-mouse secondary antibody or Chicken anti-rabbit Alexa Fluor 647 (Thermo Fisher Scientific) (in BB), coupled with BODIPY FL phallacidin 1;100 (Invitrogen B607) which stains for actin filament.

Finally, the coverslips were washed three times with DPBS then mounted on microscopy slides using VECTASHIELD® Mounting Medium H-1000 (Vector Laboratories), and sealed underneath with clean nail varnish. Slides were kept in the dark, analysed within 24h, and stored at 4°C when not in use. Samples were visualized using an epifluorescence microscope. Images were taken and channels merged using ImageJ (1.47v) to localize nuclei, actin, and focal adhesions. The latter were quantified using the focal adhesion analysis server (Berginski and Gomez 2013). Data such as focal adhesion size, count, area and cell size, were obtained from the server.

For integrin staining, primary antibodies rat anti-mouse CD29 integrin β_1 (BD Biosciences) and human integrin alpha V/CD51 antibody (R&D systems) were used combined with secondary antibodies chicken anti-rat Alexa Fluor 488 and donkey anti-goat Alexa Fluor 568 respectively. These were also combined to Alexa Fluor® 350 Phalloidin for actin staining (Thermo Fisher Scientific).

2. 13 Cell adhesion strength measurements

Cell adhesion strength to adsorbed FN on the polymer surfaces was measured using a spinning disk device, in other term, a cell detachment apparatus (CDA) (Garcia et al. 1998, García et al. 1997). This assay was carried out at Georgia Institute of Technology, Atlanta, Georgia, USA; under the supervision of Prof Andrés J. García. Substrates were incubated with 2, or 20 μg/mL human FN for 30 min at RT and then incubated with 1% BSA for 30 min at RT. 10,000 cells/cm^2 were seeded onto 25 mm substrates and allowed to uniformly attach for several hours (as indicated in legends) in media with/without serum in the incubator. Then, some substrates were treated with 10 μM blebbistatin (B0560- Sigma-

Aldrich) (inhibitor of myosin II) or 10 µM ROCK (Y-27632 dihydrochloride-Sigma-Y0503 Aldrich) inhibitor; finally, adherent cells were mounted on the spinning disk device. The experiment was performed with over eight coverslips per condition and repeated at least twice.

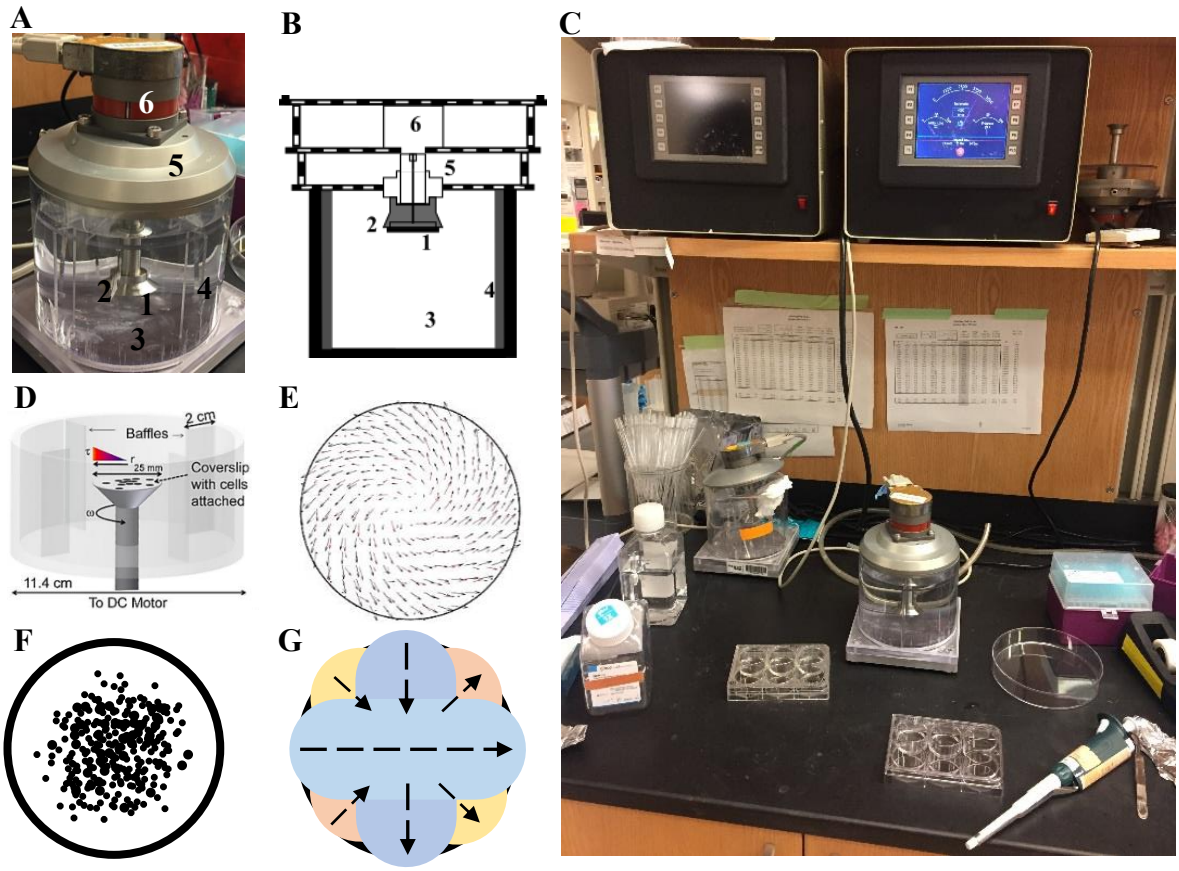

Figure 2.2 Spinning disk device. A) Image of an assembled cell detachment apparatus **(CDA). B)** Cross-sectional drawing of the device. 1, bioactive material sample; 2, spinning disk; 3, fluid chamber; 4, side baffle; 5, sleeves; 6, d.c. motor. **C)** Full spinning disk with the monitors. **D)** Schematic of spinning disk assay. **E)** Shear orientation. **F)** Schematic view of stained cells (with ethidium homodimer) after spinning. G) Schematic representation of cell counting by an automated microscope.

The CDA consists of a fluid-filled poly(methyl metbacrylate) (PMMA) cylinder in which a poly(tetrafluoroethylene) (PTFE) disc containing the sample substrate spins, (sample 25 mm diameter disc) (Figure 2.2A). The disc is driven by a d.c. motor (Figure 2.2B-D) and the speed of the spinning disc is controlled by an optical sensor connected to a tachometer (Figure 2.2C). The machine applies a linear range of forces to adherent cells (Figure 2.2D-E). The chamber apparatus is filled with DPBS with 2 mM glucose, and disk was spun for 5 min at constant speed with controlled acceleration rates at RT. After spinning, cells were immediately fixed in 3.7% PFA, permeabilised with 1% Triton X-100, and stained with ethidium homodimer (Molecular Probes, Eugene, OR, USA), a DNA-specific fluorescent

probe. Cells were counted automatically at specific radial positions using a Nikon TE300 equipped with a Ludl motorized stage, Spot-RT camera, and Image-Pro analysis system, at ×10 magnification.

Sixty-one fields (80-100 cells/field before spinning) were analysed and cell counts were normalized to the number of cells present at the centre of the disk, where negligible force is applied (Figure 2.2G). Using a non-linear computer algorithm, the fraction of adherent cells (f) was calculated by dividing the number of cells in each field by the number of cells at the centre of the array, where negligible forces are applied. The detachment profile (f versus τ) was then fit to a sigmoid curve $f = 1/(1 + \exp[b(\tau - \tau 50)])$, where τ is the surface shear stress, τ_{50} is the inflection point (shear stress for 50% detachment or the mean adhesion strength for a population of cells define as the adhesion strength) and b is the inflection slope.

Many assays are widely used to investigate the adhesion strength of cells, amongst others radial flow, hydrodynamic flow, parallel plate, washing, micromanipulation and centrifugation (Garcia and Gallant 2003). The spinning disk has advantages that it high throughout, large linear range of applied forces for each experiment and uniform surface chemical properties. A significant feature of the CDA is the application of detachment forces under constant and uniform surface chemical conditions. This system applies a well-defined range of hydrodynamic forces to adherent cells and provides sensitive measurements of adhesion strength. Factors taken in account for steady laminar flow: the velocity, temperature and concentration boundary layer thicknesses, must be constant for a given rotational speed and independent of radial distance. The resultant shear stress (τ) at the surface varies linearly with radial distance and is given by: $\boldsymbol{\tau = 0.8\, r\, (\rho\mu\omega 3)^{1/2}}$. τ is the radial distance from the centre of the disc, ρ and μ are the fluid density and viscosity, respectively, and ω is the angular velocity of the disc (rotational speed). For this configuration, cells at the centre of the sample experience negligible force, whereas cell numbers decrease toward the outside of the disk as the applied force increases.

2. 14 Extracellular matrix analysis

2. 14. 1 Immunofluorescence to quantification secretes matrix

Cells were seeded at 5,000 cells/cm^2 onto PEA and PMA coated for 1h with either Col4 (50 μg/mL) or FN (20 μg/mL) or LM (20 μg/mL) and incubated for 2h in serum-free medium condition at 37°C, 5% CO_2 after which the medium were replaced with medium with 10% FBS considering the importance of serum proteins for the reorganization process (loosening

the protein to substratum interaction (Altankov et al. 2010)). Samples were then fixed at different time points, 2h, 1, 3 and 7 days with 3.7% PFA at 4°C for 20 min and permeabilised for 5 min, blocked with DPBS/BSA 1% for 30 min.

The ability of cells to secrete and deposit the ECM Col IV, FN and LM was examined via immunofluorescence staining. For that, samples were stained with either primary monoclonal mouse anti-Collagen 4α2(IV) 1:300 (Milllipore, Cat. No. MAB1910) and polyclonal rabbit anti-LM 1:200 (Sigma, Cat. No. L9393) or polyclonal rabbit anti-FN 1:400 antibodies in BB for 1h at RT, washed 3x DPBS-/- /tween20 0.5% v/v, then incubated for 1h with secondary Cy™3 AffiniPure goat anti-rabbit (Cat. No. 111-165-003) or goat anti-mouse IgG 1:200 (Cat. No. 115-165-062) (Jackson ImmunoResearch Laboratories inc) or Alexa Fluor 488 1:200 (Jackson ImmunoResearch Laboratories inc). If the primary antibodies were not co-stained, the secondary antibodies were coupled with actin filament staining BODIPY FL Phallacidin 1:100 (Invitrogen) or Rhodamine-Phalloidin 1:100 (Life Technologies). The samples were washed 3X then mounted with Vectashield with DAPI to stain the nuclei and visualized using an epifluorescence microscope. Images were taken and channels merged using ImageJ (1.47v) to localize FN, Col4, LM, nuclei, and actin. ImageJ was also used to calculate the total amount of secreted matrix using the fluorescence integrated intensity (Berthod et al. 2006, Prewitz et al. 2015).

2. 14. 2 ELISA assay for secreted collagen

The levels/concentrations of secreted extracellular collagen 4α2(IV) was measured in an indirect ELISA using an ELISA kit in accordance with the manufacturer's instruction. 5,000 cells/cm^2 were seeded on 20 µg/mL FN substrates and were maintained in media with FBS for 7 days. Samples were washed and treated with 20 mM ammonium hydroxide to decellularize and get intact ECMs on the surfaces. Then all the samples were blocked with 1% DPBS/BSA for 30 min and incubated with primary monoclonal mouse anti-collagen 4α2(IV) diluted 1:200 in BB for 1h. Triplicate samples were washed with washing buffer then incubated for 1h at RT with HRP conjugated goat anti-mouse antibody diluted 1:10000 in BB. Colour was developed by the addition of the substrate solution (1:1 mix of H_2O_2 and tetramethylbenzydine) following a 20-min incubation at RT. At the end of the time, 1/2 volume of stop solution (H_2SO_4 2N) was added. Plates were then read in a Microspectrophotometer, Tecan NanoQuant Infinite M200 Pro plate reader (Männedorf, Switzerland) and the fluorescence were measured at 450 nm and 540 nm. All reagents were provided in the kit.

2. 14. 3 In-cell Western assay

Cells were cultured as above for 7 days, then fixed with 3.7% PFA and then permeabilised with 0.1% Triton X-100 for 5 min, blocked with DPBS/BSA 1% for 30 min for 2h followed by 3 × 10-min washing with 0.1% PBS/Tween 20. Cells were then incubated with primary monoclonal mouse anti-Collagen 4α2(IV) at 1:200 dilution in blocking buffer at RT for 1.5h. After 3 × 5-min washing with 0.1% PBST buffer, cells were incubated with 1:5000 diluted infrared-labelled secondary antibody IRDye 800CW (LI-COR, 926-32211) and 1:2000 diluted CellTag 700 Stain (LI-COR, 926-41090) at RT for 1h, followed by 5 × 5-min washing with 0.1% PBST. Substrates were then dried on white paper for infrared signal reading using an Odyssey infrared imaging system.

2. 14. 4 Passaging of mutant cells from FN-coated interfaces to glass

Cells were cultured on glass and PEA, PMA coated with FN 20 μg/mL for 7 days and then trypsinized, re-suspended in medium with FBS and seeded onto the glass. Samples were then incubated for a further 7 days. Then, samples were fixed in 3.7% PFA and processed for indirect immunofluorescence. Primary mouse anti-Collagen 4α2(IV) antibody and polyclonal rabbit anti-laminin antibody were used coupled with corresponding secondary antibodies, and processed as in section 2. 14. 1.

2. 14. 5 ER stress analysis in primary dermal fibroblasts

To study the cellular effect of Col4a2 accumulation in mutant fibroblasts, cells were processed as previously described in section 2. 14. 1. Samples were co-stained with primary monoclonal mouse anti-Collagen 4α2(IV) and polyclonal Rabbit Anti-PDI 1:100 (Stressgen) antibodies in BB for 1h at RT; then incubated for 1h with secondary Cy™3 AffiniPure goat anti-rabbit 1:100 (Jackson ImmunoResearch Laboratories inc) and Alexa Fluor 488 anti-mouse 1:100 (abcam). The samples were washed 3X DPBS+/+ /tween20 0.5% then mounted with Vectashield containing DAPI to stain the nuclei and visualized using an epifluorescence microscope. Images were taken and channels merged using ImageJ (1.47v).

2. 15 ERK1/2 phosphorylation

Levels of phosphorylation of ERK1/2 in cells seeded onto FN coated surfaces were assessed after 30 min incubation using DuoSet ELISA kit following manufacturer's instructions (DuoSetDYC1018B, R&D Systems).

2. 16 Matrix reorganisation and formation

The ability of cells to reorganise previously adsorbed ECMs was monitored by seeding 5,000 cells/cm^2 on substrates coated with Col IV 50 µg/mL, FN 20 µg/mL or LM 20 µg/mL in serum free-medium for 2h before incubation for 3 h, 1, and 3 days in serum containing medium and fixing with 3.7% PFA. Samples were stained with a polyclonal rabbit anti-LM antibody, or polyclonal rabbit anti-FN or monoclonal mouse anti-Collagen 4α2(IV) primary antibodies dissolved in 1% BSA/DPBS for 1 h, washed, and incubated with a Cy™3 AffiniPure goat anti-rabbit or mouse IgG secondary antibody for 1h coupled with actin filament staining Rhodamine-Phalloidin 1:100 before washing and mounting with Vectashield containing DAPI and visualising using an epifluorescence microscope.

2. 17 Protein quantification by Western blot

Cell scraping and protein extraction. Protein was extracted using 30 µl of radio-immunoprecipitation assay (RIPA) buffer (Table 2.3) containing 1x EDTA free protease (Roche) and 1x phosphatase inhibitors (Roche). Cells on ice were scraped using cell scrapers (Falcon®). Samples were centrifuged at 14,000 rpm and the supernatant stored at -20°C.

BCA assay. To quantification protein concentration, the BCA assay (Sigma Aldrich) was used as per manufacturer's instructions. BSA standards were made ranging from 0.1 µg to 2 µg per 50 µl dH2O. All standards and samples were analysed in triplicate in EIA/RIA 96 Well Plates (Costar®) and the colorimetric changes were analysed on the Anthos 2010 machine (at 595 nm wavelength) using ADAP plate reader software as per manufacturer's instructions. Protein levels were corrected for using zinc stain of sample gel to assess total protein in each lane of the gel and band intensity was measured using ImageJ software analysis.

SDS-PAGE Electrophoresis. Sodium dodecyl sulphate polyacrylamide gel electrophoresis (SDS-PAGE) was used to separate proteins. The SDS-PAGE gel compositions are described in (Table 2.1). All the SDS-PAGE gels were placed in a Mini PROTEAN® Tetra Cell (BIORAD) tank, and submerged in running buffer (Table 2.3) and ran at a constant voltage of 80V until the protein samples reached the bottom of the gel (~2h) or until sufficient size

separation for protein of interest had been achieved. Blots were transferred for 60 min at 350mA constant Amps.

	Composition
6%	8.65mL dH20 2.25mL 40% Acrylamide 3.8mL 1.5M Tris 150µL 10% SDS 150µL 10% Ammonia Persulphate 12µL TEMED
10%	4.8mL dH20 2.5mL 40% Acrylamide 2.5mL 1.5M Tris 100µL 10% SDS 100µL 10% Ammonia Persulphate 4µL TEMED

Table 2.1 Polyacrylamide separating gel composition

	Composition
Top gel	3.65mL dH20 760µL 40% Acrylamide 760µL 1M Tris 50µL 10% SDS 50µL 10% Ammonia Persulphate 5µL TEMED

Table 2.2 Polyacrylamide stacking gel composition

Coomassie protein loading control sample preparation. In order to obtain a protein-loading control, SDS-PAGE coomassie stained gels were used. To prepare for protein samples ranging from 5-15 µg, 4 x NuPAGELaemmli Buffer (LDS) (Invitrogen™) (v/v) and DTT (to a 0.1 mM final concentration) (v/v) were added, then denatured at 95°C for five min and kept on ice until they were loaded into the gel. 1 µl BenchMark™ ladder (Invitrogen™) was included as a size marker.

Fixing and staining the Coomassie gel. SDS-PAGE coomassie gels were fixed for 1-12 hours by mild agitation in fixing solution (Buffer conditions (Table 2.3). Protein in the gel was stained for 1-2 hours by mild agitation in staining solution (Table 2.3), then de-stained by multiple 10-min washes with mild agitation in destain solution (Table 2.3) until the stained protein bands were clear and background staining was minimal. Gels were photographed on a light box using Canon EOS Digital Rebel camera.

Western blot protein preparation. To obtain protein samples for western blot analysis ranging from 10-50 µg, samples were all prepared by adding 4 x NuPAGE LDS (Invitrogen) (v/v). DTT (v/v) was also added (to a 0.1 mM final concentration) to reduce protein samples if required. The proteins were denatured by incubation at 95°C for five min, and stored on ice, while non-denatured proteins were just stored on ice. 15 µl of Novex® Sharp Standard (Invitrogen™) or Spectra Multicolor Broad Range Protein Ladder (Thermo Scientific) were used for size reference.

Wet transfer. Gels were incubated in western transfer buffer (WTB) for 15 min. PVDF membranes were washed in 100% methanol for one min, dH20 for 5 min, and WTB for three min to hydrate it. The membranes were sandwiched with the gel, sponge and blotting paper; the cassette was placed in the Mighty Small Transphor (Amersham Biosciences) transfer tank filled with WTB. 400 mA were passed through the stack for 2h.

Semi-dry transfer. Gels were incubated in semi-dry WTB (Table 2.3) for 15 min. Immobilon® PVDF transfer membrane (Millipore) was washed in 100% methanol for one min, dH20 for five min, and semi-dry WTB for 3 min to hydrate. Thick blotting paper (Bio-Rad) were soaked in semi-dry WTB and stacked together on the transfer machine base (Fisher V20-SDB, SCIE-PLAS) and compressed to remove air bubbles. The hydrated PVDF membrane was added to the stack and the gel was positioned on top of the membrane. 0.8 mA/cm^2 was passed through the stack for 2h.

Blocking, antibody incubations and development. After protein transfer, membranes were blocked with 5% milk (Marvel) diluted into TBST buffer (m/v) (Table 2.3) for 1h at RT. Membranes were incubated with the primary antibodies diluted in 5% milk on a rocking platform or roller machine overnight at 4°C. Membranes were then washed 3X with TBS-T (0.1%) for 10 mins before addition of the secondaries. Blots were washed before licor development in a dark room for a range of times depending on signal strength to obtain the correct level of exposure using the Min-R Mammography Processor (Kodak).

- For BIP and Calnexin blots were probed using primary antibodies mouse monoclonal anti-BIP (1/40000, BD Transduction) or rabbit polyclonal anti-Calnexin (1 in 1000, Cell Signalling), secondaries were anti-mouse (1/15000) or anti-rabbit (1/15000) antibodies conjugated to fluorescent molecules diluted in 50% TBS-T (0.1%) and 50% Seablock with 0.01% SDS and incubated for 1h at RT.
- For FAK and phospho-FAK, the polyclonal mouse anti FAK (Upstate), diluted 1:2500 and polyclonal rabbit anti p-FAK (Tyr 397) (Merck Millipore) diluted 1:500 in 2% BSA-TBST were used coupled to HRP-linked donkey monoclonal anti-mouse and rabbit antibody (GE Healthcare) diluted 1:10000 in 2% BSA-TBST as secondaries for chemiluminiscent detection.
- For DDR1 activity, the primary DDR1 (C-20, sc-532, dilution 1:100) antibody was used coupled with a secondary HRP antibody.

Densitometry analysis of Western blot, coomassie gels. Densitometry was carried out using ImageJ (National Institutes of Health (NIH)) software. Images were converted to grey scale, and the band of interest was selected; ensuring the entire band was included. ImageJ removed background so only true signal was converted to a numeric representation of the band density. The selected protein bands were corrected for loading differences using a densitometry analysis of a comparative coomassie or a Memcode™ treated membrane. For the total protein gel, Pierce™ Zinc Reversible Stain Kit was used.

Buffer	**Composition**
Quick Lysis (QL) Buffer pH 8.5	0.5M Tris base, 6M EDTA 0.2% SDS 1M NaCl
RIPA Buffer	0.05M Tris base 0.15M Sodium chloride 0.1% SDS 0.01M Sodium deoxycholate 1% Triton X 100 2 PhosSTOP Phosphatase Inhibitor Cocktail Tablets (Roche)

	2 Pierce™ Protease Inhibitor Mini Tablets (Thermo Scientific).
Western Blot Running buffer (10x)	0.25M Tris base 2.5M Glycine 0.5% SDS
Western Wet transfer Buffer (wet WTB)	0.06M Tris base 0.45M Glycine 20% Methanol
Western semi-dry transfer buffer (semi dry WTB) (5x)	0.2M Tris base 0.2M Glycine 0.2% SDS Working Solution: 1:1:3 Western Transfer Buffer: Methanol:dH_2O
Blocking buffer	5% milk in TBST
10 x TBS	1.5M Sodium chloride 0.5M Tris base
1X TBS-T	0.15M Sodium chloride 0.05M Tris base 0.2% Tween20
Sample Loading Buffer (LDS 4X)	0.05 M Tris base 10% SDS 40% Glycerol 0.05M Bromophenol blue
TBE buffer (5x)	0.5M Tris base 0.5M Boric acid 0.01 M EDTA
TE buffer pH 5.5	0.1M Tris base 0.004M EDTA
Coomassie blue stain	0.01M Coomassie Brilliant Blue (Bio-Rad) 50% Methanol 10% Glacial acetic acid 40% H2O

Coomassie staining solution	0.1% Coomassie blue 10% Acetic acid 60% Methanol 40% dH2O
Coomassie de-stain solution	10% Acetic acid 30% methanol 60% dH2O

Table 2.3 Buffers

2. 18 Mechanical properties of cells and ECMs by AFM

To study mechanical properties, AFM imaging was performed using a JPK Nanowizard® 3 BioScience (JPK Instruments, Berlin, Germany). All measurements were taken in liquid (DPBS or CO_2 independent media) at 37^{o}C. Images were acquired in contact quantitative imaging (QI) mode at scan frequencies of 1Hz or less using a cantilever (as detailed below) with a resonance frequency ~75 kHz, a spring constant of ~5 N/m, and a tip radius below 10 nm. The AFM images were 256 × 256 pixels unless specified. Force spectroscopy curves were obtained, after calibration of tip sensitivity and spring constant, with a set-point of 5 nN, a zeta length of up to 5 μm, a constant duration of 1 s and at RT. Analysis were performed using the JPK data processing software (v4.3.21), and force curves were fitted with a Hertz model at 500 nm indentation to obtain the elastic/Young's modulus; more details are found in section AFM as a tool for elasticity measurements in Appendix II. Height, phase and amplitude magnitudes were recorded simultaneously for each image.

Cells were cultured on FN-interfaces for 7 days after which part of the samples were used for AFM nanoindentation on cells. Stiffness of cells was acquired using a tipless cantilever (Arrow TL1, k = 0.03 N/m, NanoWorld, Neuchâtel, Switzerland) mounted with a silica 4.83 μm sphere bead (previously incubated in 1% BSA for 30 min). The other part of the samples was used to measure the stiffness of ECMs secreted by the cells on the surfaces. To do so, the samples were decellularised to obtain intact matrix deposited by cells by treatment with 20 mM ammonium hydroxide (NH_4OH) 0,5% (w/v) in warm water (Robinson and Gospodarowicz 1984) until all the cells debris could not be seen to remove all cellular material except the insoluble ECMs. The ECMs were immunostained for the different proteins in order to observe the structure. The samples were also stained with DAPI to

confirm whether the procedure was successful. The ECMs were then scanned using a pyramidal cantilever (PNP-DB-20, k = 0.42 N/m, NanoWorld, Neuchâtel, Switzerland).

2. 19 Microscopic analysis of tissues

Col4α1 mutation was identified in SVC mice by (Van Agtmael et al. 2005). SVC mice were inviable homozygotes, henceforth, all animal tissues that were used in this study were heterogygous. Control animals were WT littermates, not C57Bl/6. Murine tissues were collected by Dr Tom Van Agtmael and Dr Frances Jones at The Central Research Facility at the University of Glasgow and stored at -80°C. Sections were cut from O.C.T. blocks to 15-µm thickness using a Leica cryostat machine at -15°C. Cryosections were fixed for 10 min in acetone at RT followed by antigen retrieval using 0.1 M HCl/KCl solution in PBS (v/v) for 10 min at RT; and then by 3 x 5 min PBS washes. After blocking in PBS containing 10% FBS for 1h, sections were incubated with primary monoclonal mouse anti-Collagen 4α2(IV) 1:300 (Milllipore, Cat. No. MAB1910) and polyclonal rabbit anti-LM 1:200 (Sigma, Cat. No. L9393) diluted in 10% FCS at 4°C overnight to visualise the BM structure. Then, samples were washed and incubated with fluorescently conjugated secondary antibodies for 1h at room temperature (JacksonLaboratories). Finally, the samples were washed 3 times then mounted with Vectashield with DAPI before visualizing using an LSM 510 confocal microscope (Zeiss) using a fixed exposure time.

2. 20 Statistical analysis

All images were analysed using ImageJ software (v1.48). The data were statistically analysed using GraphPad Prism 6 (GraphPad software, La Jolla, CA). Where relevant, one-way or Two-way ANOVA tests were performed using a Bonferroni post hoc test to compare all columns, and the differences between groups were considered significant for *$p \leq 0.05$, **$p \leq 0.01$, ***$p \leq 0.001$, and ****$p \leq 0.0001$. All error bars were standard deviation. Note that not all comparisons that are statistically significant are shown in the main text, only ones that apply to the hypothesis, differences between the WT and the MT cells on the different substrates. A complete list of significant differences for figures with multiple comparisons is shown in Appendix I.

Chapter 3

Characterisations of the Biointerfaces

Contents

3. 1 Introduction

It is of fundamental importance to understand the nature of the surface on which cells are grown in order to provide them with a reliable and robust microenvironment. Understanding and controlling the interaction of cells with synthetic materials is of great importance for regenerative medicine and biological research in general (Sipe 2002). Yet, it is established that cells do not directly interact with the material surface on which they are growing, but that their interaction depends a layer of extracellular matrix (ECM) proteins previously adsorbed onto the material for anchorage (Grinnell F. 1986, Pompe et al. 2004, Salmerón-Sánchez and Altankov 2010, Sipe 2002). This layer of ECMs, such as collagen type IV (Col4), fibronectin (FN), fibrinogen, laminin (LM) and vitronectin (VN) may come from physiological fluids *in vivo* (soluble matrix proteins of the blood) or culture medium *in vitro*. Alternatively, current biomaterials functionalisation strategies involve covalent binding and presentation of protein or adhesion peptides to enhance cell adhesion.

The composition of this adsorbed protein layer is a key mediator of cell behaviour, (García 2006, Pompe et al. 2004, Rico et al. 2014, Salmerón-Sánchez and Altankov 2010). The concentration and distribution of adsorbed ECM proteins play an important role in the biofunctionality of a synthetic material and in the understanding of the biological response to the substrates. *In vitro*, upon adsorption on substrates, ECM proteins rearrange at the cell–material interface and this is a significant phenomenon that must be considered in the design of advanced biomaterials for tissue engineering (Llopis-Hernández et al. 2013). This aspect, i.e. the behaviour of the main components of the ECMs, namely Col4, FN and LM, upon adsorption on polymeric substrates, is examined in this chapter.

As outlined in Chapter 1, ECM proteins can adopt different morphologies depending on the substrate surface onto which they are adsorbed. Specifically, the adsorption of proteins on material surfaces is a process driven both by entropy (the release of bound water molecules of the protein as it unfolds to adsorb on the surface means a significant entropy increase) and by energy (several noncovalent interactions between the molecular groups of the substrate's surface and of the protein, such as hydrogen-bonding, electrostatic, or van der Waals interactions). Both of these mechanisms eventually determine the amount and the conformation of the adsorbed proteins, (García 2006).

In this study, we have used two poly(acrylates), PEA and PMA, which have been previously employed to modulate FN adsorption and cell response in our group (Llopis-Hernandez et al. 2016, Llopis-Hernández et al. 2013, Salmeron-Sanchez et al. 2011, Vanterpool et al.

2014). They are polymers of similar chemical structure, consisting of a vinyl backbone chain with either $–COOCH_2CH_3$ or $–COOCH_3$ side groups respectively (Figure 3.2). The difference of only one methyl group in the lateral chain yields substrates with similar physicochemical properties (Gonzalez-Garcia et al. 2012). The polymers were synthetized by radical polymerization of ethyl acrylate and methyl acrylate (Sigma, St. Louis, MO), initiated by benzoin at 1 wt%, and solutions in toluene 4% w/v for PEA and 6% w/v for PMA were prepared as described in the material and method section 2. 2. Spin-coated PEA and PMA on 12 mm glass coverslips were smooth (root-mean-square (R_{rms}) < 1 nm) and homogeneous, with a thickness of ~1 μm (Vanterpool et al. 2014). ECM proteins, Col4, FN and LM were adsorbed on these polymers for 1 h at different concentrations (as indicated in the figure captions).

These substrates have been shown to modulate the adsorption, conformation and distribution of coated proteins. For instance, FN adsorbed on PMA adopts a globular conformation, whereas on PEA FN has a network or fibrillar conformation (Llopis-Hernandez et al. 2016, Llopis-Hernández et al. 2013, Salmeron-Sanchez et al. 2011, Vanterpool et al. 2014). Moreover, this difference in protein organisation results in the differential behaviour of cultured mesenchymal stem cells (MSCs) and other cells, such as myoblasts or fibroblasts. On fibrillar FN, MSCs tend to differentiate to osteoblasts, whereas on globular FN, MSCs are maintained (Gonzalez-Garcia et al. 2012, Llopis-Hernandez et al. 2016). Therefore, these polymer substrates were used in this study.

3. 2 Aims and Objectives

This chapter presents a detailed characterisation of ECMs on PEA and PMA substrate polymers. The aims were to:

- Measure the water contact angle of the interface as the wettability of the material-interface is known to influence cells attachment and adhesion.
- Quantify and analyse the density of adsorbed ECM proteins on the substrate polymers using BCA.
- Employ AFM to follow the nanoscale behaviour of adsorbed Col4 (a unique multifunctional matrix protein involved in the organisation of BMs including vascular ones), of FN (one of the earliest cell-binding proteins of the ECMs) and LM (a self-assembling heterotrimer that initiates the assembly of the BMs).

3. 3 Results and Discussions

3. 3. 1 Wettability

Wettability refers to the tendency of a fluid to spread on, or adhere to, and interact with a solid phase. It is defined by the contact angle of the fluid with the solid phase. Surface wettability by water has long been recognised as an important factor for protein adsorption and cellular interaction. Generally, hydrophilic surfaces support cell adhesion and spreading, usually attributed to the appropriate conformation of adsorbed ECM proteins, (Altankov and Groth 1997, Grinnell Frederick and Feld 1982, Hernández et al. 2007, Kowalczyńska et al. 2005, Rico et al. 2009).

To study how a liquid like water interacts with substrate surfaces coated or non-coated with ECM proteins, water contact angle (WCA) measurements were performed. 3 µl milliQ water drop were used to measure static and dynamic WCAs as detailed in Chapter 2. Contact angle hysteresis, the difference between advancing and receding CAs, can be interpreted as a measure of molecular mobility for flat surfaces with homogeneous chemistry, (Takahashi et al. 1997, Van Damme et al. 1986). In theory, if a liquid (like water) forms a drop with low WCA ($\theta < 90°$), the surface is said to be hydrophilic, otherwise the surface is hydrophobic if the WCA is high ($\theta > 90°$) (Figure 3.1) (Takahashi et al. 1997). However, generally surfaces with WCA > 70° are considered border-line hydrophobic.

The spin-coated surfaces of PEA and PMA used in this study were found to be smooth, with similar (R_{rms}) roughness of ~35 ± 7.5 × 10^1 pm and thickness of 7.5 ± 2.5 × 10^2 nm. Moreover, AFM nanoindentation determined the Young's moduli of both surfaces to be ≥1 MPa, greater than the 40-kPa stiffness threshold that cells can detect (Balaban et al. 2001, Bathawab et al. 2016).

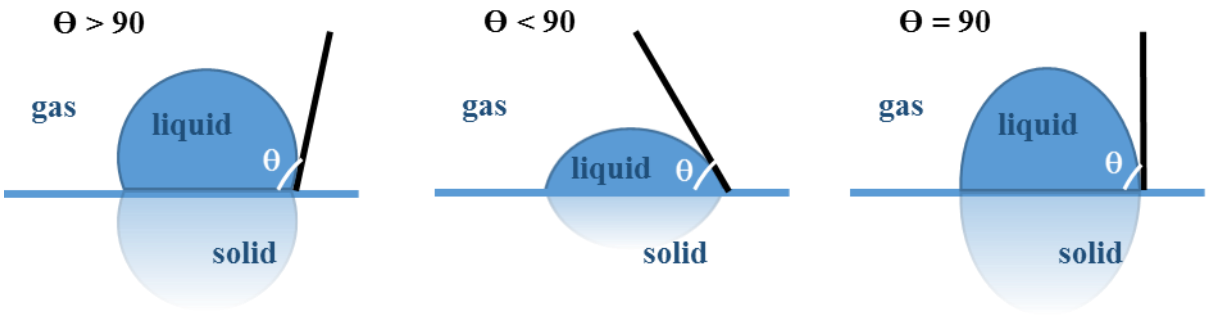

Figure 3.1. Typical states of the liquid droplets on a solid surface. Left image demonstrates a typical hydrophobic surface with a theoretical contact angle over 90°. The middle image shows a hydrophilic surface with a contact angle under 90°. The right image shows a surface with contact angle of 90°.

The data presented in (Figure 3.2A-B) showed static contact angle (SCA) and hysteresis above 70°. The advancing contact angle (ACA) and receding contact angle (RCA) are also shown (Figure 3.2C-D). In addition, after coating with LM solutions of concentrations of 2, 20, 50, and 100 µg/mL, the WCA increased slightly with solution concentration on both polymers, although higher on PEA than PMA, suggesting PEA is more hydrophobic than PMA and might present a different state of the adsorbed protein layer.

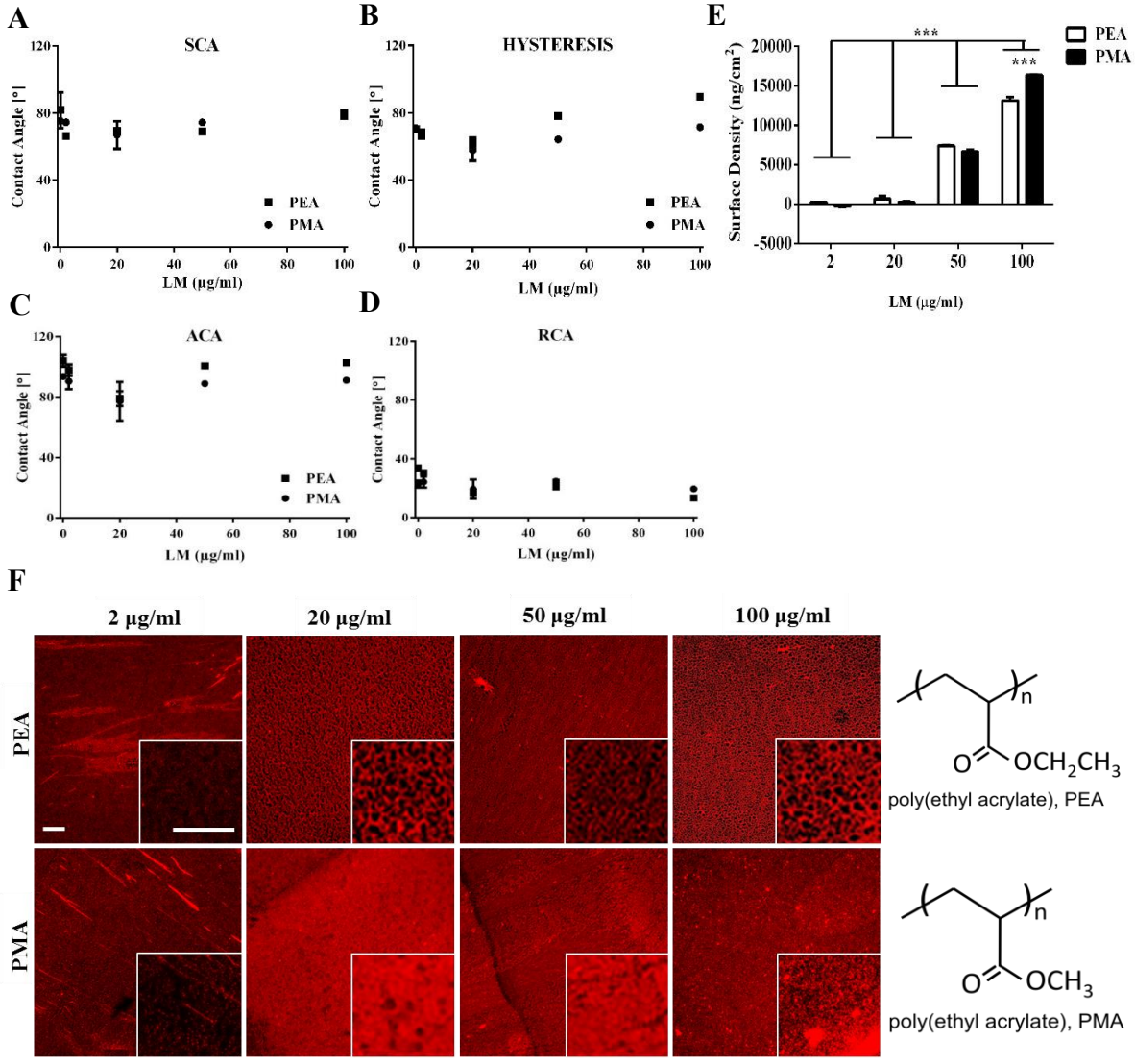

Figure 3.2. Characterization of LM-coated PEA and PMA surfaces. (**A**) SCA, (**B**) hysteresis (difference between advancing and receding contact angles), (**C**) ACA and (**D**) RCA on PEA and PMA coated from solutions with concentrations of 2, 20, 50, and 100 µg/mL LM. Each figure represents an average of 3 samples per experiment; repeated 3 times. (**E**) Surface density of LM on PEA and PMA coated from solutions of 2, 20, 50 and 100 µg/mL of LM. (**F**) Immunostaining of LM after adsorption from a solution concentration of 2, 20, 50 and 100 µg/mL, inset: high magnification images. PEA, poly(ethyl acrylate); PMA, poly(methyl acrylate); LM, laminin; SCA, static contact angle. Data presented as mean ±SD, N =9; and analysed with an ANOVA test; ***p<0.001. Scale bar: 50 µm.

Wettability of PEA and PMA polymers coated with FN solutions of concentrations of 2, 5, 10, and 20 µg/mL is shown (Figure 3.3A-B) and similarly to LM polymer interfaces, FN interfaces behaviour in dynamic contact angles differ on the two polymers. The contact angle hysteresis of FN-coated samples was higher on PEA (e.g., ~ 85º compared to ~ 70º on PMA, for concentrations in the range of 5 µg/mL to 20 µg/mL).

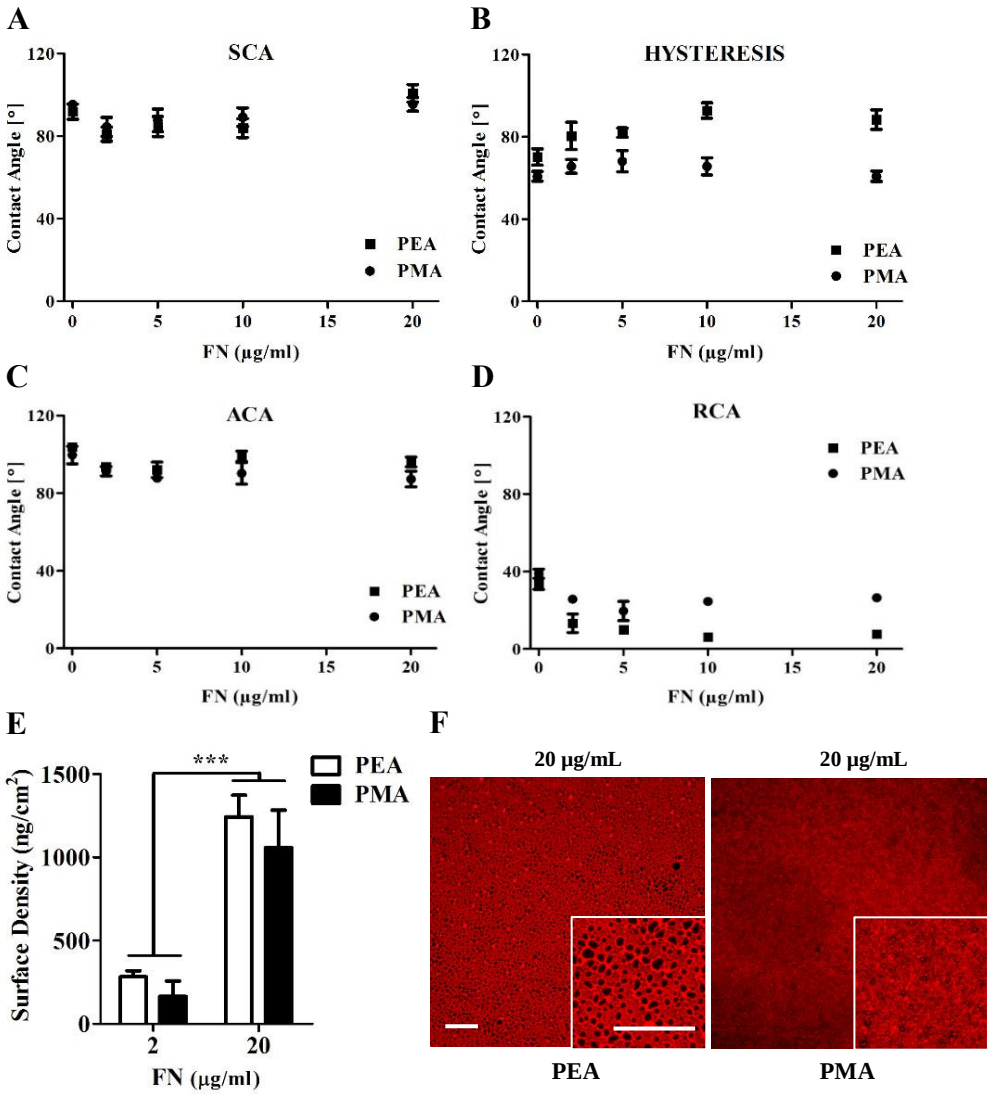

Figure 3.3. Characterization of FN coated PEA and PMA surfaces. (**A**) SCA, (**B**) hysteresis, (**C**) ACA and (**D**) RCA on PEA and PMA coated from solutions with concentrations of 2, 5, 10, and 20 µg/mL FN. Each figure represents an average of 3 samples per experiment; repeated 3 times. (**E**) Surface density of FN on PEA and PMA coated from solutions of 2 and 20 µg/mL of FN. (**F**) Immunostaining of FN after adsorption from a solution of 20 µg/mL, inset: high magnification images. FN, fibronectin. Data presented as mean ±SD, N =9; and analysed with an ANOVA test; ***p<0.001. Scale bar: 50 µm.

Finally, the wettability of the substrates coated with Col4 showed SCA remaining constant ~75^{o}; yet the hysteresis increased with Col4 solution concentrations coating (Figure 3.4A-B). In general, Figure 3.2-4A-B showed that the SCA of both polymers coated with ECM proteins solution concentrations were similar with no significant differences in the WCA suggesting that cells will not ‘‘sense’’ significant differences in wettability upon contact with these interface polymers. On another note, the differences noted for the hysteresis between PEA and PMA suggest a different state of the adsorbed protein.

3. 3. 2 Quantification of adsorbed proteins

Surface chemistry has been demonstrated to modulate proteins adsorption (such as FN) in terms of the total amount adsorption and its conformation on the material surface (Vanterpool et al. 2014). In order to determine the total amount of protein adsorbed on PEA and PMA substrate surfaces, the biochemical assay bicinchoninic acid assay (BCA) was used. ECM proteins LM, FN and Col4 were adsorbed on the substrates and the surface density calculated by measuring the depletion of protein from the coating solutions.

The surface density of LM adsorbed on PEA and PMA substrates increased with solution concentrations of 2, 20, 50, and 100 µg/mL with statistically significant differences, yet remained constant between the substrates, (e.g. ~ 650 ng/cm^2 on PEA and ~ 260 ng/cm^2 on PMA when LM is adsorbed from a 20 µg /mL solution) (Figure 3.2E). The measurements from the 2 µg/mL solution were negative as they were outside the working range of the BCA kit used.

Similarly, FN density increased with solution concentrations of 2 and 20 µg/mL, although remaining constant between surfaces, with no statistically significant differences, approximately 250 ng/cm^2 (PEA) and 150 ng/cm^2 (PMA) for the 2 µg /mL, and 1250 ng/cm^2 (PEA) and 1050 ng/cm^2 (PMA) (Figure 3.3E). In addition, Col4 surface density increased with solution concentrations of 2, 10, 20, and 50 µg/mL with significant differences and remained constant between substrates, 100 ng/cm^2, 1500 ng/cm^2, 3500 ng/cm^2 and 8500 ng/cm^2 for concentration solutions ranging from 2 to 50 µg/mL (Figure 3.4E). In summary, these results showed that the total amount of adsorbed ECM proteins increases with the concentration of the coating solution, as expected; on the other hand, no differences in the surface density were observed between PEA and PMA substrates.

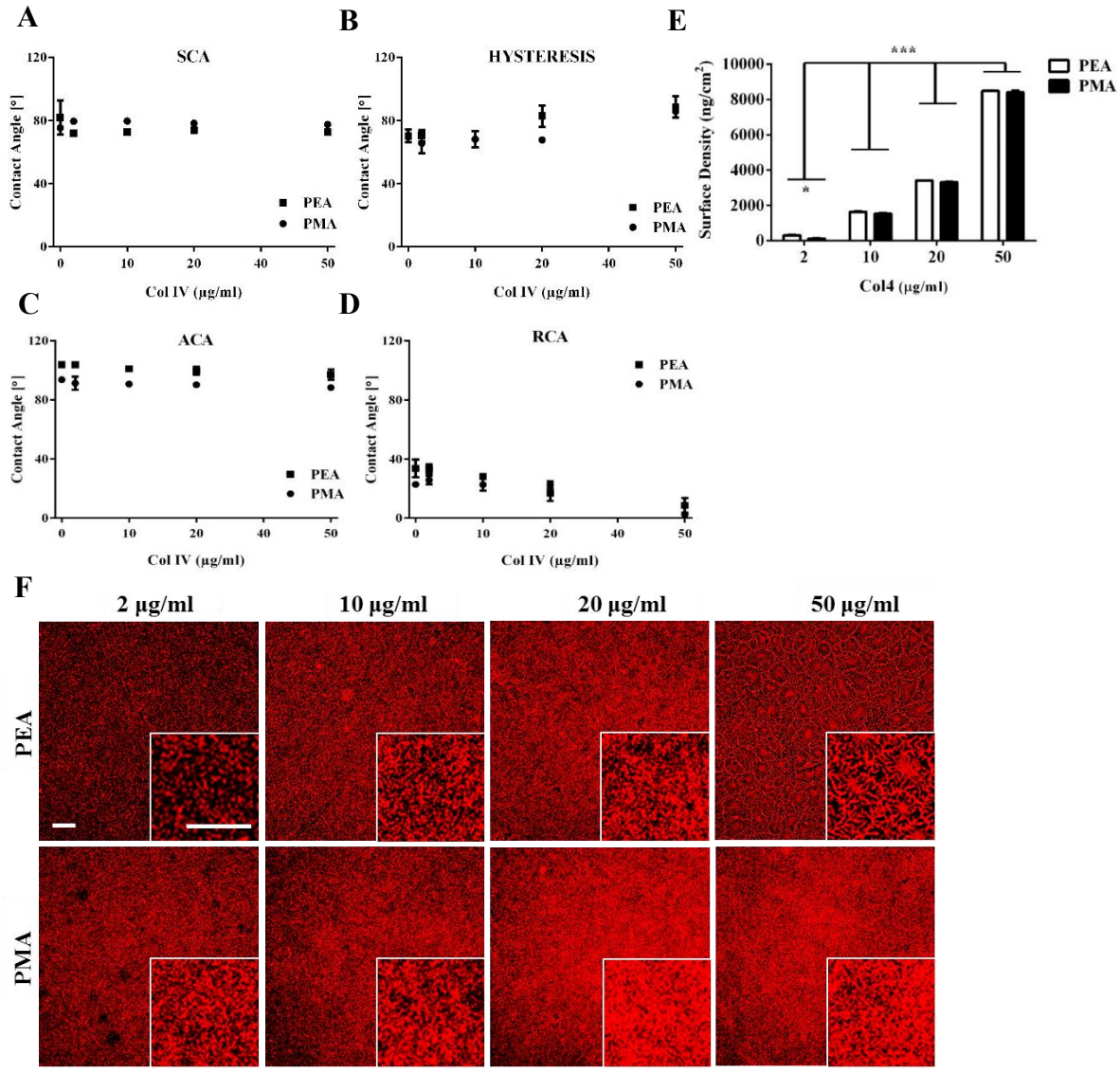

Figure 3.4. Characterization of Col4 coated PEA and PMA surfaces. (**A**) SCA, (**B**) hysteresis, (**C**) ACA and (**D**) RCA on PEA and PMA coated from solutions with concentrations of 2, 10, 20 and 50 µg/mL Col4. Each figure represents an average of 3 samples per experiment; repeated 3 times. (**E**) Surface density of Col4 on PEA and PMA coated from solutions of 2, 10, 20 and 50 µg/mL of Col4. (**F**) Immunostaining of Col4 after adsorption from a solution concentration of 2, 10, 20 and 50 µg/mL, inset: high magnification images. Col4, collagen IV. Data presented as mean ±SD, N =9; and analysed with an ANOVA test; ***p<0.001. Scale bar: 50 µm.

3. 3. 3 Immunostaining

The microscale distribution and structure of the proteins adsorbed on the polymers were assessed via staining (Figure 3.2-4F). LM showed regular network structures on PEA independently of the protein concentration. On the other hand, LM on PMA seemed to form a more uniform layer (Figure 3.2F, top row compared to lower row). FN formed densely

packed networks on PEA, while globular aggregates appeared on PMA (Figure 3.3F) in accordance to previous reports (Vanterpool et al. 2014). Col4 staining displayed a similar structural distribution on both substrates (Figure 3.4F). Although microscale distributions and structures could be observed by immunostaining of the ECM protein components, the network structures were not very clear.

3. 3. 4 Organisation of ECM proteins on substrates

Since immunostaining of the ECM proteins adsorbed on the polymers did not show detailed structures, atomic force microscopy (AFM) was used to analyse the distribution and conformation of the proteins at the nanoscale. The AFM is an exceptional tool to explore the conformation and distribution of matrix proteins at the biomaterial interface. The conformation and distribution of different ECM proteins adsorbed on various substrates have been previously studied using AFM (Cantini 2012, Coelho et al. 2011a, b, Hernández et al. 2007, Hudson et al. 1993, Khoshnoodi et al. 2008, Rodriguez Hernandez et al. 2007, Salmeron-Sanchez et al. 2011, Timpl and Brown 1996).

The current work confirms these studies. For imaging using the AFM, Rico and colleagues have shown that the phase magnitude in tapping mode AFM is a good approach to obtain significant information on protein configuration (Rico et al. 2009). Nonetheless, advances in imaging have proven that AFM height images that are combined with the phase magnitude are even excellent way to present these BM components and obtain significant information on protein configuration (Xu and Siedlecki 2017). AFM images showed Col4, FN and LM at different solution concentrations adsorbed for 10 min or 1h on the polymer substrates (Figure 3.5A-C). AFM imaging revealed clearly the nano-structure and organisation of the adsorbed protein layer compared to the immunofluorescent images, which were limited to microscale details.

Col4 is a network-forming triple helical molecule composed of three alpha chains, which self-assembles by antiparallel interactions and extensive disulphide bounding, as explained in Chapter 1 (Timpl and Brown 1996). Its monomers associate with the C-terminal globular NC1 domains to form dimers or with N-terminals to form tetramers in the BM (Hudson et al. 1993, Khoshnoodi et al. 2008, Timpl and Brown 1996). Col4 molecule structure has been extensively studied over the past decades (Hudson et al. 1993, Khoshnoodi et al. 2008, Timpl et al. 1985) and AFM has been providing significant insight, showing its structures on different surfaces (Chen and Hansma 2000, Coelho et al. 2011b).

Col4 formed similar network structures on both substrates at concentrations of 20 and 50 μg/mL, after 10 min or 1h of adsorption (Figure 3.5A). There seemed to be single molecules arrangement of Col4 formed in dimers observed after adsorption of a solution concentration of 20 μg/mL for 10 min on PEA and not on PMA. Furthermore, globular aggregates also appeared on the substrates (Figure 3.5A, shown by the green arrows). As already mentioned, in the BM, dimers form when two Col4 monomers associate with their C-terminal globular NC1 domains, this is maybe what is observed on PEA with lower Col4 concentration 20 μg/mL, otherwise they form tetramers when associated with their N-terminals, observed at higher concentration 50 μg/mL.

Globular features connected with long arms can be easily distinguished on PEA compared to PMA at time 10 min. These observations have been previously shown after adsorption on mica; typically Col4 forms dimers through intermolecular interactions of two Col4 monomers via the globular NC1 domains, (Chen and Hansma 2000). However, the globular structures disappeared after 1h adsorption time, suggesting an increase in the amount of adsorbed protein and complete saturation after extended adsorption time and distinctly interconnected network structures of tetramers laid on both substrates.

The formation of tetramers via interactions of 7S domains is presumably involved in the formation of these networks. Higher concentration solution of Col4 50 μg/mL showed denser networks and higher interconnectivity than Col4 20 μg/mL especially after 1h adsorption. This is in accordance with the amount of proteins accumulating on the surface after adsorption (Figure 3.4) (Gugutkov et al. 2009, Salmeron-Sanchez et al. 2011). Col4 formed network like structures regardless of concentration solutions on the substrates. This is characteristic for hydrophobic substrata (Coelho et al. 2011b), although higher hydrophobicity of PEA lead to formation of an augmented network structure than on PMA.

The adsorption of FN has been extensively studied on different surfaces (Altankov and Groth 1997, Kowalczyńska et al. 2005, Llopis-Hernandez et al. 2011, Llopis-Hernández et al. 2013, Salmeron-Sanchez et al. 2011, Schwarzbauer and DeSimone 2011, Singh et al. 2010, Vanterpool et al. 2014). It is found in both soluble and insoluble forms in extracellular fluids and connective tissues, respectively and is also a main component of the ECMs. AFM images confirmed structural differences of FN at the nanoscale (Figure 3.5B) showing FN 20 μg/mL distribution on both substrates after adsorption for 1 h. FN was seen unfolded leading to physiological-like interconnected fibrillar nano-networks on PEA, a (nano) network (e.g., material-driven FN fibrillogenesis). Meanwhile PMA promoted completely

different nanostructures: globular conformation; this is in accordance with previous reports (Llopis-Hernandez et al. 2011, Salmeron-Sanchez et al. 2011, Soria et al. 2007, Vanterpool et al. 2014).

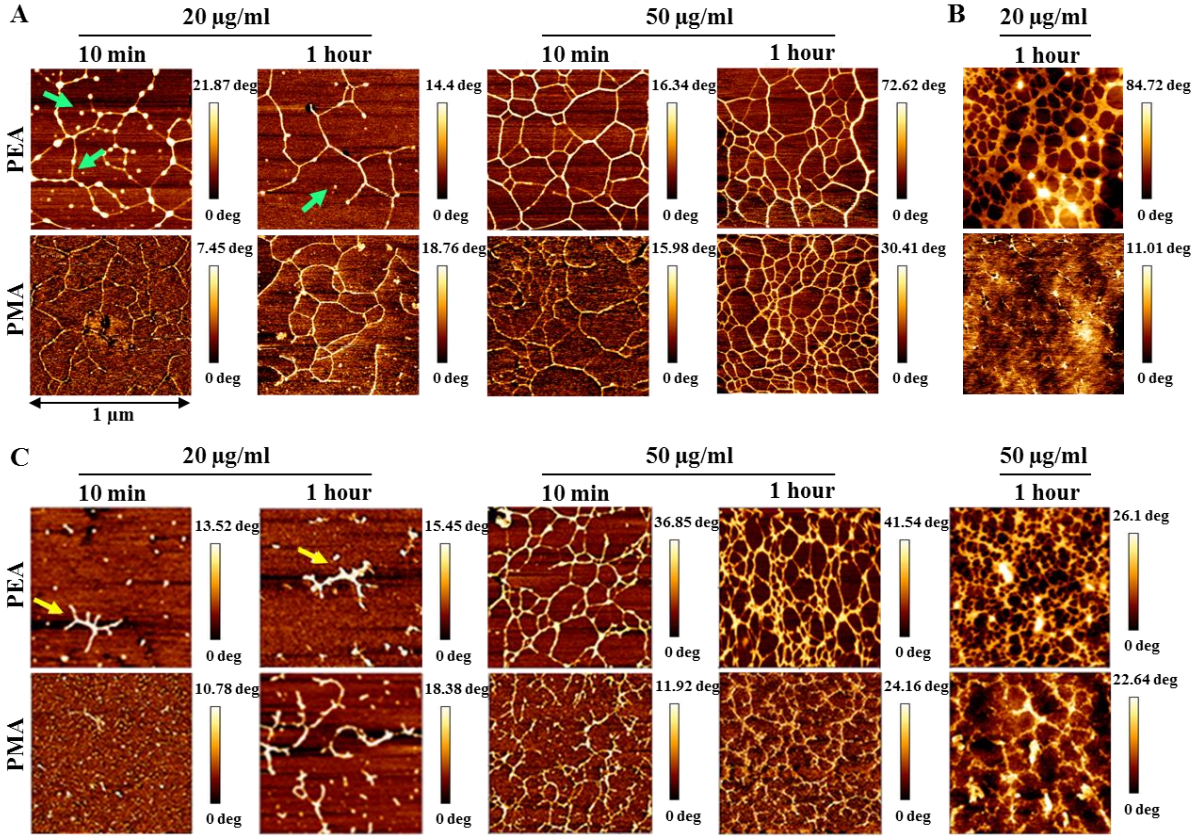

Figure 3.5. AFM images of ECM proteins. A) Col4 (20 and 50 µg/mL), **B)** FN (20 µg/mL), and **C)** LM (2, 20 and 50 µg/mL concentration) distribution after coating on PEA and PMA adsorbed for 10 min and 1 h. Green arrows show protein aggregates; white arrows show cross-shaped molecules of LM (two to five). LM, laminin; Col4, type IV collagen; AFM, atomic force microscopy.

The assembly of the BM is proposed to be initiated by LM. LM is a self-assembling heterotrimer that binds to the cell surface via integrin receptors (Beck et al. 1990, Durbeej 2010, Tzu and Marinkovich 2008). Like other ECM proteins, the structure of LM molecules has been extensively characterised in recent decades employing electron microscopy and AFM (Chen et al. 1998, Coelho et al. 2011b, Hernández et al. 2007). The maximal dimensions of the completely extended cruciform of LM molecule are expected to be 125nm long, 72nm wide, and 2.2nm thick (Chen et al. 1998, Coelho et al. 2011b). In accordance with these values, it was found that LM molecules adsorbed on PEA from lower concentrations (2 µg/mL) for 10 min or 1h appeared as cross-shaped molecules with

approximate size of 90–125nm (depending on their conformation) (Figure 3.5C, yellow arrows).

LM chains are known to combine at the centre of each chain to form cruciform-like structures (cross-shaped), Y shaped (three arms) or rod-shaped (single arm) (Hohenester and Yurchenco 2013, Timpl and Brown 1994, Yurchenco et al. 1992, Yurchenco et al. 1985). The structures on PEA were similar to two to five linked crosses like rods clustered together resulting in lamellar deposits measuring 70-100nm (Hohenester and Yurchenco 2013, Yurchenco et al. 1992, Yurchenco et al. 1985). Some globular-like proteins were also observed deposited on the substrate and little is known to why this happens; however, this has been previously reported by Hernandez and co-workers (Hernández et al. 2007). Coelho and colleagues suggested that this occurrence stresses the importance of the competition between protein–protein versus protein–material interactions to determine the conformation of LM at the material interface (Coelho et al. 2011b).

Similarly, to Col4 and FN, at higher concentration solutions from 20 μg/mL, LM formed network-like nanostructures on both substrates (Figure 3.5C). Densely packed interconnected LM networks appeared on PEA, while truncated branches appeared on PMA. At even higher concentration, 50 μg/mL, more compact protein networks were found on PEA than on PMA. AFM images correlate with both the quantification and the immunostaining.

When compared, Col4 50 μg/mL networks were more comparable to LM 20 μg/mL and to FN 20 μg/mL, and as observed in the immunofluorescence staining and quantification of the protein. The ECM proteins were adsorbed for 1h to see if the distribution would differ, but no significant differences were found for LM and Col4, although the network chains seemed thicker than at time 10 min.

In general, the ECM proteins showed similar distribution at higher concentration solutions for both 10 min and 1h of adsorption. However, these networks varied in their thickness and organisation: they formed more distinct densely packed network structures on PEA than on PMA. The prominent structures on PEA rather than the subtle protein deposition characteristic on PMA could be due to their difference in chemical composition. Nevertheless, the formation of molecular assembly in network structures by these ECM proteins could be attributed to the hydrophobicity of the substrates as reported by Coelho and colleagues on the arrangement of Col4 on substrates with controlled density of –OH groups (Coelho et al. 2011b).

3. 3. 5 Fractal dimension analysis

It has been shown that BM proteins possess a fractal nature (Hochman-Mendez et al. 2014, Zouein et al. 2014). Since the coated proteins on the substrates formed nano-network structures and displayed some fractal properties, analysis of the connectivity information (more precisely, numbers of tunnels and their homological (co)cycle classification) of fractal polyhedral were determined using fractal dimension measurements with ImageJ plugins FracLac) (Smith et al. 1996). Before analysis with the plugins, AFM images were processed as shown in (Figure 2.1). Fractal dimensions of increasing complexities were found with increasing LM concentrations, 20 to 50 µg/mL, while it remained similar for Col4 on both polymers (Figure 3. 6). It should be mentioned that neither LM nor Col4 formed network structures at lower concentrations, 2 µg/mL, therefore the images did not present fractal features from which a fractal dimension could be obtained. Furthermore, FN did not form network on PMA.

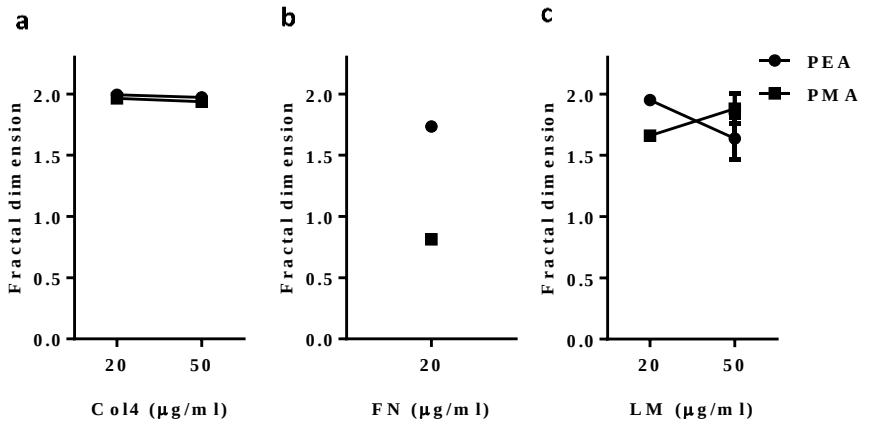

Figure 3.6. Fractal dimension analysis. (**A**) Image processing in order to prepare the image for the fractalboxcounting. (**B**) Calculation of the fractal dimension using ImageJ plugins FracLac for **a**) Col4, **b**) FN **c**) LM, on both polymers at shown concentration for 1h time.

Col4 fractal dimension was similar with no significant differences for both protein concentration (Figure 3.6Ba). Fractal dimension of FN on PEA looked similar to that of Col4 and LM on PEA and PMA (Figure 3.6Bb). Yet its organization on PMA resulted in lower fractal dimension (<1) due to its globular form. Likewise, LM fractal dimension was higher on PEA at 20 µg/mL nonetheless lower at 50 µg/mL, as the network structures lost its defined and clear polymeric-like shape caused by the amount of protein adsorbed. In contrast, the fractal dimension on PMA increased with higher concentrations, showing more interconnected networked then at lower concentrations where the chains showed short truncated branches of LM (Figure 3.6Bc).

3. 4 Conclusions

In this chapter, the surface characteristics of protein-coated material-interfaces have been described. The behaviour of the main components of the ECMs-Col4, -FN and LM-on two synthetic polymers (PEA and PMA) was examined.

The polymer substrates showed similar wettability even after the adsorption with ECM components. The wettability of the material-interface was assessed as it is known to influence cells attachment and adhesion. It showed that the wettability (static angles) of both polymers coated with different ECM proteins solution concentrations were similar with no significant differences in the WCA suggesting that cells will not ‘‘sense’’ significant differences in wettability upon contact with the these biointerfaces. The density of adsorbed ECM proteins on the substrate polymers and their subsequent distributions and organisations were analysed using BCA and AFM. Density increased with solution concentrations with statistically significant differences, yet it remained constant between the substrates.

AFM studies confirmed the differences in microstructure suggested by the immunostaining of the proteins, and further revealed that the distribution and conformation of the ECM proteins on the substrates was influenced by the concentration of the coating solutions and most importantly by the physicochemical properties of the surfaces. AFM imaging showed substratum-induced assembly of ECM proteins from a single-molecule arrangement (from low concentration solutions) to the specific networks, which were more distinctive on the more hydrophobic polymer, PEA especially fibronectin. They formed nano-network structures for the high concentration solutions as links between individual molecules caused a tendency for network assembly.

The formation of protein networks on the substrates may be the result not only of the different conformation of the molecule on the substrates, but also of the surface density of adsorbed protein. This also showed the role of the hydrophobicity of the polymers as the networks varied significantly in their thickness and were densely displayed on PEA than on PMA, the latter being less hydrophobic. These adsorbed ECM proteins showed fractal nature, with similar fractal dimension independently of the solution concentrations (for values higher than 20 μg/mL), except for FN that presented nano-network structures only on PEA and not on PMA. The fractal-like organization of these ECM proteins reflects their role as structural basis of the BMs. The results stress the importance of the underlying synthetic substrate’s surface chemistry for the biofunctional conformation of adsorbed proteins.

Chapter 4

Interaction of Wild Type Cells with Biointerfaces

Contents

4. 1 Introduction

As shown in chapter 3, surface chemistry modulates protein adsorption (including LM, FN and Col4) in terms of the total amount of protein adsorbed and of its distribution and conformation on the material surface. This implies a modulation of ECMs activity at the material interface, which has been shown to influence cell behaviour. Therefore, after surface characterisation of the substrates, cell response to these biointerfaces was investigated.

It has been established, and outlined in chapter 1, that cell response to a surface is controlled by the state of the interfacial layer of adsorbed proteins. For example, FN assembly results in protein conformation and distribution at the material interface that influence cell behaviour in focal adhesion assembly (Vanterpool et al. 2014), protein remodelling (Llopis-Hernández et al. 2013), cell differentiation (Salmeron-Sanchez et al. 2011) and in cells viability (Soria et al. 2007). Likewise, human endothelial cells and fibroblasts bind more avidly to single molecule arrangements of Col4 on hydrophilic (OH) and positively charged (NH2) substratum (Coelho et al. 2011a, b, Coelho et al. 2010) than on hydrophobic CH3 substrata (Coelho et al. 2016)

Here, this chapter focused on the analysis of adhesion, matrix secretion and remodelling using wild type cells cultured on ECMs-coated polymer substrates as illustrated in (Figure 4.1). Indeed, the next chapter will be focussed on matrix secretion by mutant cells and how the interfacial protein layer can control the behaviour of the mutant.

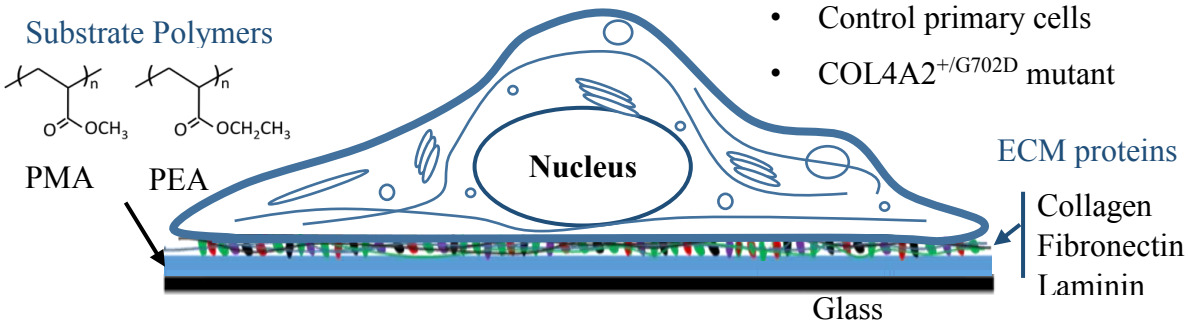

Figure 4.1 Simplified sketch of the cell-protein-material interaction. Cells interaction with the adsorbed protein layer is through integrins, transmembrane receptors that are involved in multiple cellular processes such as adhesion, migration, proliferation, matrix secretion and organisation. The chemistry of the surface substrate was manipulated to modulate protein adsorption, conformation and distribution in order to influence cells behaviour. PEA: Poly (Ethyl) Acrylate; PMA: Poly (methyl) Acrylate, consisting of similar chemistry.

4. 2 Aims and Objectives

This chapter presents assays optimisation and characterisation of cell response to the biointerfaces. The aims were to:

- Optimise cell culture and assays using wild type fibroblast cells (to minimise the usage of the limited mutant (MT) primary dermal *COL4A2*$^{+/G702D}$ fibroblasts).
- Identify differences in cell responses to the ECM-coated substrates
- Analyse matrix secretion and adhesion behaviour of wild type fibroblasts.

Control cells, age, sex, and ethnicity matched, were purchased from Tissue Culture Solutions Cell Works (UK) and used in this chapter. These cells are identified throughout this thesis as wild type (WT) fibroblasts. The mutant (MT) primary dermal *COL4A2*$^{+/G702D}$ fibroblasts were used in the following chapters.

4. 3 Results and Discussions

For all the experiments, cells were cultured in serum-free medium for the first 2h to avoid the interference and to ensure that the only proteins available were that previously coated on the substrates (Altankov G. et al. 2001), although these cells are not proteins-null and in the mid-term will secrete, create and eventually reorganize matrix network. Cells were seeded at a low density (5,000 cells/cm^2) to maximize cell–material interactions and to minimize cell-cell interactions. Beside protein-coated PMA and PEA, glass was used as another control.

4. 3. 1 Cell Adhesion

Surface wettability has long been recognized as an essential parameter for protein adsorption and cellular interaction (Altankov and Groth 1997, Grinnell and Feld 1982, Hernández et al. 2007). Generally, hydrophilic surfaces support cell adhesion and spreading, and this is most often attributed to the appropriate conformation of adsorbed matrix proteins (Grinnell and Feld 1982, Kowalczyńska et al. 2005, Rico et al. 2009). Nonetheless, some materials with very high wettability, which bind much water-like hydrogels, do not support protein adsorption and cell adhesion (Tamada and Ikada 1994). Surfaces used in this study are considered hydrophobic and increase their hydrophobicity when absorbed with ECMs as observed in chapter 3.

To study how cells respond to the ECM-polymer interfaces, a 3 h adhesion experiment was performed in serum-free conditions, focusing on the overall cell morphology, the development of focal adhesions (FAs) and actin cytoskeleton. Cells were cultured on substrate surfaces coated with different concentrations of ECM proteins and then fixed and stained for vinculin (for FAs) and actin. FAs are supramolecular structures that link adsorbed ECM at the material interface (such as PEA and PMA) with the actin cytoskeleton. Their composition, dynamics, size, and structure, depend on the surrounding matrix.

Availability of key domains from the coated protein can promote integrin clustering, which in turn can determine cell signalling and fate (Arnaout et al. 2007, Hanein and Horwitz 2012, Schiller and Fassler 2013, Wehrle-Haller 2012a, b). Besides the composition, the size of FAs, ~1 μm, are correlated with their function. FAs complexes are involved in migration and low-tension phenotypes and contain proteins such as paxillin, vinculin, and phosphorylated proteins. FAs size of ~1–5 μm are involved in intermediate tension

phenotypes; super-mature adhesions, > 5 μm, are involved in high-tension phenotypes (Biggs et al. 2009).

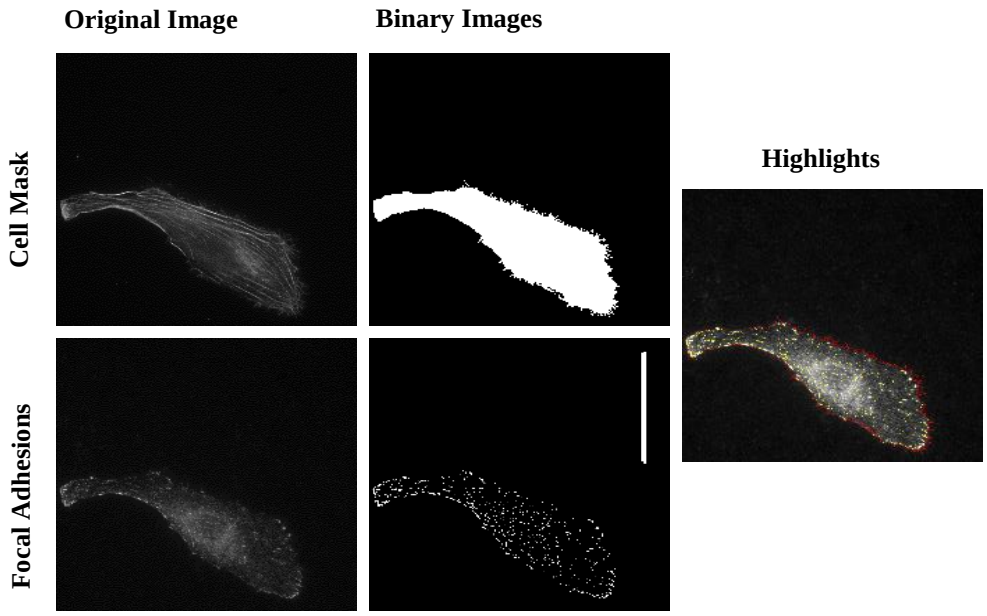

Figure 4.2 Steps of image processing for focal adhesion analysis. Scale bar: 50 μm.

To quantify the maturation level of FAs on the different surfaces with the different concentration of LM, FN and Col4 coating, frequency distributions for their size (defined as the length of the major axis of the FA plaque) were obtained through image analysis of the vinculin images as shown in (Figure 4.2). FA complexes (dot-like complexes shorter than 1 μm) were discarded from the analysis (Geiger et al. 2001). To avoid altered area and roundness values that cell overlapping would have produced, only isolated cells were used. Images were analysed with ImageJ coupled with an in-house macro processor and the values of each condition were compared.

4. 3. 1. 1 Adhesion and attachment on LM-coated substrates

Short-term cell culture experiments were performed to investigate attachment and initial adhesion of fibroblasts to the interfaces. Short-term cell attachment to LM-coated substrates (20 μg/mL) was measured using a standard protocol, allowing 20 min for attachment. Figure 4.3F showed that LM coating is essential for short-term cell attachment, as no cells were found on both bare polymer surfaces. The attachment of cells to PEA and PMA-coated with LM 20 μg/mL and to glass was similar (~85%), even when samples were washed extensively with DPBS before cell counting. This indicates that LM is important in short-term attachment of cells to surfaces.

Images of representative inverted binary representation of FAs of WT fibroblasts on PEA and PMA coated with LM from solutions of 2, 5, 10, and 20 µg/mL (Figure 4.3A). It showed high FAs distribution throughout the whole cell at lower concentration on both surfaces. Analysis of the FAs showed that there was no difference in the number of smaller FAs of fibroblast cells on both surfaces at lower LM concentration, although few differences were observed for the higher concentrations (Figure 4.3B). Similarly, the greater FAs (≥3 µm) were seen in increasing number at higher concentrations than at lower ones, and also on both surfaces. Cell size/area, FAs size, and count were also studied. There was a tendency of increasing fibroblast size on the increasing solution concentrations of LM on both substrates, although no statistical significant differences were found (Figure 4.3C).

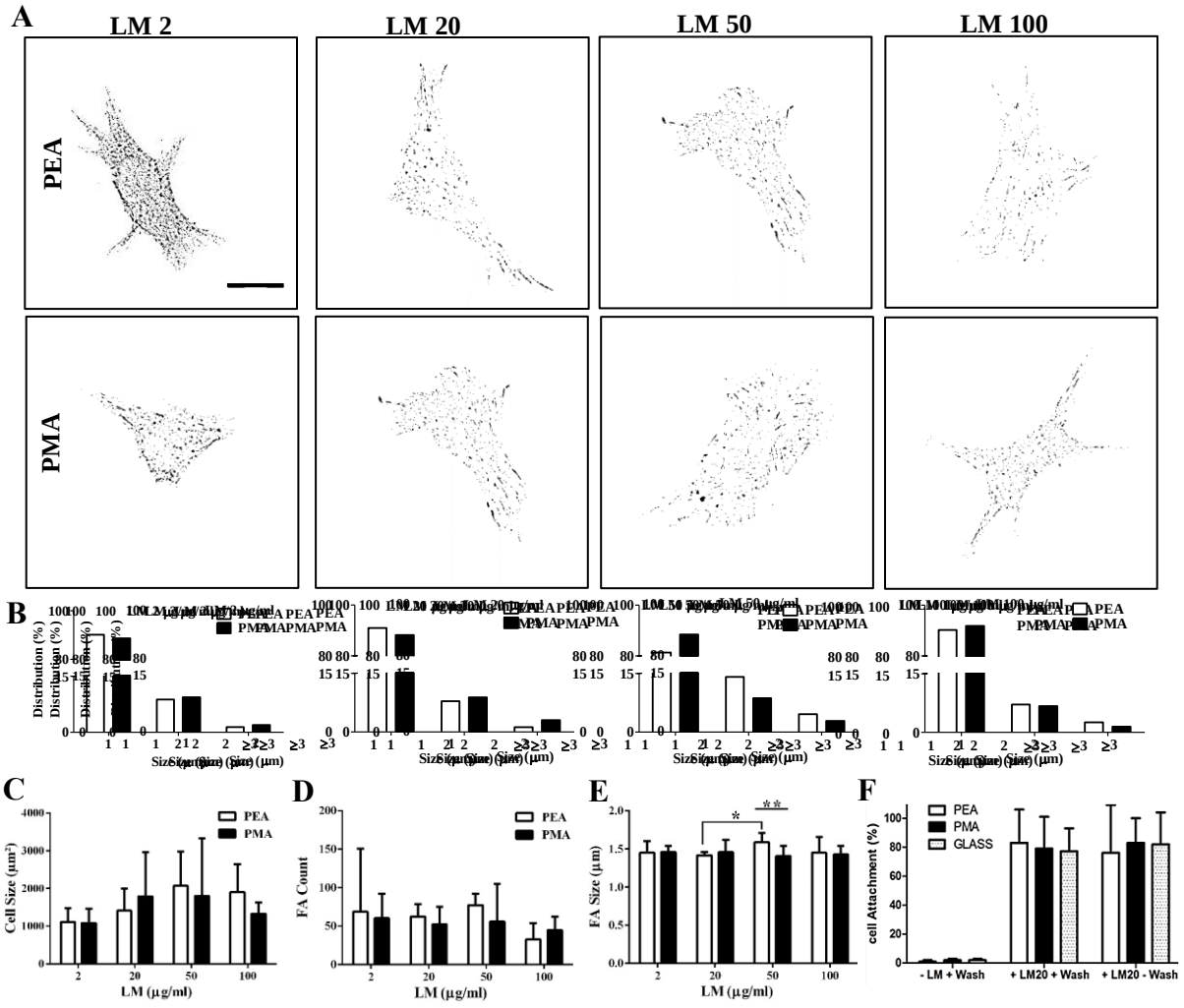

Figure 4.3 Focal adhesion quantification and cell attachment on LM coated PEA and PMA substrates. (**A**) Representative inverted binary representation of focal adhesions of WT fibroblasts on PEA and PMA-coated with different concentrations of LM. (**B**) Images in (A) were quantified to build size distribution of focal adhesions on both polymers. (**C**) Cell size on PEA and PM-coated from LM solutions of 2, 20, 50 and 100 µg/mL. (**D**) Number of FAs per cell, (**E**) size of FAs on PEA and PMA. (**F**) Cell

attachment on PEA and PMA coated from a 20 μg/mL LM solution. Scale bar: 25 μm. WT, wild type. Data presented as mean ±SD, N ≥10, and analysed with an ANOVA test; *p<0.05, **p<0.01, ***p<0.001. Bar: 50 μm.

FAs were counted for at least 10 cells for each condition and no significant differences were observed for both substrates and at all the solution concentrations (Figure 4.3D). There seemed to be fewer FAs count on PMA than on PEA. Bizarrely, these results do not support the increasing size of FAs as the protein concentration increased as well as the difference between FA sizes on both substrates as reported by another study (Vanterpool et al. 2014). FAs size was significantly different only between PEA and PMA-coated with LM50 (**p<0.01) and also PEA-coated with LM20 and LM50 (*p<0.05) (Figure 4.3E).

4. 3. 1. 2 Adhesion and attachment on FN-coated substrates

Fibroblast adhesion on FN-coated substrates was also analysed. A short-term attachment assay to 20 μg/mL of FN showed that FN is important for cell attachment to the substrates as cells did not attach in the absence of FN and extensive washing (Figure 4.4F). Similar results have been reported by Vanterpool and colleagues (Vanterpool et al. 2014). Adhesion assay of cells on polymers-coated with FN from solutions of 2 and 20 μg/mL was then performed. Images of representative inverted binary representation of FAs of WT cells on PEA and PMA-coated with FN are shown (Figure 4.4A). The images showed FAs mainly located at the cell boundaries.

Quantification of the FAs distribution showed a higher fraction of the smaller FAs (1-2 μm) with no significance difference on both substrates (Figure 4.4B). The fraction of greater FAs (≥3 μm) were lower in number yet similar on both substrates. Cells size on both substrates was similar independently of the concentration of FN, although at higher FN concentration (20 μg/mL) it was relatively higher on PMA than on PEA (Figure 4.4C). FAs count also revealed that the concentration of FN did not affect the number of FAs on both surfaces (Figure 4.4D). Likewise, FAs size was not affected (Figure 4.4E). These observations correlated with previous reports (Llopis-Hernandez et al. 2013, Vanterpool et al. 2014).

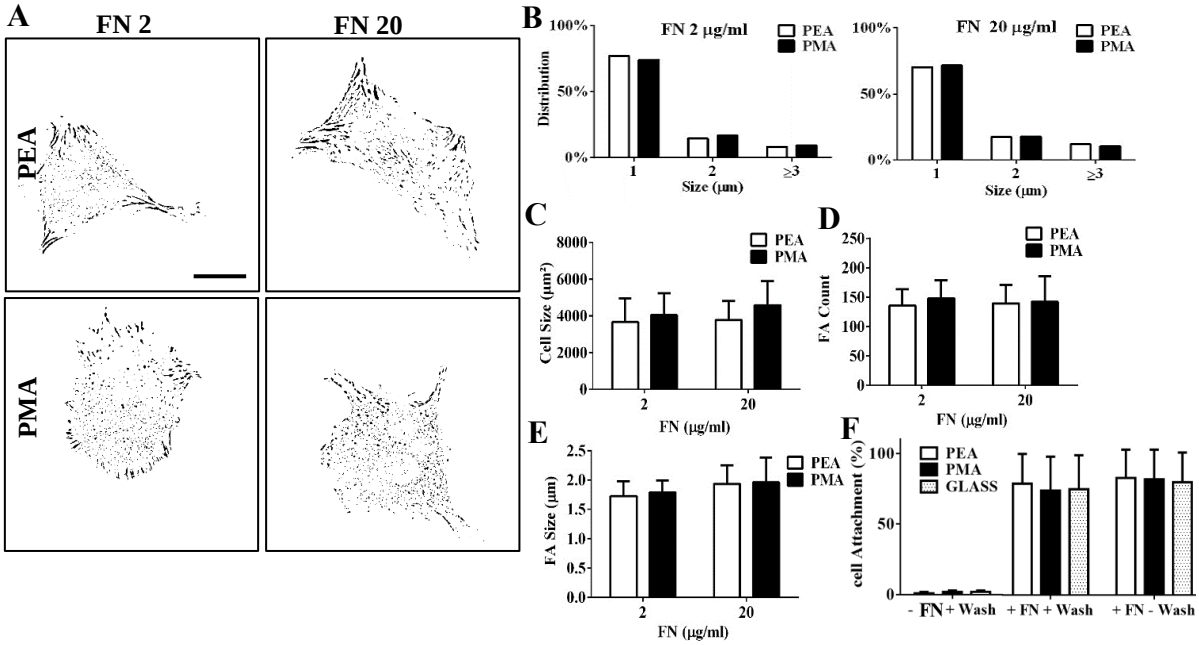

Figure 4.4 Focal adhesion assembly and cell attachment on FN coated PEA and PMA substrates. (A) Representative inverted binary representation of focal adhesions of WT fibroblasts on PEA and PMA coated with different concentrations of FN. (**B**) Images in (A) were quantified to build size distribution of focal adhesions on both polymers. (**C**) Cell size on PEA and PMA coated from FN solutions of 2 and 20 µg/mL. (**D**) Number of FAs per cell, (**E**) size of FAs on PEA and PMA. (**F**) Cell attachment on PEA and PMA coated from a 20 µg/mL FN solution. Data presented as mean ±SD, N ≥10, and analysed with an ANOVA test; *p<0.05, **p<0.01, ***p<0.001. Bar: 50 µm.

4. 3. 1. 3 Adhesion and attachment on Col4-coated substrates

Finally, cells were cultured on polymers-coated with Col4 from solutions of 20, and 50 µg/mL. The attachment assay showed once more the importance of Col4 coating in short-term cell attachment (20 min), as no cells were found on both bare polymer surfaces (Figure 4.5F). The data indicated that Col4, FN and LM are important for initial fibroblast adhesion. Images representative inverted binary representation of FAs from cells on substrates-coated with 50 µg/mL of Col4 (Figure 4.5A). Similarly to results seen in (Figure 4.3A) and (Figure 4.4A), images showed higher FA distribution throughout the whole cell especially at periphery. No apparent FAs distribution differences were observed on both polymers at both concentrations, as confirmed by the quantified distributions (Figure 4.5B).

Cells size were found to be similar at both concentrations on both substrates (Figure 4.5C). FAs count was higher on PEA than on PMA, and significantly different at 50 µg/mL concentration (Figure 4.5D). This showed that cells on PEA-coated with Col4 adhere and interact more with this surface employing more FAs, although the cell size remained similar

to PMA substrate. FAs size were similar on both polymers but were found to be greater at 50 µg/mL concentration (Figure 4.5E).

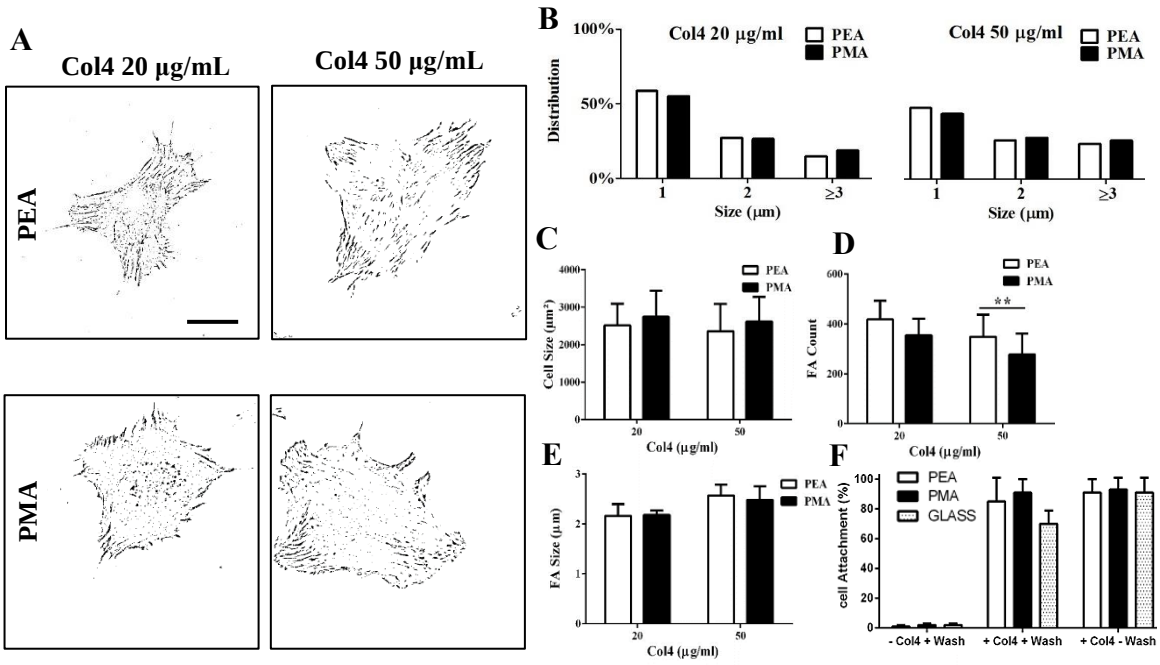

Figure 4.5 Focal adhesion assembly and cell attachment on Col4 coated substrates. (**A**) Representative inverted binary representation of focal adhesions of fibroblasts on PEA and PMA coated with different concentrations of Col4. (**B**) Images in (A) were quantified to build size distribution of focal adhesions on both polymers. (**C**) Cell size on PEA and PMA coated from Col4 solutions of 20 and 50 µg/mL. (**D**) Number of FAs per cell, (**E**) size of FAs on PEA and PMA. (**F**) Cell attachment on PEA and PMA coated from a 50 µg/mL Col4 solution. *p<0.05, **p<0.01, ***p<0.001. N-number: 12. Bar: 50 µm.

4. 3. 2 Matrix study

To investigate matrix secretion, immunocytochemistry (ICC) was performed for Col4a2, LM and FN after cells culture on PEA and PMA substrates-coated with ECM proteins (Figure 4.1). Cells were supplemented with 0.25 mM L-ascorbic acid 2-phosphate (asc-2-P, a more stable isomer) for 72 h to increase reproducibility between experiments and post-translational modifications. Ascorbic acid has an essential role in the synthesis of all collagens as it induces the latter expression and ensure proper folding (Vranka et al. 2004). Different time points were used to quantify the amount of the secreted ECMs proteins.

4. 3. 2. 1 Matrix secretion on LM interfaces

Figure 4.6A-B showed WT fibroblasts matrix secretion after culture on LM (20 µg/mL) coated polymers at different time points. Cells were stained for FN and Col4a2 to visualise the deposited/secreted proteins. The images of the stained proteins showed that WT cells began secreting matrix, especially FN, at very early time points (3h), on both PEA and PMA-coated with 20 µg/mL of LM. The secreted FN matrix also formed fibrils-like networks from day 1 on both polymer surfaces. Similar observations have been previously reported (Gonzalez-Garcia et al. 2010, Gonzalez-Garcia et al. 2012, Ilic et al. 2004, Llopis-Hernandez et al. 2011, Llopis-Hernández et al. 2013).

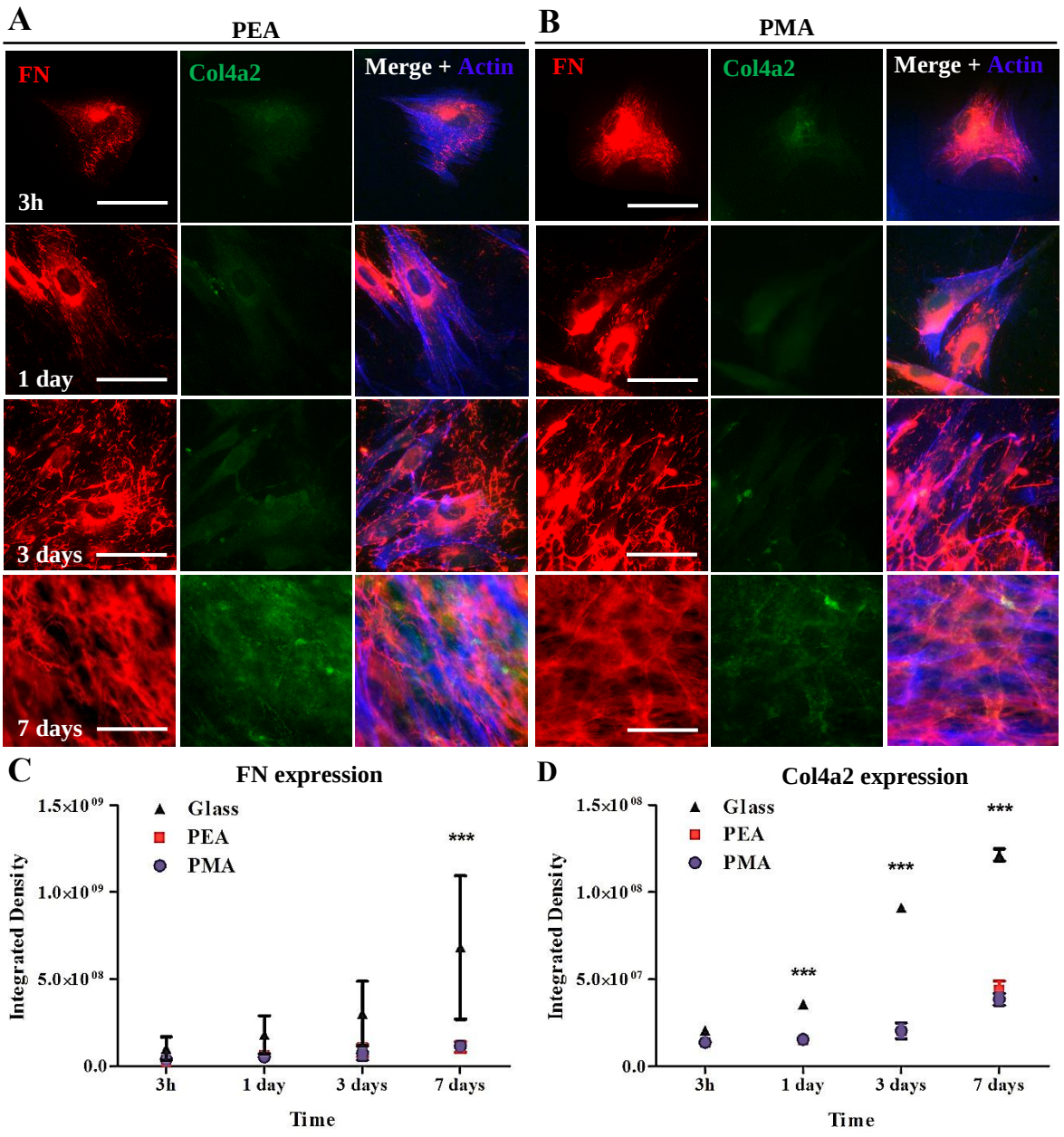

Figure 4.6 Matrix secretion by WT fibroblast cells on LM coated polymers. FN (red) and Col4a2 (green) secreted by WT cells grown on LM (20 µg/mL) coated PEA (**A**) and PMA (**B**) substrates for 2 h under serum free conditions, then with serum before fixation at different time points (3h, 1 day, 3 and 7 days). Note: no images for glass staining is shown; only the quantification is indicated in the graphs. Cells were simultaneously stained also with actin (blue). ImageJ was used to quantify protein deposition/secretion by calculating the total fluorescence intensity. Integrated density measurements of FN (**C**) and Col4a2 (**D**) proteins from full size images on PEA, PMA and glass at different time intervals. WT, wild type fibroblasts. Bar-50 µm. Data presented as mean ±SD, and analysed with an ANOVA test, ***$p<0.001$. $N \geq 5$.

In contrast, staining of secreted Col4a2 was very limited on both polymers until day 7 when it looked higher. The secreted Col4a2 at day 7 was observed forming network-like structures on both substrates, these arrangements resembled the network-like structures in the BMs (Aumailley et al. 2000, Charonis et al. 1985, Kalluri 2003). FN and Col4a2 fibrils co-localised at day 7, demonstrated by the yellow colour in (Figure 4. 6A-B). Co-localisation at this time point suggests some denaturation of both proteins increasing affinity to each other (Coelho et al. 2013).

ImageJ was used to calculate the total amount of secreted matrix using the fluorescence integrated intensity (Berthod et al. 2006, Prewitz et al. 2015). Quantification of secreted FN was observed to increase with time (as cell density also increased) on all the surfaces, although it was higher on glass than on the polymers (Figure 4.6C). These results correlate with other studies (Llopis-Hernandez et al. 2011, Sillat et al. 2012). Conversely, Col4a2 secretion remained constant until day 7 on both PEA and PMA, while it was higher on glass and increased with time (Figure 4.6D).

In general, FN and Col4a2 matrix secretion increased with time on glass and on the substrates coated with LM. These observations are in line with previous studies which indicated the increase of secreted matrix with time. For both proteins, secretion was significantly higher on glass than on the polymeric substrates. The secreted LM was not stained as this would have also stained the coated LM protein, yet the later could have been labelled with GFP and a specific antibody to the secreted LM used.

4. 3. 2. 2 Matrix secretion on FN interfaces

Secreted Col4a2 and LM by WT cells on FN-coated substrates were stained (Figure 4.7A-B). The images showed LM secretion increasing with time from 3 to 7 days as cell density increased, but no apparent differences were observed between the surfaces. Time points 3h

and 1 day are not included as the staining intensity was not good. Secreted LM on FN-coated interfaces did not form fibril networks on any surfaces at any time, and the staining remained mostly where the cells adhered. Col4a2 secretion also increased with time, yet unlike LM, it formed fibril-like network at day 7, especially on glass. Secreted LM and Col4a2 co-localised as shown by the yellow colour in the merged images. Being the major components of the BMs, LM and Col4a2 interact with each other forming the scaffold that provides specific interaction sites for the other BM components and creates a fully functional BM (Miner et al. 2004, Poschl et al. 2004).

Quantification indicated that Col4a2 secretion increased significantly with time on PEA-coated with FN and on glass, while it remained constant on FN-coated PMA (Figure 4.7C). Col4a2 secretion by the WT cells on glass was comparable to secretion on PEA-coated with FN. On the other hand, LM secretion on all the surfaces increased significantly with time from 3 to 7 days; except on PEA-FN where it remained constant.

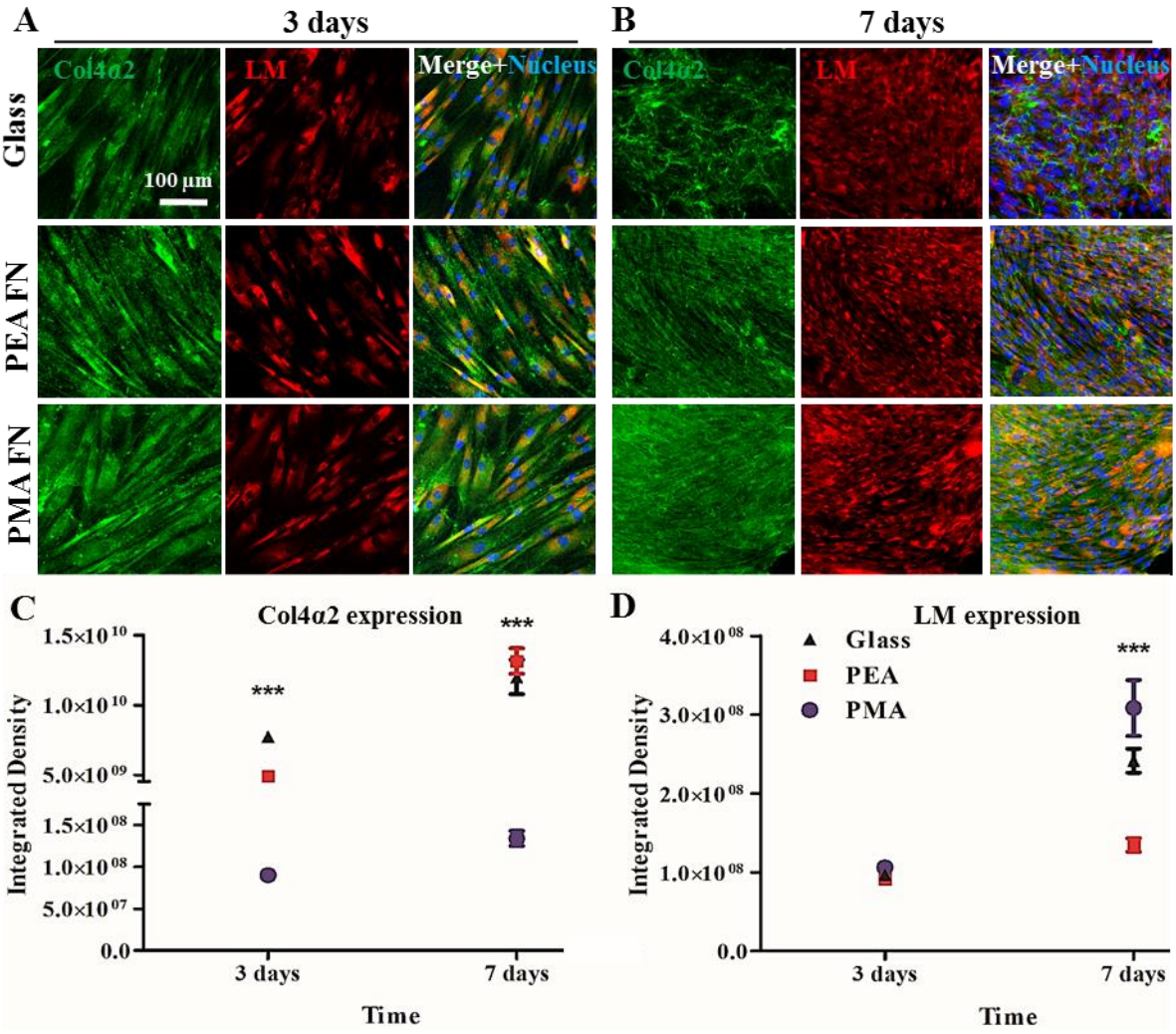

Figure 4.7 Matrix secretion by WT fibroblast cells on FN coated polymers. WT cells were grown on FN (20 μg/mL) coated PEA and PMA substrates for 2 h under serum free conditions; then with serum before fixation at different time points 3 days (**A**) and 7 days (**B**) and staining for the ECMs Col4a2 (green) and LM (red). ImageJ was used to quantify protein deposition/secretion by calculating total fluorescence intensity. Integrated density measurements of Col4a2 (**C**) and LM (**D**) proteins from full size images on PEA, PMA and glass at different time intervals. Bar-50 μm. Data presented as mean ±SD, $N \geq 5$; and analysed with an ANOVA test; ***$p<0.001$.

4. 3. 2. 3 Matrix secretion on Col4 interfaces

WT cells secretion of FN and LM was also investigated on Col4-coated PEA and PMA substrates and on glass (Figure 4.8A-C). Similarly to substrates-coated with LM, FN was secreted from an early time (3h) and secretion increased with time forming fibril-like structures on all the surfaces. Likewise, LM was observed from time 3h, but did not form fibril-like structures with time. Similarly to LM secreted on FN-coated polymers, stained LM was mostly where cells were located. Quantification of the staining showed FN secretion on Col4-coated interfaces increased with time without significance differences on all the surfaces. On the other hand, LM secretion increased with time yet with significance on glass and PMA.

The investigation of the secretion of ECMs by WT cells was an important step in understanding how fibroblasts respond to these biointerfaces. The most differences observed from these results were on FN-coated substrates. Col4a2 was highly secreted with time with significance difference on glass and PEA-FN (similar on both) compared to PMA-FN. Yet, Col4a2 was significantly secreted only on glass compared to LM-coated substrates. On the other substrates coated with either LM or Col4, secretion on the ECMs were similar independent of the surfaces. FN started to form fibril-like network structures from day 3 on all the surfaces; while Col4a2 only formed fibril at day 7 mainly on glass. LM did not form any fibrils at any time on any of the surfaces and it remained mostly where cells were located.

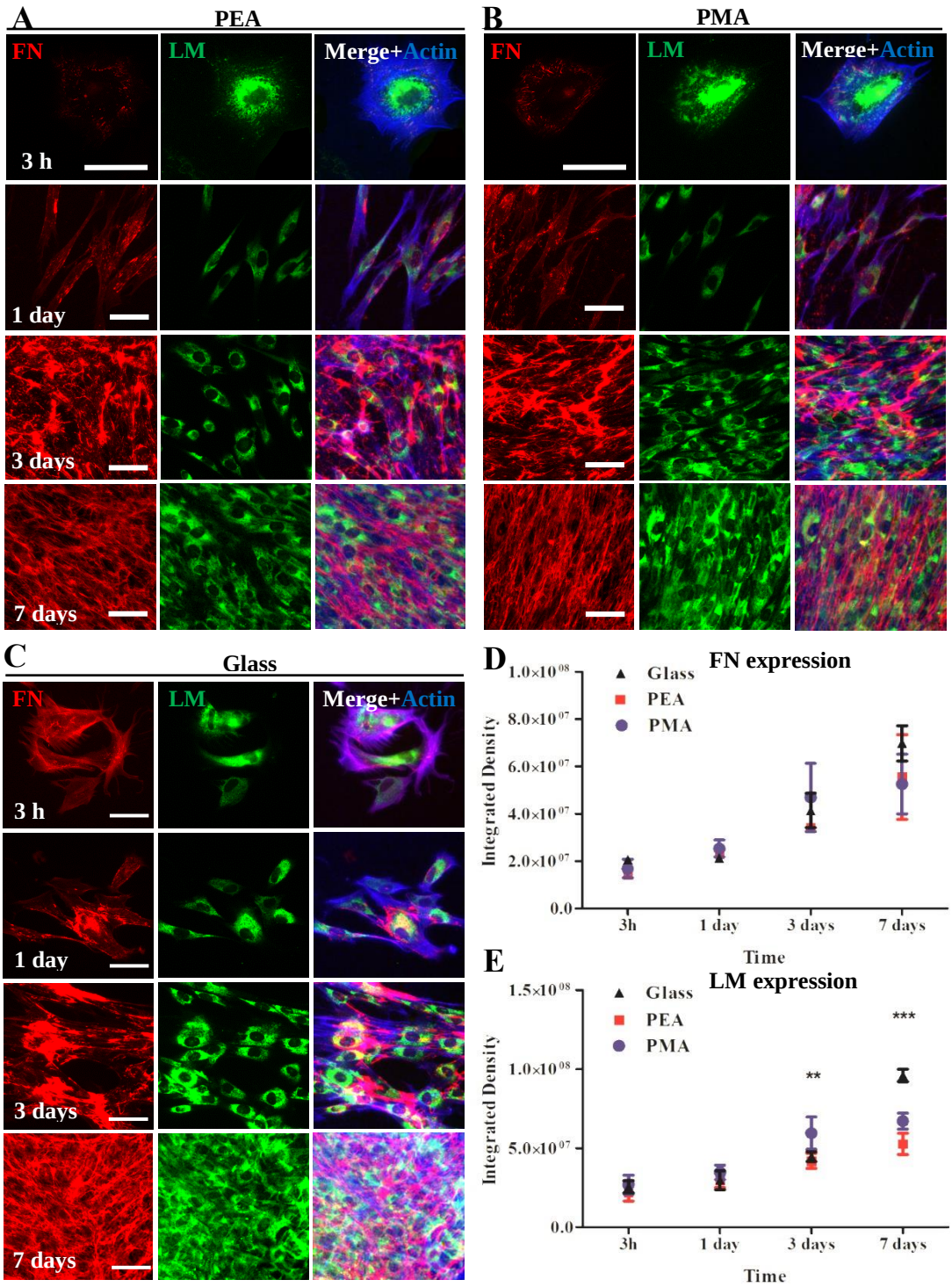

Figure 4.8 Matrix secretion by WT cells on Col4 coated polymers. Cells were grown on Col4 (50 µg/mL) coated PEA (**A**) and PMA (**B**) substrates and on glass (**C**) for 3h, 1 day, 3 and 7 days before staining for FN (red) and LM (green) and also stained with actin (blue). Integrated density measurements of FN (**D**) and LM (**E**) at different time intervals. Performed with Image J. Bar-50 µm. **p<0.01, ***p<0.001. N≥ 5.

4. 3. 3 Fibroblasts reorganisation of adsorbed ECMs proteins

Cells have been shown to remodel the matrix they interact with (Coelho et al. 2013, Maneva-Radicheva et al. 2008). Here, fibroblasts were grown on PEA and PMA coated with LM 20 µg/mL, FN 20 µg/mL or Col4 50 µg/mL at different time points. The typical morphology of WT fibroblasts adhering on LM (Figure 4.9A), FN (Figure 4.10A) and Col4 (Figure 4.11A) coated polymer substrates are shown. The low magnification images allowed to observe cells size and morphology. The high-resolution images for early time in (Figure 4.9-11B) indicated that cells on all the interfaces represented their regular flattened morphology.

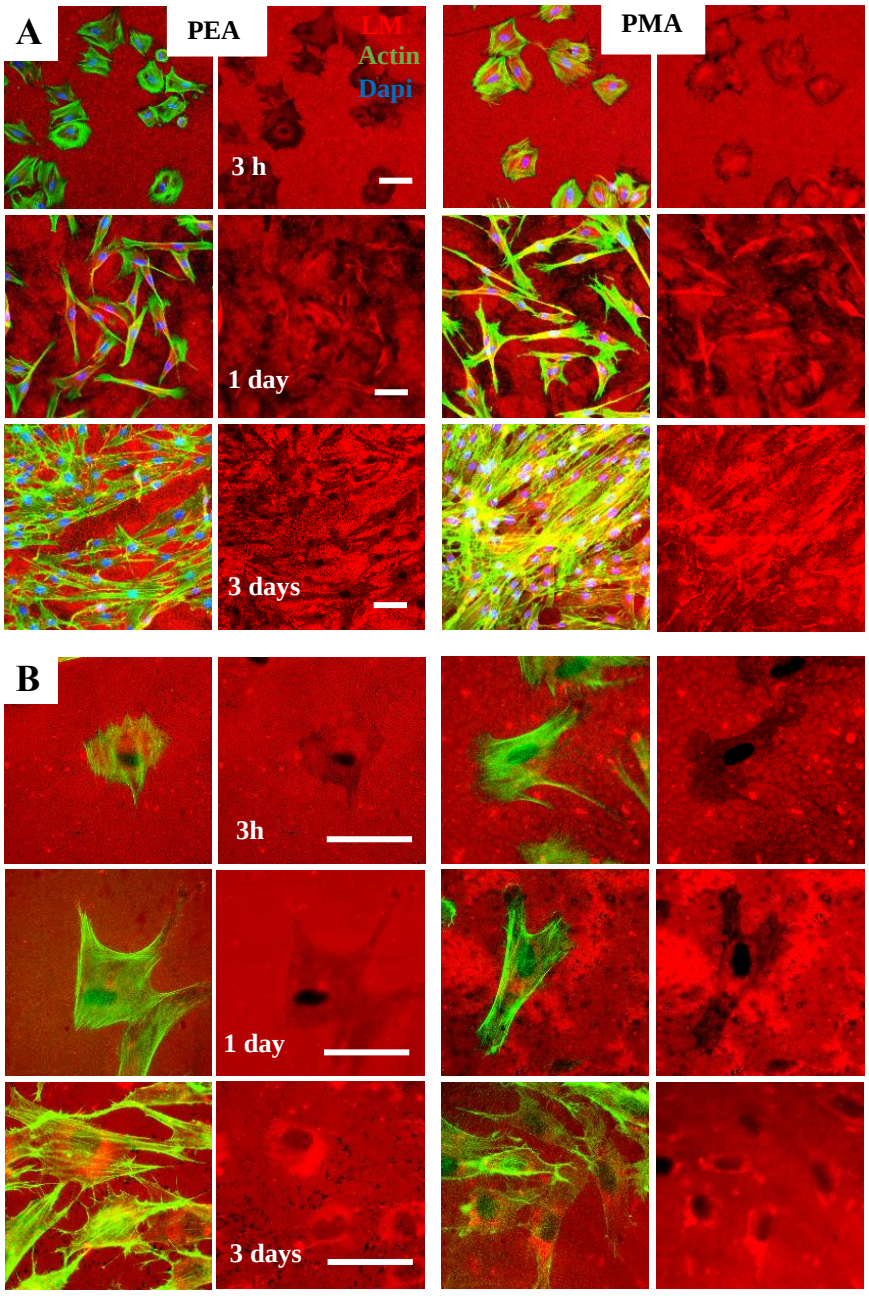

Figure 4.9 Remodelling of adsorbed laminin on the substrates by WT fibroblasts. (**A**) Low magnification images to follow the overall morphology of fibroblast cells remodelling adsorbed LM. (**B**) High magnification images. First and third columns show

fibroblasts stained with actin (Green) reorganising the coated LM, (Red). The dark zones represent the places from where the protein was removed to be arranged. Substrates were coated with LM 20 µg/mL, for 1h then cells were seeded and cultured for different time points: 3h, 1 day, and 3 days. Bars: 50 µm.

It was noted that cells on Col4 showed less efficient adhesion with appearance of both round and flattened cells suggesting delayed spreading (Figure 4.11A). Cells on Col4 were more elongated after day 1 on both polymers compared to cells on LM and FN-coated polymers. With the low magnification images, WT proliferating and density was observed increasing with time, yet the rate was slow for cells on Col4-coated interfaces.

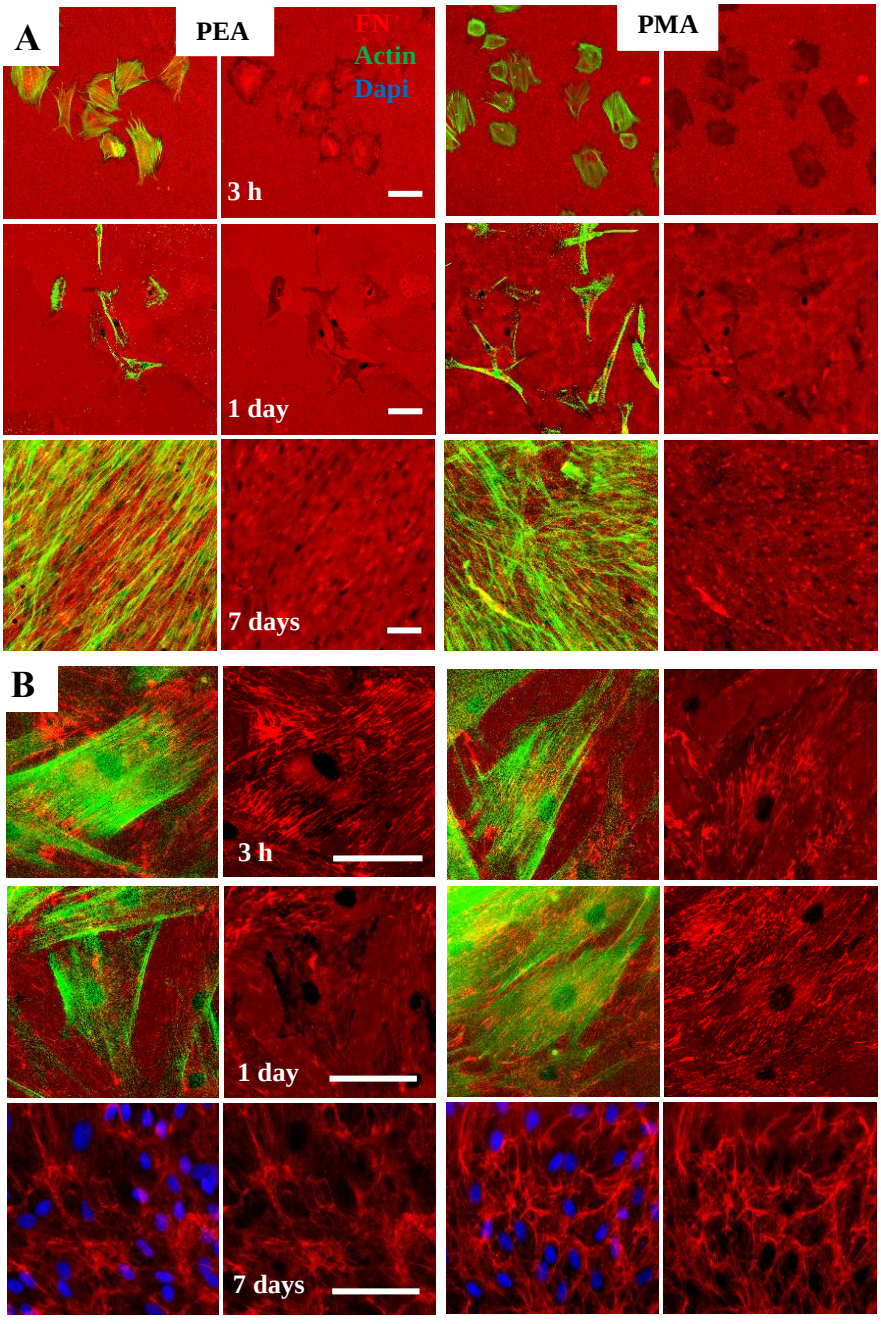

Figure 4.10 Remodelling of adsorbed fibronectin on the substrates by WT fibroblasts. (**A**) Low magnification images to follow the overall morphology of fibroblast cells remodelling adsorbed FN. (**B**) High magnification images. Actin (Green) and FN (Red). Substrates were coated with FN 20 µg/mL, for 1h then cells were seeded and cultured for different time points: 3h, 1 day, and 7 days. Bars: 50 µm.

The dark zones seen in (Figure 4.9-11B column 2 and 4) represented the areas from where the coated proteins were removed to be reorganised by cells. It was clearly seen that where the cells were located, the adsorbed LM, FN or Col4 matrix were rearranged. As time elapsed, cells started to secrete their own ECMs as the dark patches were seen being covered with high density fluorescence and formed "corona"-like reorganization. It is thought that a possible mechanism for matrix reorganization (especially Col4) is its tethering by other molecules (FN) during fibrillogenesis (Coelho et al. 2013).

There seemed to be no specific patterns observed in which the WT cells rearrange the ECMs, although LM showed more reorganisation by cells on PEA than on PMA. In general, the cells did not differentiate the rearrangement of the coated Col4, FN or LM on any of the substrates. However, it is known that the reorganisation depends on the materials surface properties. Conversely, since the polymers used have similar chemical properties, it could also be possible to get similar results although AFM coating of the proteins had proven distinctive differences in the arrangement of these adsorbed ECMs, especially for FN.

Studies have reported that two types of cell activities might happen when cells adhere onto these biomaterial interfaces: substratum (Col4, FN or LM) reorganization and its degradation via enzymatic cleavage (Coelho et al. 2013, Coelho et al. 2016, Llopis-Hernandez et al. 2011). In agreement with previously reported studies (Coelho et al. 2013, Llopis-Hernandez et al. 2011, Maneva-Radicheva et al. 2008) similar results were observed in this study.

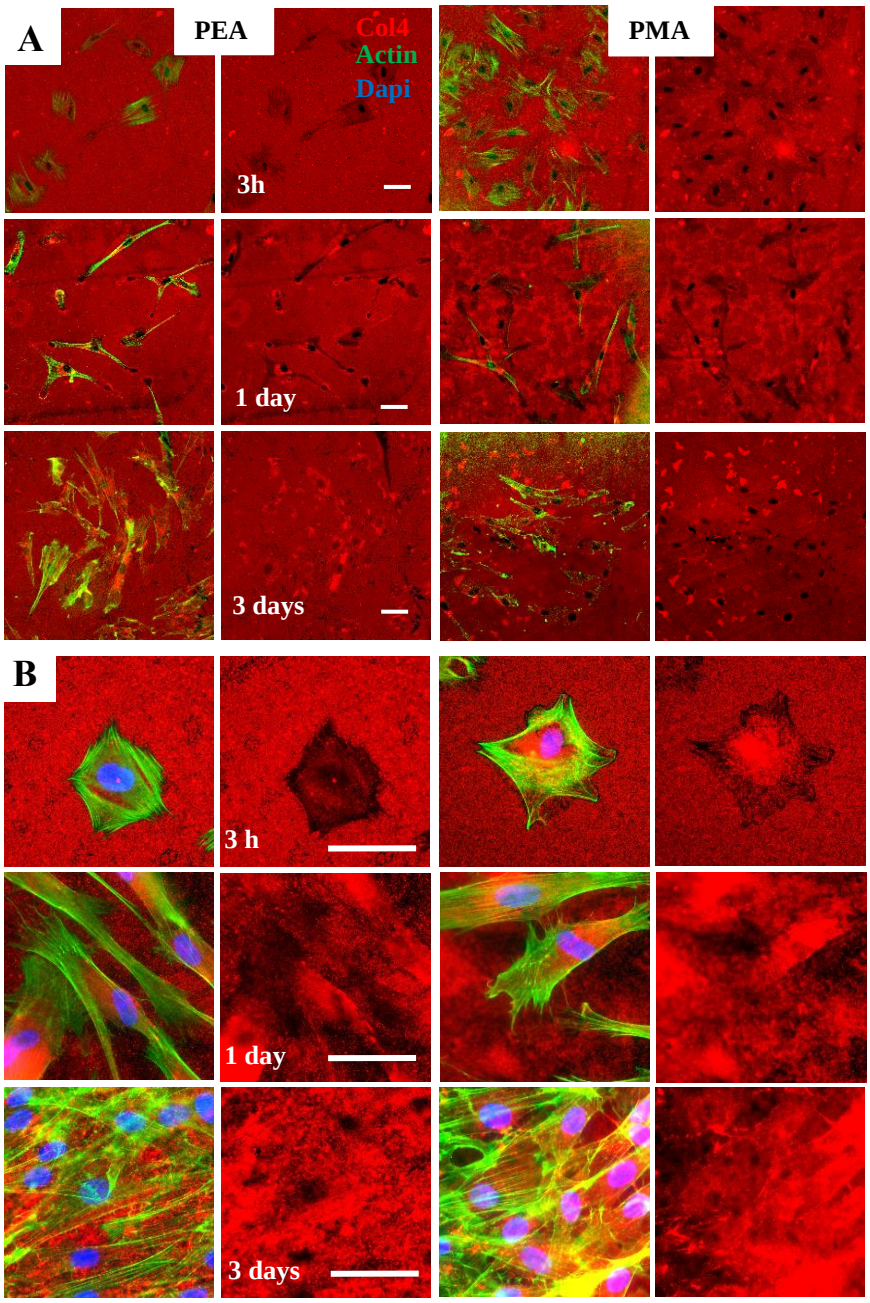

Figure 4.11 Remodelling of adsorbed Col4 on the substrates by WT fibroblasts. (**A**) Low magnification images to follow the overall morphology of fibroblast cells remodelling adsorbed Col4. (**B**) High magnification images. Actin (Green) and Col4 (Red). Substrates were coated with Col4 50 µg/mL, for 1h then cells were seeded and cultured for different time points: 3h, 1 day, and 3 days. Bars: 50 µm.

4. 4 Conclusions

Various studies have shown how different cells respond when in contact with various substrates. Here, WT fibroblasts responses on specific biointerfaces were investigated. The results showed the importance of the coating of the different ECM proteins (Col4, FN and LM) in the initial and short-term attachment of cells to surfaces. Cells adhesion on all the ECM proteins-coated substrates showed a higher fraction of the smaller FAs (1-2 μm) with no significance difference on both substrates, and lower fraction of greater FAs (≥3 μm). Results also showed that substrates-coated with LM of increasing concentrations led to an increase in cells size on both surfaces despite the FAs sizes remaining constant. Cells size, FAs count and size were independent of the different concentrations of coated-FN on both substrates. Substrates-coating with Col4 resulted in higher FA count on PEA, and significantly affected cells FAs count and size when coated with 50 μg/mL.

In general, the data showed that cells matrix secretion significantly increased with time and also formed fibril-like networks. FN was secreted at very early time points (3h), on both PEA and PMA-coated with LM and the matrix also formed fibrils-like networks after 1 day on both polymer surfaces. Secretion of Col4a2 by the cells on LM-coated substrates was very limited until day 7 when it became higher. WT cells secreted higher amount of Col4a2 on PEA-coated with FN and the amount was comparable the amount on glass. Noteworthy, the fibroblasts did not secrete high amount of Col4a2 when cultured on LM-coated substrates. The study of matrix remodelling of LM, FN and Col4 on PEA and PMA indicated that within a short culture time e.g. 3 h, WT fibroblasts not only adhere and interact with adsorbed ECMs on the biomaterial interfaces, but they are also able to mechanically translocate and remodel/reorganize the adsorbed matrix to some extent.

Chapter 5

Interaction of *COL4A2*$^{+/G702D}$ Mutant Fibroblast Cells with Biointerfaces

Contents

5. 0 Introduction

5. 1 The basement membrane

The behaviour of cells within tissues is strongly dependent on the ECM-a hierarchically organized structure consisting mostly of proteins, glycoproteins and proteoglycans. This includes the basement membrane (BM)-a specialized type of ECM that underlies all epithelial and endothelial cells, providing structural support to tissues (Kalluri 2003, LeBleu et al. 2007). The BMs contain various spatiotemporal cues that virtually impact all aspects of cell functionality, including cell signalling, growth, survival, migration, and differentiation. The BM is highly dynamic structure that is continuously being remodelled by resident cells during development, homeostasis and tissue repair. This remodelling comprises the production, deposition, and organization of BM molecules balanced by the degradation and remodelling of existing BM. Dysregulated BM remodelling may result in pathologies such as fibrosis, inflammation, or tumour progression (Kalluri 2003, LeBleu et al. 2007).

A large and growing body of evidence show that cells need to accept distinct mechanical stimuli from the surrounding structures to strengthen their connections with the cytoskeleton, and thus responding to the mechanical properties of the environment (Geiger et al. 2009, Geiger et al. 2001). As the stiffness of the surrounding ECM *in vivo* is in the same order of magnitude as cells, they tend to reorganize it mechanically in a way optimal for their functioning (Grinnell F. 1986, Hubbell 2003). Alternatively, cells can degrade the excess of ECM triggering the process of pericellular proteolysis (Cox and Erler 2011).

ECMs undergo remodelling also in contact with biomaterials as the molecular events that take place at biomaterials interface mimic to a certain extent the natural cell–ECM interaction (Altankov George et al. 2010, Llopis-Hernandez et al. 2011). Cell–materials interaction starts with the adsorption of matrix proteins from the surrounding medium (Grinnell Frederick and Feld 1982) that bind integrin with distinct integrin binding site (e.g. RGD, GFOGER, etc.) (Arnaout et al. 2007, Garcia 2005, Garcia et al. 1998, Hynes 2002, Kalluri 2002, Sun et al. 2016). When integrins bind their ligand they cluster in focal adhesion complexes where specific bidirectional signalling converges with other signalling pathways (Garcia 2005, Hynes 2002). It involves a common tyrosine phosphorylation mechanism (Geiger et al. 2001) that include focal adhesion kinase (FAK), Src, Cas, and paxillin within other important signalling molecules (Cary and Guan 1999, Horton et al. 2015, Schaller

2001, Schaller et al. 1994, Zouq et al. 2009). On the level of cell–biomaterials interaction however, depending on the conformation of adsorbed proteins, different cellular response may occur (Altankov Georgi and Groth 1997, Keselowsky et al. 2003, 2004).

5. 2 Pathology of mutations affecting α1.α1.a2(IV)

The phenotypes due to *Col4a1* mutations were first observed in mouse models (Gould et al. 2005, Van Agtmael et al. 2005). This demonstrated that mutations disrupting the collagenous region caused a high occurrence of haemorrhagic stroke at birth, with kidney and eye defects (Gould et al. 2005, Van Agtmael et al. 2005). Similarities were found between these mouse models and groups of human patients leading to the identification of *COL4A1* mutations in human disease (Breedveld et al. 2006, Gould et al. 2005, Gould et al. 2006, Plaisier et al. 2007). Then, *Col4a2* mutations (with two glycine mutations) were described in three mouse models a few years after the identification of *Col4a1* mouse models (Favor et al. 2007). Since α1(IV) and a2(IV) are obligate protein partners, it is remarkable that *Col4a2* mutant mice have an apparent absence of kidney defects, and reduced haemorrhagic stroke severity.

Collagen IV is a major structural component of the extracellular matrix (ECM) and as such, it is likely that a mutation affecting the helical region of α1.α1.a2(IV) will have an effect on the ECM. The presence of BM defects in animal models and human patients affected by mutations of glycine residues of Gly-X-Y motifs confirms that this is the case for *COL4A1* and *COL4A2* mutations (Gould et al. 2007, Jeanne Marion and Gould 2016, Jeanne Marion et al. 2012, Murray et al. 2014, Van Agtmael et al. 2010, Van Agtmael et al. 2005). It is now recognised that BM defects contribute to the pathology in diseases caused by α1.α1.a2(IV) mutations. These BM and matrix defects can be due to incorporation of mutant protein in the matrix and/or intracellular retention of mutant alpha chains in the ER, which can lead to swelling of the ER and activation of ER stress (Murray et al. 2014); this does not exclude that some mutant protein may be secreted and affect interaction with other protein.

However, the discovery that environmental events (Gould et al. 2006) and genetic background (Gould et al. 2007) can also influence phenotype development in Col4a1 mouse models suggest that BM defects are not the only contributing factor. In addition, BM defects are found in both affected and unaffected tissues in Col4a1 mouse models (Van Agtmael et al. 2005) suggesting that another mechanism may influence the pathology.

The activation of ER stress is a well-known response to *COL4A1* and *COL4A2* mutations in both humans (Gunda et al. 2014, Jeanne Marion et al. 2012, Murray et al. 2014, Verbeek et al. 2012) and mouse models (Gould et al. 2005, Gould et al. 2006, Murray et al. 2014, Van Agtmael et al. 2010, Van Agtmael et al. 2005). ER stress is a homeostatic response to inappropriate levels of unfolded or misfolded protein in the ER, evolved to protect the organism, and is often characterised by swollen ER vesicles. The ER stress response aims to protect the organism from the toxic effects of misfolded proteins by reducing general translation, increasing chaperone specific expression, and elevating protein degradation pathways (Tabas and Ron 2011).

ER stress due to accumulation of misfolded protein leads to activation of the unfolded protein response (UPR). The UPR is a homeostatic mechanism evolved to minimise damage to the organism that may be caused by the release of incomplete or incorrectly folded proteins (See review (Tabas and Ron 2011)). It is controlled by three ER membrane bound receptors, PERK, ATF6 and IRE1, that under non-stressed conditions are bound to the ER chaperone BIP, via their ER luminal domains (Harding et al. 1999, Haze et al. 1999). While the UPR is protective and will ensure that ER homeostasis is returned in the event of transient ER stress, when chronic ER stress occurs it can activate apoptotic pathways to prevent incomplete or incorrectly folded proteins being released from the ER (Rutkowski et al. 2006). Moreover, it has become increasingly clear that chronic UPR can contribute to disease pathogenesis in a variety of disorders including diseases due to mutations in matrix proteins (for review see (Bateman et al. 2009)).

5. 3 *COL4A2*$^{+/G702D}$ mutation and phenotypes

COL4A2 mutations phenotypes result in many cardiovascular diseases (CVD) including haemorrhagic stroke and familial porencephaly (Gunda et al. 2014, Ha T. T. et al. 2016, Jeanne Marion et al. 2012, Murray et al. 2014, Van Agtmael and Bruckner-Tuderman 2010, Van Agtmael et al. 2010, Verbeek et al. 2012). In addition to CVD, *COL4A2* mutations are confirmed to cause ocular, cerebral, renal and muscular defects (See reviews (Kuo et al. 2012, Meuwissen et al. 2015, Van Agtmael and Bruckner-Tuderman 2010)). This thesis focuses on a particular *COL4A2* mutation, *COL4A2*$^{+/G702D}$. Sequence analysis of human skin dermal fibroblasts (from a patient carrying the *COL4A2*$^{+/G702D}$ mutation) showed a single nucleotide change, a substitution mutation that changes the highly conserved glycine residue of a Gly-X-Y repeat for an aspartic acid (*COL4A2*$^{+/G702D}$) (Figure 1.6A-B in chapter 1). The glycine residue is located within the collagenous domain of the *COL4A2*, which in turns

forms the triple helical domain of the α1.α1.a2(IV) trimer (Murray et al. 2014). Given the size and neutral charge of the glycine residue in Gly-X-Y repeats, it is critical for the formation of the triple helical collagen domain; any substitution is thought to affect the folding of the triple helix. *COL4A2*$^{+/G702D}$ mutation is therefore expected to interfere with the triple helix 3D structure of the α1.α1.a2(IV) trimer and/or affect the trimers.

The pathogenicity resulting from *COL4A1* and *COL4A2* mutations is generally attributed to a mixture of intracellular defects and extracellular matrix defect, but their relative contribution to disease remains unclear and may be mutation and/or cell or tissue dependent. Moreover, previous data from the Van Agtmael lab has shown that the intracellular accumulation of collagen in the presence of a mutation can be influenced by the presence of genetic modifiers within the genome (Murray et al. 2014). For most if not all glycine mutations, they are associated with intracellular accumulation and extracellular deficiency of mutant heterotrimers (Jeanne M. and Gould 2017, Jeanne Marion et al. 2012) caused by COL4 (α1.α1.a2(IV)) mis-folding. The observed BM defects may thus be due to the reduced secretion and incorporation of collagen but also mutant protein may be secreted and interfere with BM function. To this day it remains to be proved the extent to which Col4a1 disease is due to the matrix defects and or ER stress but recent data support at least a contributing role for ER stress in the vascular phenotypes and at least some kidney defects.

Different clinical phenotypes of *COL4A2* in human with same mutations are now emerging. Likewise, altered phenotypes in mice with different genetic background have been reported. These data support the idea that disease outcome may be modified. It was hypothesised that culturing the mutant *COL4A2*$^{+/G702D}$ cells on substrates coated with ECM proteins LM, FN or Col4 can have effects on the cells behaviour, secretion of matrix and its degradation. It should be noted that these cells are primary cells from patients expressing the full complement of collagens such as collagen type I, etc. Previous analysis has shown that secretion of other BM components such as perlecan appeared to be unaffected by the *COL4A1 G702D* mutation (Murray et al. 2014). However, study of the secreted/deposited matrix was necessary to investigate whether the retention of Col4 allowed differential secretion of other major BM proteins. Does the intracellular accumulation of COL4A2 encompassed by the increase secretion of other ECM proteins or the latter secretion remains the same? These are questions that are aimed to be answered in this thesis.

5. 4 Effect of biointerfaces on cell behaviour

Fibroblasts are the most abundant cell type in connective tissues and are the primary cells that lay down the first provisional ECM that is rich in fibronectin (FN) (Hynes 2009). The focus on FN is motivated by the differences in the results observed in chapter 4. WT cells secreted higher amount of Col4a2 when cultured on FN-coated substrates compared to when cultured on LM-coated substrates. FN is also of great interest by the fact that it is the major component of early ECM in matrix remodelling by fibroblasts, and the fact that it changes forms dramatically on the substrates used in this study (See chapter 3) greatly influencing cell behaviour (Cantini 2012, Gonzalez-Garcia et al. 2012, Llopis-Hernandez et al. 2016, Llopis-Hernández et al. 2013, Salmeron-Sanchez et al. 2011, Vanterpool et al. 2014).

FN is a multidomain protein of the ECM consisting of two almost identical FN monomers, each approximately 220–250 kDa in molecular weight. Each FN subunit contains three modules of repeating units, each of which has distinct structures: type I, type II and type III structures (Figure 5.1A). These modules contain binding motifs that are important in facilitating the interaction of FN with cell surface receptors, such as integrins, collagen, LM and gelatin, and intramolecular units that enable self-assembly of the molecule (Singh et al. 2010).

Initial binding of integrin receptors to FN dimers leads to the activation and clustering of these receptors (Figure 5.1B). This clustering promotes further FN-FN intermolecular interactions, and tethering of FN molecules to the cell surface enables cell-mediated contractility to exert force on the FN molecule and to change its conformation. This change in conformation exposes cryptic binding sites within the FN molecule and also enables it to take a form that is more conducive to self-assembly into fibrils and in conversion of fibrils into a stabilize and insoluble form (Figure 5.1C) (Frantz et al. 2010, Singh et al. 2010). It has been shown that FN force-dependent unfolding (stretching of a single) exposes its cryptic integrin-binding sites (Klotzsch et al. 2009, Smith et al., 2007). Exposed cryptic integrin-binding results in pleiotropic changes in cellular behaviour and implicate FN as an extracellular mechano-regulator (Frantz et al. 2010, Singh et al. 2010).

FN fibril assembly involves interactions between its RGD (Arg-Gly-Asp) and synergy sequences with corresponding binding sites within cell surface receptors such as integrins. FN is mostly recognized by $\alpha V\beta_3$ and $\alpha_5\beta_1$ integrins. The primary receptor for FN matrix assembly is $\alpha_5\beta_1$ integrin, which binds to the RGD sequence in domain III_{10} and the synergy site in III_9 (Singh et al. 2010). FN self-assembly following integrin binding is mediated by

the N-terminal assembly domain and organizes the actin cytoskeleton to promote cell contractility (Mouw et al. 2014). The assembly of FN matrix impacts tissue organization by contributing to the assembly of other ECM proteins (Mouw et al. 2014, Singh et al. 2010).

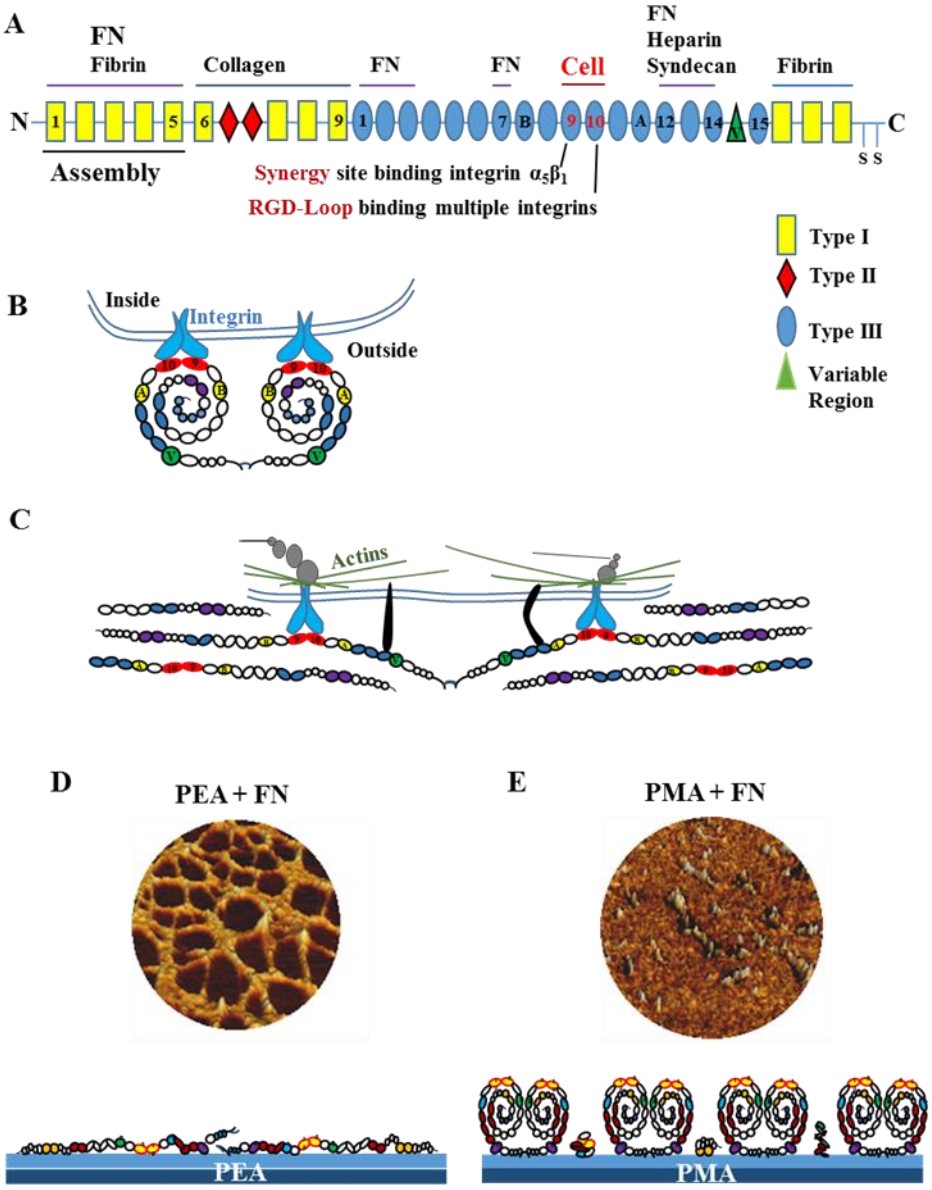

Figure 5.1 Modular protein domain structure of fibronectin. A) FN consists 12 type I modules (Yellow rectangles), 2 type II modules (Red diamonds) and 15–17 type III modules (Blue ovals). Model for the interaction between FN and $\alpha_5\beta1$ in the generation of FN fibrils. The formation of dimer is through a disulphide bond in the C-terminal region. Integrin binding sites are indicated, as well as other binding domains for FN and other proteins. **B**) Compact soluble FN binds to $\alpha_5\beta1$ (Red) via its extracellular domains. The exact organization of FN seems to depend on intramolecular interactions between $III_{2\text{-}3}$ and $III_{12\text{-}14}$, amongst other FN binding sites (blue). **C**) Binding of integrins and other receptors (black bars) to FN induces the reorganization of the actin cytoskeleton (green lines) and leads to the activation of intracellular signalling complexes (circles). Changes in cell shape allow conformational changes in FN exposing previously sequestered FN-binding domains. Fibrils form through FN-FN interactions (modified from (Mao and

Schwarzbauer 2005)). FN forms a (nano)network on PEA via the FNI_{1-5} domains (**D**), whereas a globular conformation on PMA (**E**).

As shows in chapter 3, FN undergoes a conformational change depending on surface properties. It changes from a globular structure on PMA (Figure 5.1E) to an extended structure, a physiological-like fibrillary (nano) networks on PEA (Figure 5.1D). This fibrillar conformation structure has been shown to expose cryptic binding sites within the FN molecule. Using an ELISA, the availability of the RGD (located within $FNIII_9$) cell binding domain has been shown on exposed PEA and PMA and also the PHSRN (located within $FNIII_{10}$) synergy domain more exposed on PEA (Bathawab et al. 2016, Vanterpool et al. 2014). A cell attachment assay including integrin blocking confirmed the availability of the cryptic binding sites (Salmeron-Sanchez et al. 2011, Vanterpool et al. 2014), in accordance with the theory of the exposure of these sites by FN (Klotzsch et al. 2009, Smith et al., 2007). These exposed adhesive patches influence their cell behaviour, as already mentioned above (Llopis-Hernandez et al. 2016, Reilly and Engler 2010, Vanterpool et al. 2014).

5. 5 Aims and Objectives

The objective of this chapter was to study whether the biomaterials can alter collagen mutant cells behaviour by overcoming some of the defects caused and rescuing downstream effect of ER stress. Completing our understanding of how these mutations affect cell function/behaviour will provide novel insights into Col4 disease mechanisms and increase our knowledge of Col4 mutations phenotypes.

To provide insight into effects of *COL4A2*$^{+/G702D}$ mutation and whether modification of the matrix can modulate their consequences, this chapter aims to investigate the effect of defined engineered biointerfaces on cell behaviour in *COL4A2*$^{+/G702D}$ cells. To achieve this, these were carried out:

- Analysis of the biomechanical properties of *COL4A2*$^{+/G702D}$ cells.
- Investigation in the secretion of ECM by *COL4A2*$^{+/G702D}$ cells.
- Analysis of the effect of biointerfaces on ER stress due to *COL4A2*$^{+/G702D}$ mutation.

5. 6 Results and Discussions

5. 6. 1 Effect of *COL4A2*$^{+/G702D}$ mutation on proliferation

Cells were cultured on glass and FN-coated PEA and PMA for 7 days. While culturing the fibroblasts, it was apparent that the cultures were markedly different between the control (wild type: WT) and cells harbouring the *COL4A2*$^{+/G702D}$ mutation (MT) after 7 days of culture on glass, PMA and PEA (Figure 5.2A). The WT cells formed dense confluent sheets of cells on the substrates, whilst MT cells shape was often enlarged on all the surfaces, especially glass and PMA-FN. These cells showed formation of patchy populations indicative of cell death, apoptosis. These observations were similar to previous reports of mutant cells on glass only (Murray et al. 2014). Here, it was observed that the MT cells death was reduced by culture on substrates-coated with FN and especially on PEA.

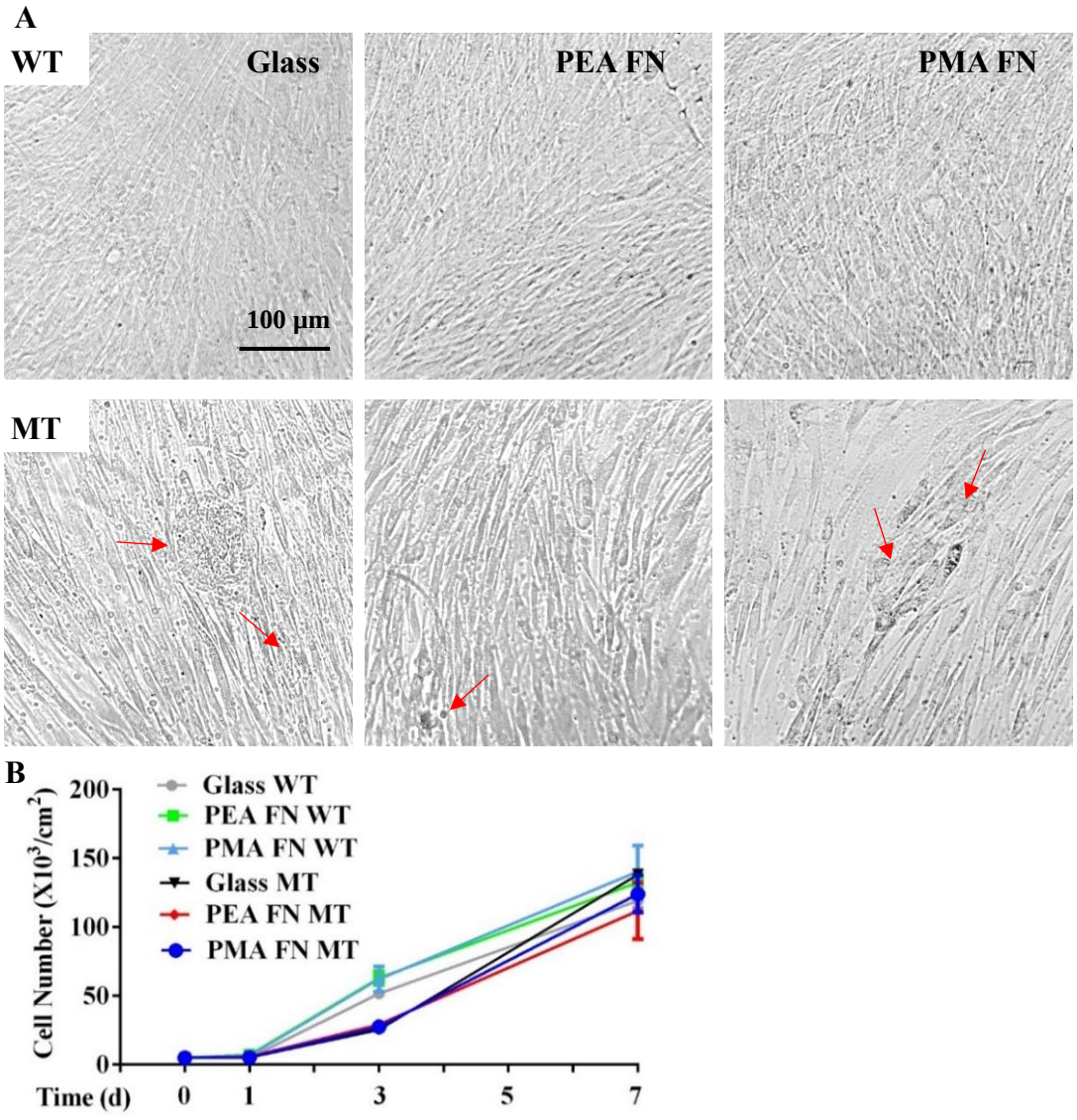

Figure 5.2 Cells morphology and proliferation. A) Light microscopy analysis of the WT and MT fibroblasts on the different substrates at day 7. Red arrows indicate apoptotic MT cells. **B**) Cells proliferation analysis at the different times: 1, 3 and 7 days. No statistically significant differences found an ANOVA test; N =3.

To determine if this apparent apoptosis is accompanied by a reduced cell proliferation, the proliferation rate of the mutant and control cells was measured using haemocytometer counting on cells cultured on glass, PMA, PEA in media containing Asc-2-P to ensure stabilize expression (Geesin et al. 1988) as well as hydroxylation of all collagens (de Clerck and Jones 1980). Consequently, all experiments pertaining to mutant cells have been performed in cell culture media containing ascorbic acid (see material and methods for details). The growth curve revealed a slow growth in the early culture of the mutants (until day 3) (Figure 5.2B) compared to the WT cells consistent with previous observations (Murray et al. 2014). After 3 days, mutant cells were observed proliferating at the same rate as the control cells on all substrates. This suggested that mutant cells have a slow proliferation rate at early time yet recover with time independent of the surfaces. This could be that the MT cells increase their proliferation rate once they reach confluency, assisted by the cell-cell interaction as this is critical to the development and function of multicellular organisms.

5. 6. 2 Matrix study of the mutant cells

Col4 is specific to the BM (Timpl and Aumailley 1989) and provides structural support to tissue including the vasculature. Any alteration in the triple helix caused by the *G702D* mutation is likely to modify the 3D structure resulting in its retention in the ER or if secreted its interaction with other ECMs proteins may be affected. As the *COL4A2* mutation causes protein mis-folding, this leads to ER-stress (due to protein retention) and BM defects due to mutant protein incorporation and/or reduced incorporation due to ER retention (Jeanne Marion et al. 2012, Murray et al. 2014, Van Agtmael et al. 2010, Van Agtmael et al. 2005).

Therefore, experiments were performed to determine the effects of our engineered biomaterial interfaces on the ability of *COL4A2*$^{+/G702D}$ mutant cells to secrete Col4a2. Pilot experiments were performed with WT primary fibroblasts to optimise the assay (Chapter 4) which indicated that Col4a2, FN and LM secretion increased with time (1, 3, 5 7 days) without major differences on both polymer interfaces. It showed that WT cells cultured on FN coated polymers especially PEA secreted higher amount of Col4a2 that was comparable to the amount secreted on glass, while it was lower on PMA-FN.

After optimisation of the protocol, experiments were then performed with mutant and WT fibroblast cells. Cells were seeded on bare glass and on PEA and PMA-coated with the ECM proteins Col4, FN and LM and incubated for 1 and 7 days after which immunocytochemistry (ICC) was performed for the ECM proteins.

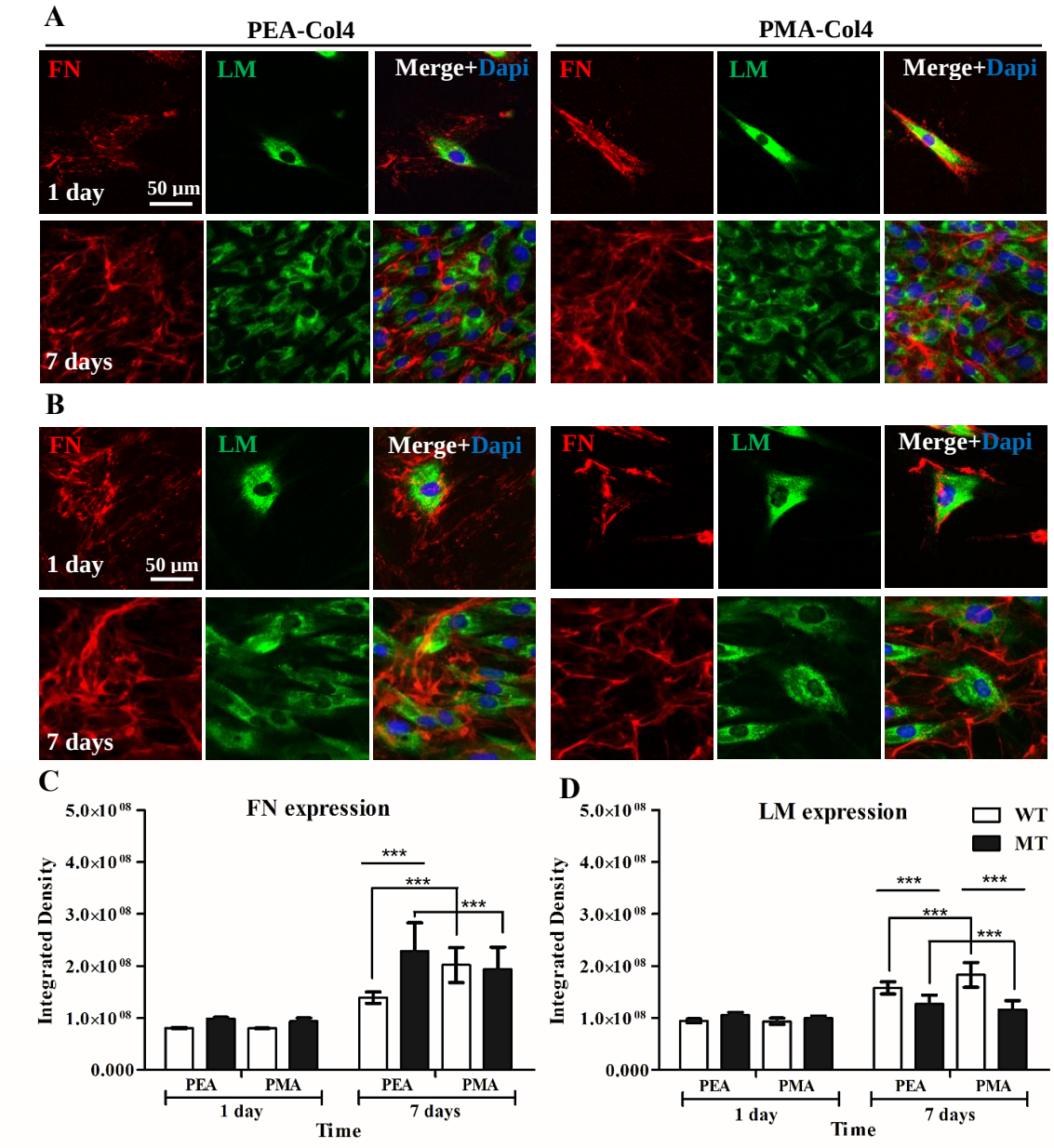

Figure 5.3 Secretion of FN and LM by WT (A) and mutant fibroblasts (B) on PEA and PMA substrates-coated with Col4. Cells were grown on PEA and PMA substrates-coated with Col4 50 µg/mL for 2h under serum free conditions; then with serum before fixation at different time points (1 and 7 days). Cells were also simultaneously stained with nucleus (Blue). Bars: 50 µm. Quantification of expressed FN (**C**) and LM (**D**) on Col4-coated polymers. Integrated density measurements (of whole image) at different time intervals performed with Image J. WT, wild type cells; MT, *COL4A2*$^{+/G702D}$ fibroblasts. Data presented as mean ±SD, N ≥10; and analysed with an ANOVA test;

***p<0.001; only differences that apply to the hypothesis, between the WT and the MT cells on the different substrates, are shown.

Matrix secretion on Col4 interfaces. Immunostaining for FN and LM in cells on Col4-coated PEA and PMA was performed for WT and for mutant (MT) cells (Figure 5.3A-B). FN was stained and formed fibril-like structures on the substratum for both cell types and substrates. LM showed staining only where cells adhered and did not formed fibril-like or network structures with time compared to FN. Staining showed low co-localisation of the two proteins. Analysis of fluorescence intensity of immuno-stained images (Berthod et al. 2006, Prewitz et al. 2015) showed that both proteins increased highly in secretion with time, in MT and WT cells (Figure 5.3C) for FN and (Figure 5.3D) for LM. These results correlate with other studies (Llopis-Hernández et al. 2013, Sillat et al. 2012). The MT cells showed a significant increase in FN secretion on PEA at day 7 than on PMA compared to the WT cells. After 7 days of culture, the amount of secreted LM was observed to be lower for the MT in comparison to WT on both substrates. Since the surfaces were coated with Col4, secreted Col4a2 was not stained as this would have stained both coated and secreted proteins with our available antibodies. At the time, there were limited resources to counter-stain with antibodies raised in different host, making this analysis not feasible.

Matrix secretion on FN interfaces. Cells were stained for Col4a2 and LM (Figure 5.4). At day 1, LM staining was mainly where the cells were located, while little staining was obtained for Col4a2 in both cell types. At day 7, the images showed LM remaining where cells were located, while Col4a2 was seen secreted by the WT on both polymers. *COL4A2*$^{+/G702D}$ mutant fibroblasts also secreted Col4a2 on both polymers. LM and Col4a2 did not appear to highly co-localise. The secreted Col4a2 was seen forming well defined network structures on PEA and PMA at day 7 for both cell types.

Quantification of the secreted proteins showed similar integrated density values of LM for both cell types and on all surfaces on day 1, and values increased with time at 7 day, being higher on glass than on the FN-coated polymers (Figure 5.4C). The MT cells values showed a significantly lower amount of secreted Col4a2 on glass at day 1 and 7 for compared to the WT (Murray et al. 2014). However, when cultured on the biomaterials, increased levels of Col4a2 were detected in the MT compared to WT at day 7. Thus, culturing on these biomaterial surfaces increased significantly Col4a2 deposition with highest levels on PEA-FN (Figure 5.4D). The secretion of Col4a2 increased with time from 1 to 7 days; this is in line with previous reports (Sillat et al. 2012). As reported in the literature, mutant *Col4a2*

causes mis-folding, accumulation and retention in the ER resulting in reduced secretion and BM defects (Jeanne Marion et al. 2012, Murray et al. 2014, Rannikmae et al. 2015, Van Agtmael et al. 2010, Van Agtmael et al. 2005). And results by Murray and colleagues showed that Col4a2 secretion by mutant cells was significantly lower compared to the WT when cultured on glass and tissue culture plastic (Murray et al. 2014).

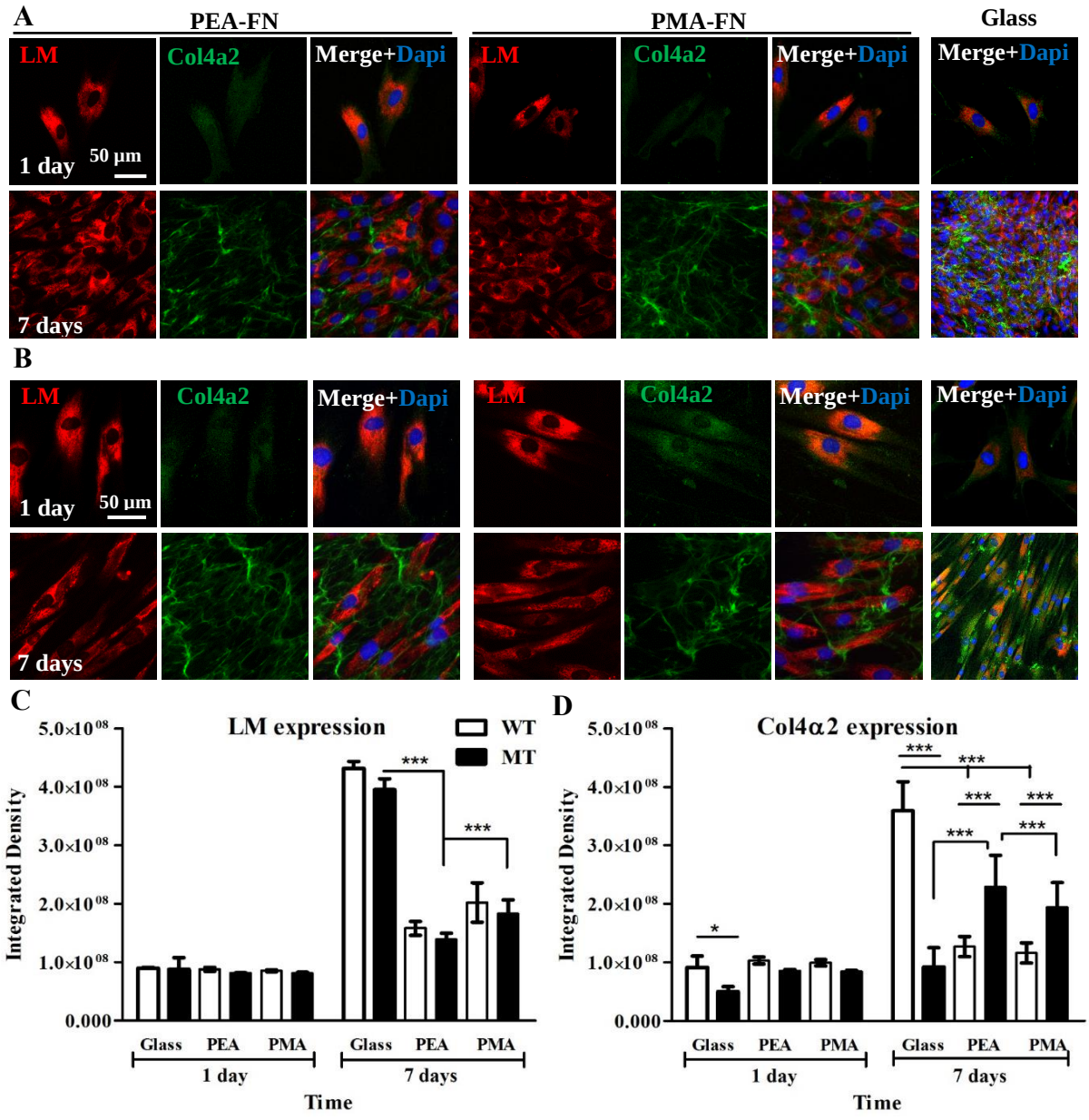

Figure 5.4 Secretion of LM and Col4a2 by control (A) and mutant fibroblasts (B) on PEA and PMA-coated with FN. Cells were grown on PEA and PMA substrates-coated with FN 20 µg/mL and on glass for 2 h under serum free conditions; then with serum before fixation at different time points (1 and 7 days). Cells were also simultaneously stained with nucleus (Blue). Bars: 50 µm. Quantification of expressed LM (**C**) and Col4a2 (**D**) using integrated density. WT, wild type; MT, *COL4A2*$^{+/G702D}$ fibroblasts. Data presented as mean ±SD, N ≥10; and analysed with an ANOVA test; *p < 0.05; ***p<0.001; only differences that apply to the hypothesis, between the WT and the MT cells on the different substrates, are shown.

Thus, these observations are interesting and unprecedented. This is a great phenomenon observed here; culture of the mutant cells on engineered biointerfaces especially coated with FN induced statistically higher secretion of Col4a2 at day 7 (Figure 5.4D) compared to when grown glass. This could suggest that the coated FN on the substrates and particularly PEA affects mutants' behaviour in a particular manner. These two synthetic polymers are known to have similar physicochemical properties modulating ECM proteins adsorption, conformation and distribution as shown in chapter 3 (Cantini 2012, Llopis-Hernández et al. 2013, Salmeron-Sanchez et al. 2011, Vanterpool et al. 2014). In turn, these material-driven FN fibrillogenesis have a wide role in cells behaviour, cell adhesion, proliferation, differentiation and many other biological processes (Salmeron-Sanchez et al. 2011, Vanterpool et al. 2014).

Observations made in this study for the significant secretion of Col4a2 by the mutants grown on FN-coated substrates may be that FN, that assembled into fibrillary networks on PEA, is likely to present the cells with an environment that allows them to possibly change signalling pathway that control protein synthesis process (folding, secretion). In addition, the formation of FN networks on PEA is known to expose cryptic integrin-binding sites binding sites (Bathawab et al. 2016, Frantz et al. 2010, Singh et al. 2010, Vanterpool et al. 2014) like the cell attachment domain (RGD sequence) to the mutants allowing changes in cell behaviour. FN fibrillary network structures on PEA might modulate the protein signalling pathway of Col4a2 of the mutant cells, even though, these remain widely speculative until further analysis of the signalling pathway (MAPK/ERK pathway) is examined (Chapter 6).

Given the apparent formation of a Col4a2 network (Sillat et al. 2012) with features of fractals, possible fractal dimensions were investigated for the two substrates. Fractal dimension analysis of secreted Col4a2 showed values higher on PEA-FN for the MT cells compared to the WT cells without significance difference, but the values were similar on PMA-FN for both cell types (Figure 5.5). Similar observations have been shown by growing cells on orientated PEA fibres, spatially organised secreted FN matrix were observed along oriented fibres and an altered arrangement on random ones (Gugutkov et al. 2009). While secreted FN and Col4 formed network-like scaffolding, LM did not form any. Furthermore, it did not present fractal feathers. The secreted Col4a2 on glass by the MT cells did not form network structures that fractal dimensions could be analysed.

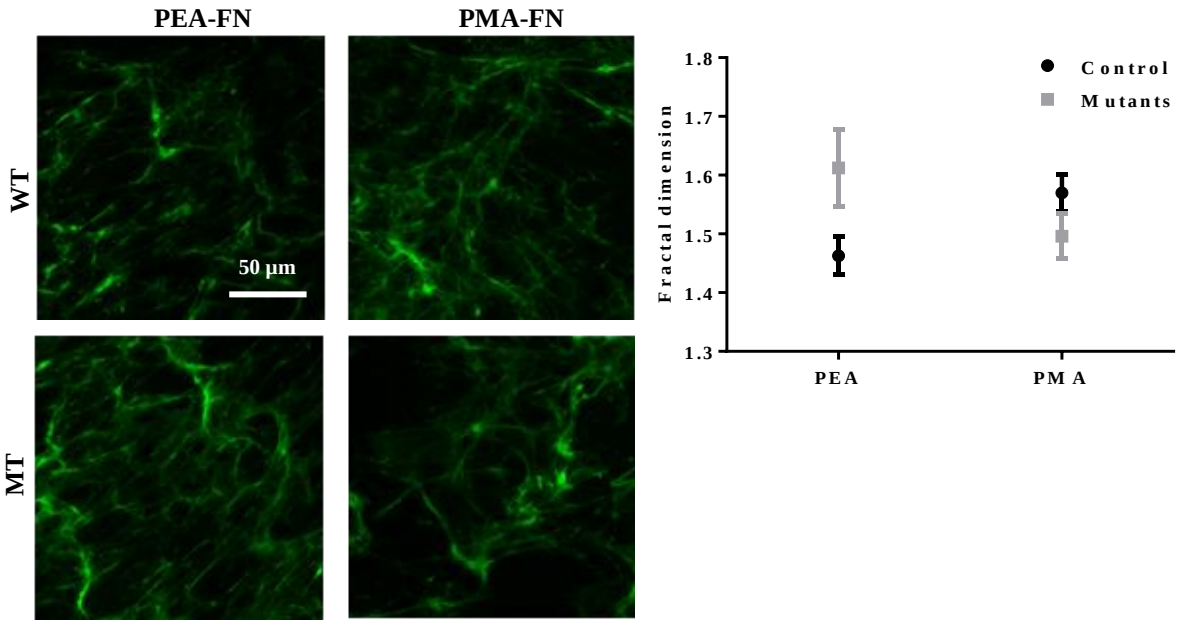

Figure 5.5 Fractal dimension analysis of secreted Col4a2 at day 7 in images from Figure 5. 4.

Matrix secretion on LM interfaces. Furthermore, matrix secretion was analysed on substrates-coated with LM. At day 1, FN was secreted by both cells types and the mutants were observed to have secreted more on PMA with a similar trend on PEA, while there was little Col4a2 secretion (Figure 5.6A-B). At day 7, there was a large presence of secreted FN by both cells on both polymers.

Quantification of the integrated intensity showed higher FN secretion by mutants on both surfaces, also increasing with time (Figure 5.6C). This observation was similar with the FN secreted by mutants when cultured on the Col4 interface (Figure 5.3C). Interestingly on the other hand, quantification of Col4a2 showed low secretion with little increase over time (Figure 5.6D). These observations are striking as when the cells were cultured on FN interfaces, Col4a2 was observed in a large amount with time.

It is noteworthy that Col4 is not fibrillar collagen and characteristically it is seen in the BMs where it assembles in a sheet-like structure providing the major structural support for organ-specific cells (Coelho et al. 2013, Coelho et al. 2011a, b, Hudson et al. 1993, Poschl et al. 2004). Col4a2 was observed rearranged into network structures on the substrates, suggesting that the driving force for Col4a2 reorganization is the association with FN fibrils. It also co-localised with FN confirming active involvement of FN in the reorganization process. Indeed, the association between Col4a2 and FN is not surprising, as a FN molecule has at least two binding sites for collagens (Larsen et al. 2006, Mao and Schwarzbauer 2005) and

corresponding binding sites for FN have been identified on the collagen molecule (Coelho et al. 2013, Sottile and Hocking 2002, Velling et al. 2002, Zoppi et al. 2004).

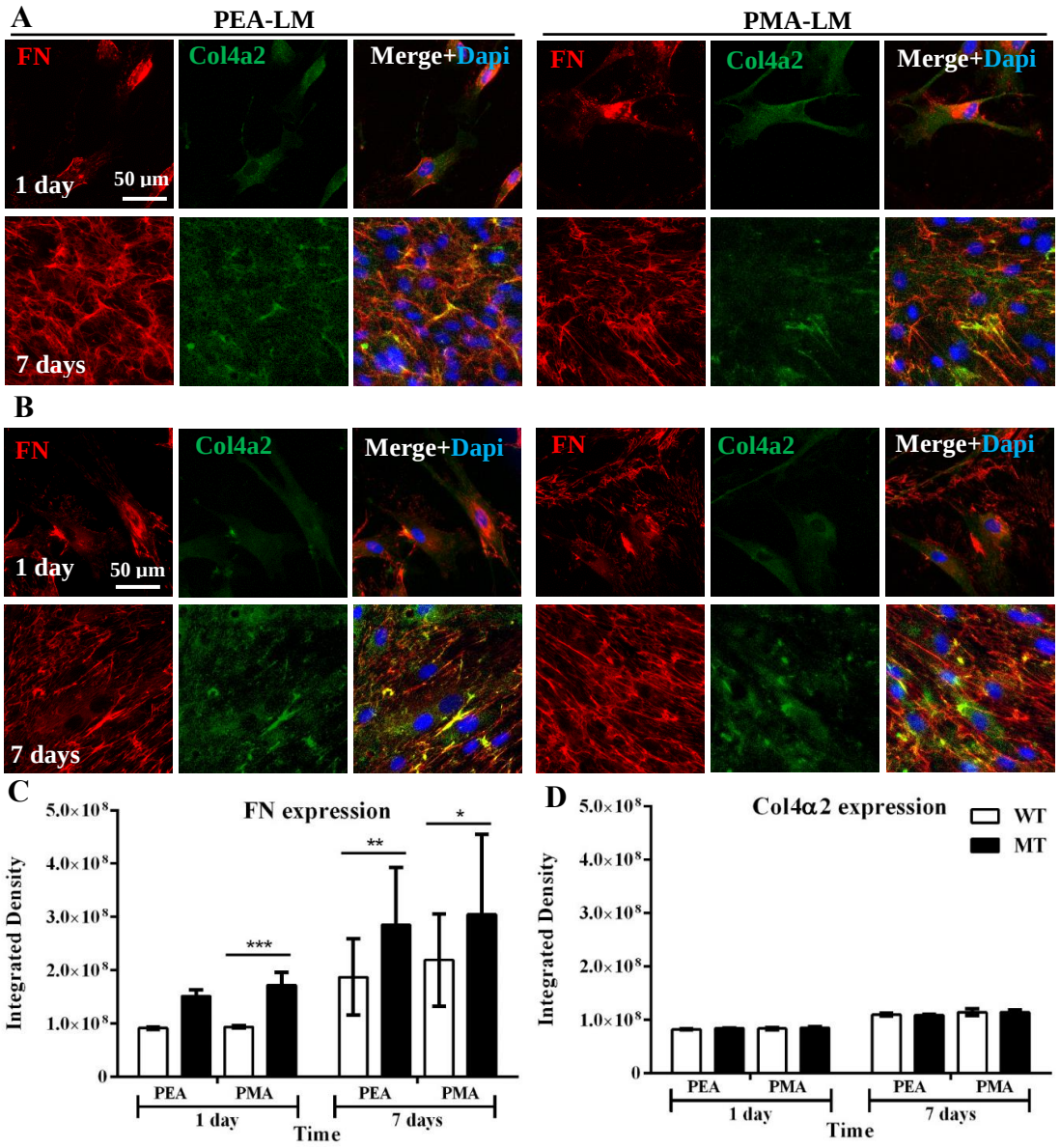

Figure 5.6 Secretion of FN and Col4a2 by control (A) and mutant fibroblasts (B) on PEA and PMA-coated with LM. Cells were grown on PEA and PMA substrates-coated with LM 20 µg/mL for 1 and 7 days. Quantification of expressed FN (**C**) and Col4a2 (**D**) on LM-coated polymers. WT, wild type cells; MT, *COL4A2*$^{+/G702D}$ fibroblasts. Analysed with an ANOVA test; *p<0.05, **p<0.01, ***p<0.001; only differences that apply to the hypothesis, between the WT and the MT on the different substrates, are shown. N ≥15.

FN involvement is supported by its characteristics. FN is synthesized by many types of cells, including fibroblasts, which assemble it into a fibrillar network. FN undergoes conformational changes during assembly that expose FN-binding sites and promote intermolecular interactions important for the fibril formation. Of course, the role of other matrix proteins like LMs or any other ECM component cannot be excluded. Particularly for

LM, studies have shown that it tends to form a joint network with Col4 upon adsorption, which could significantly affect the process of remodelling (Coelho et al. 2013, Coelho et al. 2011a, b).

5. 6. 3 FN-coated substrates effect on mutant cells

Since the layer of fibrillar FN network on PEA induced the high secretion of Col4a2 in mutant cells, it was decided to perform the rest of experiments on FN (20 µg/mL) coated substrate polymers in order to get an understanding of this phenomenon. As observed in chapter 3 and in (Figure 5.1) PEA and PMA modulate FN adsorption, conformation and distribution; and differences in conformation result in cell differential cell behaviour. Coated FN takes a globular structure PMA (Figure 5.1E) to extended fibril network on PEA (Figure 5.1D). The physiological-like fibrillary (nano) networks on PEA allows FN to exposes cryptic binding sites within the FN molecule. Exposed cryptic integrin-binding results in pleiotropic changes in cellular behaviour and implicate FN as an extracellular mechano-regulator (Frantz et al. 2010, Singh et al. 2010). This could explain why FN induces the secretion of Col4a2 in the MT cells. This is to say that the physiological-like fibrillary (nano) FN networks on PEA induce an alleviation mechanism in the mutant cells to overcome the effect of the mutation.

To directly assess extracellular Col4a2 staining without detecting intracellular protein, the cells were stained for laminin and Col4a2 without permeabilisation. This is important as the mutation is known to cause intracellular retention of collagen. Figure 5.7 showed results similar as seen in (Figure 5.4). Col4a2 formed fibril-like network on day 7 on all the substrates, while LM did not; furthermore, the two proteins showed co-localisation on all the surfaces by both cell types. Quantification of Col4a2 showed higher secretion by mutant cells with time (1 to 7 days) and especially on FN-coated PEA compared to secretion on glass and FN-coated PMA (Figure 5.7B). The WT cells also secreted higher Col4a2 and LM with time. This showed that the coated FN ECM on PEA induced Col4a2 secretion in mutants.

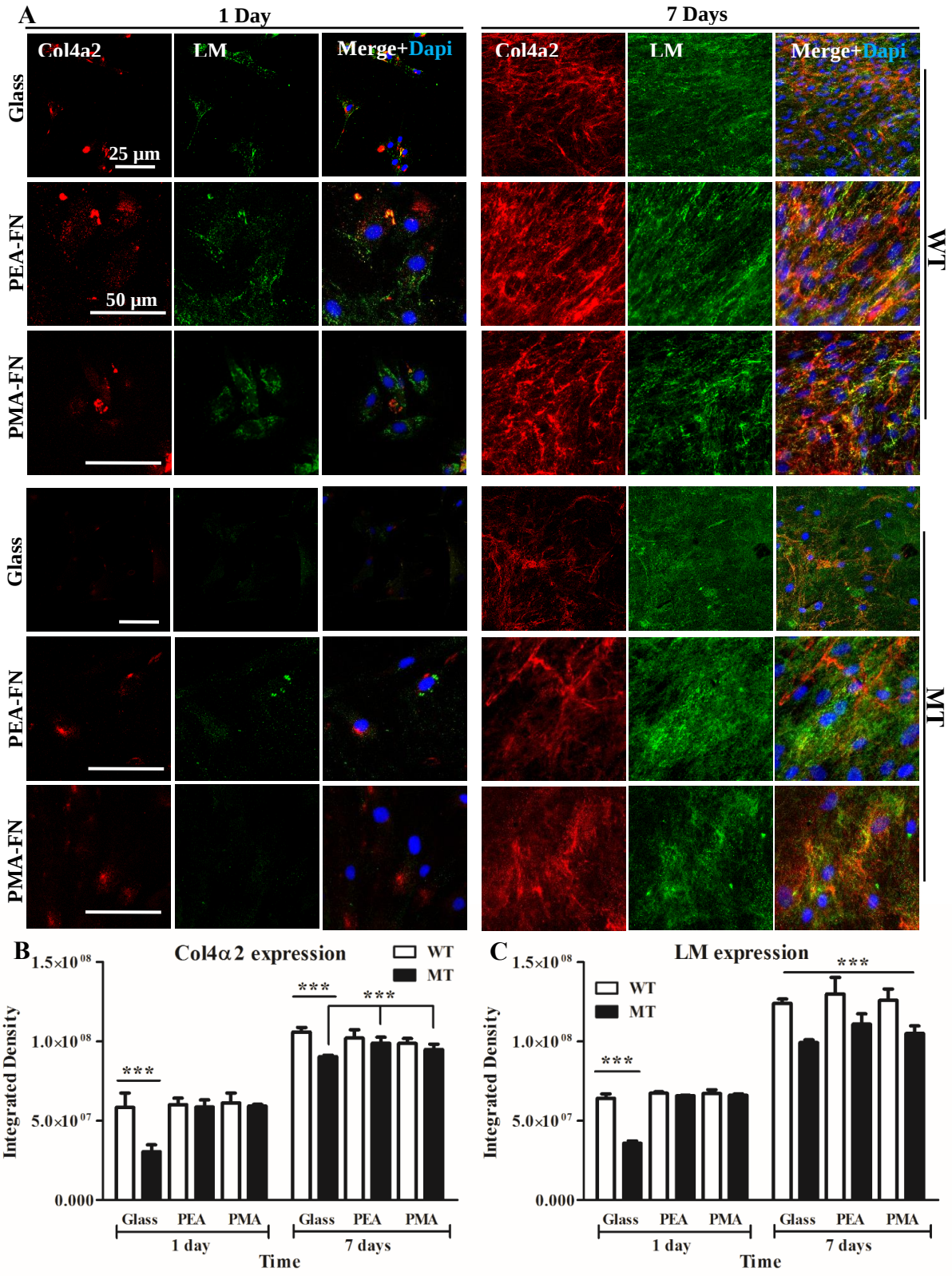

Figure 5.7 Quantification of secreted Col4a2 and LM by control and mutant fibroblasts on PEA and PMA-coated with FN with no permeabilisation. A) Cells were grown on PEA and PMA substrates-coated with FN 20 µg/mL for 2 h under serum free conditions; then with serum before fixation at different time points (1 and 7 days). Cells were not permeabilised before staining in order to only stain for extracellular proteins. Quantification of expressed Col4a2 (**B**) and LM (**C**). Integrated density measurements (of whole image) at different time intervals performed with ImageJ. WT,

wild type; MT, *COL4A2*$^{+/G702D}$ fibroblasts. Data presented as mean ±SD, N ≥10; and analysed with an ANOVA test; ***p<0.001.

Furthermore, secretion of Col4a2 was quantified for culture with and without serum (Figure 5.8). Col4a2 secretion by both WT (Figure 5.8A) and MT (Figure 5.8B) cells was similar despite the absence of serum at early time (1 day); although at day 7 the secretion of Col4a2 was higher for culture supplemented with serum. Secretion of LM also followed the same trend (Figure 5.8C-D); with similar secretion at day 1 but higher for serum supplemented culture of both WT (Figure 5.8C) and MT cells (Figure 5.8D).

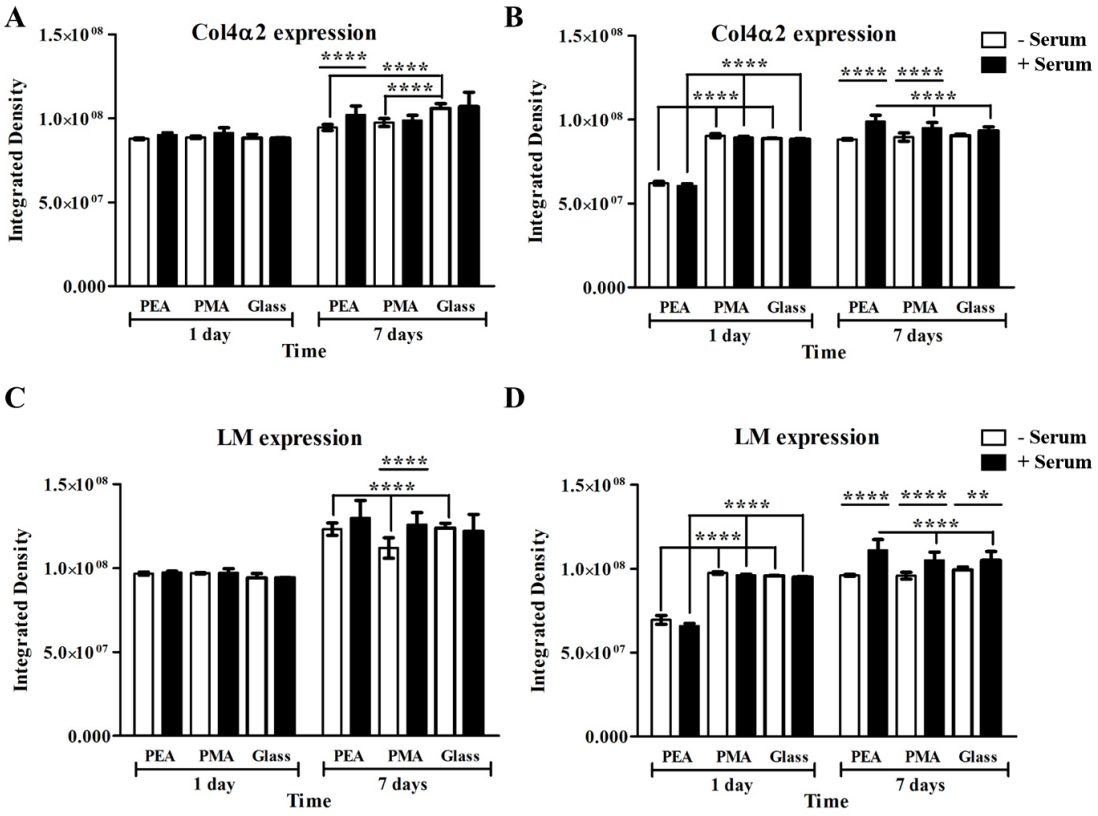

Figure 5.8 Quantification of secreted Col4a2 in mutants cultured with and without serum. Col4a2 and LM in WT fibroblast (**A** and **C**) and mutants (**B** and **D**) cultured on FN-coated polymers for 1 and 7 days with and without serum fixed and stained without permeabilisation. Integrated density measurements of images from Figure 5.7 including images of samples cultured without serum performed with ImageJ. *p<0.05, **p<0.01, ***p<0.001, ****p<0.0001; N-number: <10.

Quantification of secreted Col4a2 using other assays. Cells cultured for 7 days reached a high confluence, and staining of ECMs without permeabilisation may not allow the observation of secreted ECMs located under the thick layer of cells. Therefore, a decellularization assay was employed to quantify the secreted Col4a2. ECMs scaffolds derived from cultured cells have been extensively studied for use in tissue engineering, and

several methods have been developed to prepare cultured cell-derived ECM scaffolds (Lu et al. 2012, Robinson and Gospodarowicz 1984). Decellularization treatments with 2 M or 8 M urea for 10 minutes, 0.1% Triton™ X-100 (TX100) for 5 min, and 20 mM ammonium hydroxide (NH_4OH) for 5 min were used to remove all cellular material except the insoluble ECMs (Robinson and Gospodarowicz 1984). The different treatments were used in order to optimise which method most successfully remove cellular components.

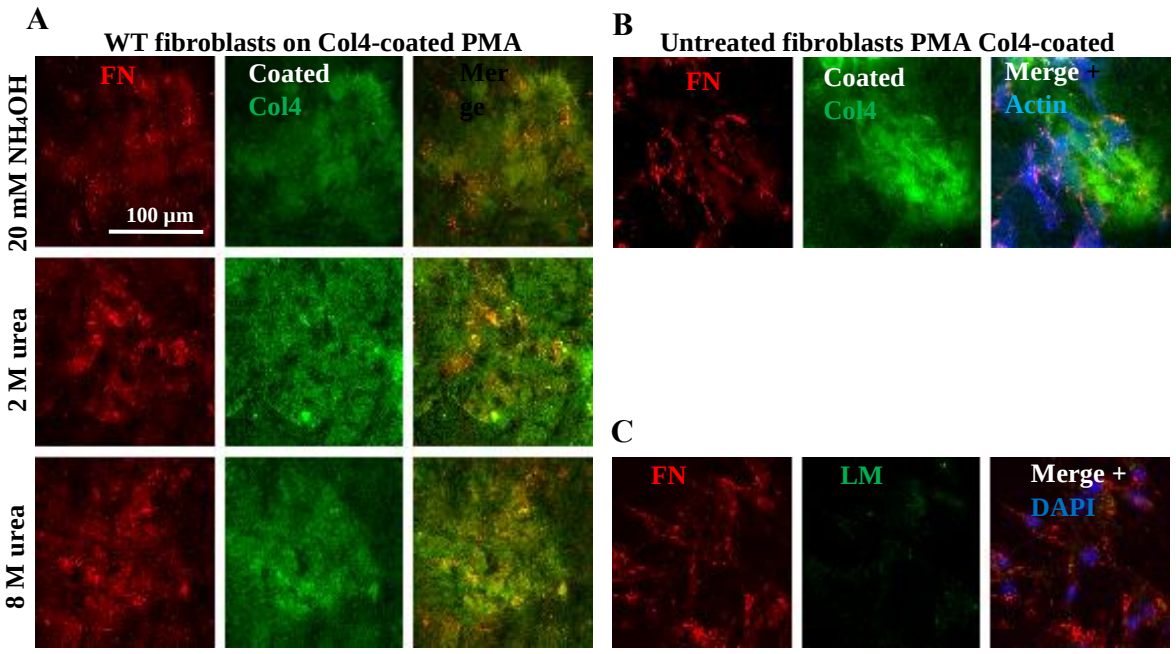

Figure 5.9 Optimisation of cell removal without disturbing the coated and secreted matrix. (A) WT fibroblasts were cultured on Col4-coated PMA for 1 day and then the cells were removed by the indicated treatment, 20 mM NH_4OH for 5 min, 2 M or 8 M urea for 10 minutes, then stained for the coated Col4 and secreted FN; staining with DAPI was used to confirm removal of cell nuclei. For control conditions, cells were not treated and stained in similar manner (**B**) or LM **(C)**. 0.1% Triton™ X-100 results not shown, but were similar.

To screen for cellular material after the various extractions, samples were stained for DAPI to confirm the removal of cell nuclei. The coated Col4 was also stained in order to observe if treatment affected the deposited protein structure, knowing in advance the structure of Col4-coated on these polymers (Ha Tran Le Bao et al. 2013). The secreted FN was stained to observe the intact structure of secreted ECM. Figure 5.9A showed successful removal of cells from the surface polymer (PMA) without the disturbance of the coated Col4 protein nor the secreted FN, compared to the untreated samples (Figure 5.9B-C). The secreted FN protein also appeared similar as in untreated samples. These observations confirmed that these treatments can remove cellular components from a surface without disturbing the

coated or secreted matrix. Therefore, the decellularization method with NH_4OH was used for further investigation.

Secreted Col4a2 and LM by both cell types cultured on FN-coated PEA and PMA substrates were stained and the integrated density quantified (Figure 5.10A-B). The samples showed a well-defined network of Col4a2 and LM on the interfaces as seen with non-decellularised samples. Despite decellularization, Col4a2 still displayed network structures. No obvious DNA staining were observed after treatment with NH_4OH. The MT cells secreted LM in lower amount than WT cells. Quantified Col4a2 showed similar secretion on PEA by both cell types but different on PMA as the MT secreted statistically less Col4a2 on the latter. Moreover, the MT secreted significantly higher Col4a2 on PEA than on PMA. In contrary, the WT secreted more Col4a2 on PMA than on PEA. This once more confirms the higher secretion of Col4a2 by the MT on PEA than on PMA.

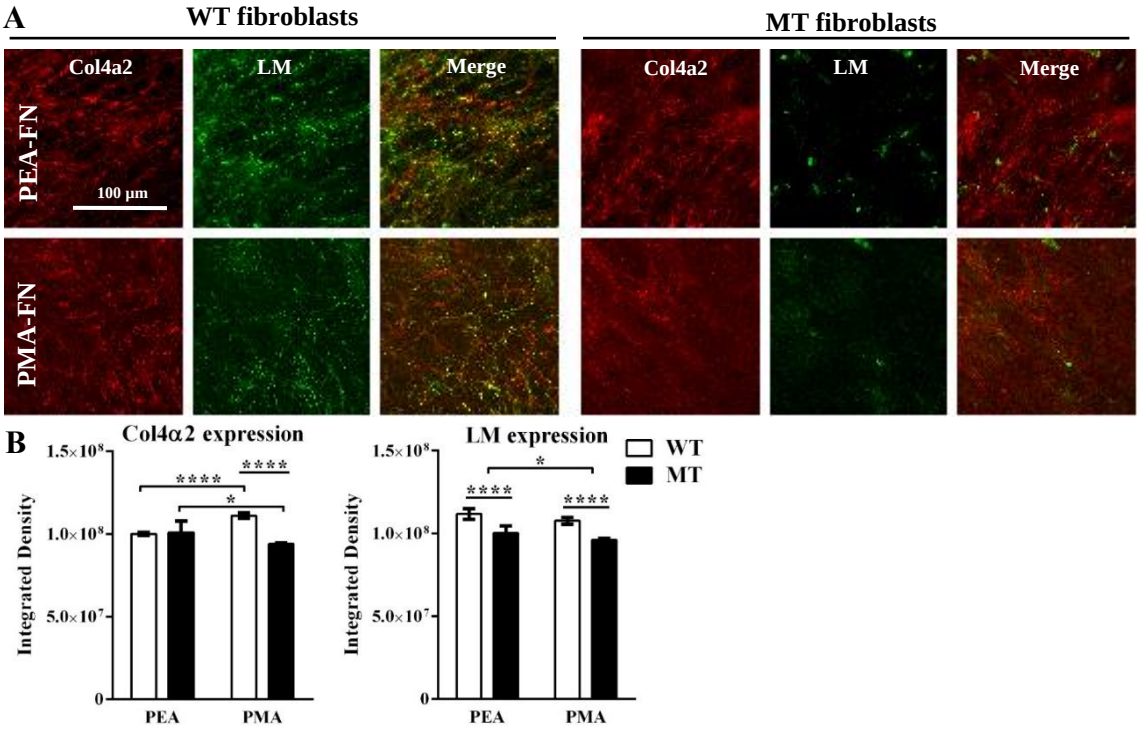

Figure 5.10 Quantification of secreted matrix after decellularization. A) Staining of Col4a2 and LM by control and mutant fibroblasts on PEA and PMA-coated with FN after cells treatment with 20 mM NH_4OH. Human fibroblasts were grown on PEA and PMA substrates-coated with FN 20 µg/mL for 2 h under serum free conditions; then with serum before fixation after 7 days. Cells were also simultaneously stained with DAPI as a nuclear stain (But none could be stained). **B**) Quantification of expressed Col4a2 and LM in WT and MT cells cultured on FN-coated polymers. Integrated density measurements at different time intervals performed with ImageJ. Data presented as mean ±SD, N ≥5; and analysed with an ANOVA test; *p<0.05, **p<0.01, ***p<0.001; N=12.

Other assays were employed to confirm the higher secretion of Col4a2 on FN-coated PEA substrate by mutant *COL4A2*$^{+/G702D}$ cells. In-cell-western was carried out (Figure 5.11A) for cells cultured on FN-coated substrates for 7 days staining for Col4a2 (Figure 5.11B). Despite not showing any statistical differences, the values showed similar trend as the results shown in figure below. Col4a2 secretion by the MT cells was higher on FN-coated PEA than on glass and PMA. The WT secreted similar amount of Col4a2 on PEA and glass than on PMA.

Likewise, quantification of Col4a2 using an ELISA assay also showed higher values of Col4a2 for MT cells on FN-coated PEA compared to glass and PMA-FN (Figure 5.11C). Similar trend of values was observed with the WT; the WT secreted same amount of Col4a2 on PEA and PMA than on glass. These results further confirm the higher secretion of Col4a2 on FN-coated PEA as observed in the immunofluorescence quantification. The results demonstrate the potential of using biointerfaces as a tool to investigate this mutation. The PEA-FN biointerface can influence the *COL4A2*$^{+/G702D}$ cells to secrete Col4a2 to levels similar to normal cells.

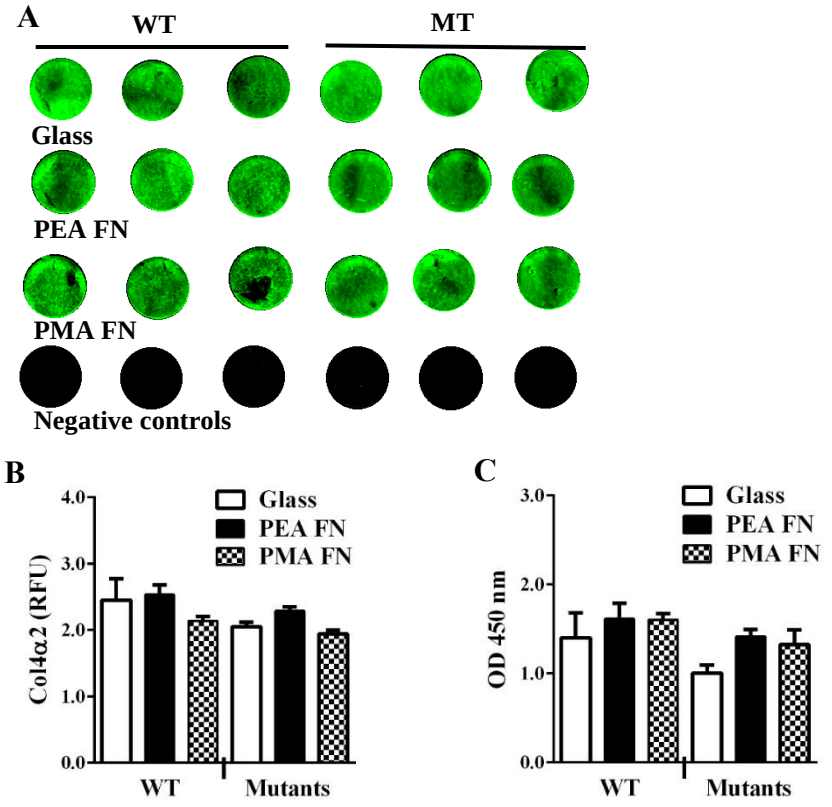

Figure 5.11 Quantification of secreted Col4a2 by mutants. In-cell Western assay for Col4a2 of cells on FN-coated substrates after 7 days culture; fluorescence images of the samples **(A)** and quantifications **(B).** In addition, an enzyme-linked immunosorbent assay (ELISA) was performed for Col4a2 after decellularization of cells cultured on FN coated substrates for 7 days culture **(C).** Negative controls show secondary antibody only and the substrates only. RFU, relative fluorescence units. ANOVA showed no statistically significant differences between samples. Data presented as mean ±SD, N =3.

5. 6. 4 Does FN-coated PEA have lasting effect on mutant cells?

Data so far have shown that mutant *COL4A2*$^{+/G702D}$ fibroblast cells secreted higher amount of Col4a2 on FN coated PEA interface after 7 days culture. However, what remains unknown is whether the mutant cellular disease phenotypes were ameliorated/alleviated. Since these mutant cells began secreting higher amount of Col4a2 on FN-coated PEA, could it be possible that the protein synthesis and secretion process was also altered? Thus, to test whether these cells were relieved from the consequence of Col4a2 accumulation in the ER, the mutant cells were initially cultured on the FN interfaces for 7 days as in all previous experiments; then cells were trypsinized and cultured further on glass for a further 7 days. Samples were then stained for Col4a2 and LM to observe whether cells secreted the protein as the control fibroblast.

Trypsinized mutants previously grown on the FN-coated polymers secreted Col4a2 protein that formed network structures on the new glass surface (Figure 5.12A), although in all previous data MT cells generated Col4a2 with less pronounced network structures compared to the WT cells. LM staining also appeared similar as to the other examples shown in previous figures. Quantification of the fluorescence integrated density of Col4a2 showed higher values for MT cells deriving from PEA-FN compared to glass and PMA-FN.

Secretion of LM also showed similar trend to that of Col4a2. Integrated density showed a higher level of secreted LM on PEA FN by the MT cells compared to PMA FN and glass. Once more like Col4a2, the WT cells secretion of LM on PEA-FN was lower than on PMA-FN and on glass. It is not clear why the WT cell in this case secreted low ECMs on PEA-FN. LM secretion by the MT cells on glass was also lower compared to WT cells.

These observations reflect the previous data presented in this chapter. This suggest that the FN biointerface alter the MT cells behaviour by appearing to allow cells to overcome at least some of the effects of the mutations relating to the intracellular retention of Col4a2. The data also showed that FN-coated PEA had a lasting effect on mutant cells. These biomaterials provided a well-defined microenvironment that allowed the MT to ameliorate/alleviate the cellular disease phenotypes. These are very interesting observations, the *COL4A2*$^{+/G702D}$ cells secreting higher amount of Col4a2 on glass after culture on FN-coated PEA. Hence, the ER stress levels of these mutant cells were investigated to probe whether the level of Col4a2 accumulation was yet affecting these cells.

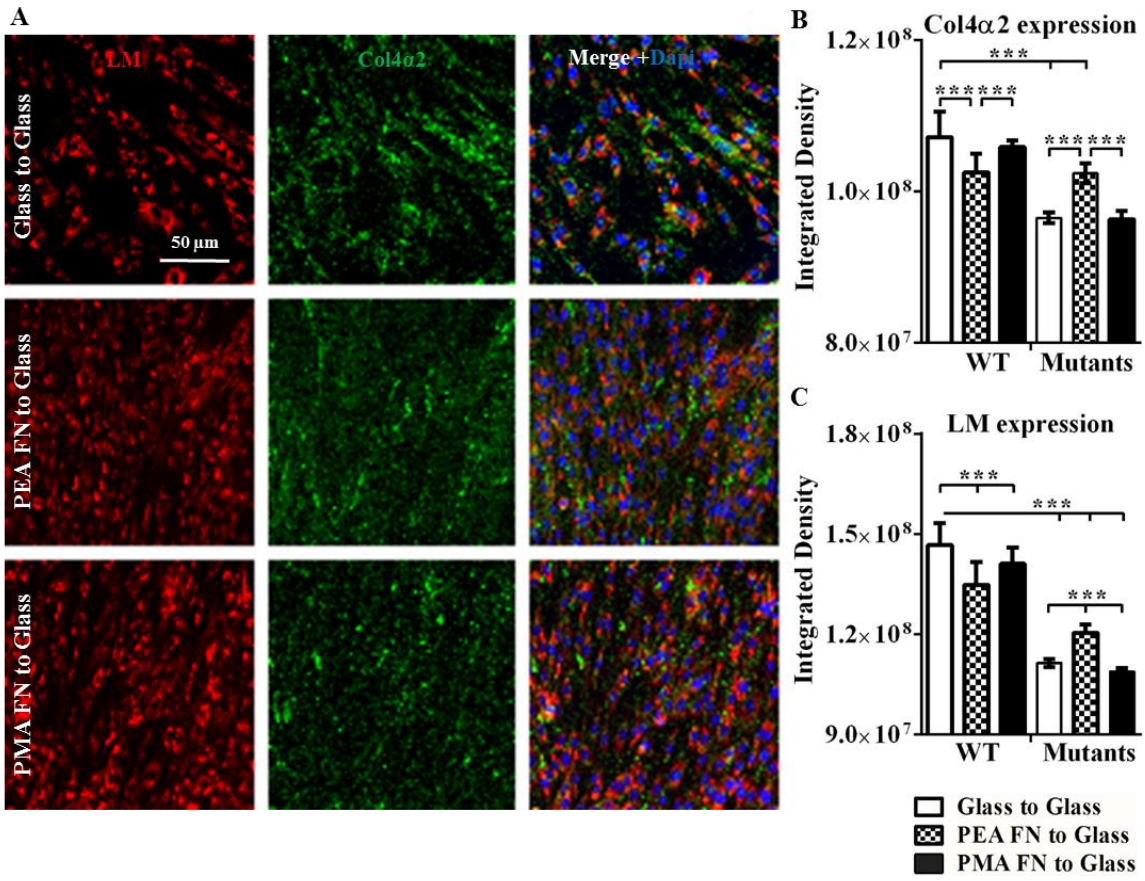

Figure 5.12 Culture of mutants from FN-substrates on glass. Cells were cultured on FN20-substrates for 7 days with serum and then trypsinized and seeded onto new substrates without FN coating for 7 days including serum. (**A**) Immunofluorescence images of Col4a2 and LM expression by mutant fibroblasts on glass after culture on PEA and PMA-coated with FN. Scale bars: 50 µm. Quantification of expressed Col4a2 (**B**) and LM (**C**) in control and mutant fibroblasts. Integrated density measurements using ImageJ (of whole image). Data presented as mean ±SD, N ≥12; and analysed with an ANOVA test; **p<0.01; ***p<0.001.

5. 6. 5 ER stress in *COL4A2*$^{+/G702D}$ fibroblast cells

ER swelling in *COL4A2*$^{+/G702D}$ fibroblasts. Since mutant fibroblasts showed higher Col4a2 secretion on FN-coated substrates, ICC was performed for the ER marker protein disulphide isomerase (PDI) to investigate whether the surfaces were able to reduce ER volume and collagen IV retention in the ER. Staining of PDI was located inside the cells at both time points and for both cell types (Figure 5.13A-B). At day 7, there was co-localisation of Col4a2 with PDI in both cell types, suggesting that despite the higher secretion of Col4a2 on PEA-FN by the MT cells, there could be an amount of accumulated Col4a2 that was contained primarily within the ER. The increased PDI staining in both cell types suggested that these cells contained larger ER areas. Nevertheless, biomaterials appear to modulate protein secretion of the MT cells.

Quantification of PDI integrated density showed higher values for MT cells on all the surfaces particularly on glass compared to the WT at day 1, consistent with previously published data (Murray et al. 2014). However, after 7 days the WT PDI values were higher than that of the MT cells on all the surfaces. The values showed lower PDI staining in MT cells on PEA-FN and PMA-FN compared to glass, suggesting less ER swelling in the mutants on FN-coated substrates.

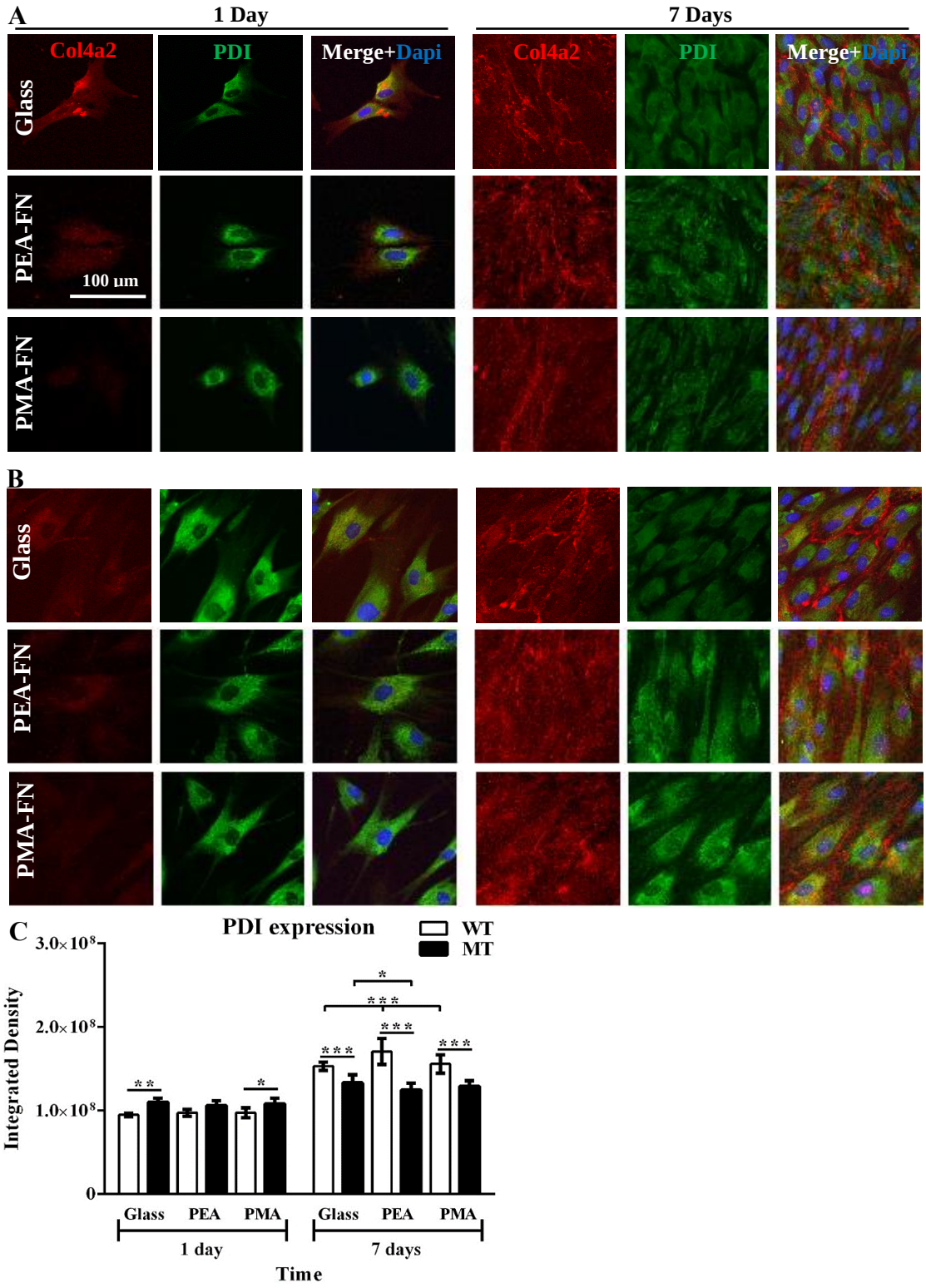

Figure 5.13 Col4a2 and PDI staining. Staining of Col4a2 and PDI in WT (**A**) and MT fibroblasts (**B**), also simultaneously stained with nucleus (Blue). Cells were cultured on PEA and PMA substrates-coated with FN 20 µg/mL then with serum before fixation at different time intervals (1 and 7 days). Quantification of PDI integrated density measurements (**C**) (whole image) performed with ImageJ. Data presented as mean ±SD, N ≥12; and analysed with an ANOVA test; *p<0.05, **p<0.01, ***p<0.001. N≥12.

Basal levels of ER stress in *COL4A2*$^{+/G702D}$ fibroblasts. To investigate whether the decrease in ER volumes observed within the MT cells cultured on the FN interfaces are associated with decreased ER stress levels, the protein levels of chaperones BIP and calnexin were measured using western blot. The two are ER chaperones involved in protein folding and quality control. Both chaperones levels were found to be higher in MT cells cultured on glass compared to the WT confirming that the MT cells undergo ER-stress activation (Figure 5.14A-B) (Jones et al. 2016, Murray et al. 2014). Intriguingly, both BIP and calnexin levels were elevated in both cell types on the FN interfaces.

The elevated levels of the chaperones in both WT and MT cells correlated with the increased amount of secreted Col4a2. As increased chaperone levels elevate protein folding capacity of the cells, this data support the hypothesis that our surfaces may increase protein folding capacity which result in secretion of Col4a2. It was also noticed that MT BIP level on PMA FN was lower than glass.

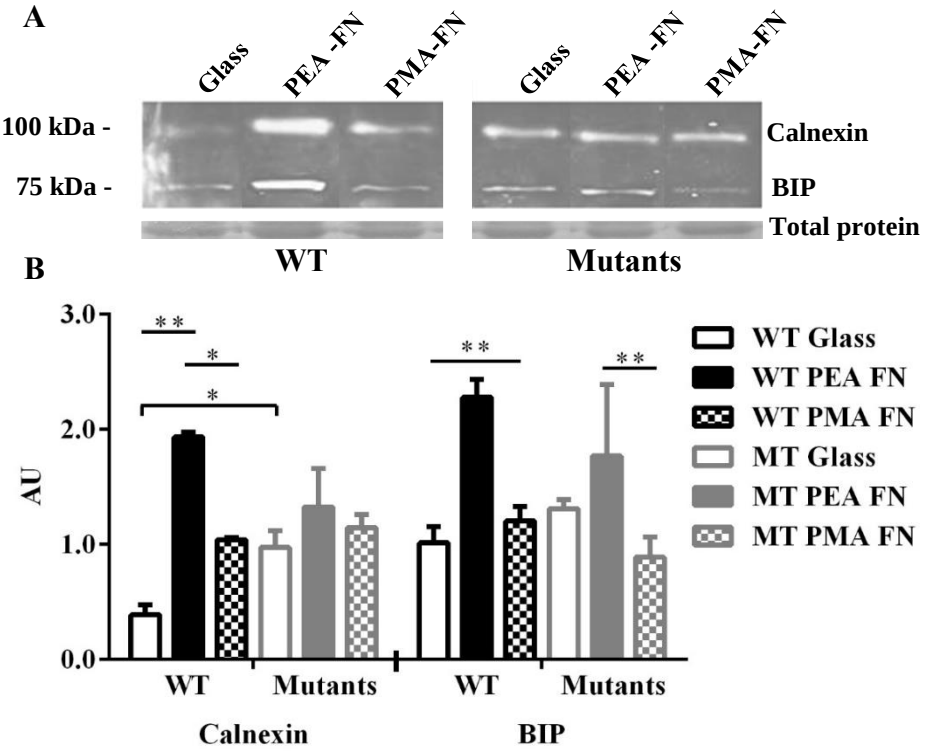

Figure 5.14 Initial analysis of ER stress markers in cells by Western blot. A) Western blot analysis of Calnexin (90 kDa) and BIP (78 kDa) levels in cell lysates from control (WT) and mutant *COL4A2*$^{+/G702D}$ cultured for 7 days; total protein zinc stain from the same lysates. **B**) Densitometry of western blots shown in arbitrary units (AU). WT, wild type; MT, mutant. Data presented as mean ±SD, N =4; and analysed with an ANOVA test; *p<0.05, **p<0.01.

5. 6. 6 Mechanical properties of *COL4A2*$^{+/G702D}$ fibroblasts

Mechanical properties, especially stiffness, of individual cells and their surrounding extracellular matrices (ECMs) play important roles in many biological processes including cell growth, motility, division, differentiation, tissue homeostasis, stem cell differentiation, tumour formation and wound healing (Discher et al. 2005). Cell mechanical stiffness has been demonstrated to be mostly determined by the ECMs and the cytoskeleton, mainly the networks of actin and intermediate filaments and other proteins associated with them. Changes in stiffness of live cells and ECM are often signs of changes in cell physiology or diseases in tissues. Henceforth, monitoring the mechanical stiffness of living cells can provide a novel way to monitor cell physiology, to detect and diagnose diseases, and to evaluate the effectiveness of drug treatments (Thomas et al. 2013).

Among the multitude of methods applied to measure the stiffness of cells and tissues, particle-tracking microrheology, magnetic twisting cytometry, micropipette aspiration and microindentation. The latter using an atomic force microscope (AFM) provides a way to efficiently characterize the micro-scale stiffness for a variety of materials ranging from metal surfaces to soft biological tissues and cells. Few limitations are accounted with this method including uncertainty in contact point determination, applicability of the Hertz model, and the potential to physically damage the cells or soft biological tissues. Microindentation applies an indenter with selected geometry and measure the applied force from the bending of the AFM cantilever. Hence, fitting of the force-indentation curve to the Hertz model for the corresponding tip geometry provides quantitative measurements of material stiffness (Young's moduli).

Elasticity of *COL4A2*$^{+/G702D}$ cells. The mechanical stiffness of cells and ECMs were measured to investigate effect of the mutation on the biomechanical properties of cells and the ECM. Cells were cultured for 7 days on FN-coated substrates then microindentations were performed on living cells (on top the nucleus) in CO_2 independent media with an AFM in contact force mapping mode with a tipless cantilever mounted with a 4.85 µm bead. Figure 5.15A showed the stiffness of the WT and MT fibroblasts. The MT cells were 10-fold softer

than the WT cells on all the surfaces. The stiffness distribution of WT cells population ranged mainly from 500 to 1000 Pa on glass, from 2000 to 5000 Pa on PEA FN, and from 500 to 1500 Pa on PMA FN (Figure 5.15B). Likewise, the stiffness distribution of MT cells population ranged mainly from 10 to 50 Pa on glass, from 100 to 350 Pa on PEA FN, and from 25 to 150 Pa on PMA FN (Figure 5.15C). Relative frequency distribution of stiffness in fractions is shown in (Supplementary Figure S5.1).

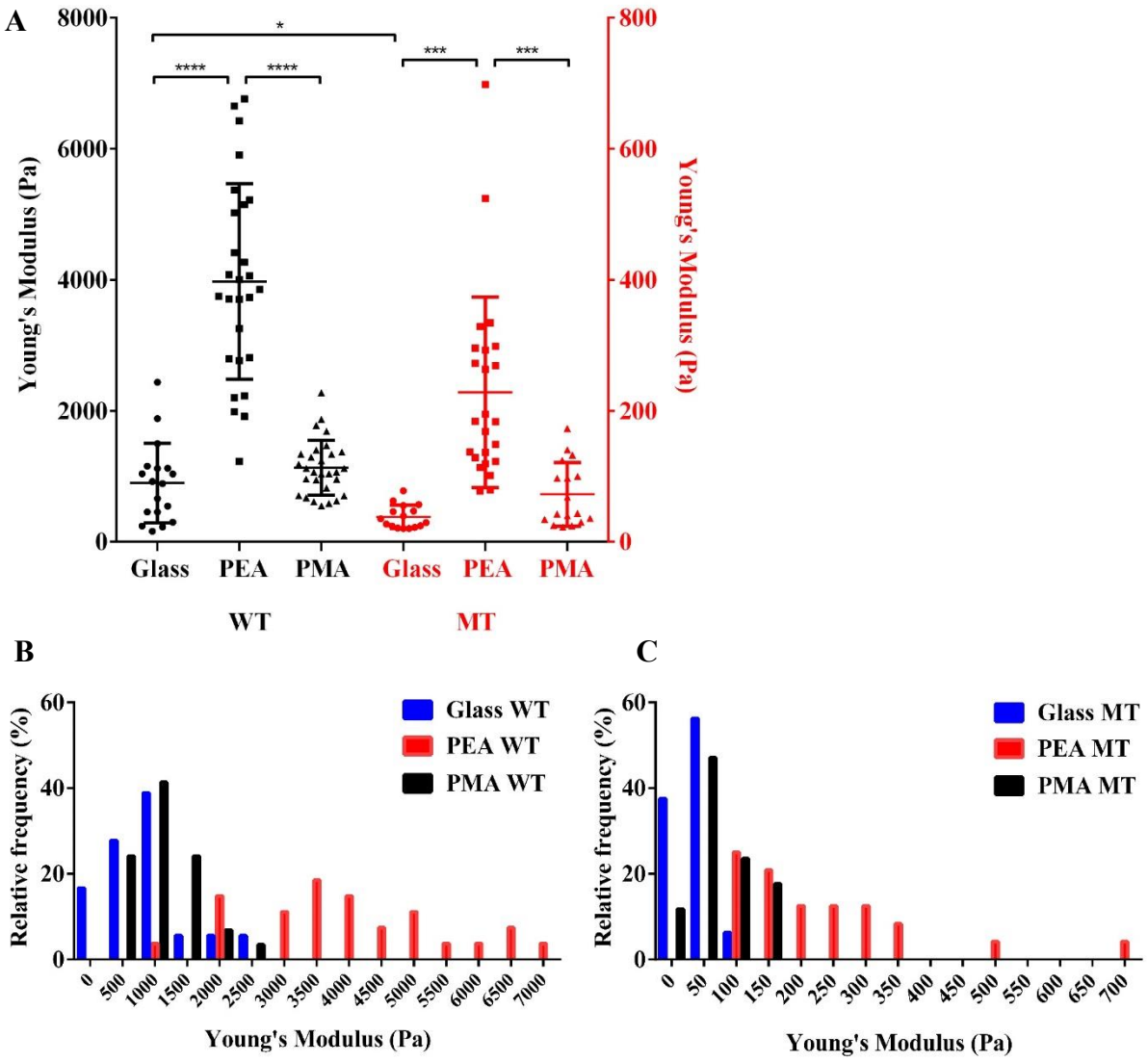

Figure 5.15 Cell stiffness analysis. A) Stiffness of cells on the different substrates using AFM force mapping. Stiffness distribution of WT **(B)** and MT **(C).** Cells were cultured on FN coated substrates for 7 days and then scanned live in media using AFM in contact force mapping mode with a tipless cantilever mounted with a 4.85 µm bead. Data presented as mean ±SD, N ≥12; and analysed with an ANOVA test; *p<0.05, **p<0.01, ***p<0.001, ****p<0.0001; only relevant statistical differences are shown. WT, wild type; MT, mutant cells.

This is the first time the stiffness of the *COL4A2*$^{+/G702D}$ cells has been measured. Culture of these cells on PEA coated with FN seemed to induce significantly higher stiffness than on glass, and even PMA-FN. This is related to the networks of actin and intermediate filaments inside the cells as the mechanotransduction of cells is largely dependent on the cytoskeletal structure and the pre-stress in the cytoskeleton (Ngandu Mpoyi et al. 2016, Wang et al. 2002). Further investigations on cell adhesion behaviours can be found in chapter 6 to correlate how these MT cells adhere on the network forming FN on PEA. The MT cells difference in stiffness compared to the WT cells is an index suggesting that these cells have different behaviours, and in terms of matrix, they may secreted different types of ECMs than the WT cells, as observed by the reduced secretion of Col4 *in vivo* (Jones et al. 2016, Van Agtmael et al. 2010).

Elasticity of ECMs. Thus, AFM measurements of secreted ECMs by the cells were performed. After 7 days culture, cells were decellularised using 20 mM NH_4OH and the intact matrix in PBS were scanned using AFM in quantitative imaging mode. Decellularization for AFM imaging is a delicate process that requires accurate processing and great care in order not to disturb the matrix as it can detach from the surface and begin to float in PBS (Figure 5.16).

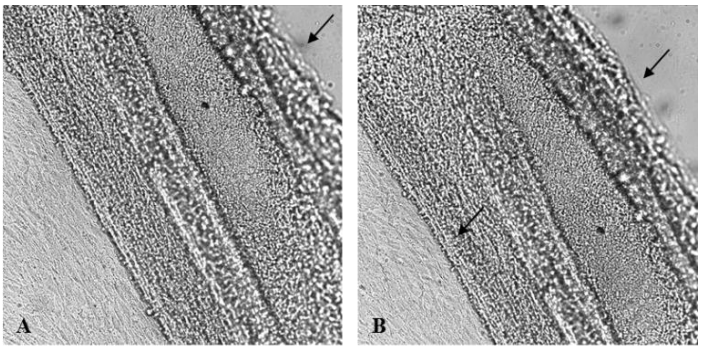

Figure 5.16 Brightfield images of decellularised ECM for AFM scanning. If great care is not observed, the matrix layer will be disturbed. Here is an example of decellularised ECM from WT cells after 7 days culture on glass. The images indicate matrix detachment from the surface and floating from the top right corner and rolling on itself from **A** to **B** (shown by the black arrows).

The Young's modulus of secreted ECMs by the *COL4A2*$^{+/G702D}$ and WT cells was measured by AFM using pyramidal tip (see experimental procedures). Figure 5.17A-C showed AFM image scanning of secreted ECMs by *COL4A2*$^{+/G702D}$ cells after cell decellularization. The average Young's modulus was analysed using the Hertz model on the force curves. The Young's modulus ranged mainly from 4.5 to 14 kPa on glass, 7.5 to 18 kPa on PEA, and 4.3 to 11.5 kPa on PMA (Figure 5.17D). The stiffness of the secreted ECMs by MT cells was significantly higher on PEA than on glass and PMA.

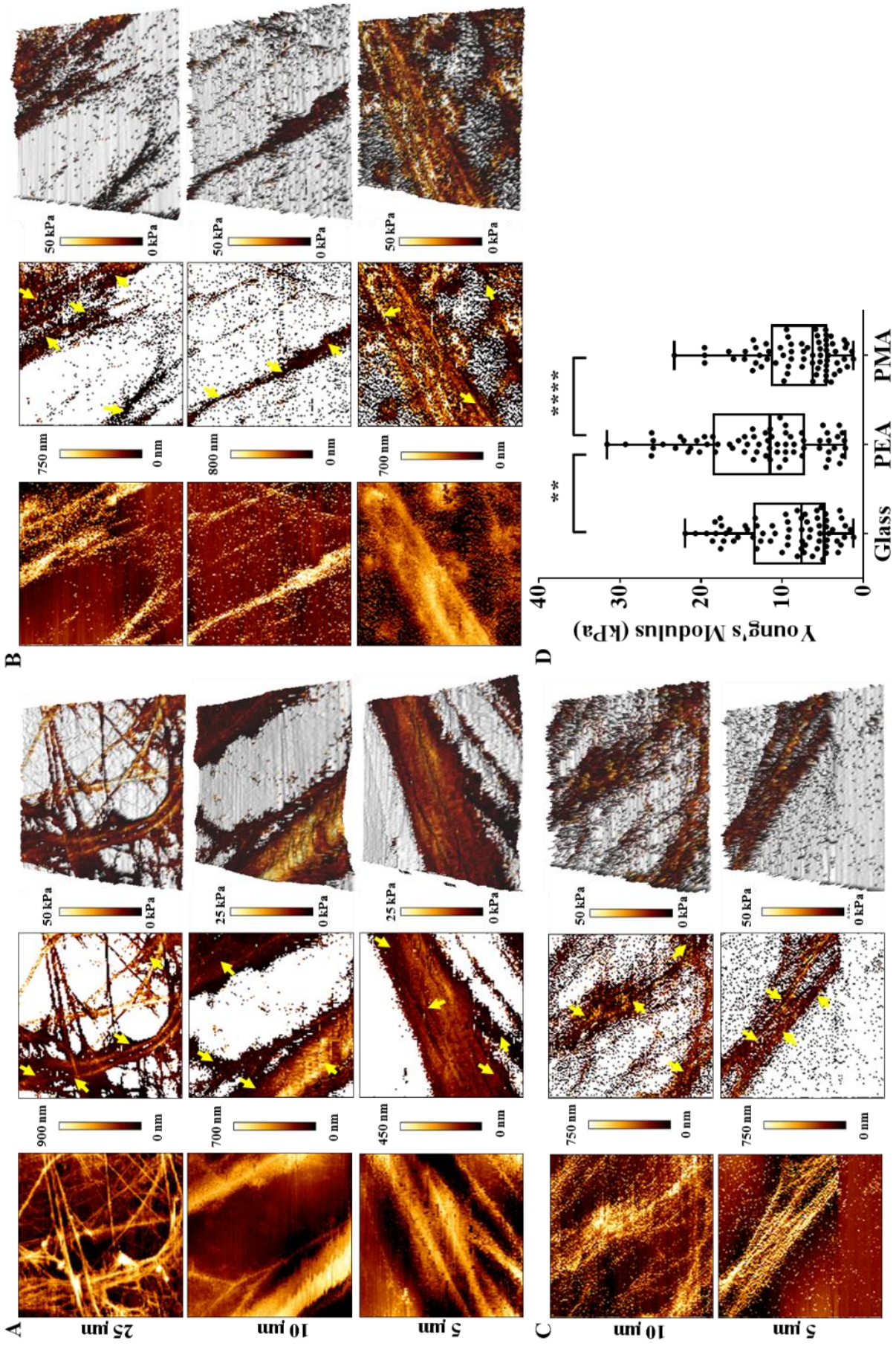
A
25 μm
10 μm
5 μm
900 nm
0 nm
700 nm
450 nm
50 kPa
25 kPa
0 kPa
B
750 nm
800 nm
700 nm
C
D
Young's Modulus (kPa)
40
30
20
10
0
**
****
Glass
PEA
PMA

Figure 5.17 AFM imaging of ECMs after decellularization of *COL4A2*$^{+/G702D}$ cells. Mutant cells were cultured on FN-coated PEA (**A**), PMA (**B**), and glass (**C**) for 7 days and then decellularized using 20 mM ammonium hydroxide (NH_4OH) solution, leaving the intact ECMs; then AFM quantitative imaging was carried in DPBS using a pyramidal tip. Height images (first column), elasticity-processed images using the Hertz model (second column) and 3D images of the processed images (third column). The average Young's modulus of ECMs obtained using the Hertz model (**D**) of at least 20 measurements (N ≥20) were analysed taken from the yellow arrows. Data presented as mean ±SD; and analysed with an ANOVA test; **p<0.01, ****p<0.0001.

Figure 5.18A-B showed AFM images of the WT control cells on PEA and PMA. The average Young's modulus ranged mainly from 20 to 43 kPa on PEA and 1.5 to 6.5 kPa on PMA (Figure 5.18C). The stiffness of secreted ECMs was statistically higher on PEA than on PMA. No AFM images were obtained for WT cells on glass as ECMs were detaching while decellularizing. Summarising the Young's moduli of ECMs secreted by the WT and the MT cells, the stiffness of WT' ECMs was 10-fold significantly higher than that of MT's, especially on PEA. These values correlated with the trend of cells stiffness observed in (Figure 5.15).

The ECMs elasticity measurements were made using sharp pyramidal tips. Measurements using spherical tips (used in cells stiffness measurement) were also made to confirm these observations and the elasticity values were found to be similar. In general, these observations indicated that cells secreted ECMs of the order of stiffness; for example, secreted ECMs by the WT cells on glass would have lower stiffness compared to ECMs secreted by WT cells on PEA-FN as the WT cells on PEA-FN have higher stiffness than on glass. The trend in the mechanical properties of secreted ECMs followed the stiffness of the cells. The material substrate on which the cells were cultured seemed to have an effect on the cells, yet it was not clear why cells and ECMs on PEA-FN had higher stiffness than on glass and PMA. This could be due to the amount of secreted ECMs or to the nature of the secreted proteins; hence, it would be interesting to investigate the degradation and stability of Col4 and how these cells adhere to these interfaces.

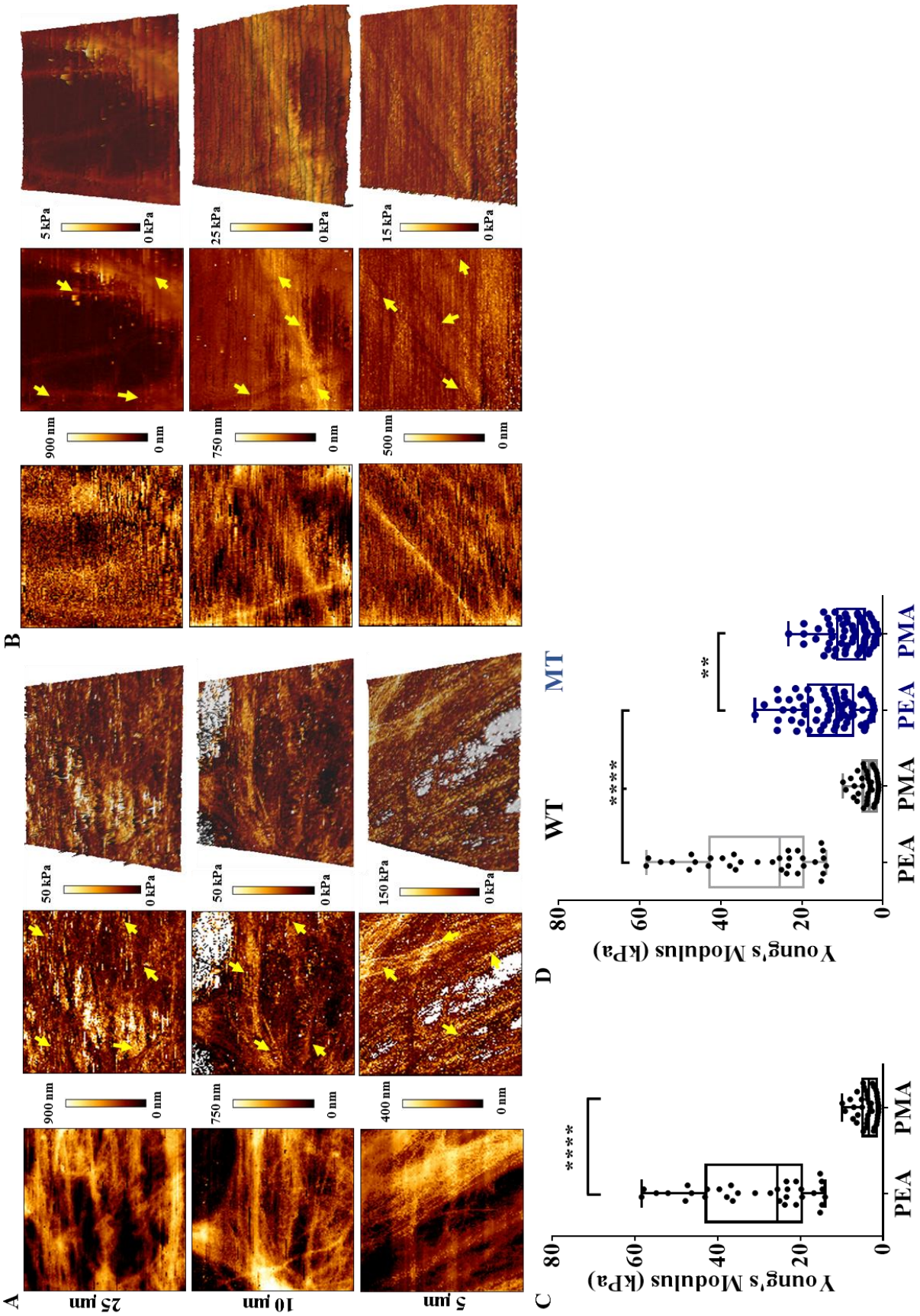
A
25 μm
10 μm
5 μm
900 nm
0 nm
750 nm
400 nm
50 kPa
150 kPa
0 kPa
B
5 kPa
25 kPa
15 kPa
900 nm
750 nm
500 nm
C
Young's Modulus (kPa)
PEA
PMA
****
D
WT
MT
PEA
PMA
PEA
PMA
****
**

Figure 5.18 AFM imaging of ECMs after decellularization of wild type control cells. WT cells were cultured on FN coated PEA (**A**) and PMA (**B**) and processed as described above. Height images (first column), elasticity-processed images using the Hertz model (second column) and 3D images (third column). The average Young's modulus of WT' ECMs obtained using the Hertz model (**C**). Comparison between WT (black) and MT (blue) ECMs Young's moduli on PEA and PMA (**D**). At least 20 measurements (N ≥20) were analysed taken from the yellow arrows. Data presented as mean ±SD; and analysed with an ANOVA test; **p<0.01, ***p<0.001, ****p<0.0001; only important statistical differences are shown. MT, mutant; WT, wild type.

5. 6. 7 Compositional basement membrane defects

To establish the effect of *COL4A2*$^{+/G702D}$ mutation on the BM, AFM quantitative imaging was performed to analyse its structure integrity and biomechanical properties, providing fundamental insight into stiffness and adhesion forces. This was done under physiological conditions (not fixed or stained) as this has not been done previously. Heterozygous mutant mice (e.g. Col4a1$^{+/SVC}$ [SVC, Neonatal lethality due to ICH, recurrent adult intracerebral haemorrhage (ICH), anterior segment dysgenesis, cataracts, medullary atrophy, glomerulopathy, proteinuria, polyuria, haematuria (Van Agtmael et al. 2010) which carry a glycine to aspartic acid mutation [G1064D] (Van Agtmael et al. 2005) were used for this study, as they are an excellent model for collagen IV disease as the phenotypic similarities between these mice and patients led to the identification of the human mutations (Vahedi and Alamowitch 2011).

Brightfield image of a 15 μm unfixed and unstained mice aorta cryosections from which AFM scanning was performed was shown (Figure 5.19A). It was not possible to acquire AFM images with very high details of the unfixed and unstained mice aorta sections. Since no BM structures could be identified with the AFM, IHC of aorta sections was carried out to enable localisation of the BM in relation to Col4a2 and laminin (Figure 5.19B-C) as this would also reveal the BM composition and structure. This once more proved difficult as images showed staining of the whole section, indicating that the elastin found in aorta was also stained (Figure 5.19B-C). Hence it was not possible to identify the location of the BM by IHC. Instead, mice kidney sections were used.

Kidney sections were stained for Col4a2 and laminin to enable localisation of the BM. The BM of the Bowman's capsule was of interest as it contains the α1.α1.a2(IV) network. Confocal images showed that the SVC animals had significantly weaker Col4a2 staining in the Bowman's capsule compared with WT, but no significant changes were detected for LM in both WT and SVC mice (Figure 5.20A-B). The Col4a2 signal also appeared less sharp

indicating more BM incorporation of mutant Col4a2. This showed that mutation in Col4a2 causes BM defect, agreeing with previous data (Murray et al. 2014).

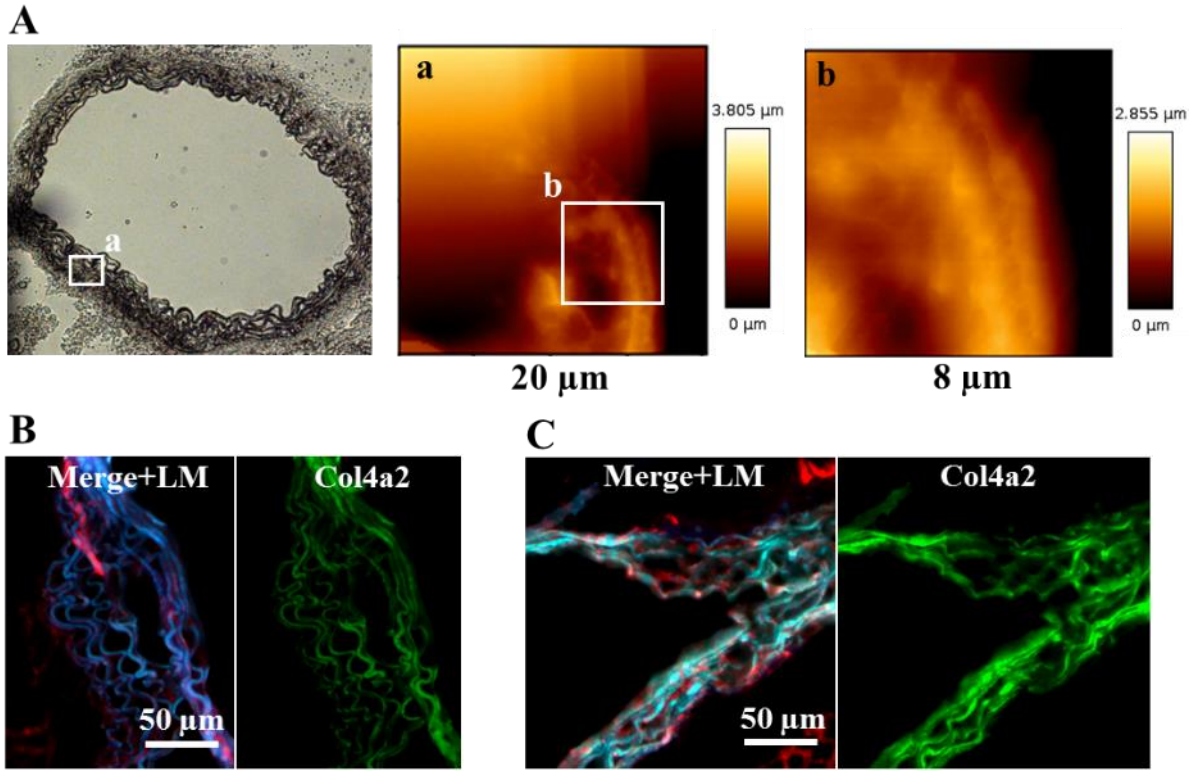

Figure 5.19 Analysis of the effect of mutants on BM structural integrity. Brightfield image of 15 µm unfixed and unstained mice aorta section (**A**); from which AFM scanning was performed (a-b). IHC of Col4a2 and laminin localisation in aorta sections from WT (**B**) and SVC mice (**C**). Inset box shows higher magnification. Green: Col4a2, Red: laminin (LM), blue: nuclei.

To analyse the changes in more detail, unfixed and unstained mice kidney cryosections were AFM scanned in liquid to measure the mechanical properties of defective BM under physiological conditions. Once again, it was not possible to acquire detailed images. Yet, it is possible to observe in details the BM of mice kidney sections fixed with acetone using AFM as demonstrated in (Figure 5.20C) (Images are courtesy of Dr Marco Cantini). The figure showed a well-structured BM for the WT and a disrupted BM with a bulge in SVC. It also showed reduced average stiffness for the WT sample, 200 MPa versus 100 MPa for SVC. This furthermore proved that mutation into *COL4A2* causes BM defects.

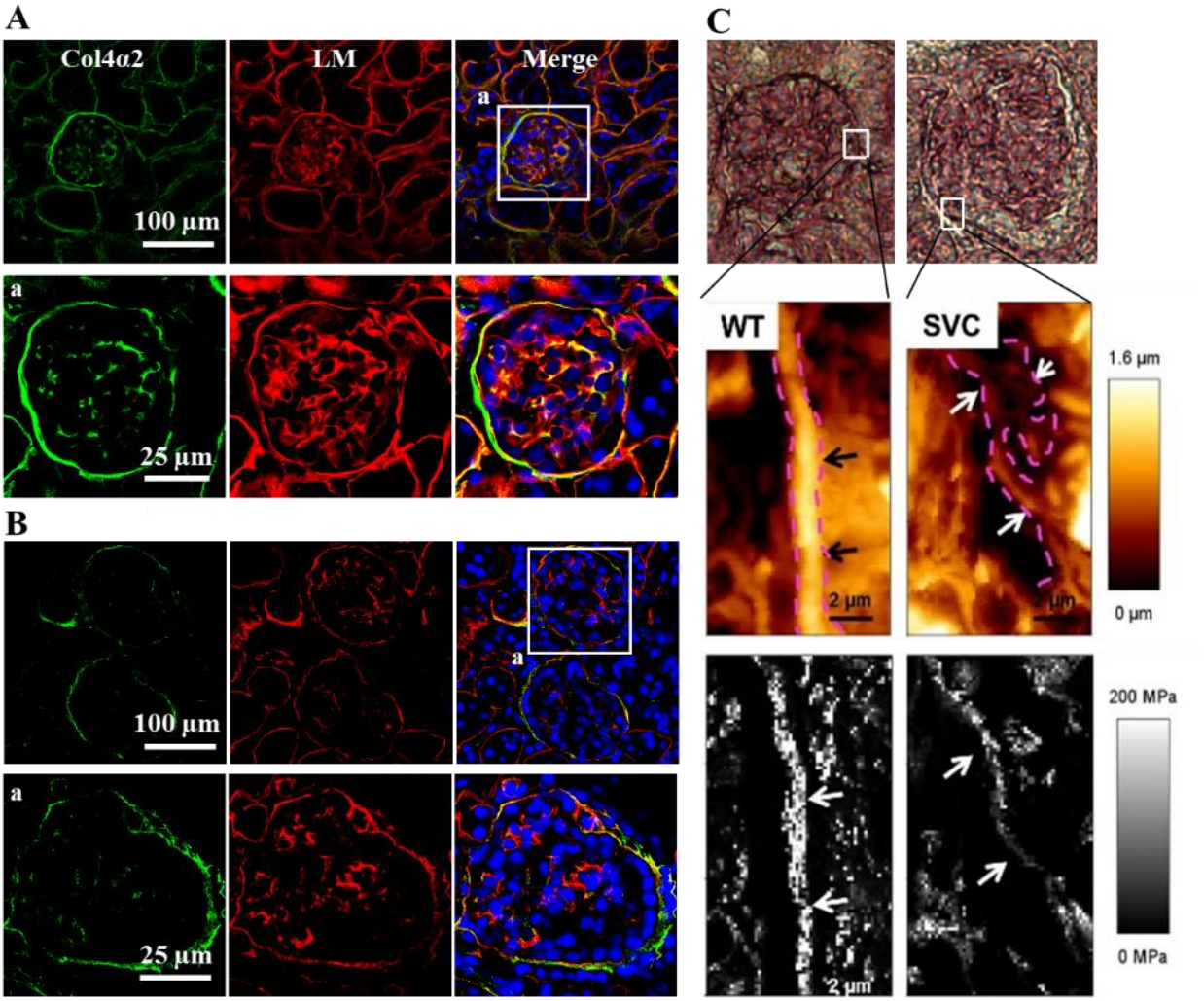

Figure 5.20 Analysis of the effect of mutants on BM composition and structural integrity. IHC of Col4a2 and laminin localisation in kidney sections from WT (**A**) and SVC mice (**B**). Green: Col4a2, Red: laminin (LM), Blue: nuclei, White: merge. (**C**) Example of an AFM analysis of the BM of the Bowman capsule (outlined in pink and arrows); courtesy of Dr Marco Cantini, University of Glasgow. Inset box shows higher magnification. Scale bars indicate height (µm) (top) and stiffness (MPa) (bottom).

5. 6. 8 Matrix reorganisation

Cells may alter their environment and adhesion mechanism by secreting or manipulating the extracellular matrix. Following the analysis of how *COL4A2*$^{+/G702D}$ cells secrete the ECMs, an assay was performed to investigate how fibroblasts reorganise matrix. Cells were seeded for 1 or 7 days on substrates adsorbed with ECMs, and the coated ECMs were stained. First, the reorganization of Col4 by WT and MT cells on the synthetic polymers was examined (Figure 5.21). Both cell types were able to mechanically remove and reorganize adsorbed Col4 in a specific linear pattern, and they also showed similar degree of reorganisation on the two polymers, observed by the appearance of dark zones of protein removal. It is reported

that ECMs reorganization takes place in the early time of cell adhesion, within 3h cells tend to reorganize it environment.

Col4 rearrangement was mostly seen at day 1 as at day 7 cells secreted a large amount of ECMs that covered the surface, corroborating with disappearance of the dark zones of protein removal. Col4 and secreted FN or LM were also viewed simultaneously to confirm the cooperative mechanism of reorganization previously observed for fibroblasts (Supplementary Figure S5. 2). It is thought that a possible mechanism for Col4 reorganization is its tethering by FN molecules during fibrillogenesis (Coelho et al. 2013). Indeed, the typical fibrillar pattern of secreted FN co-localized almost completely with the substratum rearranged Col4, resulting in violet when merged (Supplementary Figure S5. 2A) yet secreted LM did seem to co-localize with coated Col4 (Supplementary Figure S5. 2B). Thus, these results show that cells were able to mechanically translocate adsorbed Col4 in fibril-like pattern that frequently co-localize with FN matrix fibrils.

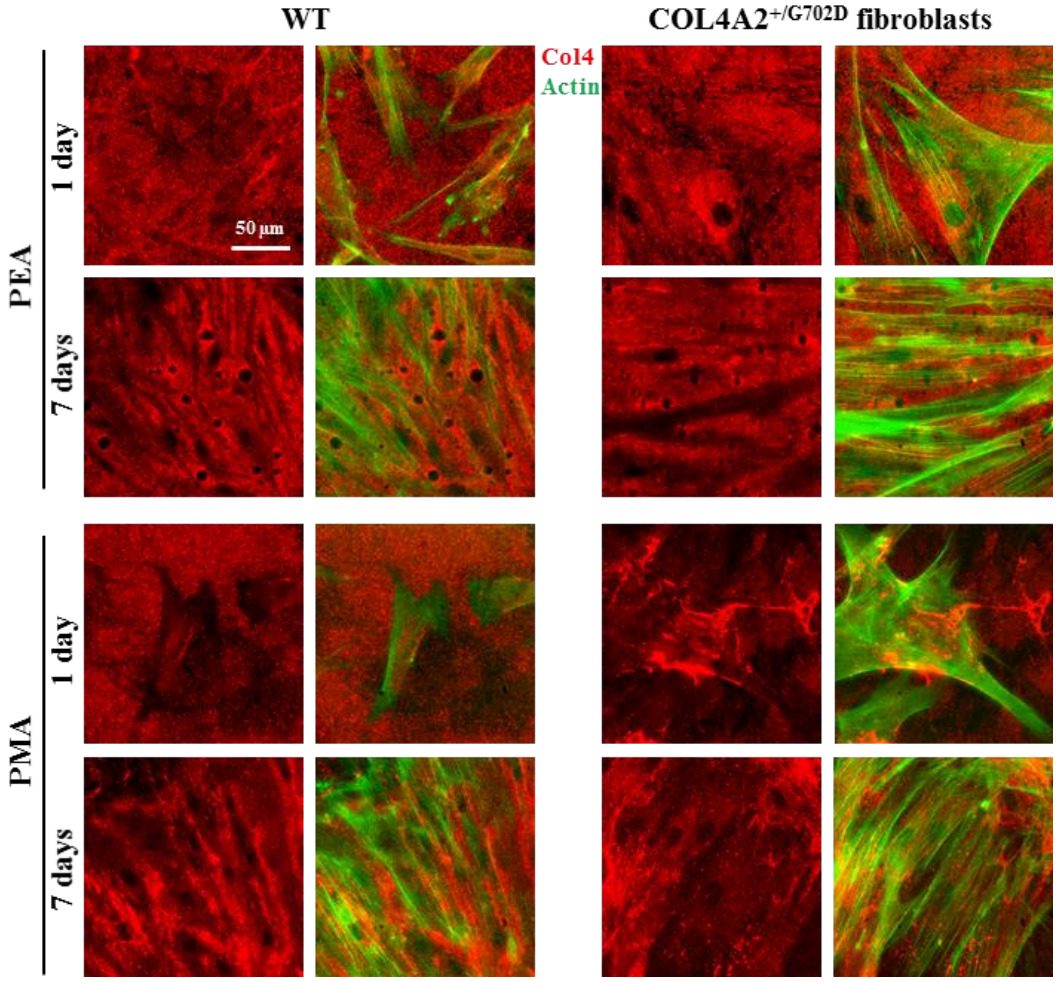

Figure 5.21 Remodelling of Col4 matrix by mutant fibroblasts on PEA and PMA polymers at different time points (1 and 7 days). Col4-coated matrix (Red) and actin (Green). Scale bars: 50 µm.

Then, the reorganization of FN by WT and MT cells on the synthetic polymers was also investigated (Figure 5.22). Results showed both cell types on PEA and PMA not only interacting with adsorbed matrix, but also tend to reorganize in some patterns making dark zone at cell borders representing mechanical translocation of adsorbed matrix from the places from where the protein was initially and removed to be arranged using cells secreted proteases (Coelho et al. 2013). Cells were also observed to secrete their own ECMs as the dark patches were covered with high density fluorescence and formed "corona"-like reorganization of FN at the periphery (Maneva-Radicheva et al. 2008). Fibrillar patterns of FN were seen increasing with time points on both substrates. Rearranged FN was clustered predominantly at cell borders in a specific linear (fibril-like) pattern, which is similar, but not identical to the substratum associated Col4 fibrils seen above. The fibrillar patterned FN-coated on the substrates did not seem to co-localize with the secreted Col4a2 (Supplementary Figure S5. 3).

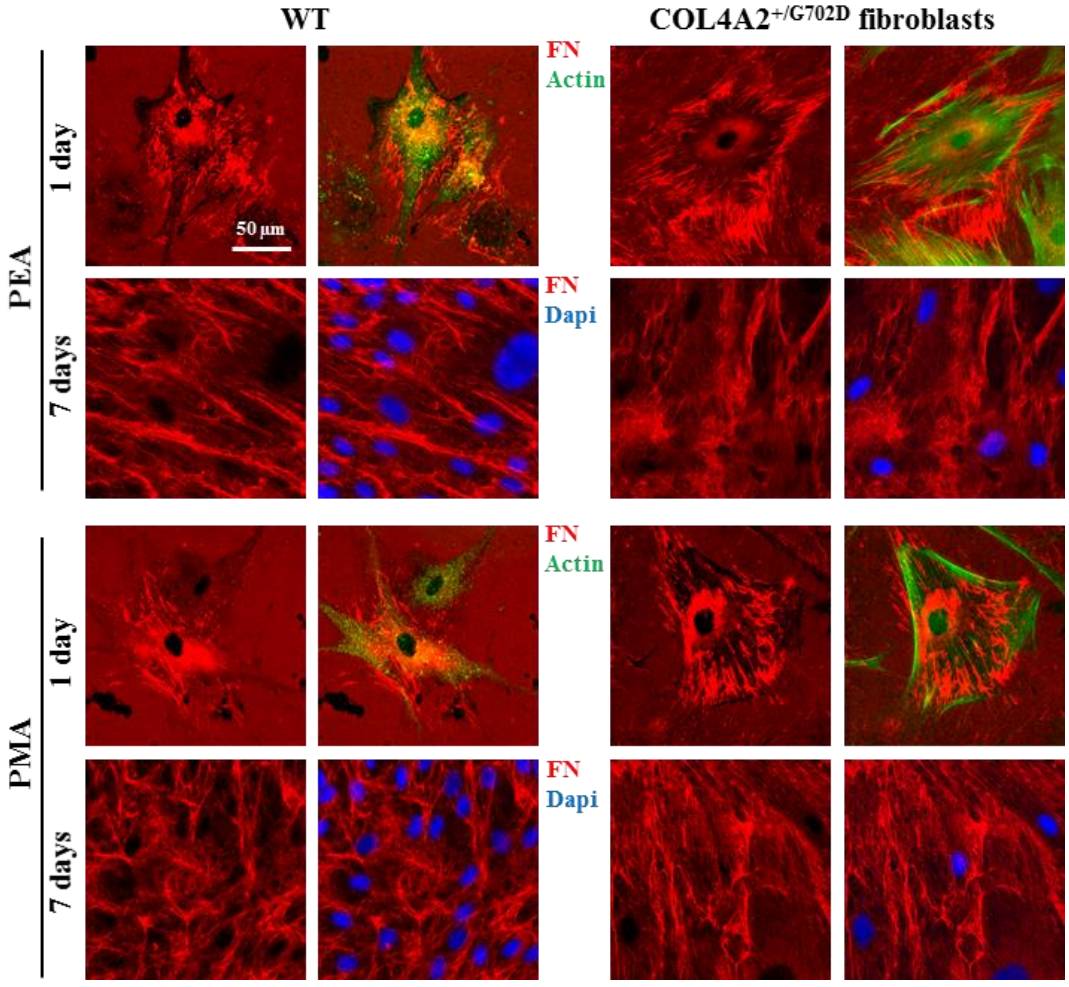

Figure 5.22 Remodelling of FN matrix by mutant fibroblasts on PEA and PMA polymers at different time points (1 and 7 days). FN-coated matrix (Red) and actin (Green) and nucleus (Blue). Scale bars: 50 µm.

Finally, LM reorganization by cells on the polymers was also investigated (Figure 5.23). Once more, both WT and MT cells were observed to rearrange the coated LM protein. Yet, unlike reorganisation of Col4 or FN, WT and MT cells seemed to remodel LM to a lesser extent. This correlates with how cells also secreted ECMs when cultured on the LM-coated substrates. As seen (Figure 5.6), after 7 days culture on LM-coated substrates, Col4a2 was not secreted in high amount compared to ECMs secreted on Col4 or FN-coated substrates (Coelho et al. 2011b). Small amount of ECM was secreted on the LM substrates by both WT and MT cells correlating with the reorganisation of the substratum LM. This suggested lower cell activity on the LM interfaces compared to the Col4 and FN substrates. Rearranged LM did not co-localize with secreted Col4a2 (Supplementary Figure S5. 3).

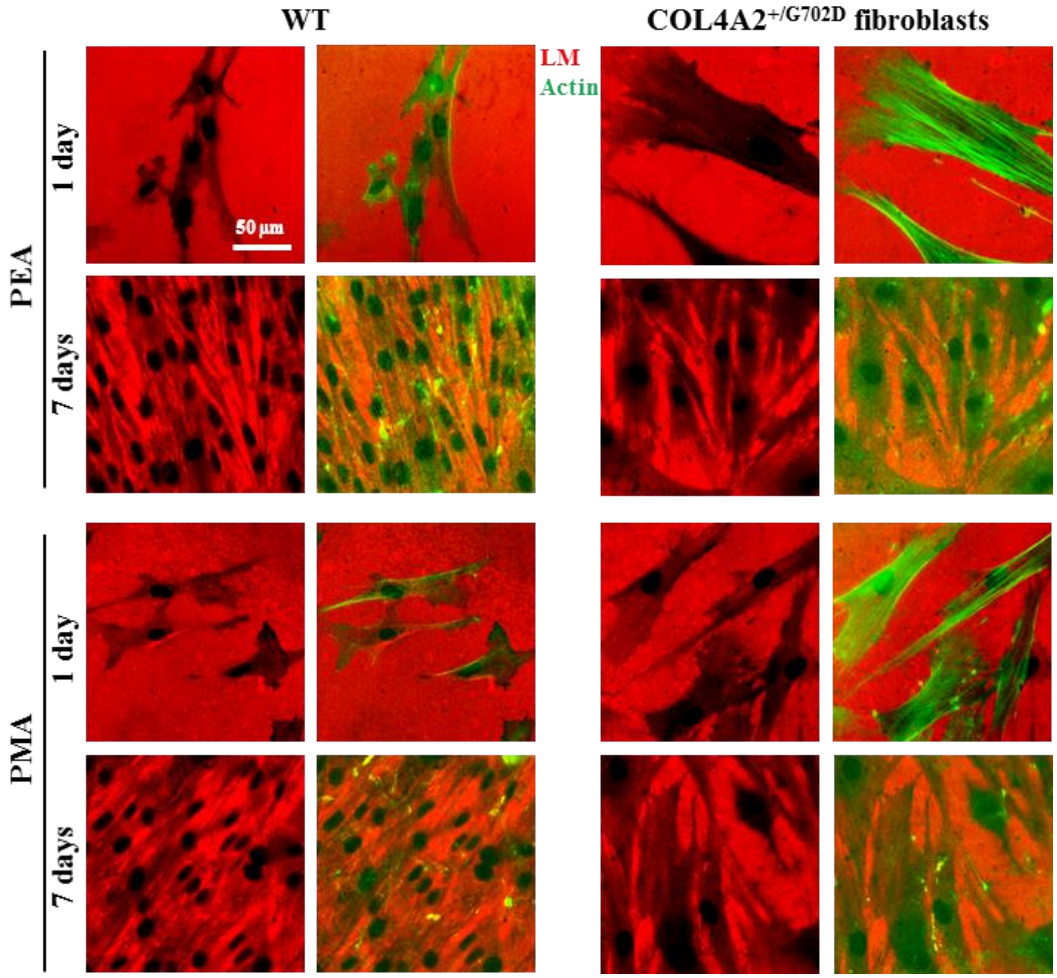

Figure 5.23 Remodelling of LM matrix by mutant fibroblasts on PEA and PMA polymers at 1 and 7 days). LM-coated matrix (Red) and actin (Green). Scale bars: 50 µm.

In summary and agreement with previously reported studies (Coelho et al. 2013, Maneva-Radicheva et al. 2008), this analysis of matrix reorganisation by both WT and MT cells on PEA and PMA substrates showed that after adhesion, cells interacted with the substratum and moreover were able to mechanically translocate adsorbed matrix in some ways. Both

cell types did not differentiate the rearrangement on neither coated Col4, FN nor LM. Studies have reported that two types of cell activities might happen when cells adhere onto these bio-material interface: substratum (Col4, FN or LM) reorganization and its degradation via enzymatic cleavage. Moreover, it is also known that the reorganisation depends on the materials surface properties.

5. 7 Conclusion

This chapter details the effect of engineered biointerfaces on the behaviour of *COL4A2*$^{+/G702D}$ mutant cells. Since these cells were characterised to secrete lower amount of Col4a2, the cells were subjected on ECMs coated synthetic polymer interfaces. Interestingly, altered behaviour by the *COL4A2*$^{+/G702D}$ cells was observed when cultured on FN substrates. The mutant cells were observed to secrete a higher amount of Col4a2 on FN-coated PEA. The findings are unprecedented and show that cells behaviour can be influenced by biomaterials. The results concluded that FN biointerface, the layer of physiological-like fibrillary nano-networks on PEA, can induce the secretion of Col4a2 from the mutant cells. This was associated with increased levels of molecular chaperones and reduced ER area, suggesting increased protein folding capacity of the cell and perhaps reduced ER stress, and altered biomechanical proteins of the cells. Results also showed that *COL4A2*$^{+/G702D}$ cells do not only interact with the biomaterial interfaces, but they are also able to mechanically translocate adsorbed ECMs.

Investigation into the mechanical properties of *COL4A2*$^{+/G702D}$ fibroblast cells revealed a 10-fold decrease in cell stiffness compared to the WT control cells. This decrease is attributed to the cross-linked F-actin, to the changes in the matrix molecules that make up the ECM, to the fluctuations in the degree of protein cross-linking that occurs due to matrix-modifying enzymes, and to the alterations in the remodelling process. Likewise, the stiffness of ECMs secreted by the MT cells were found to be 10-fold lower than that of the WT cells confirming the state of the cells. Concluding, mutant cells and their ECMs were 10-fold softer than the WT cells, and both cell types and ECMs stiffness were higher on PEA-FN. Mutation in *COL4A2* was shown by confocal imaging of stained Col4a2 and LM to cause BM defect as weaker Col4a2 staining showed the disrupted BM structure in the mutant sample, furthermore confirming the involvement of the mutation in BM diseases. Combined, the data presented in this chapter suggests that just by culturing cells on matrices the behaviour of mutant cells can be partially rescued.

Chapter 6
Cell Adhesion and Signalling

Contents

6. 0 Introduction

6. 1 Cell Adhesion and signalling

Cell adhesion to extracellular matrix (ECM) components is an important process for the development, maintenance, organization, and repair of numerous tissues. It provides anchorage triggering signals that direct cell survival, migration, cell cycle progression, and expression of differentiated phenotypes. Cell adhesion to the ECM is central to biomaterials, tissue engineering, and biotechnological applications (Anselme et al. 2000, Gumbiner 1996, Sipe 2002).

It is widely recognised that cells do not directly interact with the material surface on which they are seeded. Indeed, their adhesion onto synthetic surfaces is mediated by a layer of adsorbed ECM proteins previously adsorbed onto the material, either from the physiological fluids *in vivo* or initially adsorbed on a biomaterial surface *in vitro* (Anselme et al. 2000, García 2006, Gumbiner 1996, Salmerón-Sánchez and Altankov 2010, Sipe 2002). Cell adhesion to ECMs is critical to a cascade of cellular events including but not limited to cell spreading, migration, growth, apoptosis, bidirectional signalling during morphogenesis, and tissue homeostasis (Reddig and Juliano 2005). These processes regulate cellular homeostasis and govern cell fate (Berrier and Yamada 2007, Disatnik and Rando 1999).

Adhesion of cells to ECM proteins such as collagen (Col), fibrinogen (FB), fibronectin (FN), laminin (LM) and vitronectin (VN) is initiated as a surface phenomenon and primarily mediated by transmembrane heterodimeric receptors that belong to the integrin family (Aiyelabegan and Sadroddiny 2017, Hynes 2002, Jansen et al. 2017, Sun et al. 2016). Integrins are a family of transmembrane receptors that serve as a link between the extracellular environment and the cytoskeleton. They initiate several intracellular signalling pathways acting also as mechanical transducers, controlling cell motility, cytoskeleton reorganization amongst other complex cellular processes (Burridge 2017, Garcia 2005, Hynes 2002, Jansen et al. 2017).

Cell adhesion to ECMs is a highly regulated and complex process that involves recruitment of integrins to the cell surface, activation, and mechanical coupling to extracellular ligands (Garcia et al. 1998a, Jansen et al. 2017). Recruited receptors mechanically coupled to the cell surface are reinforced by structural and signalling proteins cluster together at the adhesive sites forming focal adhesions (FAs) that connect the actin cytoskeleton to further stabilize the adhesions.

FAs are supramolecular structures that link proteins at the material interface (such as PEA and PMA used in this study) with the actin cytoskeleton. Their composition, dynamics, size, and structure, depend on the surrounding matrix. FAs ~2–5 μm are involved in intermediate tension phenotypes; super-mature adhesions > 5 μm are involved in high-tension phenotypes (Biggs et al. 2009). They are complexes, mature adhesion sites that contain structural and signalling proteins such as vinculin, talin, and -actinin, focal adhesion kinase (FAK), Src, paxillin, and p130Cas. The signalling proteins play the initial step in the organization of mid- and long-term processes such as differentiation and migration, (Aiyelabegan and Sadroddiny 2017, Geiger et al. 2001, Sun et al. 2016).

FAK, a non-receptor tyrosine kinase that activates in response to cell-ECM adhesion and inactivated by dephosphorylation after detachment or trypsinization, is involved in FA development (Aiyelabegan and Sadroddiny 2017, Hanks et al. 1992, Sun et al. 2016). FAK triggers a wide variety of signalling pathways involved in cell motility, invasion, proliferation, cell cycle and development, (Beggs et al. 2003, Braren et al. 2006, Cary and Guan 1999, Mitra et al. 2005, Parsons 2003) and contributes to integrin activation directed towards the generation and enhancement of cell-ECM adhesive forces (Jansen et al. 2017, Mitra et al. 2005, Sun et al. 2016). FAK activation is mainly dictated by Tyr-397 autophosphorylation. This phosphorylation creates a high-affinity site for the SH2 domain of Src, recruiting and activating Src in the FA complexes (Schaller et al. 1994). When Src binds to phosphoTyr-397, other FAK residues are also phosphorylated. Activated FAK interacts with signalling and adaptor proteins, including p130Cas, Grb2, paxillin, Shc and PI-3k kinase, thereby initiating intracellular signal transduction cascades (Cary and Guan 1999, Mitra et al. 2005, Schaller 2001, Zouq et al. 2009) that, in turn, regulate cellular processes such as proliferation, migration, survival, and differentiation.

Besides triggering adhesion through FA development, both integrins and signalling proteins such as FAK are deeply involved in other cellular processes, including transcription and protein synthesis and secretion. These are amongst the wide variety of cellular processes directed by the mitogen-activated protein kinase (MAPK) signalling pathway (Provenzano et al. 2009). MAPK superfamily includes ERK1/2 amongst hundreds of kinases (Roskoski 2012) and is involved in an amplificatory cascade where an initial trigger, which can be integrin-mediated signalling, activates a series of kinases which substrates are other kinases. This signalling cascade can be divided into three tiers; (1st) MAP3K or MAPK kinases, which phosphorylates MAP2K (MAPK kinases, 2nd). Substrates of MAP2K are MAPK (3rd) namely ERK1/2 (Biggs et al. 2009, Provenzano et al. 2009, Roskoski 2012).

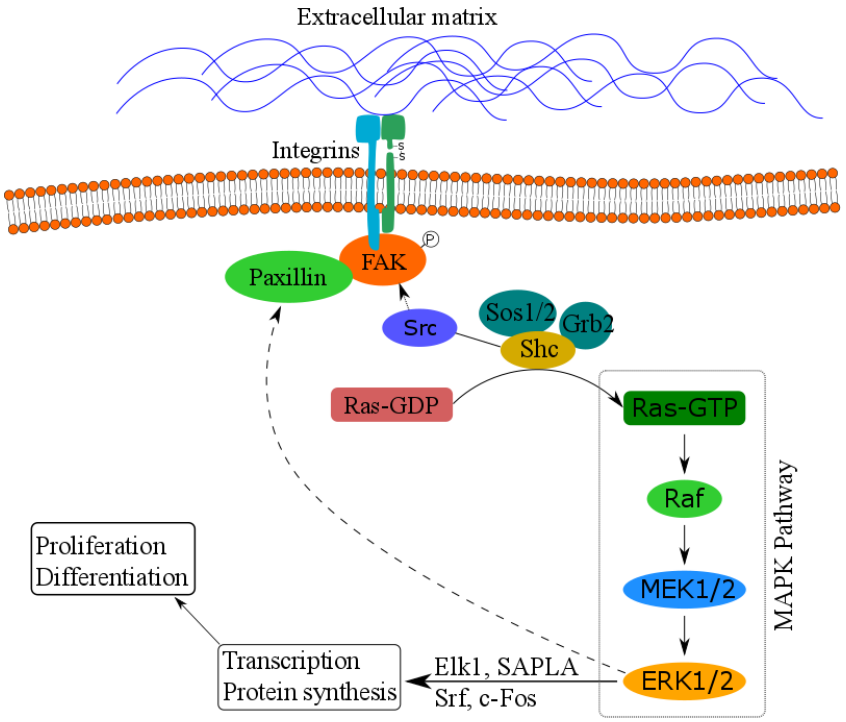

Figure 6.1 Integrin dimerization activates the MAPK pathway-signalling cascade, which results in enhanced focal adhesion formation and maturation via paxillin phosphorylation. MAPK signalling pathway also activates several genes involved in cell proliferation and migration.

Cell proliferation, one of the most important events related to newly developed tissue, is tightly controlled by the Ras-Raf-MEK-ERK pathway (Roskoski 2012). Integrin dimerization can trigger this pathway, in response to extracellular events such as interaction with ECM proteins (FN, Col, LM and others) (Figure 6.1) (Garcia 2005, Mouw et al. 2014, Weinberg et al. 2017). Dimerization of integrin subunits leads to Ras activation, via exchange of GDP by GTP, the active form. Ras-GTP is responsible for the subsequent activation of the Raf kinase family (Raf-A, B and C), in a complex multistage process involving homo- and hetero-dimer formation (Roskoski 2010). Raf activates MEK1/2 (MAP/ERK kinases) whose only substrates are ERK1 and ERK2. MEK1/2 are Tyr-Thr kinases, phosphorylating Thr202/Tyr204 in ERK1 and Thr185/Tyr187 in ERK2. Active ERK1/2 are promiscuous kinases, with 175 known substrates including paxillin, a protein that plays a prominent role in focal adhesion complexes. This activation helps in the formation of mature adhesion complexes (Liu Z. X. et al. 2002, Yoon and Seger 2006).

Mechanical properties, surface topography, chemistry and functionalization are different parameters widely used to influence cell behaviour including cell adhesion, spreading, proliferation, and differentiation, however, the mechanisms that trigger different signalling pathways at the material interface is not completely understood. The effect of substrate

properties in protein adsorption and cell responses-particularly intracellular signalling pathways-has been extensively studied (See review by (González-García et al. 2015)).

6. 2 Cell adhesion strengthening and focal adhesion assembly

Focal adhesions are discrete adhesive plaques, as mentioned above. They have emerged as putative mechanosensors for extracellular stimuli, as many of the molecules implicated in mediating signal transduction in response to mechanical stimuli are found at FAs, including Src, FAK, Rho, and talin (Geiger et al. 2009, Riveline et al. 2001, Wang H. B. et al. 2001, Wang N. et al. 2002, Weinberg et al. 2017). For instance, external forces exerted on integrins enhance FA assembly and increase the strength and rigidity of the linkage between integrins and the actin cytoskeleton (Geiger et al. 2009, Riveline et al. 2001). Not only do FAs transmit external mechanical signals (converting them to biochemical signals), but external force can regulate the types of FAs that cells form (Geiger et al. 2009) and this study suggests that FAs formed under different biophysical environments transmit different signals to the cell, leading to different cell behaviours. Recent studies have provided exciting evidence showing that p130Cas, a focal adhesion adaptor protein, serves as an important force sensor in cell-ECM adhesion-dependent mechanotransduction (Sawada et al. 2006).

FAK has been implicated in mechanosensing by the finding that FAK-null cells cannot detect differences in ECM rigidity (Wang H. B. et al. 2001). Normal cells will migrate preferentially on rigid substrates; FAK-null cells do not show this preference. The phosphorylation of FAK at its autophosphorylation site, Y397, seems to be involved in the mechanosensing response because FAK is phosphorylated when mechanical strain is applied to smooth muscle and endothelial cells (Wang H. B. et al. 2001).

Furthermore, FA assembly plays a key role in the generation of strong traction forces (Balaban et al. 2001, Gallant et al. 2005, Garcia 2005). FA assembly also contributes to cell adhesion strengthening by distributing bond forces along the cell-substrate interface (Gallant et al. 2005, Lotz et al. 1989). Cell adhesion strengthening is stated to be a two-step process consisting of initial integrin-ligand binding followed by rapid strengthening (Lotz et al. 1989). The strengthening response is understood as a three stage process that includes (a) initial integrin-ligand binding and simultaneous increase in cell-substrate adhesive area (initial attachment and spreading), (b) increased receptor recruitment to the adhesive interface (clustering) and (c) interactions with cytoskeletal components involving recruitment of intracellular proteins that lead to enhanced force distribution at the adhesive site via local membrane stiffening (focal adhesion assembly).

Pioneering work to quantify the adhesion strength and provide a mechanism for cell adhesion strengthening to FN has been done by Gallant et.al (Gallant et al. 2005). Their work found that FA assembly (FA size and distribution), integrin-ligand bond strength and cytoskeletal architecture play a major role in modulating adhesion strength by distributing bond forces along the cell-substrate (Gallant et al. 2005). They used a spinning disk device to measure the cell adhesion strength (See Figure 2.4 chapter 2) (Garcia et al. 1998a, García et al. 1997).

The spinning disk technique uses shear stress generated from a rotating disk device. As detailed in the method chapter 2. In short, cells are seeded on circular 25 mm glass and PEA-FN and PMA-FN coverslips. Substrates containing adherent cells are placed on the rotating disk and spun in buffer at prescribed speeds (Garcia et al. 1998a, García et al. 1997). The fluid flow associated with the disk rotation applies a well-characterized hydrodynamic force to adherent cells. The hydrodynamic force increases linearly with radial position along the surface of the sample, such that cells at the centre of the sample experience negligible forces, whereas cell numbers decrease toward the outside of the disk as the applied cell detachment force increases (Figure 6.18). The adherent fractions of cells were quantified using microscopy and by counting the number of cells using an automated image processing software (García et al. 1997).

The spinning disk technique has been used to investigate various types of cell-substrate interactions for wide range of applications such as quantifying the adhesion strength of an osteoblast-like cell on bioactive glass (Garcia et al. 1998a, García et al. 1997) and human bone marrow cells on hydroxyapatite (Deligianni et al. 2005). The assay has been used to show the role of FAK in promoting integrin activation to enhance the generation of cell–ECM adhesive forces (Michael et al. 2009, Mitra et al. 2005). The effect of surface charges on different substrates has also been studied using HT-1080 cells following FN coating (Miller and Boettiger 2003). García and colleagues (Garcia et al. 1998b) were able to measure the short- and long-term adhesion strength of IMR-90 human fibroblasts adhered to FN-coated glass using the spinning disk technique.

The existence of a linear relationship between the adhesion strength and ligand density, which is directly related to the number of $\alpha_5\beta_1$–FN bonds has been initially suggested (Desai et al. 2009). Integrin–FN bonds are preferentially localized to FA structures and require an activated form of $\alpha_5\beta_1$ that can bind FN. The phosphorylation of FAK through Tyr-397 appears to be an early event in $\alpha_5\beta_1$-integrin-mediated signalling and is linearly correlated to the number of receptor–ligand bonds and the level of bound integrins. Overall, it is suggested

that phosphorylation of Tyr-397 is required for the functional effects of FAK on integrin binding rate and adhesion strengthening.

Therefore, the spinning disk assay was used to measure the cell adhesion strength of *COL4A2*$^{+/G702D}$ cells cultured on FN-coated substrates focusing on four factors, incubation time influence on adhesion strength, role of contractility, serum effect and fibronectin density effect on adhesion strength. This assay was carried out at the Georgia Institute of Technology, Atlanta, Georgia, USA under the supervision of Prof Andrés J. García. Other common adhesion assays together with their advantages and disadvantages are listed in Table 2.1, chapter 2, (See also review (Ahmad Khalili and Ahmad 2015)).

Investigations in this chapter were performed to correlate with results observed in the previous chapter 5. The functional roles of FAs extend beyond stabilizing adhesions and transduce mechanical signals at the cell-ECM interface in various signalling events. Although biochemical events explain signalling mechanisms in a cell, a mechanistic understanding of the cell adhesion process provides essential information on various cues that control mechanoresponse, mechanosensation, and mechanotransduction (Shattil et al. 2010). Abnormalities in adhesive interactions are often associated with pathological states, including blood clotting and wound healing defects as well as malignant tumour formation, (Jin and Varner 2004, Wehrle-Haller and Imhof 2003).

6. 3 Aims and Objectives

Integrin-mediated cell adhesion to the ECM is central to regulate cell survival and migration, differentiation and proliferation, mechanotransduction and also affect extracellular matrix assembly (Shattil et al. 2010). At the tissue level, cell adhesion is important in the pathological and physiological processes that regulate the tissue morphogenesis. Besides triggering adhesion through FA development, both integrins and signalling proteins such as FAK are deeply involved in other cellular processes including protein synthesis and secretion. Therefore, after investigating the effect of the biointerfaces on *COL4A2*$^{+/G702D}$ secretion of extracellular matrix, this chapter aims to:

- Investigate the effect of defined engineered biointerfaces on *COL4A2*$^{+/G702D}$ mutant cells adhesion.
- Investigate the role of cell signalling in inducing *COL4A2*$^{+/G702D}$ mutant cells cultured on FN interfaces to secrete Col4a2.
- Analyse the contribution of FA complex and cytoskeleton in modulating cell-substrate adhesion strength.

6. 4 Results and Discussions

6. 4. 1 Cell adhesion

Following the investigation of matrix secretion of *COL4A2*$^{+/G702D}$ mutant cells in chapter 5, considerable questions were raised as to how the mutant cells adhere on the synthetic FN matrices assembled at the material interface and what signalling pathways were involved. The organization of proteins involved in the formation of focal adhesion (FA) complexes provides an opportunity to learn more about the effectiveness of cell-substrate-interactions.

To gain insights into the mechanisms controlling cell adhesion on material-driven FN networks, a short-term cell culture experiment was performed to investigate initial adhesion and response of *COL4A2*$^{+/G702D}$ mutant cells to the FN-coated surfaces, focusing on the development of FA complexes. Early cell adhesion experiments (2h and 4h) were performed in serum-free conditions (unless otherwise) after coating the surfaces from a solution containing 20 μg/mL of FN. Cells were seeded at a low density (5,000 cells/cm^2) to maximize cell–material interactions and to minimize cell-cell interactions.

Influence of fibronectin density on cell adhesion. FN density has been shown to influence cell behaviour including adhesion (Cantini 2012, Coelho et al. 2011a, b, Dupont-Gillain et al. 2004, Garcia et al. 1998a, Llopis-Hernández et al. 2013, Vanterpool et al. 2014). Here also, the effect of the availability of ligands on cell adhesion was investigated. Cells cultured on substrates coated with 2 and 20 μg/mL solution concentrations of FN and on glass as control in media under serum free conditions, were fixed after 2h and stained for paxillin, a protein that plays a prominent role in FA complexes, at different time points. Images of representative inverted binary representation show well-defined FA plaques (Figure 6.2A).

With the intention of quantifying the maturation level of the FAs on the different surfaces, frequency distributions for their size (defined as the length of the major axis of the FA plaque) were obtained through image analysis of the paxillin images (process detailed in Figure 4.7). Focal complexes, dot-like complexes shorter than 1 μm, were discarded from the analysis (Geiger et al. 2001). To avoid altered area and roundness values that cell overlapping would have produced, only isolated cells were used. Images were analysed with ImageJ coupled with an in-house macro processor, and the values of each condition were compared.

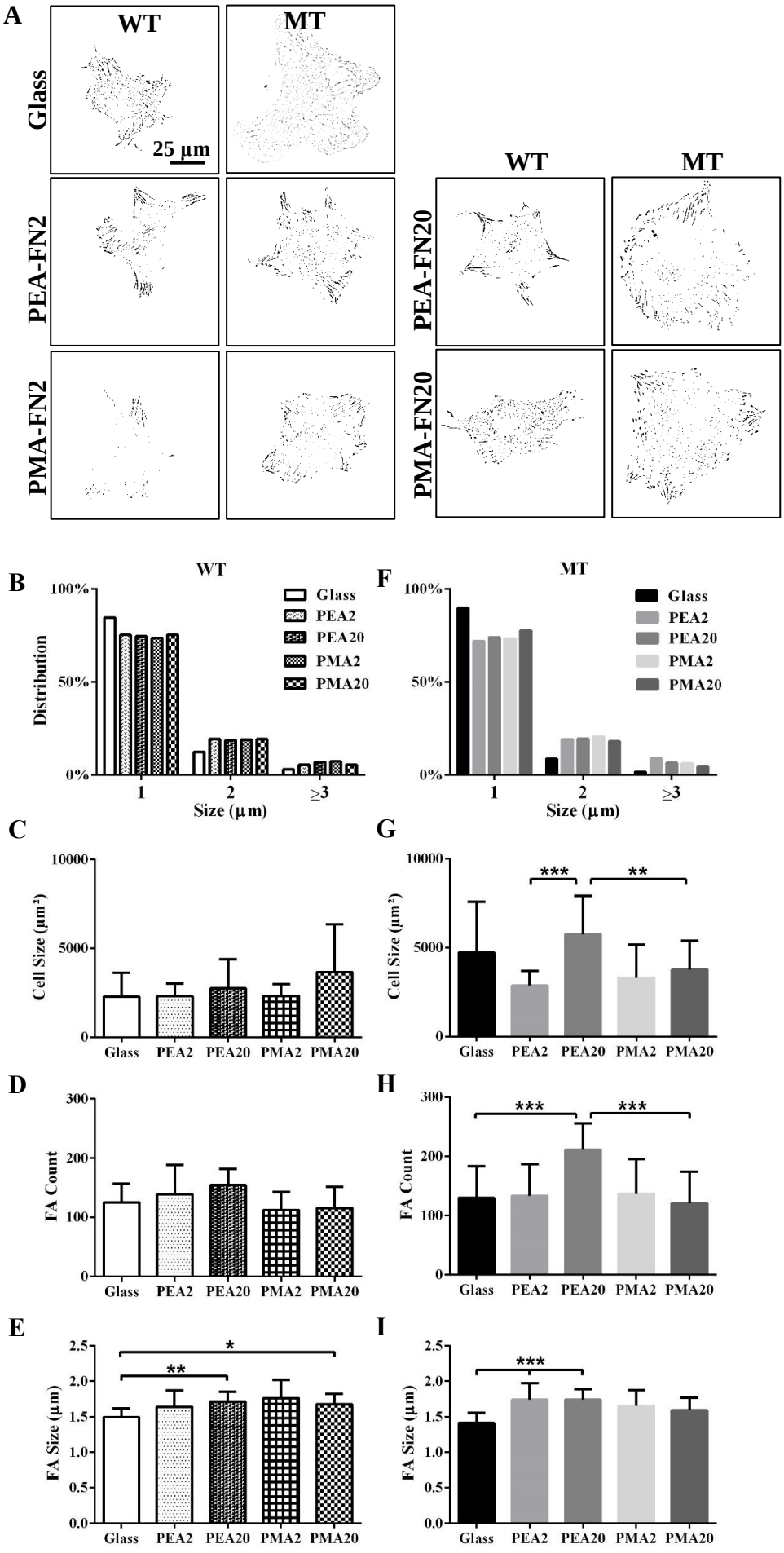
A
WT
MT
Glass
25 μm
PEA-FN2
PMA-FN2
PEA-FN20
PMA-FN20
B
WT
Distribution
100%
50%
0%
Glass
PEA2
PEA20
PMA2
PMA20
1
2
≥3
Size (μm)
F
MT
C
Cell Size (μm²)
10000
5000
0
G
***
**
D
FA Count
300
200
100
H
E
FA Size (μm)
*
2.5
2.0
1.5
1.0
0.5
0.0
I

Figure 6.2 Adhesion quantification: influence of fibronectin density. A) Representative inverted binary representation of focal adhesions of WT and MT fibroblasts (5,000 cells/cm^2) on glass and PEA and PMA coated with 2 and 20 µg/mL FN for 2h in media under serum free conditions, fixed and then stained for paxillin. Size distribution of focal adhesions of WT (**B**) and MT Cells (**F**). Also analysed were cell size of WT (**C**) and MT (**G**); number of FAs per cell in WT (**D**) and MT (**H**); size of FAs in WT (**E**) and MT (**I**). WT, wild type; MT, *COL4A2*$^{+/G702D}$ mutant cells. Data presented as mean ±SD, N ≥12; and analysed with an ANOVA test; *p<0.05, **p<0.01, ***p<0.001. Original images in (Supplementary figure S6.3).

The FA frequency distribution of WT and MT cells, respectively is shown (Figure 6.2B&F). Higher fraction of smaller FA plaques was found compared to the longer FAs (2-3 µm and over) on all the surfaces. The trend was similar for both cells indicating no effect of FN concentrations. WT cell size was not affected by the FN concentration (Figure 6.2C), while the MT cell size was affected only on PEA, being greater on higher FN concentration (20 µg/mL) (Figure 6.2G). Similar to cell size, WT FA count was independent of FN concentration; however, the MT showed significantly higher FA count on PEA coated with the higher FN concentration (Figure 6.2D&H). Interestingly, both cells FA size was not influenced by FN concentrations (Figure 6.4E&I). FA sizes for WT cells were significantly greater on FN-coated PEA and PMA than on glass; similar observations were made for the MT FA sizes.

It is evident that FN concentration has little effect on the WT cells, while it influenced MT cell size, FA count and size especially on PEA coated with FN20. This could be why FN-coated PEA assembled into fibrillary networks induced the secretion of Col4a2 in MT cells. The fibrillary FN nanonetworks may expose cryptic epitopes that induce signalling pathways in *COL4A2*$^{+/G702D}$ mutants allowing the secretion of Col4a2 (Bathawab et al. 2016, Frantz et al. 2010, Klotzsch et al. 2009, Reilly and Engler 2010).

Time evolution effect on cell adhesion. To investigate how cell adhesion on the biointerfaces is influenced by time, cells cultured in medium supplemented with 10% serum were stained for paxillin. Images of representative inverted binary representation showed well-defined FA plaques developing on all the surfaces at 2h (Figure 6.3A) and at 4h (Figure 6.3B), where they were located at the end of prominent stress fibres (Figure 6.8-9). There were no distinctive differences in the appearance of FAs from WT and MT cells at both time points and on all surfaces.

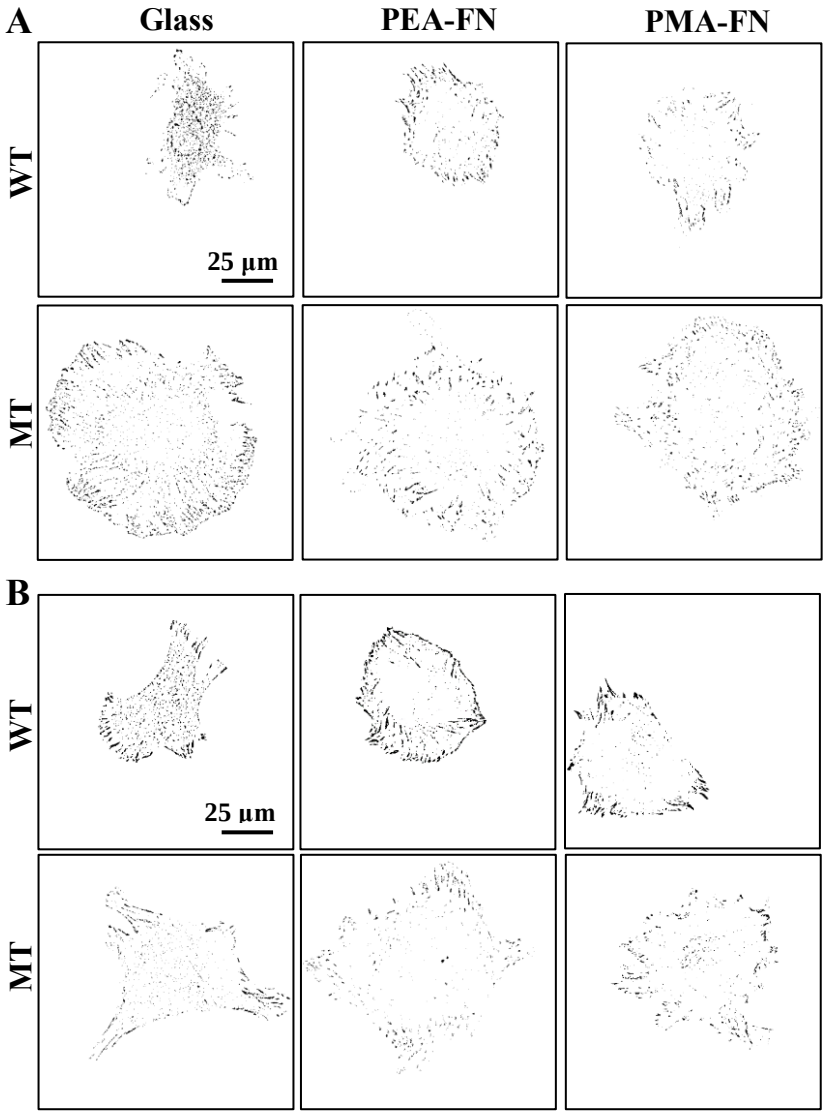

Figure 6.3 Focal adhesion assembly on glass and FN-coated PEA and PMA substrates after 2 and 4h. Representative inverted binary representation of focal adhesions of WT and MT fibroblasts (5,000 cells/cm^2) on glass and PEA and PMA coated with 20 µg/mL FN for 2h (**A**) and 4h (**B**) in media supplemented with 10% FBS, fixed and then stained for paxillin. WT, control wild type; MT, *COL4A2*$^{+/G702D}$ mutant cells. Original images in (Supplementary figure S6.1).

The frequency distribution was similar on glass and FN-coated PEA and PMA for WT and MT cells (Figure 6.4A-B). There was higher fraction of smaller FA plaques (1 to 2 µm) compared to the longer FAs (2-3 µm and over) on all the surfaces for both cell types. The WT cells smaller plaques were noticed to decrease with time on each surface while the MT remained constant. Cell size otherwise called "spreading area", FAs count and size were also analysed. MT size was significantly higher on glass at both times and increased significantly from 2 to 4h (Figure 6.4C). The size of WT cells seemed to decrease with time, whereas it remained constant for the MT cells at both times on all the surfaces except from glass where

it was significantly higher after 4h. It is suggested that this could be due to WT cells beginning migration, whistle the MT cells were still trying to adhere to the substrates; the latter are known for slow proliferation rate at early time (until day 3 as seen in chapter 5) (Murray et al. 2014). The size difference values reflected the images seen in (Figure 6.3).

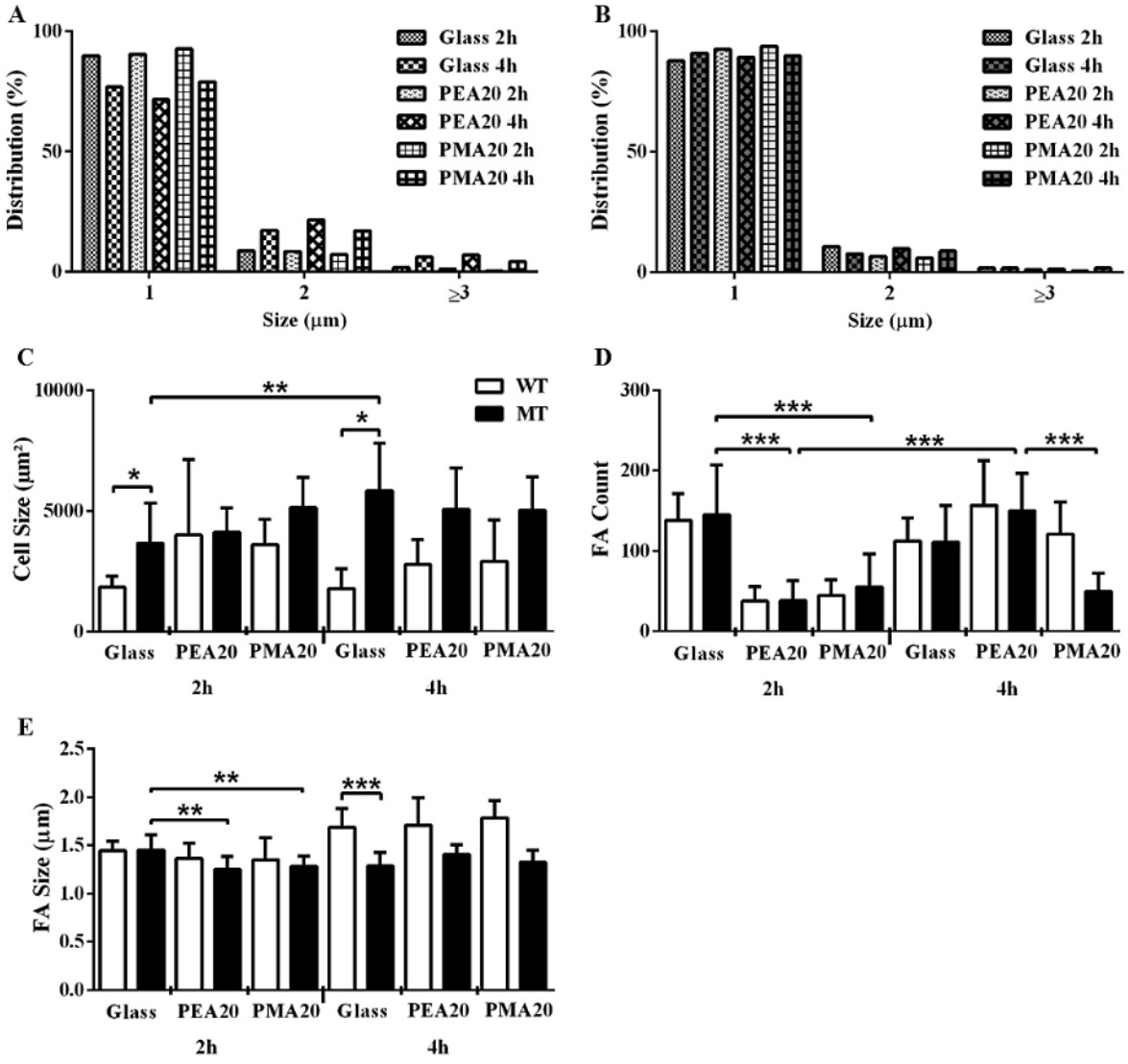

Figure 6.4 Analysis of adhesion of cells to the substrates over time. Images in Figure 6.3 were used to quantify and build size distribution of focal adhesions (FAs) of WT (**A**) and MT cells (**B**) (5,000 cells/cm^2) on glass and PEA and PMA coated with FN 20 µg/mL at different time points (2 and 4h) in media supplemented with 10% FBS. Also calculated were cells size (**C**), number of FAs per cell (**D**); and size of FAs (**E**). WT, wild type; MT, *COL4A2*$^{+/G702D}$ mutant cells. Data presented as mean ±SD, N ≥12; and analysed with an ANOVA test; *p<0.05, **p<0.01, ***p<0.001; only relevant statistical differences are shown. Original images in (Supplementary figure S6.2).

Although cells size differences were observed between the WT and MT cells on glass, this was not translated in the FAs number (Figure 6.4D). No statistical differences in FA count were found between the WT compared to MT cells on any of the surfaces. However, there

was a higher FA count (with significance) on glass than on FN-coated PEA and PMA at 2h. Nonetheless, FA count increased significantly with time for cells on FN interfaces, and remained constant for both cells. FA size also did not differ for both cell types on the surfaces with the exception on glass after 4h (Figure 6.4E). In general, FA size remained constant on all the surfaces for both cell type yet increased for the WT cells as a function of time but not for MT cells. On the other hand, MT cells on glass had greater FA size than on PEA and PMA at 2h, yet FAs size remained constant on all the surfaces independent of the time.

Serum effect on cell adhesion. Then, the effect of serum on cell adhesion onto the FN interfaces was investigated. Serum contains numerous kinds of growth factors and cytokines which contribute to the activation of the signal pathways related to survival and proliferation of the cells (Brunner et al. 2010, Grinnell and Feld 1982). Besides, serum starvation has been demonstrated to highly increase integrins affinity state enhancing cell adhesion to FN (Altankov et al. 2001). Hence, this a potent tool used in molecular and cellular biology experiments. Cells were cultured for 2 and 4 h on the FN (20 μg/mL) interfaces in medium with and without 10% FBS (Figure 6.5A&D).

The graphs showed no effect of serum starvation on cell size for both WT and MT at both time points. Once more MT cell size was higher than the WT cells. Interestingly, supplemented serum had an effect on the FA count. For instance, serum addition significantly decreased FA count for both cell types on FN interfaces at 2h; and the contrary was seen after 4h as FA count increased with serum (Figure 6.5B&E). This could suggest low adhesion at early time increasing time. FA count correlated with the size of FA as similar differences were observed for both cell types (Figure 6. 5C&F). The WT cells seemed to have bigger FA size that the MT.

Role of contractility on cell adhesion. To explore the role of contractility on *COL4A2*$^{+/G702D}$ mutants adhesion to the FN interfaces, cells were treated with 10 μM blebbistatin (BB), a potent inhibitor of myosin-II-specific ATPase, which has been used to inhibit contraction of invertebrate and mammalian muscle preparations containing non-muscle myosin, and also with 10 μM Y27632, an inhibitor of Rho-associated protein kinase. These inhibitors of contractility (Both BB and Y27632) affect the cytoskeleton resulting in cell morphology changes (Darenfed et al. 2007, Liu Zhenan et al. 2010) and also affect adhesion strength and FA assembly (Gallant et al. 2005).

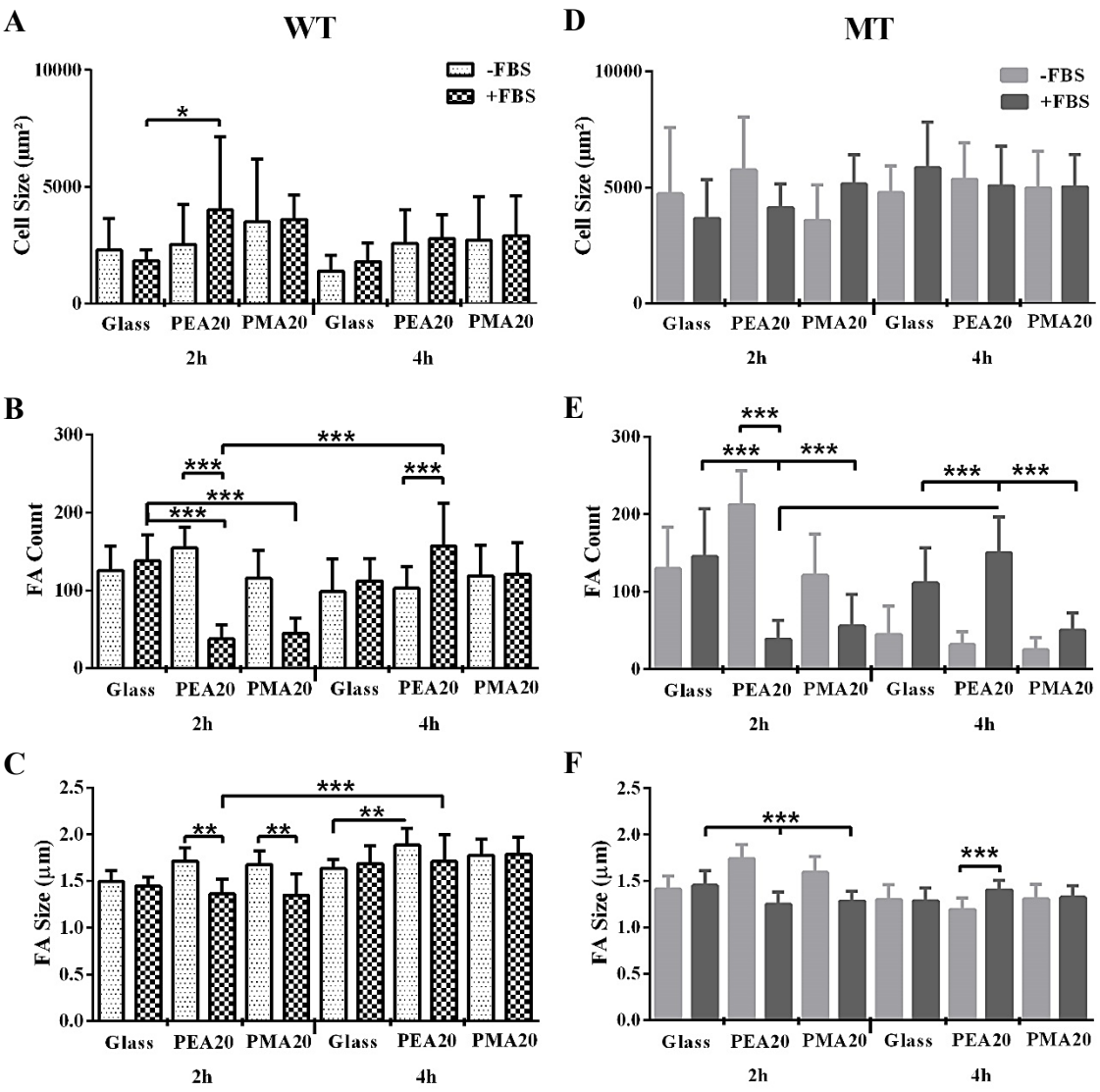

Figure 6.5 Adhesion quantification: serum effect. Images from Figure 6.2 and Figure 6.3 were used for the size distribution of focal adhesions of WT (**A**) and MT cells (**E**) on the substrate polymers. Also analysed were cell size of WT (**B**) and (**F**) on PEA and PMA-coated with a solution of 20 µg/mL FN with or without 10% serum and fixed at 2 or 4h; number of focal adhesions per cell in WT (**C**) and MT (**G**); size of a focal adhesions in WT (**D**) and MT (**G**). WT, wild type; MT, mutants; *p<0.05, **p<0.01, ***p<0.001; only relevant statistical differences are shown; N-number: 12.

Images of representative inverted binary representation of WT and MT cells treated with BB were shown (Figure 6.6B). Well-defined FAs were observed for both cell types, and mainly located at cell extremities. Cells morphology did not seem to be affected when compared to the untreated images (Figure 6.6A) except from few cell protrusion of MT cells on PEA-FN and PMA-FN.

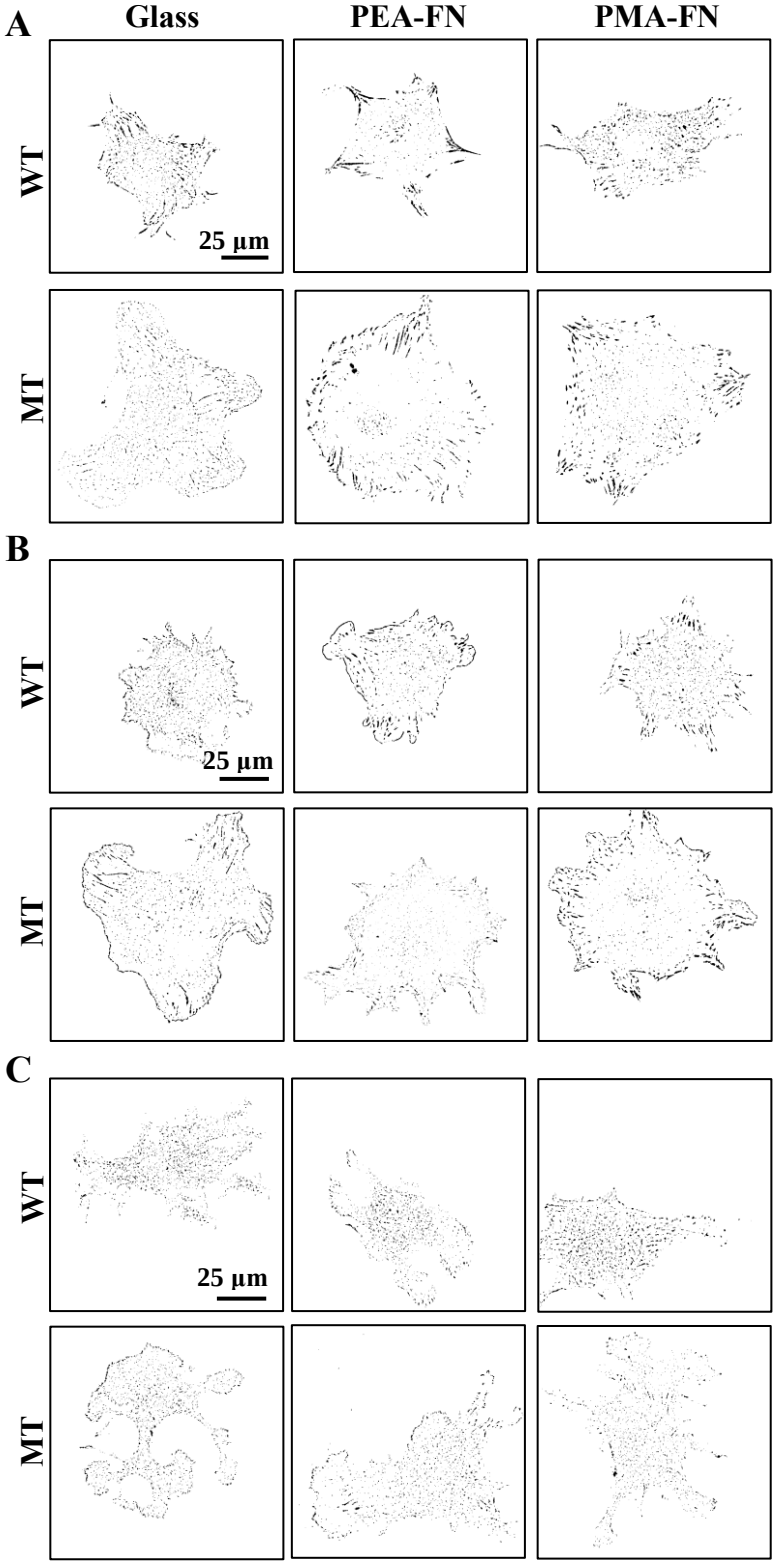

Figure 6.6 Focal adhesion assembly on FN coated PEA and PMA substrates treated with cytoskeleton drugs. Representative inverted binary representation of focal adhesions of WT and MT fibroblasts on glass and PEA and PMA-coated with 20 µg/mL FN and incubated for 2h under serum free conditions before being fixed and stained for paxillin (**A**). Samples were supplemented with 10 µM blebbistatin (BB) (**B**) or 10 µM Y27632 (**C**) for 30 min before fixation. WT, control wild type; MT, mutants.

Cells treated with 10 μM Y27632 displayed randomly distributed FAs throughout the cells and not at the edge compared to untreated or BB treated cells (Figure 6.6C). Their FAs looked more grainy like (small dots) than the usual long dots seen in untreated cells. Both WT and MT cells were seen elongated and the morphology was greatly affected. FA frequency distribution of cells treated with BB and with Y27632 (Figure 6.6) were quantified. The trend distribution of smaller and greater FAs size was similar for both cell types treated with BB and Y27632 (Figure 6.7A&E). Higher fraction of smaller FA plaques was found compared to the longer FAs (>2 μm) on all the surfaces by both cells. BB and Y27632 had no effect on WT cells size on any of the surfaces (except from the morphology), yet they decreased statistically MT cells size on PEA-FN (Figure 6.7B&F).

FA count of WT cells on glass was not much affected by the treatment with BB or Y27632 but was significantly affected on PEA-FN and PMA-FN. BB increased the FA count and Y27632 decreased it for WT on PEA-FN and PMA-FN; and this could be due to the coated FN (Figure 6.7B-C). Similarly, drug treatment affected the MT FA count only on PEA and PMA but unlike the WT cells, BB reduced FA count (Figure 6.7G). Since FA count was affected by treatment with myosin II inhibitors, FA size was quantified. Once more, BB and Y27632 greatly affected both cell types only on FN coated PEA and PMA but not on glass (Figure 6.7D&H).

In summary, inhibitors of contractility had an effect on the FAs count and size of WT cells only on FN-coated substrates. The inhibitors seemed to have little effect on the morphology and size of WT cells on all the surfaces. Conversely, they disrupted the cytoskeleton of the MT cells resulting in cells morphology and size change, including FAs count and size, especially on FN-coated substrates. This indicated that these cells utilise different cytoskeleton fibres when on glass than on the FN interfaces. It suggested that the cells adhere strongly to the coated FN compared to when on glass.

It is noteworthy to mention that cells were incubated with the inhibitors for 30 min before fixation to allow cells to adhere to the surfaces for minimum time of 2h. This means that the effect of the drugs on the cells would have been short, indicating the mild effect on WT cells size. This is short treatment comparing to the treatment reported in most literatures of over 2h (Dumbauld et al. 2010, Garcia et al. 1998a). In the case of the MT cells, these cells stiffness have been shown in chapter 5 to be 10-fold softer than the WT cells, suggesting that they would be greatly affected by the inhibitors of centrality compared to the WT cells. Nonetheless, it interesting to observe that the cytoskeleton has a great role in cells adhesion.

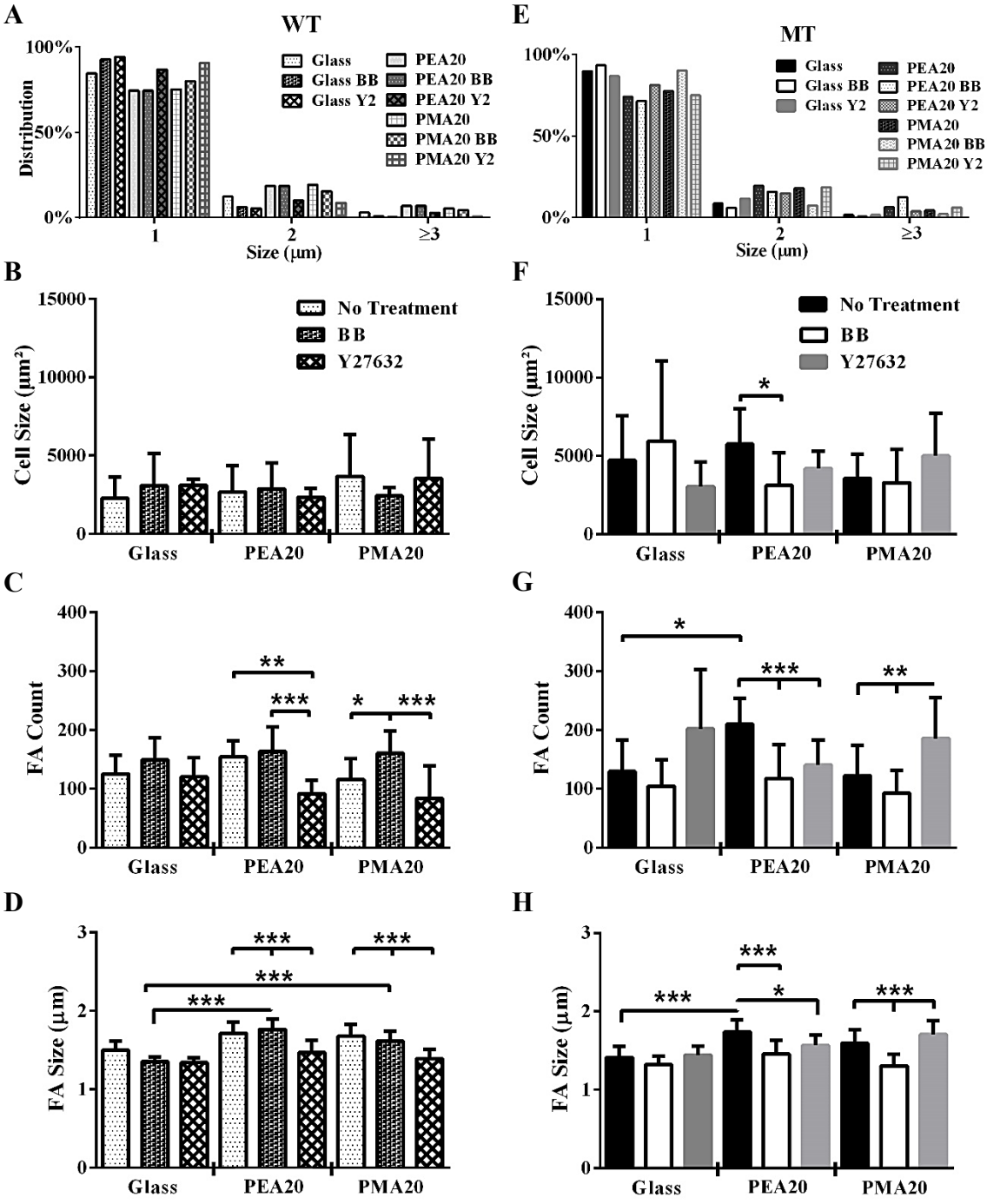

Figure 6.7 Adhesion quantification: role of contractility. Images in (Figure 6.6) were used for size distribution of focal adhesions of WT (**A**) and MT (**E**) on the substrate polymers. Also analysed were cell size of WT (**B**) and MT (**F**) on PEA and PMA coated with a solution of 20 μg/mL FN in media under serum free conditions; number of focal adhesions per cell in WT (**C**) and MT (**G**); size of a focal adhesions in WT (**D**) and MT (**G**). WT, wild type; MT, mutants. BB, blebbistatin; Y27632, ROCK inhibitor. Data presented as mean ±SD, N ≥12; and analysed with an ANOVA test; *p<0.05, **p<0.01, ***p<0.001.

6. 4. 2 Cell signalling

To assess whether the FN-coated substrates, especially PEA, trigger the adhesion-signalling pathway in *COL4A2*$^{+/G702D}$ mutant cells to influence the secretion of col4α2, a number of signalling pathways were analysed including integrin expression, the phosphorylation of FAK and ERK1/2 and the DDR1.

Signalling by integrins. Integrins binding to the adsorbed FN in the secretion of col4α2 by *COL4A2*$^{+/G702D}$ cells was studied. $\alpha_5\beta_1$ and $\alpha V\beta_3$ heterodimers are referred to as the main FN receptors (Schaffner et al. 2013), the first one is the classical FN receptor that provides primary adhesion mechanism, and the second one recognizes vitronectin. Integrins are also involved in intracellular signalling and, thus, a diverse range of cell functions. They recognize specific sequences of ECM proteins such as the arginine-glycine-aspartic acid tripeptide (RGD) present in several proteins such as fibronectin and vitronectin, providing a trans-membrane link between the ECM and actin cytoskeleton (Hynes 2002).

β_1 and αV integrins binding to FN-coated materials together with paxillin were analysed via immunostaining, following the overall cell morphology, cell adhesion quantities and spreading of WT (Figure 6.8) and MT cells (Figure 6.9). Paxillin staining of both cell types showed well-developed FA plaques that were mainly located at the end of prominent stress fibres on all the substrates, with the exception of the MT on glass (Figure 6.9), this could suggest the low secretion of Col4 by the MT cells. Both integrins were expressed by both cell types adhering on FN coated substrates. β_1 staining showed well pronounced clusters resembling FA contacts for the WT cells, but not for the MT where it was dispersed throughout the cells. The αV staining was not similar to β_1, it showed a rather diffuse pattern in the entire cell on FN-coated substrates for the MT compared to the WT cells.

FA and β_1 represented a linear organization along with actin stress fibres. This revealed that $\alpha_5\beta_1$ is the main receptor involved during the initial cell interaction with the material-driven FN network, as it happens for the interaction of cells with natural physiological matrices; these observations correlated with a study by (Llopis-Hernández et al. 2013). β_1 binding has been related to the simultaneous availability of the synergy and RGD sequences within FN (Llopis-Hernández et al. 2013). $\alpha V\beta_3$ has been reported to be mainly expressed by cells on PMA-FN where FN is adsorbed as discrete aggregates. In this state, FN synergy sequence availability is hindered, thus cell adhesion mostly occurs through the αV receptor, which only needs the exposition of the RGD sequence (Llopis-Hernández et al. 2013). Fluorescence integrated density quantification was performed (Figure 6.14).

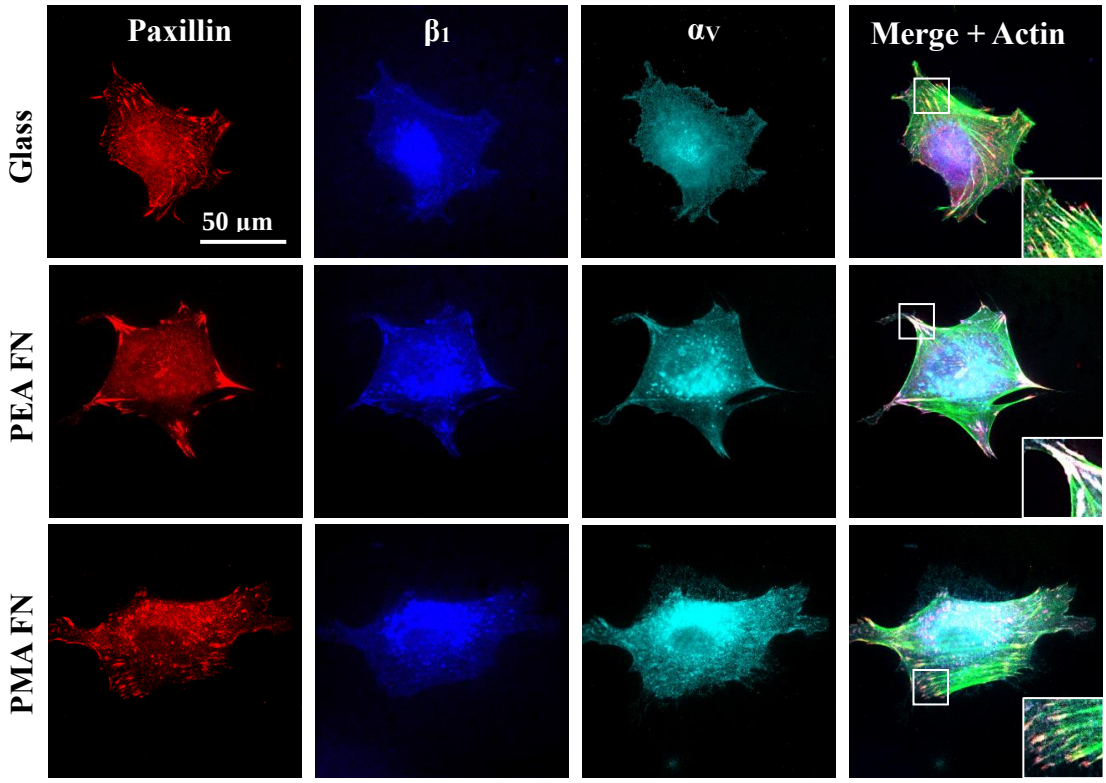

Figure 6.8 Integrins and focal adhesion immunostaining of WT. Expression of β_1 and αV integrins and of focal adhesion protein paxillin by WT fibroblasts adhering to 20 µg/mL FN-coated substrates for 2h under serum free conditions.

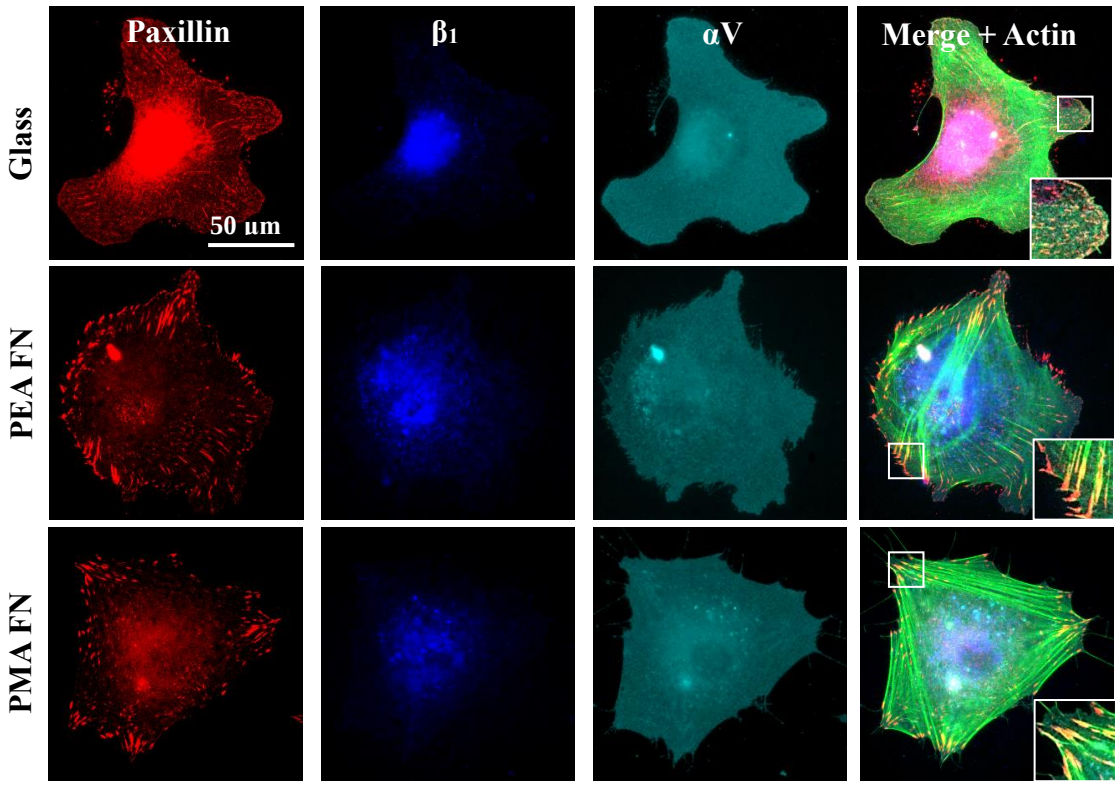

Figure 6.9 Integrins and focal adhesion immunostaining of MT. Expression of β_1 and αV integrins and of focal adhesion protein paxillin by MT fibroblasts adhering to 20 µg/mL FN-coated substrates for 2h under serum free conditions.

To gain insight into the involvement of cell contractility on integrin expression and cell adhesion, cells were treated with 10 µM BB and Y37632. Treatment of cells with these inhibitors of contractility has been reported to reduce integrin expression, for example they greatly reduce αV expression in myofibroblasts (Wipff et al. 2007). In general, cells were found to spread on all surfaces but the cytoskeleton was not well-developed compared to untreated samples shown above. The WT morphology and actin cytoskeleton were better pronounced after treatment with BB (Figure 6.10) than the MT cells (Figure 6.11) which were highly affected showing elongation of cells and actin cytoskeleton not completely developed and only peripheral stress fibres observed.

FAs in WT cells were well-developed and located at cell periphery on the FN-substrates than on glass. In contrast, FAs in MT had a more diffused pattern on all the surfaces. β_1 expression formed structures resembling FA contacts in the WT cells than in the MT which was diffusely dispersed. αV integrins in the WT appeared in a rather linear pattern, resembling fibrillar adhesions compared to the diffused display in MT cells, yet in the latter it was more pronounced than the β_1.

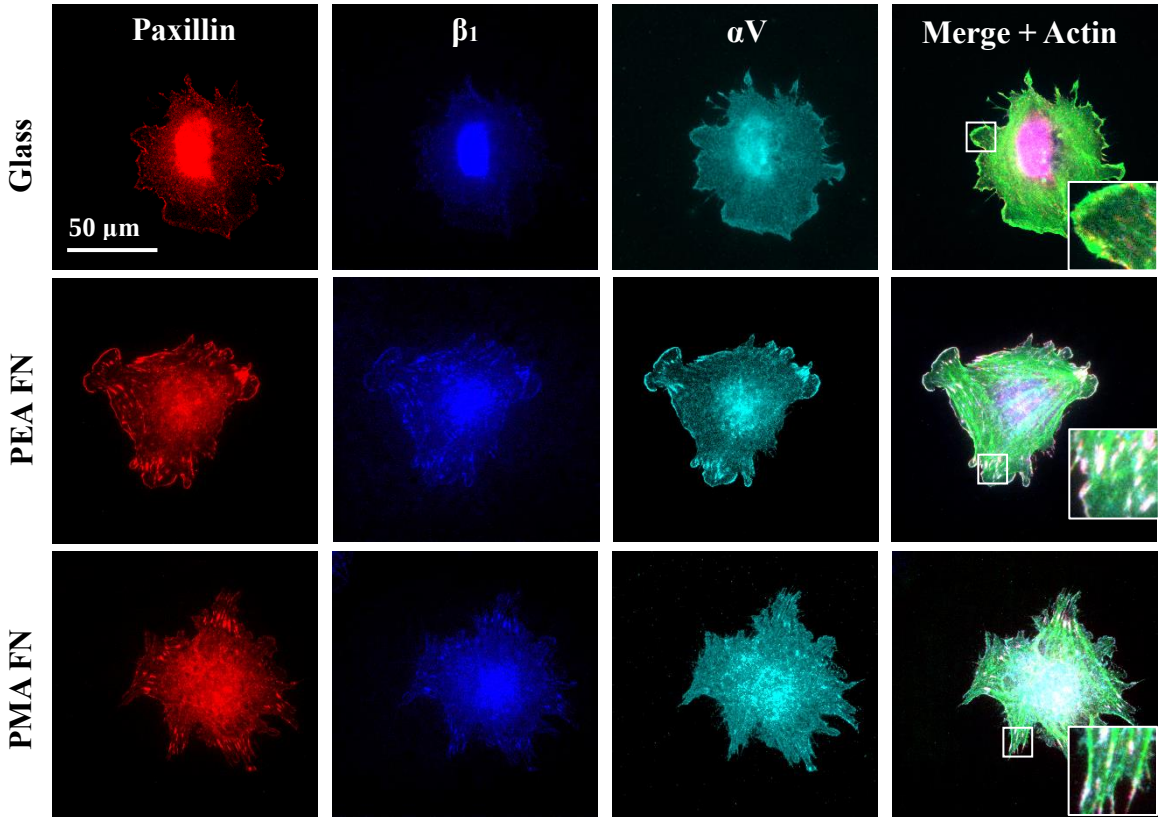

Figure 6.10 Integrins and focal adhesion immunostaining of WT cells treated with blebbistatin (BB). β_1 and αV integrins and FA protein (paxillin) staining in WT cells on 20 µg/mL FN-coated substrates for 2h under serum free conditions also and supplemented with BB 30 min before fixation and staining.

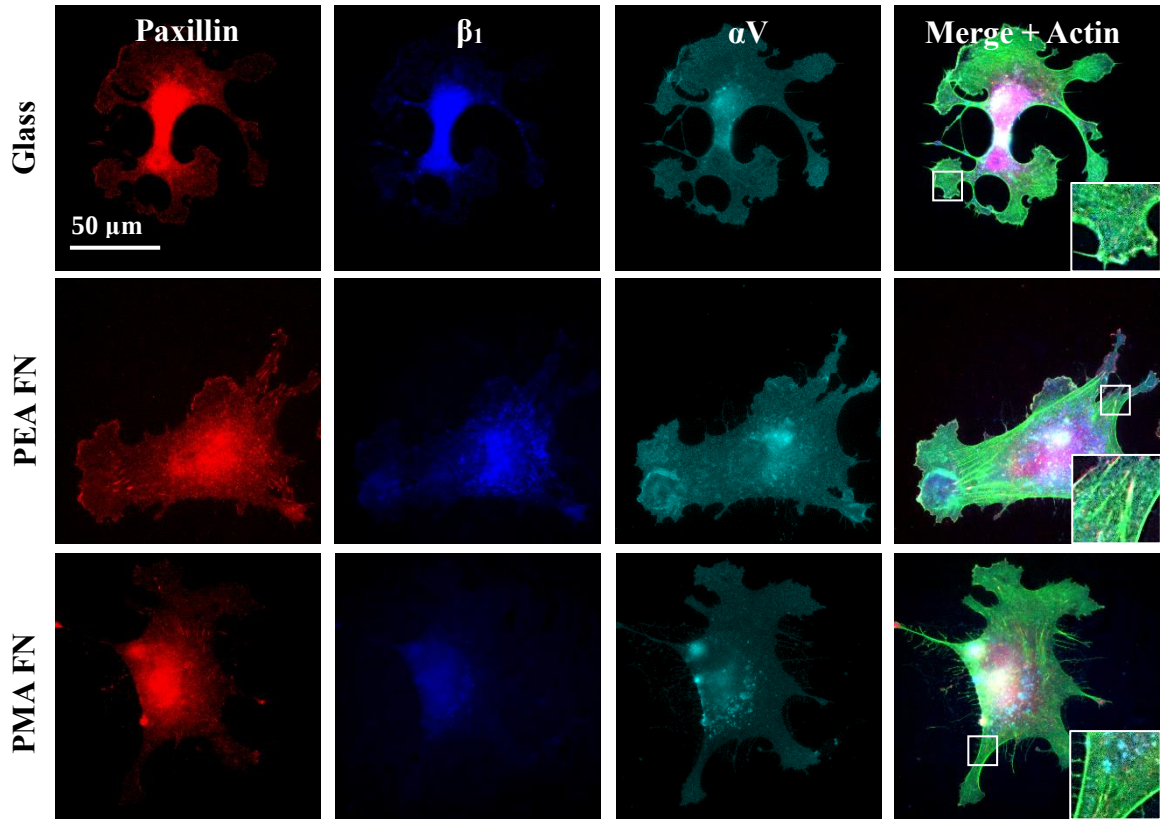

Figure 6.11 Integrins and focal adhesion immunostaining of MT cells treated BB. β_1 and αV integrins and paxillin staining in MT cells on 20 µg/mL FN-coated substrates for 2h without serum also and supplemented with BB 30 min before fixation and staining.

Interestingly, treatment with Y27632 affected the WT cells on all the surfaces especially on glass (Figure 6.12) more than the MT (Figure 6.13) as seen by the cells morphology. The MT cytoskeleton was more developed than that of the WT cells. It showed formation of prominent F-actin fibres terminating in well-developed FA complexes on glass and PMA but not on PEA, Figure 6. 14. While the WT showed a more dispersed actin distribution (either lacking stress fibre formation or mostly peripheral staining). FAs in WT cells had diffuse patterns while in MT they represented a rather linear organization along with actin stress fibres. β_1 integrins staining was diffused throughout both WT and MT cells, but with less background in the MT. WT cells expression of αV showed diffuse distribution, and this was similar to for the MT cells.

These results indicated that both cells types express β_1 and αV integrins on all the surfaces but increased staining was observed for cells on FN-coated substratum, suggesting the implication of adhesive proteins in cell adhesion. The data showed that the two drugs have different inhibition mechanisms on these cells. BB highly reduced the expression of both β_1 and αV integrins in MT cells compared to the WT cells. This correlated with the stiffness of MT cells as treatment with BB would induce more contractility hence reduced integrins. On

the other hand, Y27632 decreased both integrin expressions of WT cells on the surfaces especially on glass while it had reduced effect on the MT cells integrin expressions. These results showed the involvement of integrin in cell material interaction that is mediated by ECM proteins. Integrin expressions are involved in intracellular signalling and, thus, a diverse range of cell functions including gene expression, protein secretion and cell adhesion (Bischof et al. 1995, Kundu et al. 2009, Merna 2014, Werb et al. 1989).

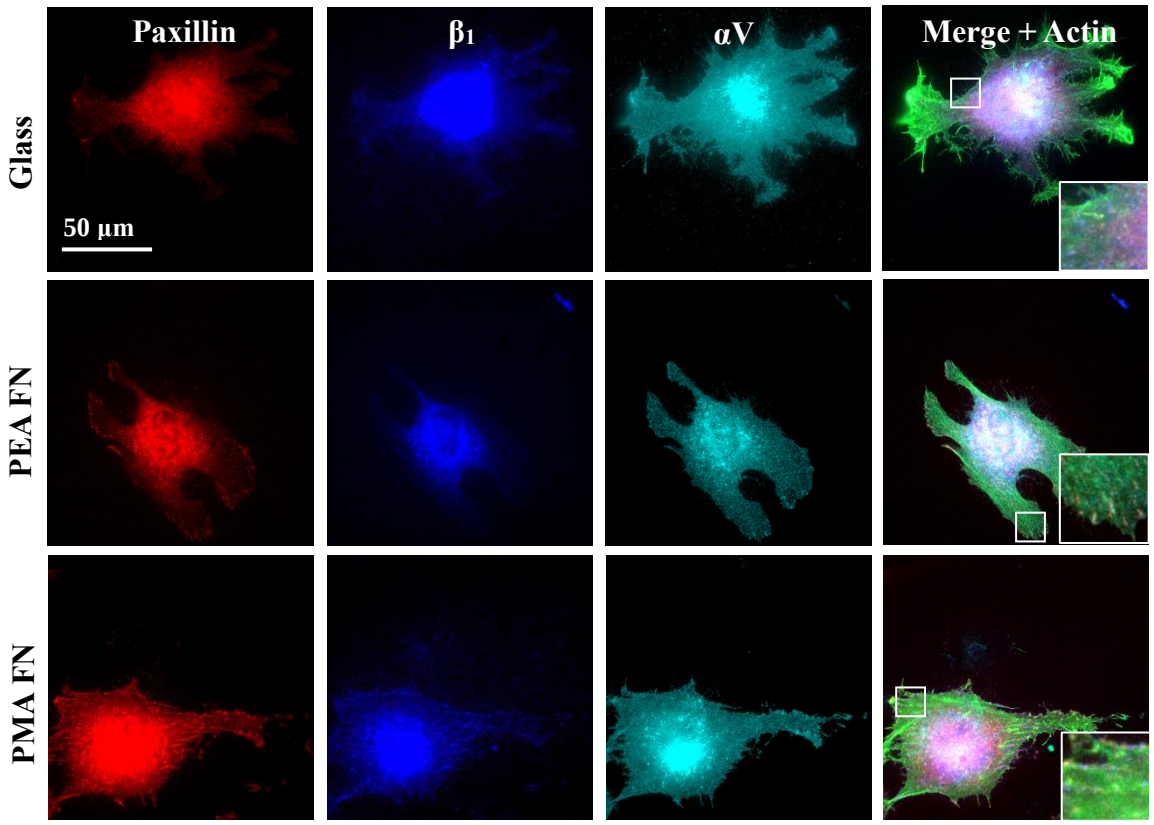

Figure 6.12 Integrins and focal adhesion immunostaining of WT treated with ROCK inhibitor. Expression of β_1 and αV integrins and paxillin by WT cells on 20 µg/mL FN-coated substrates for 2h without FBS and supplemented with RI 30 min before fixation.

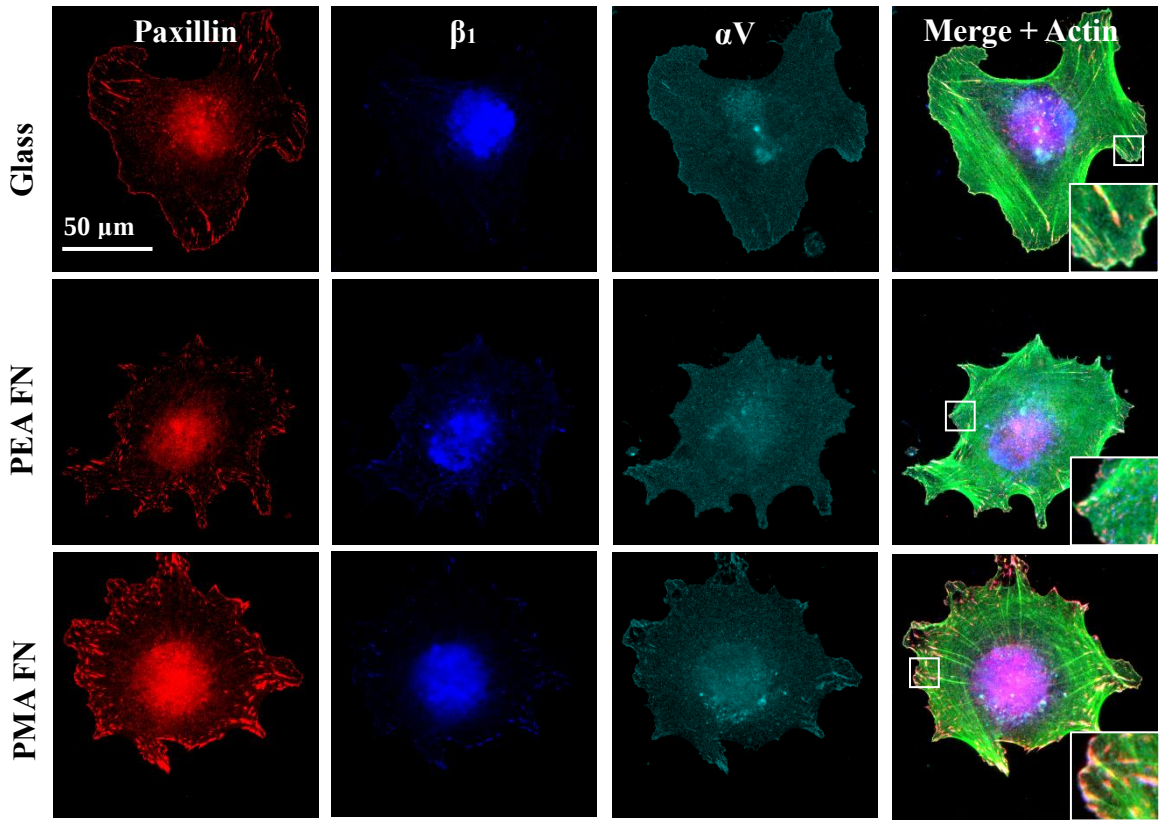

Figure 6.13 Integrins and focal adhesion immunostaining of MT treated with ROCK inhibitor. Expression of β_1, αV integrins and paxillin by MT cells on 20 µg/mL FN-coated substrates for 2h without FBS and supplemented with RI 30 min before fixation.

To measure the expression of integrin in both cell types, quantification of fluorescence-integrated density of stained integrins in (figures 6.8-13) above was performed (Figure 6.14). This could provide with the adhesion state on the FN-coated substrates compared to glass. Total αV and β_1 integrins were generally higher in the MT than the WT cells. β_1 integrin was observed higher on FN-coated substrates especially on PEA, indicating the involvement of FN fibrillar network in cell adhesion and signalling. αV quantification showed low expression in the WT cells compared to MT cells although the images displayed well stained integrin. This could be due to the expression being more like FA in WT cells than dispersed with high background in the MT cells.

Statistical differences were found only on PMA-FN, glass with BB, PEA-FN RI and PMA-FN RI for αV and only on PMA-FN RI for β_1. αV co-localising with FAs was higher for the MT than the WT cells, while β_1 was similar for both cells. The ratio of total to integrin co-localising with FAs was similar for β_1 in both cells types while it was higher for αV in WT cells compared to the MT cells.

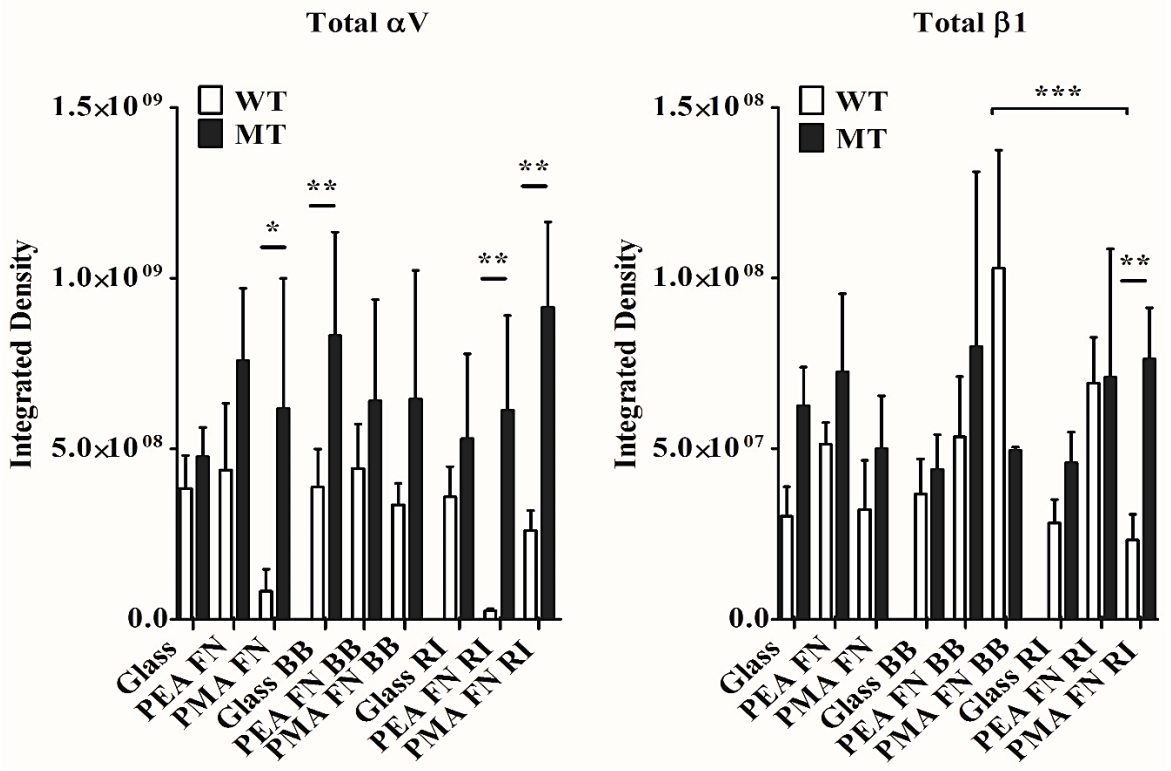

Figure 6.14 Integrin quantification. Quantification of fluorescence integrated density of αV and β_1 integrin from Figure 6.8, Figure 6. 9, Figure 6. 10, Figure 6. 11, Figure 6. 12 and Figure 6. 13. First column shows total integrin; second column: integrin co-localising with FAs; third column: ratio between total integrin with integrin co-localising with FAs. BB, blebbistatin; RI, ROCK inhibitor. Data presented as mean ±SD, N ≥10; and analysed with an ANOVA test; *p<0.05, **p<0.01, ***p<0.001; only relevant statistical differences are shown. Further analysis are presented in Supplementary figure S6.5.

FAK phosphorylation analysis. Signalling was also investigated via phosphorylation of focal adhesion kinase (pFAK) that is activated after integrin binding and clustering (Mitra et al. 2005). FAK is part of the FA complexes and activate multiple signalling pathways that regulate cell migration, survival, proliferation and differentiation (Manning et al. 2002, Roskoski 2010, 2012). Phosphorylation of Tyr-397, the autophosphorylation site in FAK and a binding site for Src and PI-3 kinase (Reiske et al. 1999, Schaller et al. 1994) was examined by immunofluorescence and western blotting. FAK phosphorylation is an intermediary step between adhesion and downstream targets, including MAPK pathways. As a result, Tyr-397 autophosphorylation of FAK plays a central role during many cells behaviour including proliferation that is influenced by protein regulation (Aiyelabegan and Sadroddiny 2017, Biggs et al. 2009, Burridge 2017).

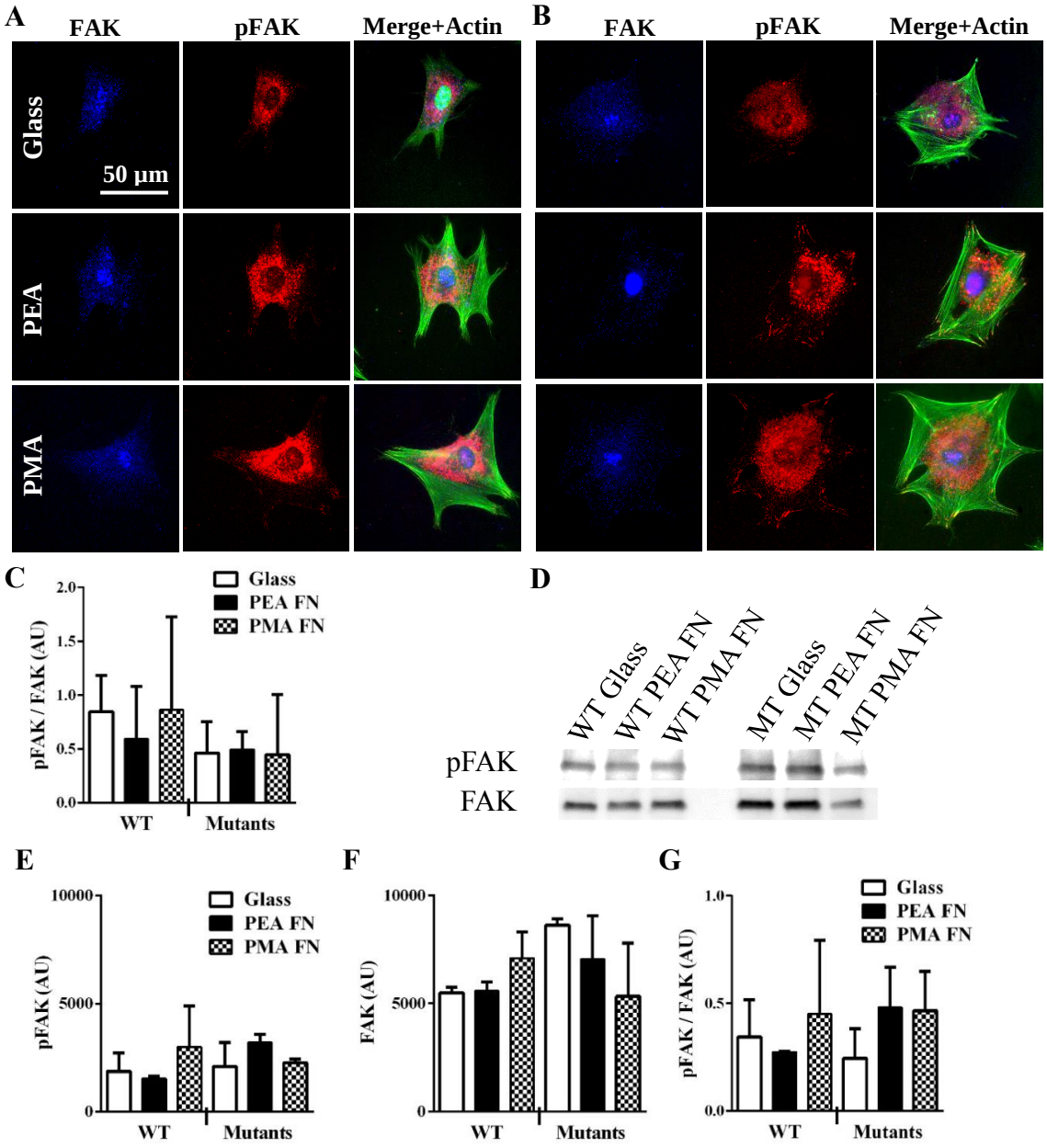

Figure 6.15 FAK phosphorylation analysis by immunofluorescence (IF) and western blot (WB). IF images staining of FAK and phospho-FAK in WT (**A**) and MT cells (**B**). Integrated density was quantified and a ratio of the values presented (**C**). Representative images of WB membranes with detected FAK and pFAK proteins in cells lysates after 2 h incubation (**D**); bands were analysed for pFAK (**E**), FAK (**F**) and a ratio also calculated (**G**). N= 3. No statistically significant differences were found for the ratio of both IF and WB values.

Cells were seeded at an initial density of 5,000 cells/cm^2 (for IF) and 20,000 cells/cm^2 (for WB) in FBS-free medium to rule out the presence of any external FN influence on the material surface. After 2h, IF staining of both WT and MT cells on glass displayed few distinctive FAK and pFAK, which were mainly located in the centre of the cells (Figure 6.15A-B). However, on the FN-coated substrates, both cell types displayed well-developed

FAK, showing accumulation of FAs at sites and mainly at periphery, though the pFAK staining was less pronounced; this corroborated with the FA count observed in (Figure 6. 3D). A ratio of pFAK to FAK fluorescence intensity showed lower value for the WT cells on PEA-FN compared to glass and PMA-FN, although slightly increased value for MT on PEA-FN cells than on glass and PMA-FN yet, with no significant differences (Figure 6.15C).

For Western blotting, cells were lysed and the protein extract was purified and subjected to a 7% SDS-PAGE electrophoresis. Bands corresponding to FAK and pFAK were visualized and quantified by densitometry using ImageJ. FAK bands intensity remained approximately constant for both cell types on all the surfaces; whereas the pFAK bands value were significantly higher for MT cells (Figure 6.15D). Quantification of the bands intensity revealed pFAK levels were lower for WT cells on PEA-FN compared to PMA-FN and glass. In contrast, pFAK levels for MT cells were higher on PEA-FN than on PMA-FN and glass, once again with no significant differences (Figure 6.15E).

On the other hand, FAK levels was similar for WT cells on glass and PEA-FN, nonetheless elevated on PMA-FN. MT cells FAK levels were higher on glass than on FA-coated PEA and PMA, yet with no significant differences (Figure 6.15F). Similar to the IF quantification, the ratio of pFAK to FAK by WB showed lower levels on PEA-FN compared to glass and PMA-FN for WT cells, but higher values on PEA-FN than glass and PMA-FN for MT cells (Figure 6.15G), once more no statistically significant differences were found. The results of the WT cells correlated with a study that showed higher levels of pFAK on PEA than PMA, although lower than glass, revealing enhanced signalling from the substrate-assembled FN networks (Llopis-Hernández et al. 2013). The enhanced phosphorylation of FAK in MT cells on PEA-FN could suggest the role of the material-driven FN network assembled on PEA in inducing *COL4A2*$^{+/G702D}$ mutant cells to secrete Col4a2.

ERK1/2 phosphorylation analysis. Signalling was then assessed in cells early adhesion behaviour via ERK1/2 phosphorylation, a downstream effector which is activated via the mitogen activated protein kinase (MAPK) branch of GF receptor and integrin signalling (Olsson et al. 2006). A 30-minute culture of *COL4A2*$^{+/G702D}$ mutant and WT cells on FN interfaces was used to quantify the amount ERK1/2 phosphorylated on Thr-202/Tyr-204.

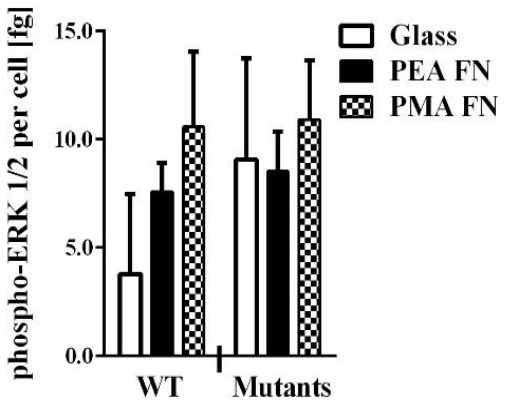

Figure 6.16 ERK1/2 in WT and MT cells on glass and FN-coated PEA and PMA. ELISA quantification of pERK1/2 after 30 min incubation. ANOVA showed no statistically significant differences between samples. Data presented as mean ±SD, N =3.

As indicated in the introduction of this chapter, ERK1/2 are two isoforms of the extracellular regulated kinase, a kinase pertaining to the MAPK regulatory pathway, involved in transcription and protein synthesis/secretion processes (Biggs et al. 2009, Mitra et al. 2005, Provenzano et al. 2009, Roskoski 2012). FN is known to trigger the activation of this pathway via dimerization of the $\alpha_5\beta_1$ integrin. ERK1/2 phosphorylation levels for WT was lower on glass than on PEA-FN, and in turn the latter was lower to PMA-FN with no statistical significance differences. MT cells also expressed similar phosphorylation levels on all the surfaces (Figure 6.16). ERK1/2 has been previously shown to be higher on PEA than on PMA in human umbilical vascular endothelial cells (Moulisová et al. 2017).

ERK1/2 is crucial for gene expression and DNA synthesis. Analysis showed integrin expression independent of the surfaces in all the cell types. It is also interesting to note that ERK1/2 phosphorylation, an event taking place upstream to the formation of FA complexes and the subsequent activation of the MAPK signalling pathway, correspond to the FAK phosphorylation shown above. This indicates that FN coating on PEA is affecting these signalling pathways to a lesser extent; hence, pointing to other pathways. It should be noted that FAK and ERK1/2 phosphorylation experiments were carried at specific time; these pathways could still affect the cells at different times.

DDR1 signalling analysis. Widely expressed mammalian adhesion receptors for fibrillar collagens include the $\alpha_2\beta_1$- and $\alpha_{11}\beta_1$-integrins and the disk-shaped receptor tyrosine kinases discoidin domain receptors (DDRs) (Leitinger and Hohenester 2007). Integrins and DDRs bind distinct and separate motifs in native fibrillar collagen (Vogel et al. 1997). DDR1 is a tyrosine kinase transmembrane receptor together with DDR2 expressed in several cell types

and organs and mainly regulates collagen synthesis and degradation, and monitors ECMs component formation. On activation by binding to fibrillar or soluble collagens, DDR1 regulates cell adhesion, differentiation, migration and proliferation (Vogel et al. 1997).

Immunostaining images displayed DDR1 mainly expressed on the membrane surface for both cell types on all surfaces (Figure 6.17A). WB analysis detected DDR1 expression levels on glass being significantly higher for the MT than the WT cells (Figure 6.17B-C). However, there was no significant differences in DDR1 levels for both cell types on the FN interfaces. The DDR1 levels was higher for WT cells on FN-coated PEA and PMA than on glass. For the MT cells, DDR1 levels were lower on the FN coated polymers than on glass, though PEA levels were higher than PMA.

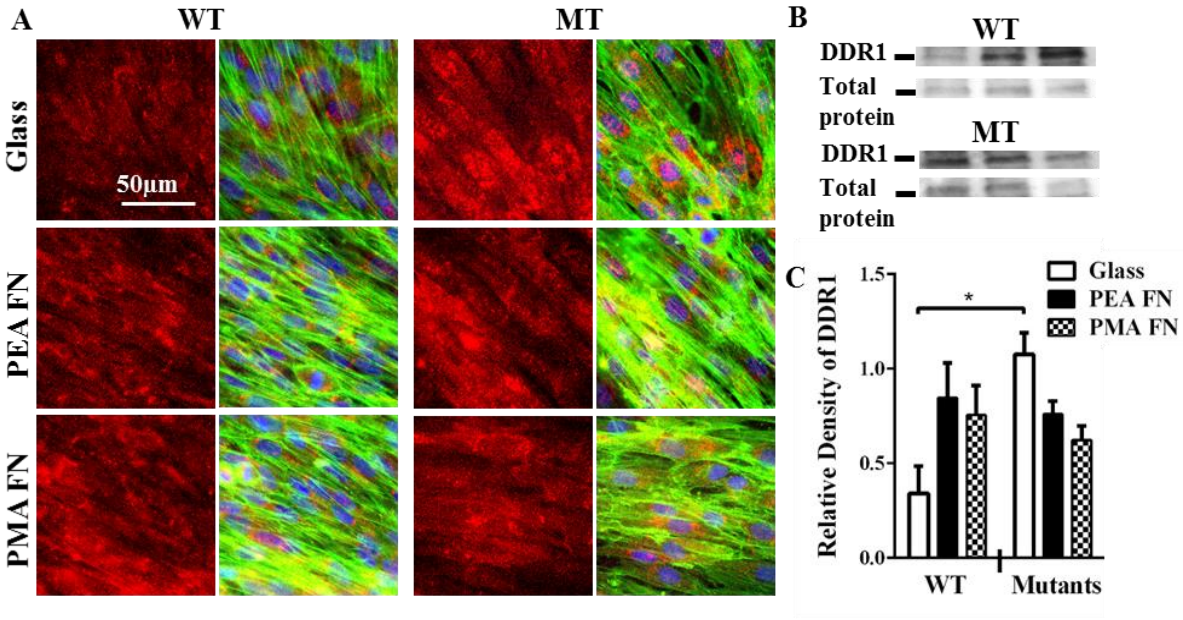

Figure 6.17 DDR1 (125 kDa) protein expression levels in the WT and MT cells were assessed using immunofluorescence (**A**) and western blot (**B**). The WB bands show traces of DDR1 in cells grown on FN coated substrates for 5 day (**C**). Total protein was used as the internal standard. Data are shown as the mean ± SD; N= 3. *p < 0.05.

6. 4. 3 Analysis of cell adhesion strength

Then, to explore how the *COL4A2*$^{+/G702D}$ mutant cells adhere onto the biointerfaces, the cell adhesion strength was measured to gain insight into how they interact with the biointerfaces. While various methods were developed to characterize cell adhesion, here cell adhesion strength was quantified using a well characterized spinning disk hydrodynamic shear assay that has been used extensively for investigating structure function relationships among adhesive components (Gallant et al. 2005, Garcia 2005, Garcia et al. 1998a). This method

was particularly used due to its access at the Georgia Institute of Technology under the supervision of Prof Andrés J. García. This system applies a well-defined range of hydrodynamic forces to a population of cells adhered to the biointerfaces and provides sensitive measurements of adhesion strength. To analyse data, detachment profiles (f versus τ) were fit to a sigmoid curve ($f = 1.0/(1.0 + \exp[b(\tau - \tau_{50})]$) to obtain the shear stress for 50% detachment (τ_{50}) that allowed for quantitative comparisons between experimental conditions, τ_{50} is defined as the adhesion strength (Figure 6.18). For all the cell adhesion strength values presented here, only the sigmoid curve profiles that resembled the one in Figure 6.18 or the control glass were used as some of the sigmoid curves shifted to the right not allowing fitting. Thus only 80% of the profiles were used for the bar values indicated.

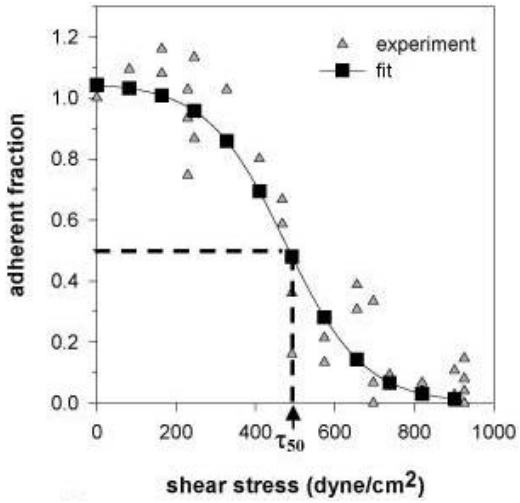

Figure 6.18 Characteristic detachment profile. Shown is fraction of adherent cells (f) as a function of surface shear stress (τ). Adapted from (Gallant et al. 2005).

Incubation time influences on adhesion strength. To investigate if adhesion time influenced cell adhesion strength, cells were seeded for 2 and 4h before being spun for 5 min at 6000 rpm. After spinning, remaining cells were fixed, stained, and counted at specific radial positions. The fraction of adherent cells (f) was calculated by dividing the number of cells in each field by the number of cells at the centre of the array, where negligible forces are applied. Representative detachment profiles indicating fraction of adherent cells versus applied shear stress for WT and MT cells respectively are shown (Figure 6.19A&B), additional profiles in Supplementary figure S6.6.

Adhesion strength was comparable for both cell types on each substrate, although higher for the MT than WT cells on glass at time 2h (Figure 6.19C). Adhesion strength was found to be statistically higher for both WT and MT cells on the FN-coated substrates (especially on PEA) than on glass independent of the time. Incubation time of cells on PEA-FN and PMA-

FN influenced adhesion strength as after 4h it decreased significantly for both cells. The decrease in adhesion strength after time could suggest migration of cells, as at early time they tend to attach to sense the environment.

Assembly of FAs complexes, especially at the periphery, has been reported to contribute significantly to adhesion strength (Balaban et al. 2001, Gallant et al. 2005, Garcia and Gallant 2003). Here, adhesion strength on the FN interfaces correlated with the FA study further above. Recruitment and clustering of integrins into the focal complexes (seen in Figure 6. 8-13) lead to increases in adhesion strength. In this study also, observations were consistent with the increased adhesion strength of cells onto the adhesive FN coated on the substratum (Figure 6.19C), in agreement with previous report (Garcia and Gallant 2003).

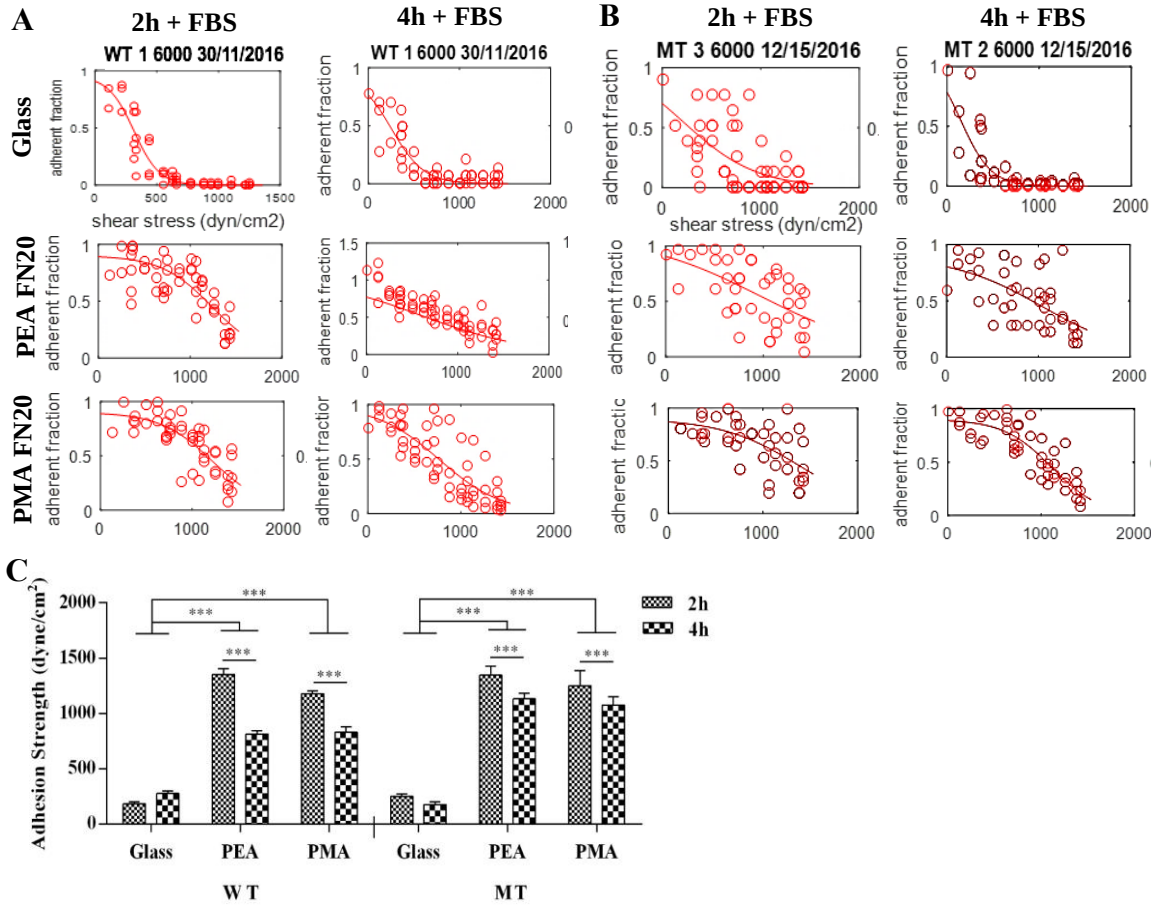

Figure 6.19 Cell adhesion strength measurements: time evolution. Samples detachment profile showing fraction of adherent cells versus applied shear stress for WT (**A**) and MT cells (**B**) adhering to substrates coated with FN solutions of 20 µg/mL for 2 and 4 h in media supplemented with 10% serum. Additional profiles in Supplementary figure S6.6. Experimental points were fit to sigmoid to obtain the shear stress for 50% detachment (τ_{50}) using 80% of the profiles (**C**). 50000 cells were seeded on 25 mm coverslips and spun for 5 min at 6000 rpm after incubation. Data presented as mean ±SD, N ≥5; and analysed with an ANOVA test; ***p<0.001. FBS, fetal bovine serum; MT, mutant; WT. wild type.

Role of contractility in adhesion strength. Cytoskeletal interactions and FA plaque assembly have been shown to enhance adhesion strength by significantly increasing the stiffness of anchoring sites (Balaban et al. 2001, Garcia and Gallant 2003). The role of cell contractility on adhesion strength is shown (Figure 6.20), additional profiles in (Supplementary figure S6.7). The profiles showed that disruption of the actin cytoskeleton with BB and Y27632 yielded background levels of adhesion, indicating the adhesive force was in part provided by the actin cytoskeleton.

In general, both BB and Y27632 treatments had different effect on adhesion strength of the WT and MT cells. BB and Y27632 decreased adhesion strength of WT cells on glass, however, they increased adhesion strength of MT cells. The two drugs decreased adhesion strength of MT cells on PEA-FN, inversely increasing WT cells strength. Similar results have been shown by (Dumbauld et al. 2010) who observed that reductions in adhesion strengthening by inhibitors of contractility correlated with loss of vinculin and talin from focal adhesions without changes in integrin binding. It is not clear why these drugs affect these cells lines so differently. It could be due to the difference in cells stiffness.

Interestingly, treatment of MT cells on PEA-FN with Y27632 resulted in detachment profiles that could not yield any τ_{50} values (Figure 6.20). This corroborated directly with observation made about FAs and integrins expressions; MT cells on PEA treated with Y27632 showed lower cell size, FAs count and smaller FAs size (Figure 6.7). In contrast, Y27632 did not have the same effect on WT cells. On PMA-FN, both drugs reduced the adhesion strength of both cell types.

The various patterns of the effect of these drugs on cells on the different surfaces have been observed and are thought to be related to cell signalling which occurs during interaction of cells with the materials mediated by integrins and ECM proteins (Dumbauld et al. 2010). Signalling include FAK-dependent, integrin and vinculin-containing FA assembly, that modulate adhesion strengthening via contractility. The involvement of cytoskeletal interactions in the strength of adhesion accounted for the observed enhancements in adhesion strength, showing the role on contractility in cell adhesion on surfaces (Gallant et al. 2005).

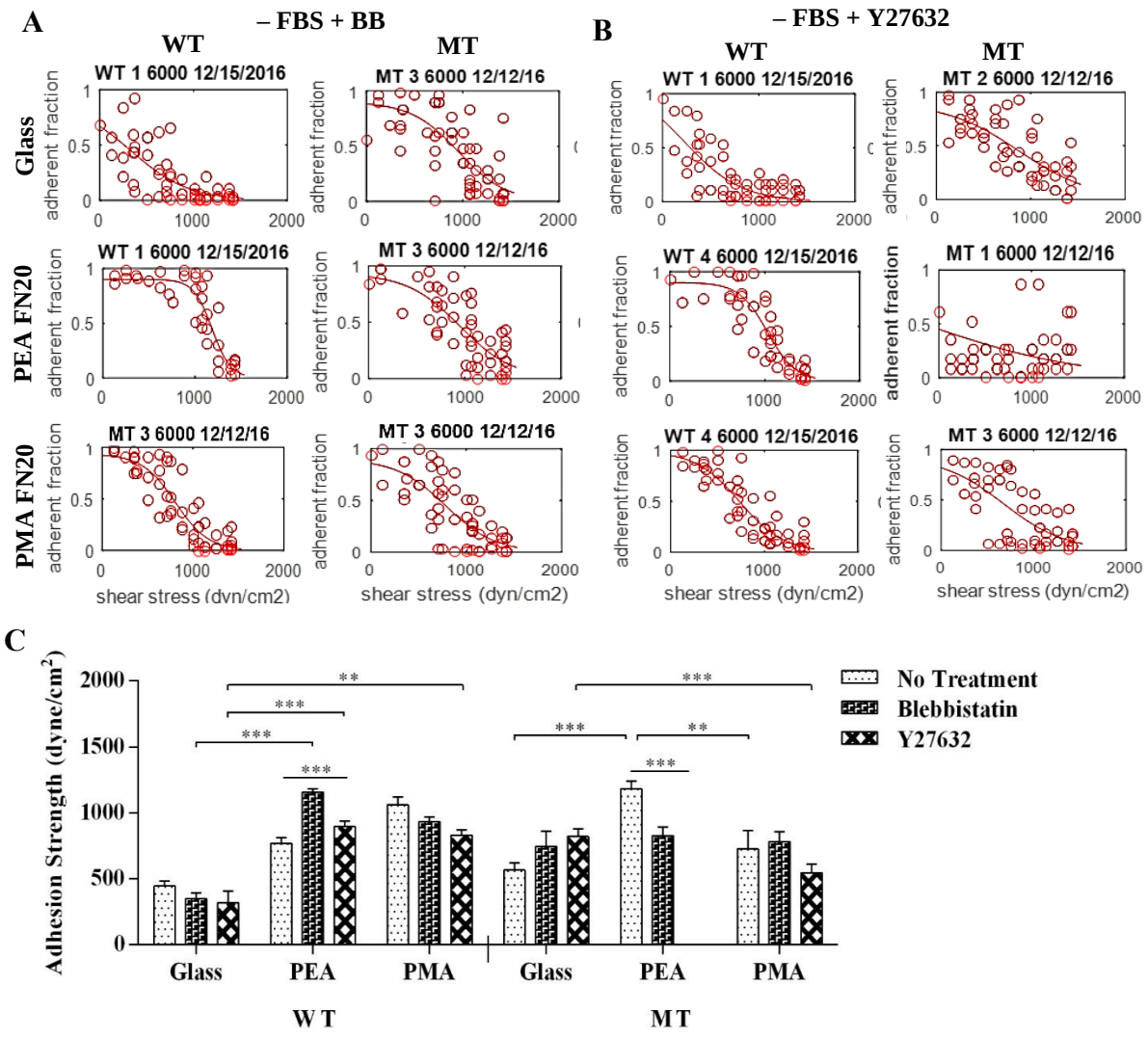

Figure 6.20 Cell adhesion strength measurements: role of contractility. Samples detachment profile showing fraction of adherent cells versus applied shear stress for cells treated with 10 µM of BB (**A**) and Y27632 (**B**) adhering to substrates coated with FN solutions of 20 µg/mL for 2 h under serum-free conditions. The shear stress for 50% detachment (τ_{50}) (**C**). Samples were spun for 5 min at 6000 rpm after incubation. BB, blebbistatin; Y27632, Rock inhibitor. **p<0.01, ***p<0.001; N-number: 6.

Serum effect on adhesion strength. Then, the influence of serum starvation on cell adhesion strength was investigated (Figure 6.21A-B) and (Supplementary figure S6.8). The graph showed statistically lower adhesion strength for both cell types on glass when serum starved. In contrast, serum starvation significantly increased adhesion strength of both WT and MT cells on the FN interfaces. The increase in adhesion strength reflected results seen in FA quantification influence by serum starvation (Figure 6.5). FA size has been established as a putative mechanotransducer that provides for a direct correlation to cellular traction (Balaban et al. 2001). Addition of serum to the medium decreased FA size (Figure 6.5), furthermore decreasing adhesion strength. This decrease is thought to be due to the large

amount of proteins and growth factors provided to cells allowing them to proliferate and migrate at early time than cells starved (Gallant et al. 2005, Garcia and Gallant 2003).

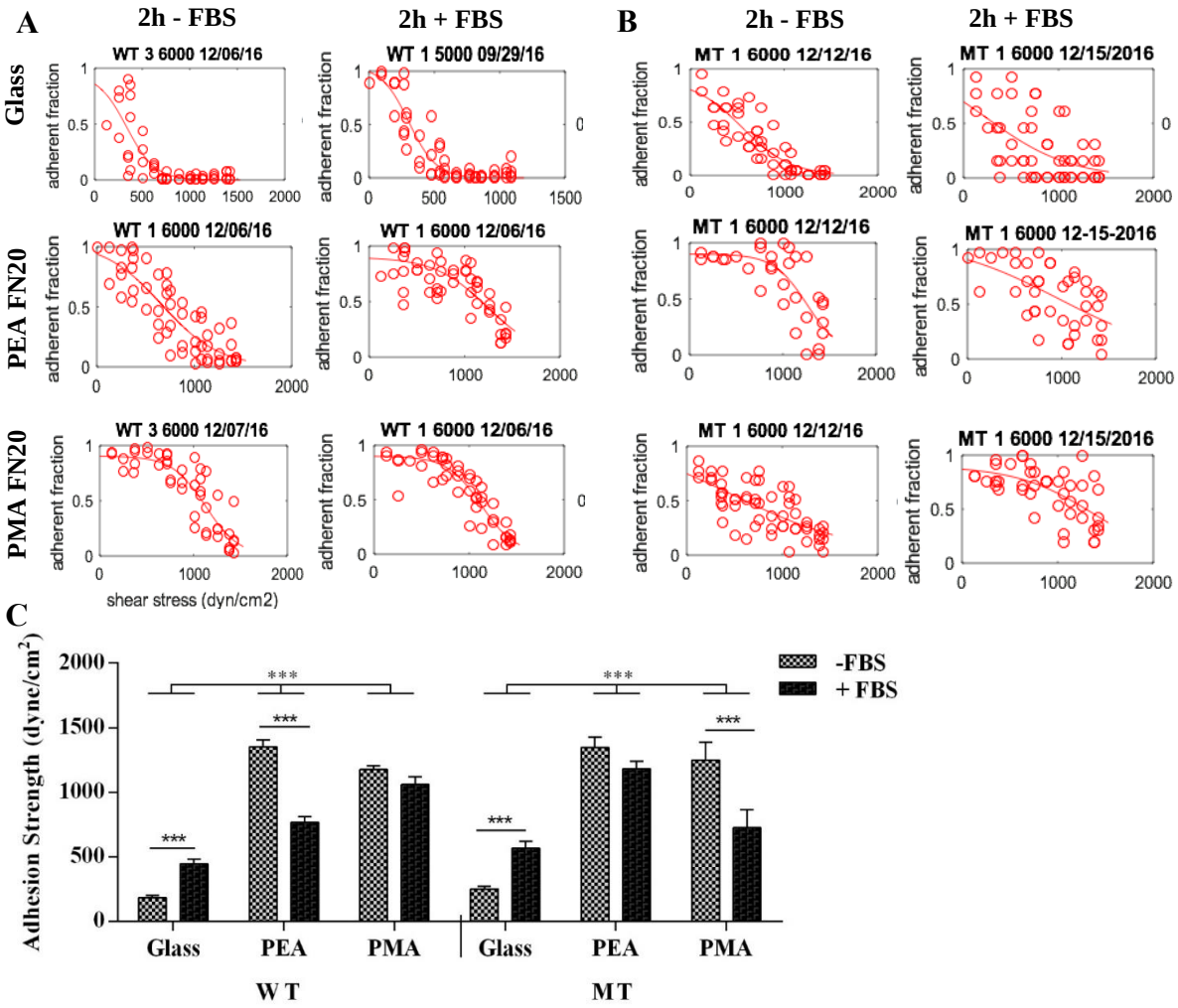

Figure 6.21 Cell adhesion strength measurements: serum influence. Samples detachment profile showing fraction of adherent cells versus applied shear stress for WT (**A**) and MT cells (**B**) adhering to substrates coated with FN solutions of 20 µg/mL for 2 h in the presence or absence of serum. Experimental points were fit to sigmoid to obtain the shear stress for 50% detachment (τ_{50}) (**C**). Data presented as mean ±SD, N ≥5; and analysed with an ANOVA test; ***p<0.001.

Fibronectin density effect on adhesion strength. Finally, to examine the relationship between adhesion strength and FN density, substrates coated with different concentrations of FN were analysed (Figure 6.22A-B) and (Supplementary figure S6.9). As expected, increasing the FN coating concentration generated a family of sigmoids that shifted to the right with increasing concentration, indicating a direct relationship between ligand density and adhesion strength (Garcia et al. 1998a, Garcia et al. 1998b). The graph confirmed that increasing FN concentration directly influenced adhesion strength. Adhesion strength for MT cells on PEA coated with FN20 µg/mL was statistically higher than that with 2 µg/mL

and on PMA-FN20 µg/mL and glass (Figure 6.22C). The WT cell strength also increased with higher FN concentration on the substrates. Larger and higher FAs together with higher adhesion strength have been shown on higher availability of ligand (FN), this is due to cells attached strongly to the underlying adhesive FN (Dumbauld et al. 2010, Garcia et al. 1998a, Garcia et al. 1998b, Llopis-Hernández et al. 2013, Vanterpool et al. 2014).

Taken together, these results demonstrated that ligand density, serum deprivation and actin-myosin contractility accounts for the increases in adhesion strength, in agreement with previous reports (Dumbauld et al. 2010, Garcia et al. 1998a, Garcia et al. 1998b).

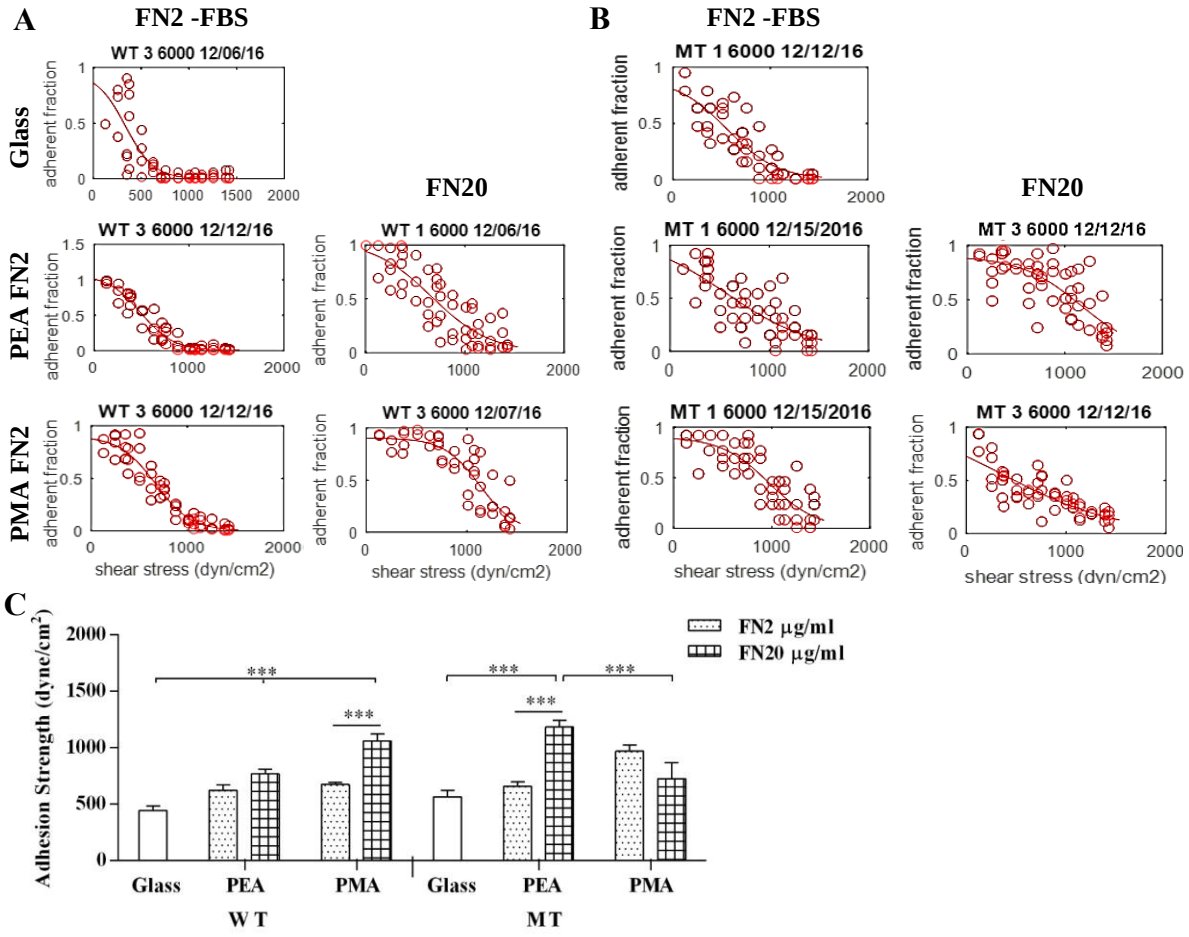

Figure 6.22 Cell adhesion strength measurements: influence of fibronectin density. Samples detachment profile showing fraction of adherent cells versus applied shear stress for WT (**A**) and MT cells (**B**) adhering to substrates coated with FN solutions of 2 and 20 µg/mL for 2 h - FBS. Experimental points were fit to sigmoid to obtain the shear stress for 50% detachment (τ_{50}) (**C**). Data analysed with an ANOVA test; ***p<0.001; N≥6.

6. 5 Conclusions

Observations in this chapter correlated with how the MT cells secrete a higher amount of Col4a2 on PEA-FN than on PMA-FN and glass. The results showed that the MT cells size was larger compared to the WT cells over time and this did not translate into FAs count, as the latter did not differ between the WT and MT cells on any of the surfaces. Nonetheless, FA count increased significantly with time for both cell types on FN-coated substrates. Yet again, FA size remained constant for the MT cells on all the surfaces and also followed the increasing trend for the WT cells. WT cell size, FA count and size was independent of the density of FN, whereas MT cells size and FA count and size increased with FN density only on PEA-FN. The absence or presence of serum in the media only affected both cells FA count and size not cell size. Inhibitors of contractility had different effect on both cell types, yet they both greatly affected the adhesion of cells on FN-coated substrates.

Cell signalling by integrin showed that the cells, especially the WT cells, expressed well pronounced $\alpha_5\beta_1$ integrin clusters resembling FA, and $\alpha V\beta_3$ integrin expression was more diffused. Cytoskeleton inhibitors showed the involvement of cell contractility on integrin expression and cell adhesion as the F-actin was greatly disrupted yet integrin expression remained similar. Signalling showed enhanced phosphorylation of FAK in MT cells on PEA-FN suggesting the role of the material-driven FN network assembled on PEA in inducing *COL4A2*$^{+/G702D}$ mutant cells to secrete Col4a2. ERK1/2 signalling also did not show any differences in the mutant on any of the surfaces. This concluded that FN coating on PEA is affecting these signalling pathways to a lesser extent in the *COL4A2*$^{+/G702D}$ mutant cells; hence, pointing to other pathways. Signalling of collagen by DDR1 also showed less expression in the MT cells on FN-coated substrates. To this extend, the signalling pathways explored in this work were less conclusive on the effect of FN-coated PEA assembled into fibrillary networks induction of the secretion of Col4a2 by MT cells.

The *COL4A2*$^{+/G702D}$ cells could be exerting different forces while interacting with the biointerfaces. This was shown by the greater cell adhesion strength of the MT cells on FN-coated substrates especially on PEA-FN over time compared to glass. Cell adhesion strength was found to reduce with the addition of serum for both cell types independent of the surfaces; and increasing the FN coating concentration increased adhesion strength on the polymer substrates for all cell types, and particularly for the MT cells on PEA-FN20. Concluding, these adhesion strength results showed ligand density, serum deprivation and actin-myosin contractility account for the increases in adhesion strength.

Chapter 7

Overall Discussions and Conclusions

Contents

7. 0 Overall Discussions

Col4 is a basement membrane (BM) (Timpl and Aumailley 1989) component that provides structural support. Mutations that could alter the nature of this protein can affect its structure and function, causing disease. There are many mutations found in the *Col4* gene, and in this study, cells harbouring the *COL4A2*$^{+/G702D}$ mutation were used. This glycine mutation is likely to interfere with the triple helix structure of the α1.α1.α2(IV) trimer (Murray et al. 2014), potentially affecting the 3D structure of the protein. This ultimately, causing its retention in the ER or, if secreted, can alter its interaction with other ECMs proteins. This eventually leads to BM defects (due to mutant protein incorporation or its absence) and ER-stress (Jeanne et al. 2012, Murray et al. 2014, Van Agtmael et al. 2010, Van Agtmael et al. 2005). Clinically, this mutation caused intracerebral haemorrhage and familial porencephaly y (Gunda et al. 2014, Verbeek et al. 2012), in line with many other collagen IV mutations (reviewed by (Khoshnoodi et al. 2008, Vahedi and Alamowitch 2011, Van Agtmael and Bruckner-Tuderman 2010)). Traditionally, haemorrhagic stroke is considered to be caused by weakened blood vessels due to BM defect, although recent evidence also supported the contribution of ER stress (Murray 2014, Gould 2015)

Therefore, considering the economic and social impact of haemorrhagic stroke on the society and the absence of any specific treatment, in part due to our limited understanding of disease mechanisms, this project was designed to explore whether biointerfaces could alter the mechanisms in *COL4A2* mutation leading to differential ECM expression. The latter indeed provide well-defined microenvironments to interrogate the cells and provide insights into pathological and physiological cell behaviour. For the sake of this study, *COL4A2*$^{+/G702D}$ fibroblast cells were cultured on various biomaterial interfaces, composed of two poly(alkyl-acrylates) PEA and PMA, coated with LM, Col4, or FN; their behaviour, especially in terms of secretion of ECM proteins was then investigated.

7. 1 Secretion of Col4a2 is altered on FN assembled on PEA

Results showed that *COL4A2*$^{+/G702D}$ mutant cells secreted higher amounts of Col4a2 when cultured on FN-coated PEA, but not when cultured on glass, FN-coated PMA, Col4 or LM-coated surfaces as shown by several approaches throughout this project such as immunofluorescence (including without permeabilisation, to rule out the possibility of staining intracellular Col4a2 and after a decellularization assay), In-cell western and ELISA. These results were interesting and unprecedented.

As shown in chapter 3, FN adsorption on PEA led to the assembly of distinctive physiological-like fibrillar nanonetworks, whilst the protein maintained a globular structure on PMA. This confirmed previous results (Gonzalez-Garcia et al. 2012, Llopis-Hernández et al. 2013, Vanterpool et al. 2014) and makes FN on PEA an interesting protein interface. This conformational change of FN has been in fact shown to have a great influence on cell behaviour, namely adhesion, proliferation and differentiation (Moulisová et al. 2017, Llopis-Hernández et al. 2013, Llopis-Hernandez et al. 2016, Rico et al. 2009, Salmeron-Sanchez et al. 2011, Vanterpool et al. 2014). Here, we have observed that these FN nanonetworks have a positive effect on ECM secretion by mutant cells, as the nanonetworks induce the mutant cells to secrete Col4a2 similar to normal cells. This is not a potential treatment but is potential tool to monitor effectiveness of treatment. Hence, this biointerface proves to assist in the alleviation of cellular disease phenotypes (some effects of the mutation) of *COL4A2*$^{+/G702D}$ fibroblasts. The LM and Col4 coatings, on the other hand, appeared to form network structures independently of the polymer substrate to which they were adsorbed, and did not influence the secretory behaviour of mutant cells.

FN assembly on PEA is mediated via the FNI_{1-5} domains in a similar way to cell-mediated FN fibrillogenesis (Mao and Schwarzbauer 2005, Salmeron-Sanchez et al. 2011). This fibrillar structure exposes cryptic binding sites within the FN molecule, enabling it to take a form that is more conducive to self-assembly into fibrils (Salmeron-Sanchez et al. 2011, Vanterpool et al. 2014). This material-driven FN matrix favours an enhanced exposure of the synergy cell binding domain, which the *COL4A2*$^{+/G702D}$ fibroblasts might recognise, influencing their behaviour and matrix secretion (Llopis-Hernandez et al. 2016, Reilly and Engler 2010, Vanterpool et al. 2014). Exposed cryptic integrin-bindings on FN have been in fact demonstrated to result in pleiotrophic changes in cellular behaviour, implicating FN as an extracellular mechano-regulator (Frantz et al. 2010, Singh et al. 2010, Salmeron-Sanchez et al. 2011, Vanterpool et al. 2014). Material-driven FN fibrillogenesis influence on cell behaviour shows the importance of FN in tissue engineering; FN is an important ECM protein for cell adhesion to the matrix as well as for guiding cell migration in vertebrate embryos (Mouw et al. 2014). Besides, mutant cells morphology was observed to be larger compared to the WT cells, and they formed apoptotic patches of cells on glass (Murray et al. 2014) and on PMA-FN although these patches were reduced on PEA-FN. This could be related to cells favouring the network fibril of FN formed on PEA than the aggregate structures on PMA or the nude glass.

Both WT and MT cells secrete FN with time when cultured on LM and Col4 coated substrates (Figure 5.3 and Figure 5.6). FN secretion was detected after 1 day and formed fibril structures, supported by data from (Llopis-Hernández et al. 2013). In contrast, in both cell types LM was mainly located where cells adhered at all times (1 and 7 days) when cultured on Col4 and FN coated substrates (Figure 5.3 and Figure 5.4). Furthermore, LM did not form networks, although when staining was performed without permeabilisation, it displayed poor network structures (Figure 5.7).

Secreted FN and Col4a2 by cells on LM coated substrates were observed to co-localise. Similarly, LM and Col4a2 secreted by cells on FN coated substrates, and also FN and LM secreted by cells on Col4-interfaces co-localised. All these ECM proteins are known to interact with each other in the BM (Kalluri 2003, LeBleu et al. 2007, Timpl and Aumailley 1989). LM is thought to be the centrepiece of the network and initiates BM formation. LM is the first component in the assembly of the BM; followed by Col4 that provides the scaffold (Poschl et al. 2004). The initial deposition of LM polymers is facilitated by cell-surface proteins such as integrins (especially β_1 integrin) and dystroglycans via site-specific interactions, and then Col4 polymers associate with the LM networks on the cell surface via nidogen/entactin bridging (Figure 1.2) (Aumailley et al. 2000, Charonis et al. 1985, Willem et al. 2002). Henceforth, this scaffold provides specific interaction sites for the other BM components and creates a fully functionally BM.

7. 2 Secretion of Col4a2 and mechanical properties of the cell

In this study, remodelling of ECM proteins at the material interface observed by IF and AFM does not only happen with adsorbed ECMs but also with ECMs secreted by the cells. High magnification IF images of secreted FN (Figure 5.3) and Col4a2 (Figure 5.4) displayed fibril-like network remodelling on the substrates. This is in line with what is observed in the BM (Kalluri 2003, LeBleu et al. 2007, Timpl and Aumailley 1989). Additionally, after decellularization, the secreted ECMs (stained Col4a2, and to a lesser extend LM) displayed well defined fibril network structures on the interfaces as seen with non-decellularised samples. Furthermore, the AFM image scanning of secreted ECMs (Figure 5.17 and Figure 5.18) corroborated these observations. This concluded that the secreted ECMs have similar nature to the physiological ones.

The secreted Col4a2 network structures, similar to the network structures observed after Col4 adsorption, displayed a fractal nature (Sillat et al. 2012), similarly to the physiological-

like mesh of network observed in tissues (Kalluri 2003, LeBleu et al. 2007, Timpl and Aumailley 1989). Analysis showed that the fractal dimension of the secreted Col4a2 was higher on PEA for the mutant cells compared to the WT cells, though it was similar for both cells on PMA. Similar observations have been shown by growing cells on orientated PEA fibres, spatially organised secreted FN matrix were observed along oriented fibres and an altered arrangement on random ones (Gugutkov et al. 2009). It should however also be considered that evidence support an interaction between fibronectin and α1α1α2(IV) around residue 580 within the triple helical domain (Laurie et al. 1986, Parkin et al. 2011), perhaps stabilising the secreted collagen network.

While the mechanism underlying this phenomenon is unclear, it may potentially indicate that fibrillary FN (assembled on PEA) has a role to play in Col4 synthesis and secretion. As cells do not secrete Col4a2 when cultured on LM interfaces, this suggested that this effect is specific to FN assembled on interfaces that appears to affect MT cells and enable a partial rescue of the retention and intracellular accumulation of Col4a2. Intriguingly, the FN coated network appeared to affect the cellular programme of the cells as after culture on FN-coated PEA for 7 days, the mutant *COL4A2*$^{+/G702D}$ fibroblasts retained the ability to secrete Col4a2 when re-cultured on glass. This rescue in secretion was associated with associated with increased levels of molecular chaperones Bip and Pdi and reduced ER area, suggesting increased protein folding capacity of the cell and perhaps reduced ER stress, and altered biomechanical proteins of the cells.

The *COL4A2*$^{+/G702D}$ mutation and other mutations in mice results in lower secretion and incorporation into the BM of Col4 (Jeanne et al. 2012, Murray et al. 2014). Stiffness analysis showed that the MT cells and their ECMs were 10-fold softer than the WT cells, directly indicating effects on matrix stiffness associated with these mutations. Importantly, these cells were significantly stiffer on PEA-FN than on glass and PMA-FN. It is thought to be related to the higher amount of secreted Col4 that form networks and demonstrated fractal dimension on this particular interface, the PEA-FN, and also due to the nature of secreted ECMs. The stiffness of these cells was linked to the networks of F-actin and intermediate filaments inside the cells (observed in lower amount in the MT than in the WT cells) as the cells mechanotransduction is largely dependent on the cytoskeletal structure and the pre-stress in the cytoskeleton (Dumbauld et al. 2010, Gallant et al. 2005, Garcia et al. 1998b, Wang N. et al. 2002)

Inhibition of crosslinking in collagen has been shown to significantly reduce the stiffness of aorta; this is consistent with structure modifications such as higher degrees of cross-link between collagen fibrils (Bruel et al. 1998). Likewise, *COL4A1* mutation has been shown to be genetically associated with vascular stiffness. Indeed, it is also thought that *COL4A2*$^{+/G702D}$ mutation affects Col4 cross-linking, resulting in lower stiffness. Considering the appearance of the cells and their stiffness, one can link the effect of the mutation on these cells to cancer cells that have been demonstrated to have a decrease in stiffness compared to healthy cells, giving benefits for tumour invasion (Efremov et al. 2014).

7. 3 Secretion of Col4a2 and cell adhesion

Different signalling pathways were analysed in order to understand the behaviour of mutant cells on the FN nanonetworks. To investigate potential mechanisms by which PEA-FN is able to modify the mutant cells, various experiments were performed to investigate cell adhesion and matrix-cell signalling pathways. The organization of proteins involved in the formation of focal adhesion (FA) complexes provides an opportunity to learn more about the effectiveness of cell-substrate-interactions. The MT cells were observed to be larger on all the surfaces compared to the WT cells, yet both cell types size decreased with time. It is been shown that cell size correlates with FA quantity and quality (Vanterpool et al. 2014). Yet, in this case, the larger MT cells did not have higher FA count or size than the WT cells. Thus, one potential reason may be the reduced stiffness of the matrix produced by these cells. However, smaller plaques of WT cells decrease with time on each surface while the MT remained constant, indicating difference in cell adherence.

Therefore, integrin recruitment was analysed. Cells have been demonstrated to adapt to their environment by changing the collection of integrins expressed, and their distribution, according to the ligands available and the differentiation state of the cells (Coelho et al. 2016, Garcia et al. 1998b, Llopis-Hernández et al. 2013, Wilson et al. 2005). Because of upregulation (and localization) of integrins when their preferred ligand is available, it is possible that differential integrin expression reflects distinct FN adsorption profiles characteristic of underlying surface properties.

Both WT and MT cells formed $\alpha_5\beta_1$ integrin clusters resembling FA, while $\alpha V\beta_3$ integrin expression was more diffused. FAs, as shown by paxillin staining, and $\alpha V\beta_1$ represented a linear organization along with actin stress fibres, revealing that $\alpha_5\beta_1$ is the main receptor involved during the initial cell interaction with the material-driven FN network, as it happens

for the interaction of cells with natural physiological matrices (Llopis-Hernández et al. 2013). Binding of $\alpha_5\beta_1$ has been related to the simultaneous availability of the synergy and RGD sequences within FN (Llopis-Hernández et al. 2013). Unlike $\alpha_5\beta_1$, $\alpha V\beta_3$ was weak in all the cells on all the surfaces. This integrin is mainly expressed by cells on PMA-FN where FN is adsorbed as discrete aggregates. Cell adhesion to the aggregate form of FN mostly occurs through the $\alpha V\beta_3$ receptor, which only needs the exposition of the RGD sequence as the synergy sequence availability is hindered (Llopis-Hernández et al. 2013). Interestingly, the results also concluded that differences in integrins expression observed on different materials may account for observed variations in cell behaviour (Jin and Varner 2004, Salmeron-Sanchez et al. 2011, Schaffner et al. 2013, Sun et al. 2016). It showed that in serum starvation, cells switched to stationary behaviour resulting in stronger adhesion to FN (particularly at higher density), confirmed by the co-localisation of $\alpha_5\beta_1$ integrins in FA contacts on both cells. Experiments were performed with 2 initial hours without serum.

Drugs affecting cell contractility are used widely used to study various cellular process (Darenfed et al. 2007, Dumbauld et al. 2010, Garcia et al. 1998b, Liu et al. 2010, Salmeron-Sanchez et al. 2011). Treatment with cytoskeleton inhibitors greatly affected focal adhesion complexes and strength (especially on PEA), although each drug had different effect on both cell types. The adhesion strength was higher on FN-coated substrates than on glass. This indicated that constant cell spreading area and migration, and peripheral adhesive complexes accounted for 100% of the adhesion strength. FAs dynamically respond to changes in cell contractility and externally applied forces and have emerged as candidate mechanotransducers (Balaban et al. 2001, Rubin et al. 2006, Shattil et al. 2010).

Focal plaque assembly, including interactions with vinculin, appear to strengthen adhesive domains by recruiting the actin cytoskeleton and increasing local membrane stiffness (Garcia and Gallant 2003, Wang N. et al. 2002). Integrin binding to the FN, especially on PEA also has been shown to induce higher adhesion strength associated with its effect on the actin filament (Dumbauld et al. 2010, Garcia et al. 1998a, Garcia et al. 1998b). In addition, phosphorylation and dephosphorylation events, including interactions with FAK and src, also modulate adhesion strength through cytoskeletal associations (Gallant et al. 2005, Garcia and Gallant 2003, Wang H. B. et al. 2001).

Our analysis of adhesion strength is based on the theoretical work of Bell (Bell 1978) and Hammer and Lauffenburger (Hammer and Lauffenburger 1987) and later refined by (Garcia et al. 1998a, b). The adhesion model considers a spherical cell with a single class of receptors

attaching to a surface through uniformly distributed receptor-ligand complexes. The applied hydrodynamic force is dependent on cell shape; for spherical cells, exact solutions have been derived (Hammer and Lauffenburger 1987). Observed variables in the adhesion strength profiles could be associated with the conditions of the experiment. At first, cells used in these experiments adhered and had a flat non-spherical shape. Then, spinning of a coverslip took 5 min, and having over 5 replicates, this means that the last sample had a further 25 min incubation compared to the first spun one. This is thought to have induced the varied sigmoid curves as incubation time is thought to influence the adhesion strength. Furthermore, the variation in values could be due to the relationship between adhesion strength and ligand density and receptor density as shown by (Garcia et al. 1998a, b).

The biological response of the material-driven FN network could potentially be due to the following phenomena that occur at the cell–material interface after FN assembly into physiological-like fibrils: (a) the availability of the integrin binding sequence, (b) α_5 integrin expression, which leads to enhanced FA formation and cytoskeleton development, and (c) enhanced phosphorylation of FAK affecting integrin signalling. Thus, cell adhesion occurs primarily through the specific $\alpha_5\beta_1$ receptor occupancy, with enhanced focal adhesion formation and FAK signalling. However, this work suggests that there is little signalling influence from FAK, ERK1/2 and DDR1, although this could be due to probing time of these pathways. It is apparent that the MT cells have other signalling pathways triggered in order to begin the secretion of Col4a2 when cultured on the fibrillar FN network formed on PEA.

7. 4 Overall Conclusions

The data support the hypothesis that biomaterials may alter the behaviour of *COL4A2*$^{+/G702D}$ mutant cells by overcoming some of the defects caused by the mutation and rescuing the downstream effect of the ER stress. It was observed that interaction of mutant cells with an ECM protein, fibronectin, assembled into fibrillar networks on a synthetic polymer PEA influenced phenotypic fate by altering protein synthesis and secretion. The results show the properties of materials, in particular protein adsorption on different surfaces and protein assembly influence on cell fate, correlating with other (Ballester-Beltrán et al. 2017, Salmeron-Sanchez et al. 2011). This work shows that biomaterials can alter *COL4A2* mutant cells behaviour by overcoming the secretion defects and rescuing downstream effects of ER stress. Understanding the mechanisms by which the fibrillar FN on PEA results in increased Col4a2 secretion by mutant *COL4A2*$^{+/G702D}$ cells, and if it affects signalling via cell surface

receptors or perturb intercellular communication via morphogens are unresolved and important questions that need further investigation. Nonetheless, these data provide a basis to enhance our knowledge in understanding the biological consequences (function/behaviour) of *COL4A2* mutations, which is critical to developing personalized therapeutic strategies for intracerebral haemorrhage and pathologies due to collagen IV mutations.

7. 5 Future perspectives

Detailed analysis of how FN affects the mutants especially on PEA and the possible modification of cellular pathways would provide a clear understanding of these results. Nonetheless, these are promising observations, as the mutants can overcome the retention of Col4a2 while cultured on the FN-PEA interface. This would prove to be a novel *in vitro* model characterisation of how modulating the matrix in a controlled manner is able to modify the cellular responses and sequelae to Col4 mutations.

Other assays could be used to quantify the amount of secreted Col4a2. While other have used transfection of cells in order to quantify the intracellular and extracellular amount of Col4a2 (Jeanne et al. 2012), this does not assess expression and secretion at endogenous levels. However, expression analysis of Col4a2 in the mutant cells using microarrays and/or proteomics could also be employed as it provides a good profile results. qPCR could be used to investigate Col4a2 at the gene level. The secretion rates could also be assessed via pulse-chase analysis of newly synthesised proteins (S-methionine labelled) by COL4A2 immunoprecipitation from cell lysates and media to determine secreted versus intracellular COL4A2 levels. The amount of secreted Col4a2 could also be quantified after longer culture on the FN interfaces to be certain the cells retain the ability to secrete high level of Col4a2.

In addition, recently introduced method that combines click chemistry and pulsed stable isotope labelling with amino acids in cell culture to selectively enrich and quantify secreted proteins could also be used as the combination of these two labelling approaches allows cells to be studied irrespective of the complexity of the background proteins (Eichelbaum et al. 2012). In parallel, the thermal stability of secreted collagen IV could be assessed via its sensitivity to trypsin digestion over a range of temperatures to inform on triple helix folding of the secreted Col4a2 (Fritsch et al. 2009).

Cell surface distribution of integrin receptors could be assessed using FACS analysis, as this would allow a good quantification of the cell adhesion as primary interaction between cells

and adhesion proteins occurs via integrins (Zoppi et al. 2004). This would help to understand more on the adhesion of the MT cells on the FN-coated PEA interface as differences in integrin expression on different surfaces might account for variations in cell adhesion and alternative signalling pathways. Furthermore, alternative signalling pathways could also be assessed to get an understanding of the effect of this biointerface on the mutant behaviour. There is also a need to show that the biointerface effects observed are also valid for other mutations within col4 and to generalise other types of collagen or matrix proteins.

As with any approach, this project and the methodologies employed have limitations. When analysing cell cultures, it must be considered that the surface of a plastic culture flask or glass cover slip is not biomimetic to the normal dermal fibroblast environment *in vivo*, (Birgersdotter et al. 2005, Cukierman et al. 2002). It would be of great value to repeat these experiments using a three-dimensional cell culture model to see if this changed characteristics such as adhesion, and expression profiles. Growing cells in an environment more similar to that of the ECM would provide a far more accurate reflection of the cells behaviour in the body. It would be interesting to probe the differences in secreted Col4a2 by the *COL4A2*$^{+/G702D}$ fibroblasts when grown in FN hydrogels. Growth of C_2C_{12} and MSCs in FN hydrogels has indicated that this material has a great effect on the cell differentiation; proving that employing synthetic hydrogels as ECM mimics is becoming important to garner biologically relevant conclusions from *in vitro* cell culture (Tibbitt and Anseth 2009). In addition, sandwich-like culture could be employed as it has demonstrated some advantages providing confined microenvironments to manipulate cell fate e.g. tuning myogenic differentiation (Ballester-Beltran et al. 2014, Ballester-Beltrán et al. 2017).

Appendix I: Supplementary figures

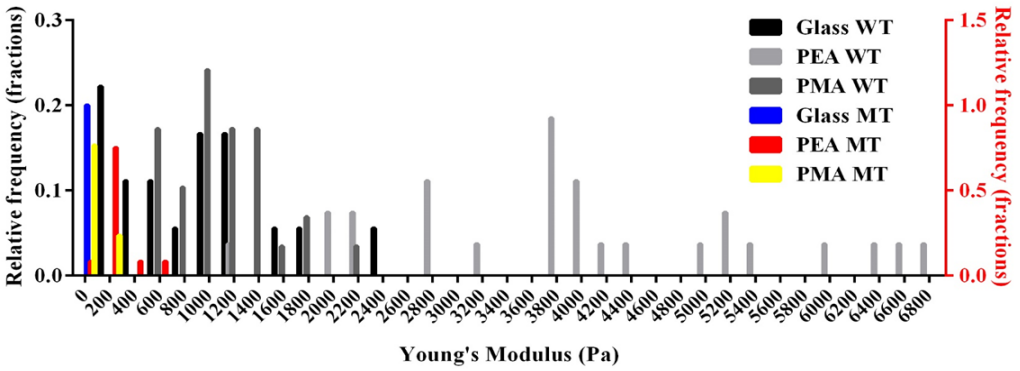

Supplementary figure S5.1 Combined cell stiffness distributions of WT and MT

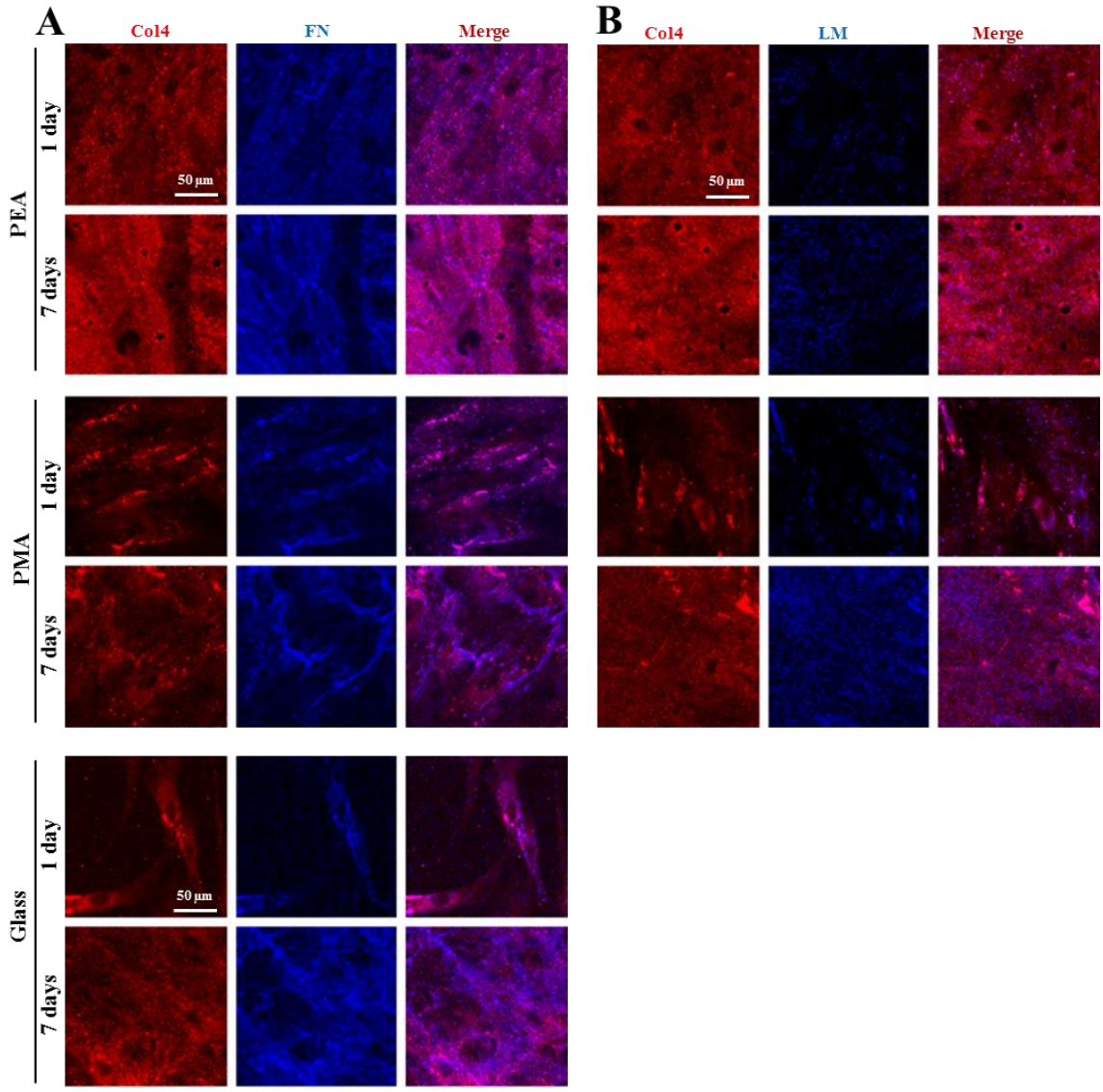

Supplementary figure S5.2 Remodelled Col4 matrix co-localisation with secreted FN (A) or LM (B) by mutant fibroblasts on PEA and PMA polymers and glass at different time points (1 and 7 days). Scale bars: 50 µm.

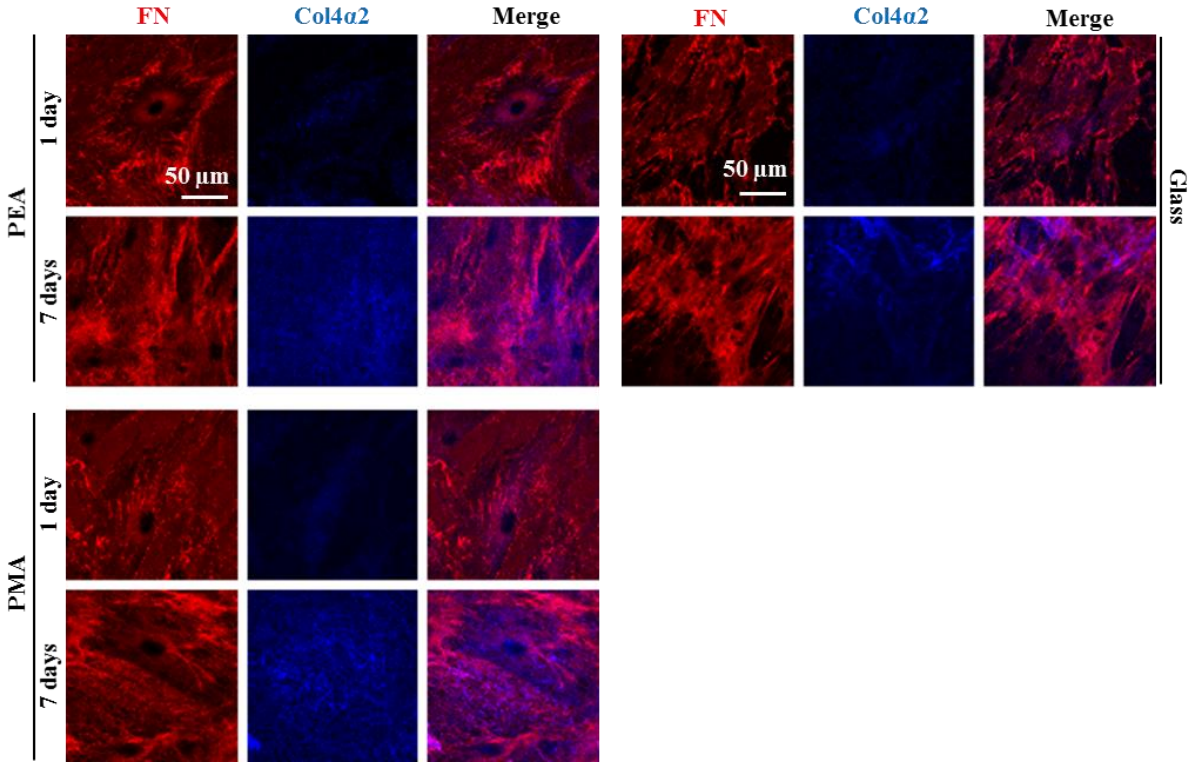

Supplementary figure S5.3 Remodelled FN matrix co-localisation with secreted Col4a2 by mutant fibroblasts on PEA and PMA polymers and on glass at different time points (1 and 7 days). Scale bars: 50 µm.

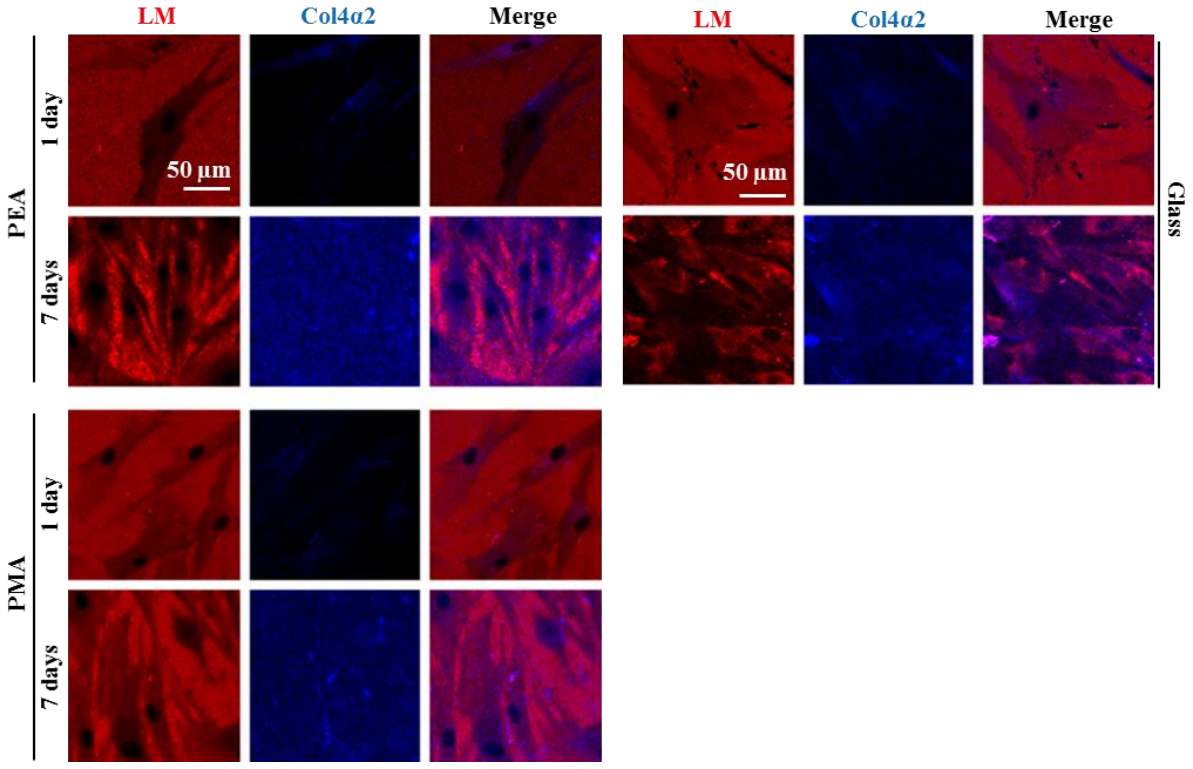

Supplementary figure S5.4 Remodelled LM matrix co-localisation with secreted Col4a2 by mutant fibroblasts on PEA and PMA polymers and on glass at different time points (1 and 7 days). Scale bars: 50 µm.

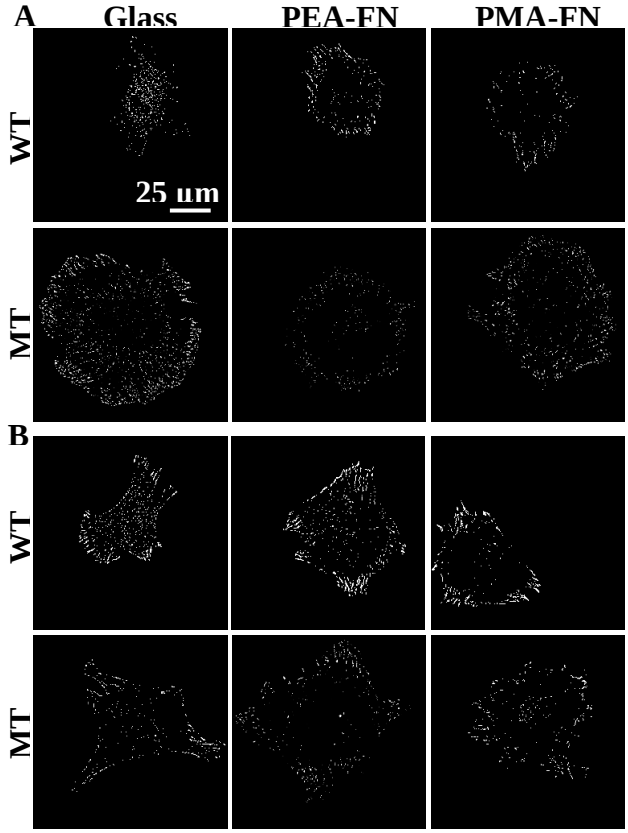

Supplementary Figure S6.1 Focal adhesion assembly on FN coated PEA and PMA substrates after 2 and 4h. Images of focal adhesions of WT and MT fibroblasts (5,000 cells/cm^2) on glass and PEA and PMA coated with 20 µg/mL FN for 2h (**A**) and 4h (**B**) in media supplemented with 10% serum, fixed and then stained for paxillin. WT, control wild type; MT, *COL4A2*$^{+/G702D}$ mutants.

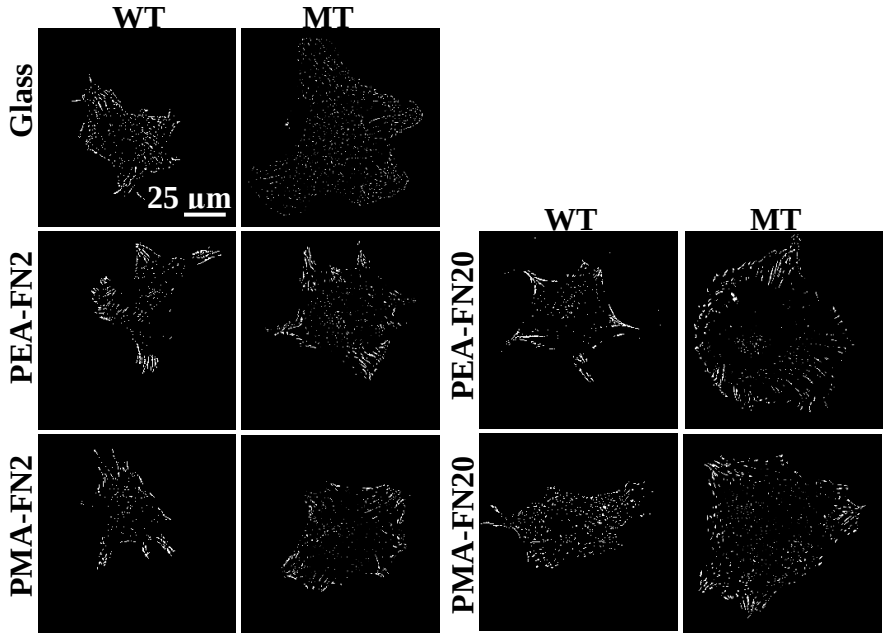

Supplementary Figure S6.2 FA assembly on PEA and PMA-coated with 2 and 20 µg/mL FN. Images of FAs of WT and MT fibroblasts (5,000 cells/cm^2) on glass and PEA and PMA coated with 2 and 20 µg/mL FN for 2h in media under serum free conditions, fixed and then stained for paxillin. WT, control wild type; MT, *COL4A2*$^{+/G702D}$ mutants.

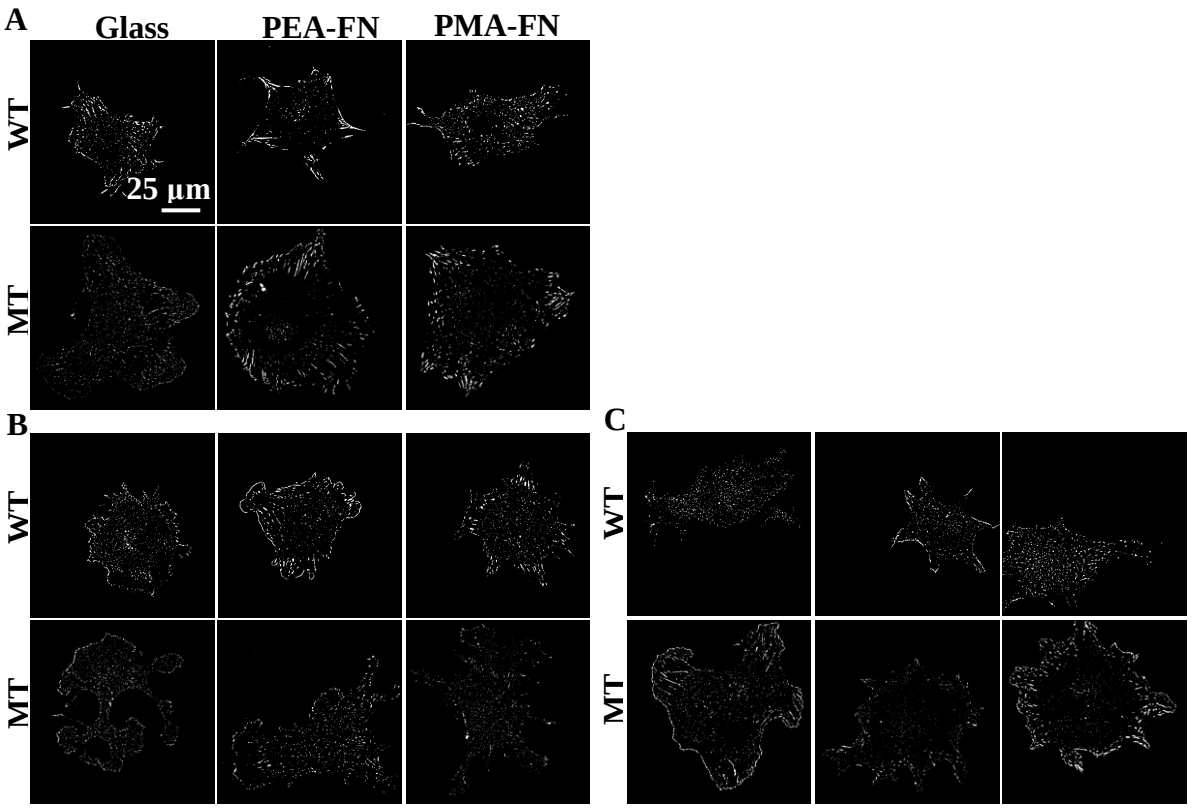

Supplementary Figure S6.3 Focal adhesion assembly on FN coated PEA and PMA substrates treated with cytoskeleton drugs. Images of focal adhesions of WT and MT fibroblasts on glass and PEA and PMA-coated with 20 µg/mL FN and incubated for 2h under serum free conditions before being fixed and stained for paxillin (**A**). Samples were supplemented with 10 µM blebbistatin (BB) (**B**) or 10 µM Y27632 (**C**) for 30 min before fixation. WT, control wild type; MT, mutants.

Multiple comparison	Mean diff.	P value
Figure 5.4 LM expression		
7 Days: WT Glass vs WT PEA FN	-273400000	***
7 Days: WT Glass vs WT PMA FN	-229400000	***
7 Days: WT Glass vs MT Glass	-36380000	***
7 Days: WT PEA FN vs WT PMA FN	44000000	***
Figure 5.4 Col4α2 expression		
1 Day: MT Glass vs MT PEA FN	34830000	*
1 Day: MT Glass vs MT PMA FN	33910000	*

Supplementary Figure S6.4 Complete table list of the significantly differences of the figures.

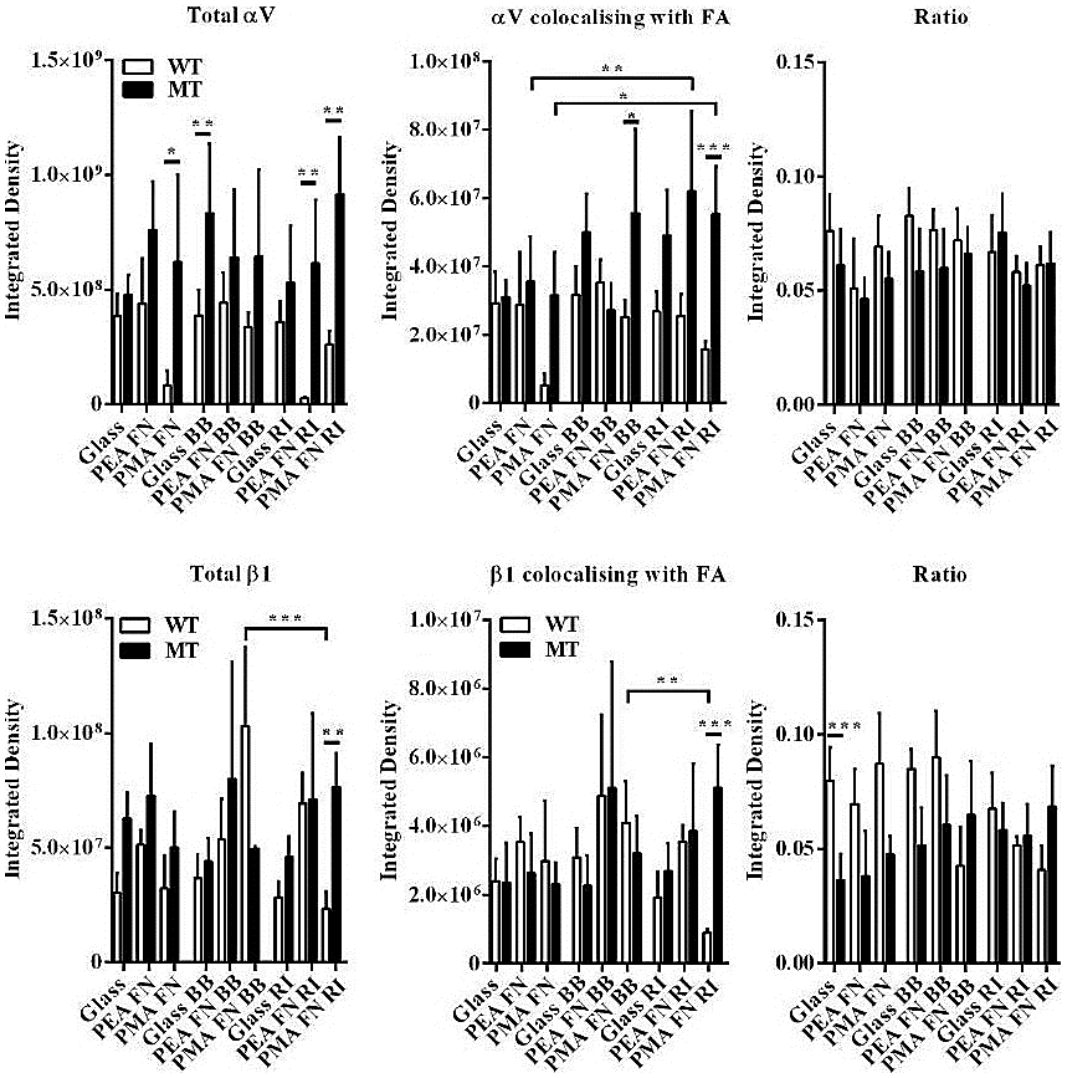

Supplementary Figure S6.5 Integrin quantification. Quantification of fluorescence integrated density of αV (top row) and β1 (bottom row) integrin from Figure 6.8, Figure 6. 9, Figure 6. 10, Figure 6. 11, Figure 6. 12 and Figure 6. 13. First column shows total integrin; second column: integrin colocalising with FAs; third column: ratio between total integrin with integrin colocalising with FAs. BB, blebbistatin; RI, ROCK inhibitor. Data presented as mean ±SD, N ≥10; and analysed with an ANOVA test; *p<0.05, **p<0.01, ***p<0.001. **Below is a complete table list of the integrin** significantly differences.

Multiple comparison	**Mean diff.**	**P value**
Total αV		
WT PMA FN vs MT PMA FN	-536900000	*
WT Glass vs MT Glass	-443900000	**
WT PEA FN RI vs MT PEA FN RI	-587800000	**
WT PMA FN RI vs MT PMA FN RI	-654200000	***
MT Glass RI vs YMT PMA FN RI	-385100000	*
αV co-localising with FA		
MT PEA FN vs MT PEA FN RI	-26440000	**
MT PMA FN vs MT PMA FN RI	-23880000	*
MT PEA FN BB vs MT PEA FNRI	-34810000	**
WT PMA FN BB vs MT PMA FN BB	-30500000	*
WT PEA FN RI vs MT PEA FN RI	-36500000	***
WT PMA FN RI vs MT PMA FN RI	-39720000	***

Multiple comparison	**Mean diff.**	**P val**
Total β1		
WT PMA FN vs WT PMA FN BB	-70700000	***
WT Glass BB vs WT PMA FN BB	-66160000	***
WT PEA FN BB vs WT PMA FN BB	-49400000	***
WT PMA FN BB vs MT PMA FN BB	53370000	*
WT PMA FN BB vs WT PMA FN RI	79650000	***
WT PMA FN RI vs MT PMA FN RI	-53070000	**
β1 co-localising with FA		
WT PMA FN BB vs WT PMA FN RI	3196000	*
WT PMA FN RI vs MT PMA FN RI	-4221000	***
Ratio		
WT Glass vs MT Glass	0.04335	***
WT PEA FN vs MT PEA FN	0.03157	*
WT PMA FN vs MT PMA FN	0.03948	*
WT PMA FN vs WT PMA FN BB	0.04468	***
WT PMA FN vs WT PMA FN RI	0.04632	**
WT Glass BB vs MT Glass BB	0.03342	*
WT Glass BB vs WT PMA FN BB	0.04244	***

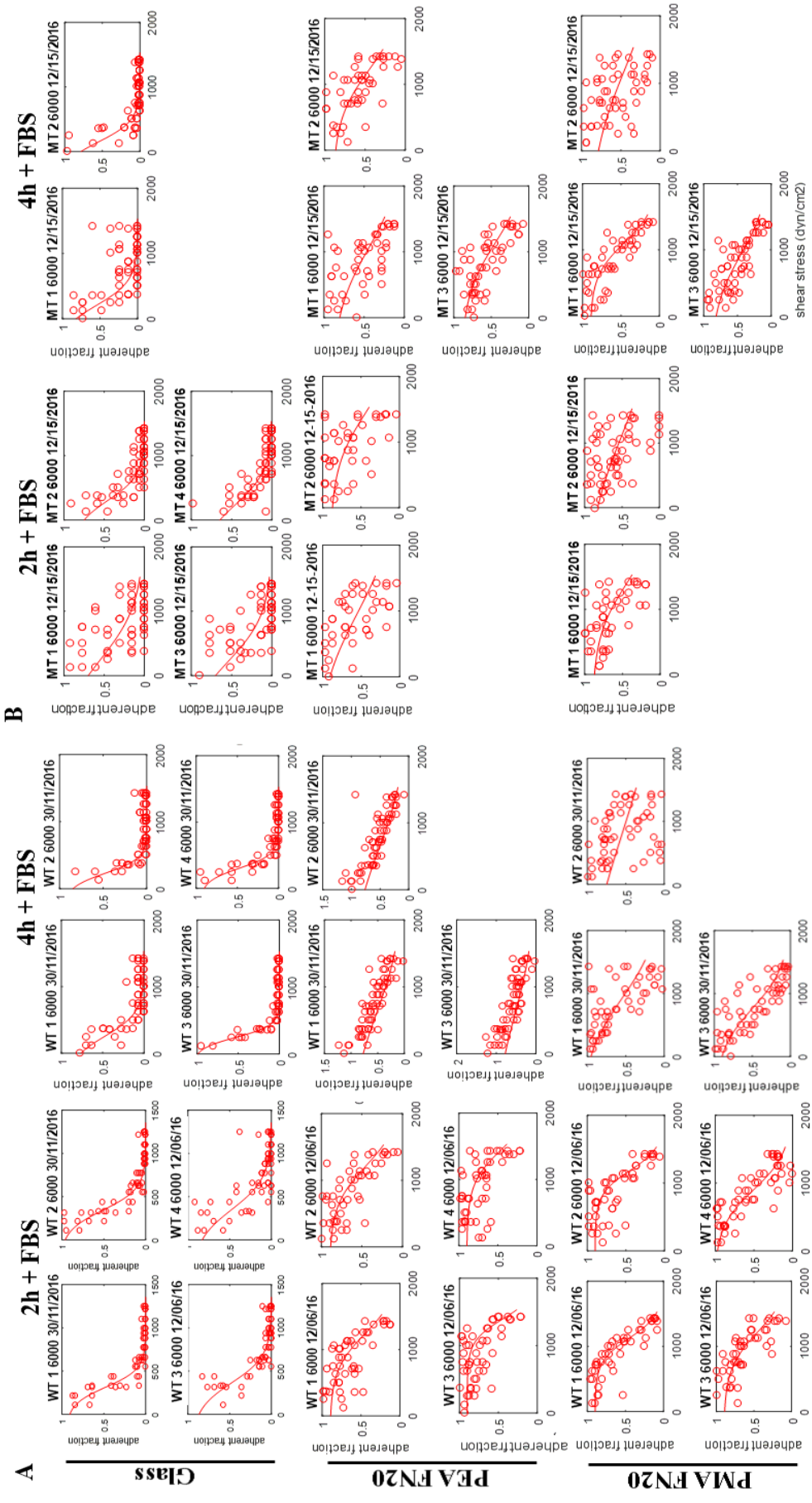

Supplementary Figure S6.6 Cell adhesion strength measurements: Time evolution. Detachment profile showing fraction of adherent cells versus applied shear stress for WT (A) and MT cells (B) adhering to substrates coated with FN solutions of 20 µg/mL for 2 and 4 h +/- FBS.

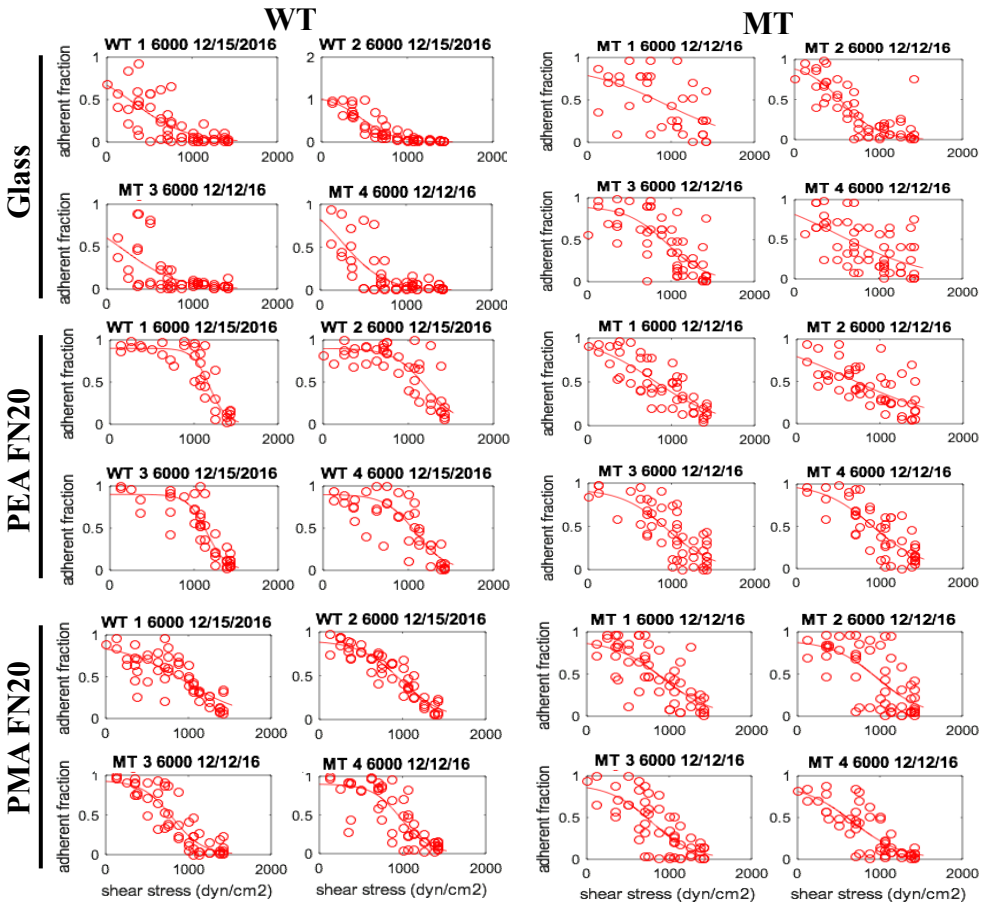

Supplementary Figure S6.7 Cell adhesion strength measurements: Role of contractility. Detachment profile showing fraction of adherent cells versus applied shear stress for cells treated with BB (Above) or with Y27632 (Below) adhering to substrates coated with FN solutions of 20 µg/mL for 2 h - FBS.

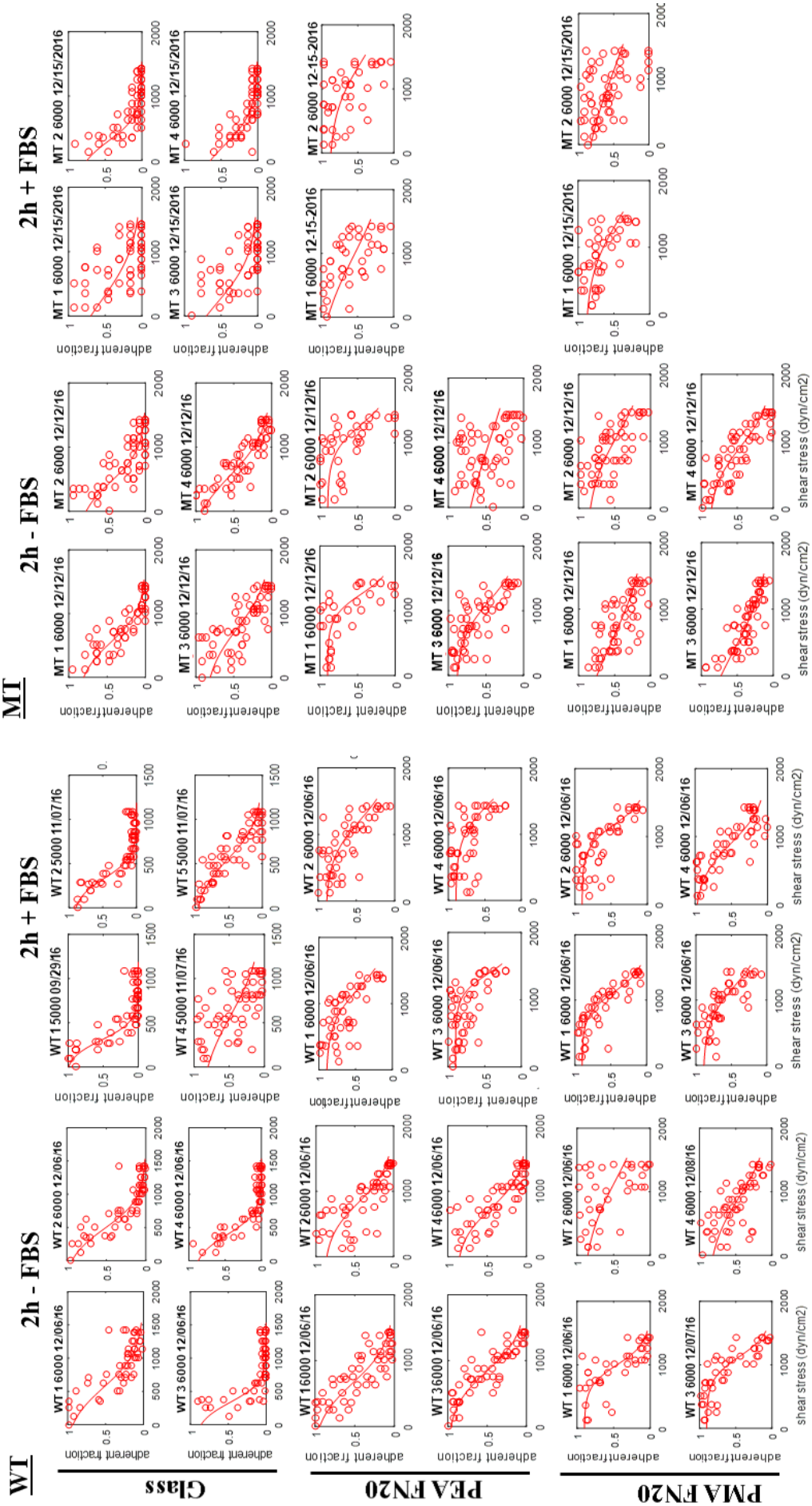

Supplementary Figure S6.8 Cell adhesion strength measurements: Serum starvation influence. Detachment profile showing fraction of adherent cells versus applied shear stress for WT (A) and MT cells (B) adhering to substrates coated with FN solutions of 20 µg/mL for 2 h +/- FBS.

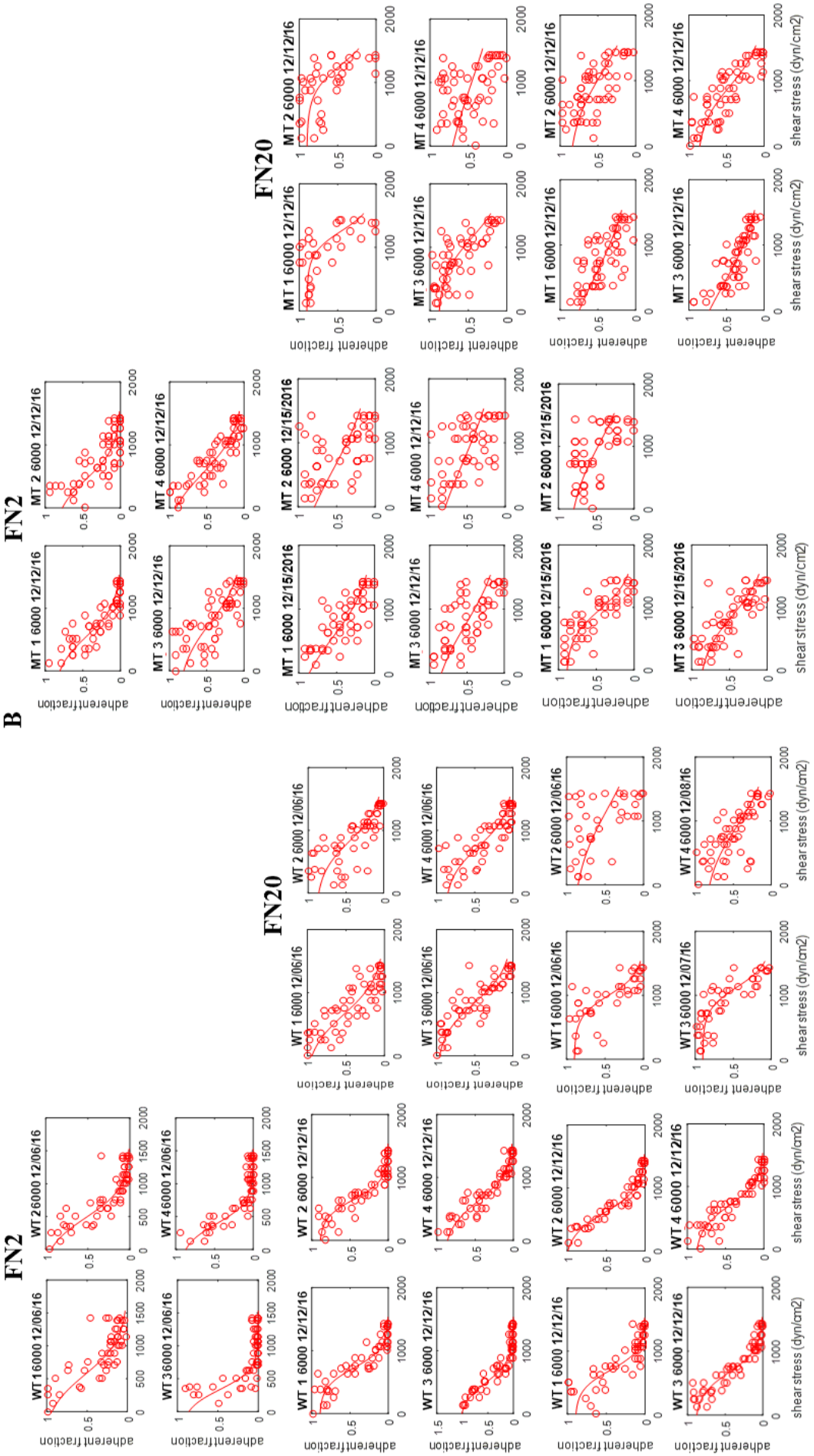

Supplementary Figure S6.9 Cell adhesion strength measurements: Influence of fibronectin concentration. Detachment profile showing fraction of adherent cells versus applied shear stress for WT (A) and MT cells (B) adhering to substrates coated with FN solutions of 2 and 20 µg/mL for 2 h - FBS.

Appendix II: AFM

Principles of operation: The AFM uses a very sharp stylus or tip mounted at the end of a flexible cantilever (Figure A1.1) to probe and map the morphology of the sample surface. AFM images consist of a series of parallel line contours acquired by scanning the surface of a specimen using the sharp tip with an extremely small (nanonewtons) tracking force. As the tip is scanned across the specimen, the net interaction force between the molecules on the sample surface and tip apex deflects the cantilevered-tip. The tip-deflection is sensed by detecting the angular deflection of a laser beam reflected off the cantilever, which is converted to electrical signals by photodetectors (Figure A1.1A). An electronic feedback loop keeps the cantilever deflection and the tracking force constant by moving the sample up and down as the tip traces over the contours of the surface.

An image is obtained by plotting the vertical motion (z) of the tip and hence the sample height (z) as a function of specimen lateral position (XY). By choosing a very soft cantilever (low spring constant k), the imaging force can be in the range of interatomic forces (about 10^{-9} Newton), thus the name "atomic force" microscopy. Precise lateral and vertical position of the sample with respect to the probe is controlled by a computer-driven piezoceramic scanning stage. Depending on the design, the scanner may move the sample relative to a stationary probe or scan the probe over a stationary sample. The state of the art AFM used in our study uses a Z-scanner to control the vertical position of the probe (stationary in the XY plane) and a XY scanning stage to control the sample horizontal position.

There are two commonly used imaging modes to acquire sample topography with AFM: contact (static) mode and tapping (dynamic or intermittent contact) mode. In the contact mode imaging, the electronic feedback loop keeps the cantilever deflection and hence the tracking force constant during the raster-scanning of a sample. In the tapping mode, the cantilever beam is oscillated near its resonant frequency and interaction between tip and sample will alter the oscillation amplitude. The feedback loop maintains constant oscillating amplitude by keeping a constant interaction force (which translates to a fixed distance) between the tip and sample and the raster-scanned probe traces out the surface height contour of the sample.

AFM was used to analyse protein organization on material surfaces and to assess the biomechanical properties (*e.g.* elastic modulus) of cells and ECMs (Coelho et al. 2011), as they play important roles in many biological processes including stem cell differentiation, tumour formation, and wound healing. The uniqueness of this tool allows for the study even

under physiological conditions. It provides high-resolution images with resolution smaller than a nanometre (Binnig et al. 1986).

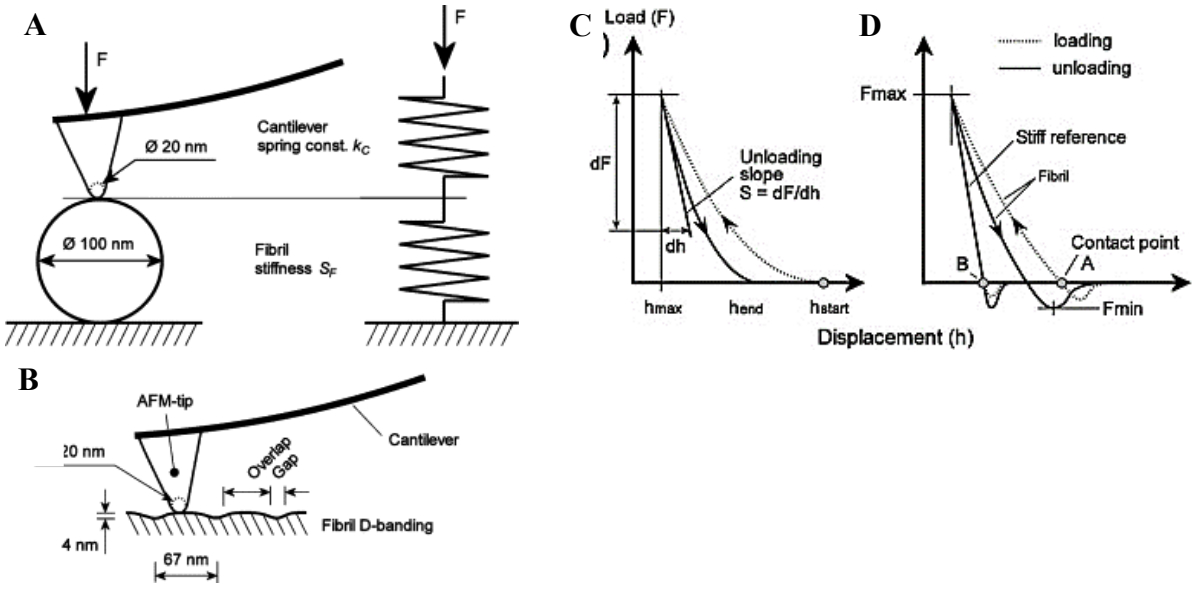

Appendix Figure A1.1 Illustration of AFM nano-indentation and interpretation of the force curve. A) Arrangement of AFM tip, cantilever, and ECMs fibril during nano-indentation. The AFM tip being stiff compared to the cantilever and the fibril, the arrangement can be described by two springs connected in series. The dimensions of the AFM tip apex and the fibril diameter are to scale. B) The longitudinal section of a collagen fibril shows the D-banding structure consisting of an overlap and gap region repeating every ~67 nm. The dimensions of the AFM tip apex and the fibril D-banding are to scale. C-D) Schematic of typical indentation curves obtained using nano-indentation on an elastic-plastic sample. The slope of the initial unloading curve S = dF/dh is related to the reduced modulus according to $S_F=\beta\times (2/\pi^{1/2}) \times Er\times A^{1/2}$; (stiffness, S_F, at the inception of unloading is related to the reduced modulus, E_r; the measured, projected, or cross-sectional contact area, A, and β is a variable, which takes into account nonaxisymmetry of the indenter and large strains. C) Indentation without attractive interfacial forces. D) Interfacial forces altering the shape of the curves; the intersection point between the horizontal (nondeflected cantilever) and the slope (deflected cantilever) is defined as the contact point. The indentation is the difference in the contact point positions (measured in vertical AFM piezo displacement) between loading a stiff sample and loading the fibril. Modified from (Wenger et al. 2007).

AFM as a tool for elasticity measurements: In the imaging modes, the AFM tip is raster scanned over the surface of the sample, which gives the surface topography of the sample. AFM can also be used to study the mechanical characteristics of soft samples at nanometre resolutions, including single cells (Figure A1.2) (A-Hassan et al. 1998). For instance, to scan a cell, the force mapping mode is used. The cantilevered AFM tip is pushed against the sample surface, the repulsion force deflects the cantilever. This interaction between the tip and the sample is commonly represented by the force curve (Figure A1.1C-D). The degree

of cantilever deflection is dependent on the stiffness of the sample. For a soft sample, the tip penetrates deeper into the sample and thus the cantilever deflection is less (Figure A1.1D) (loaded) compared to that of a hard impenetrable surface (Figure A1.1D) (unloaded).

The indentation depth of the AFM tip pushing into the sample can be determined by comparing force curves on the soft tissue with force-curves on a hard glass substrate. This force mapping process can be repeated after moving the tip laterally to the next measuring point thus creating a force-volume plot over the whole scan area. The mapping can achieve a spatial resolution of < 10 nm. The elastic or Young's modulus of the tissue can be calculated based on these force curves using the Hertz model: $F = \frac{4}{3}\frac{ER^{0.5}}{(1-\nu^2)}\delta^{1.5}$ (Spherical tip of radius) or $F = \frac{2E\ tan\emptyset}{\pi(1-\nu^2)}\delta^2$ (Sharp cone tip of opening angle 2Ø) (A-Hassan et al. 1998, Laney et al. 1997). Where F is the applied force, ν is the Poisson's ratio, δ is the depth of tip indentation into the sample, α is the half angle of the AFM tip, E is the Young's modulus, and ν is the Poisson's ratio. Note: When δ is more than 10% of the sample thickness (cell height), the measured cell stiffness is affected by the substrate stiffness. The thickness of peri-nuclear region is usually on the order of a few micrometres. Therefore, only the first 200-500 nm of F-δ curve is fit to the Hertz model.

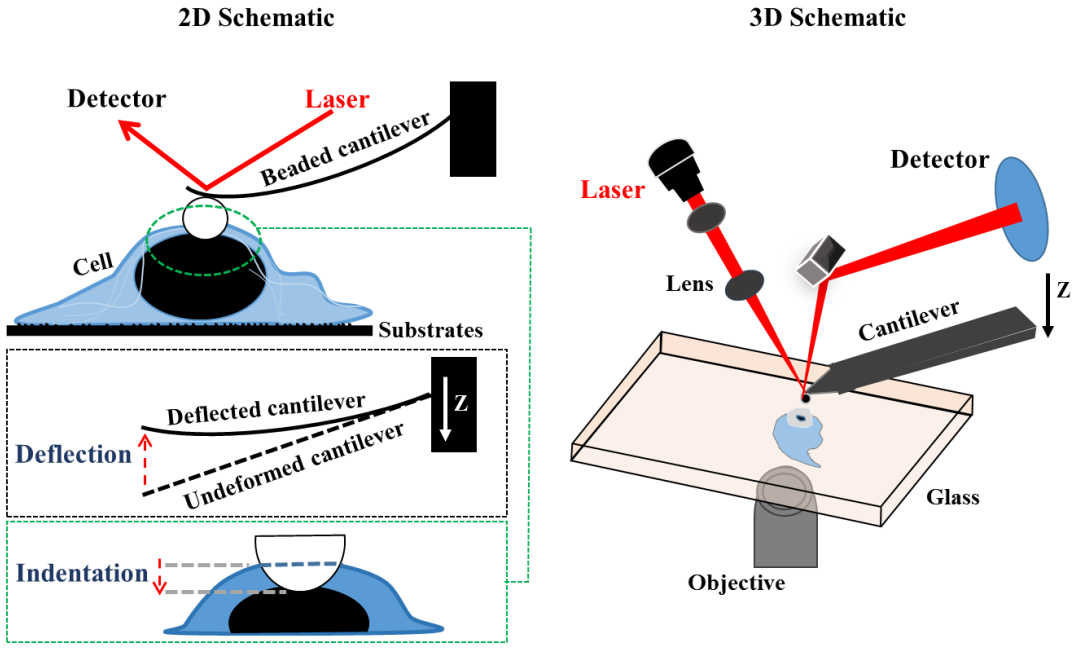

Appendix Figure A1.2 Process of imaging ECMs and cells and measuring mechanical properties with an AFM probe. 10 measurements were recorded for 10 independent point or cells suspended in PBS or CO_2 independent medium (respectively). Deflection was measured as the cantilever probed the sample surface. It was then used to calculate Young's Modulus using a Hertz model. 2D and 3D representation of Atomic Force Microscopy (AFM) imaging a healthy cell with a beaded cantilever.

References

Abràmoff MD, Magalhães PJ, Ram SJ. 2004. Image processing with ImageJ. Biophotonics international 11: 36-42.

Ahmad Khalili A, Ahmad MR. 2015. A Review of Cell Adhesion Studies for Biomedical and Biological Applications. International Journal of Molecular Sciences 16: 18149-18184.

Aiyelabegan HT, Sadroddiny E. 2017. Fundamentals of protein and cell interactions in biomaterials. Biomed Pharmacother 88: 956-970.

Alavi MV, Mao M, Pawlikowski BT, Kvezereli M, Duncan JL, Libby RT, John SW, Gould DB. 2016. Col4a1 mutations cause progressive retinal neovascular defects and retinopathy. Sci Rep 6: 18602.

Alberts B, Johnson A, Lewis J, Raff M, Roberts K, Walter P. 2007. Molecular Biology of the Cell. London: Garland Science.

Altankov G, Groth T. 1997. Fibronectin matrix formation by human fibroblasts on surfaces varying in wettability. Journal of Biomaterials Science, Polymer Edition 8: 299-310.

Altankov G, Hecht J, Dimoudis N. 2001. Serum-free cultured keratinocytes fail to organize fibronectin matrix and possess different distribution of beta-1 integrins. Exp Dermatol 10: 80-89.

Altankov G, Groth T, Engel E, Gustavsson J, Pegueroles M, Aparicio C, Gil FJ, Ginebra M-P, Planell JA. 2010. Development of provisional extracellular matrix on biomaterials interface: lessons from in vitro cell culture. Pages 19-43. Advances in Regenerative Medicine: Role of Nanotechnology, and Engineering Principles, Springer.

Anselme K, Bigerelle M, Noel B, Dufresne E, Judas D, Iost A, Hardouin P. 2000. Qualitative and quantitative study of human osteoblast adhesion on materials with various surface roughnesses. J Biomed Mater Res 49: 155-166.

Arikawa-Hirasawa E, Watanabe H, Takami H, Hassell JR, Yamada Y. 1999. Perlecan is essential for cartilage and cephalic development. Nat Genet 23: 354-358.

Arnaout MA, Goodman SL, Xiong JP. 2007. Structure and mechanics of integrin-based cell adhesion. Curr Opin Cell Biol 19: 495-507.

Aumailley M, Wiedemann H, Mann K, Timpl R. 1989. Binding of nidogen and the laminin-nidogen complex to basement membrane collagen type IV. Eur J Biochem 184: 241-248.

Aumailley M, Has C, Tunggal L, Bruckner-Tuderman L. 2006. Molecular basis of inherited skin-blistering disorders, and therapeutic implications. Expert Rev Mol Med 8: 1-21.

Aumailley M, Pesch M, Tunggal L, Gaill F, Fassler R. 2000. Altered synthesis of laminin 1 and absence of basement membrane component deposition in (beta)1 integrin-deficient embryoid bodies. J Cell Sci 113 Pt 2: 259-268.

Aumailley M, Battaglia C, Mayer U, Reinhardt D, Nischt R, Timpl R, Fox JW. 1993. Nidogen mediates the formation of ternary complexes of basement membrane components. Kidney Int 43: 7-12.

Aumailley M, et al. 2005. A simplified laminin nomenclature. Matrix Biology 24: 326-332.

Avram MM, Fein PA, Borawski C, Chattopadhyay J, Matza B. 2010. Extracellular mass/body cell mass ratio is an independent predictor of survival in peritoneal dialysis patients. Kidney Int Suppl: S37-40.

Baetscher M, Pumplin DW, Bloch RJ. 1986. Vitronectin at sites of cell-substrate contact in cultures of rat myotubes. J Cell Biol 103: 369-378.

Balaban NQ, et al. 2001. Force and focal adhesion assembly: a close relationship studied using elastic micropatterned substrates. Nat Cell Biol 3: 466-472.

Bateman JF, Boot-Handford RP, Lamande SR. 2009. Genetic diseases of connective tissues: cellular and extracellular effects of ECM mutations. Nat Rev Genet 10: 173-183.

Bathawab F, Bennett M, Cantini M, Reboud J, Dalby MJ, Salmerón-Sánchez M. 2016. Lateral Chain Length in Polyalkyl Acrylates Determines the Mobility of Fibronectin at the Cell/Material Interface. Langmuir 32: 800-809.

Baur AM, Gamberger TI, Weerda HG, Gjuric M, Tamm ER. 1995. Laminin promotes differentiation, adhesion and proliferation of cell cultures derived from human acoustic nerve schwannoma. Acta Otolaryngol 115: 517-521.

Beck K, Hunter I, Engel J. 1990. Structure and function of laminin: anatomy of a multidomain glycoprotein. Faseb j 4: 148-160.

Beggs HE, Schahin-Reed D, Zang K, Goebbels S, Nave KA, Gorski J, Jones KR, Sretavan D, Reichardt LF. 2003. FAK deficiency in cells contributing to the basal lamina results in cortical abnormalities resembling congenital muscular dystrophies. Neuron 40:501-14.

Bell G. 1978. Models for the specific adhesion of cells to cells. Science 200: 618-627.

Berginski ME, Gomez SM. 2013. The Focal Adhesion Analysis Server: a web tool for analyzing focal adhesion dynamics. F1000Res 2: 68.

Berrier AL, Yamada KM. 2007. Cell-matrix adhesion. J Cell Physiol 213: 565-573.

Berthod F, Germain L, Tremblay N, Auger FA. 2006. Extracellular matrix deposition by fibroblasts is necessary to promote capillary-like tube formation in vitro. J Cell Physiol 207: 491-498.

Biggs MJ, Richards RG, Gadegaard N, Wilkinson CD, Oreffo RO, Dalby MJ. 2009. The use of nanoscale topography to modulate the dynamics of adhesion formation in primary osteoblasts and ERK/MAPK signalling in STRO-1+ enriched skeletal stem cells. Biomaterials 30: 5094-5103.

Bischof P, Haenggeli L, Campana A. 1995. Integrins and adhesion molecules: Gelatinase and oncofetal fibronectin secretion is dependent on integrin expression on human cytotrophoblasts*. Human Reproduction 10: 734-742.

Bissell MJ, Radisky D. 2001. Putting tumours in context. Nat Rev Cancer 1: 46-54.

Borza DB, Bondar O, Ninomiya Y, Sado Y, Naito I, Todd P, Hudson BG. 2001. The NC1 domain of collagen IV encodes a novel network composed of the alpha 1, alpha 2, alpha 5, and alpha 6 chains in smooth muscle basement membranes. J Biol Chem 276: 28532-28540.

Boutaud A, Borza DB, Bondar O, Gunwar S, Netzer KO, Singh N, Ninomiya Y, Sado Y, Noelken ME, Hudson BG. 2000. Type IV collagen of the glomerular basement membrane. Evidence that the chain specificity of network assembly is encoded by the noncollagenous NC1 domains. J Biol Chem 275: 30716-30724.

Bowman W. 1840. On the Minute Structure and Movements of Voluntary Muscle. Philosophical Transactions of the Royal Society of London 130: 457-501.

Braren R, Hu H, Kim YH, Beggs HE, Reichardt LF, Wang R. 2006. Endothelial FAK is essential for vascular network stability, cell survival, and lamellipodial formation. J Cell Biol 172: 151-162.

Breedveld G, de Coo IF, Lequin MH, Arts WF, Heutink P, Gould DB, John SW, Oostra B, Mancini GM. 2006. Novel mutations in three families confirm a major role of COL4A1 in hereditary porencephaly. J Med Genet 43: 490-495.

Brunner D, Frank J, Appl H, Schoffl H, Pfaller W, Gstraunthaler G. 2010. Serum-free cell culture: the serum-free media interactive online database. Altex 27: 53-62.

Burridge K. 2017. Focal Adhesions: a personal perspective on a half century of progress. Febs j.

Cantini M, González-García, C., Llopis-Hernández, V., and Salmerón-Sánchez, M. 2012. Material-driven fibronectin fibrillogenesis. In: Proteins at Interfaces III State of the Art. Horbett T, Brash JL, Norde W, (eds.) American Chemical Society: Washington, DC; pp. 471–496; 2012.

Cary LA, Guan JL. 1999. Focal adhesion kinase in integrin-mediated signaling. Front Biosci 4: D102-113.

Charonis AS, Tsilibary EC, Yurchenco PD, Furthmayr H. 1985. Binding of laminin to type IV collagen: a morphological study. J Cell Biol 100: 1848-1853.

Chen CH, Hansma HG. 2000. Basement membrane macromolecules: insights from atomic force microscopy. J Struct Biol 131: 44-55.

Chen CH, Clegg DO, Hansma HG. 1998. Structures and dynamic motion of laminin-1 as observed by atomic force microscopy. Biochemistry 37: 8262-8267.

Coelho NM, Salmerón-Sánchez M, Altankov G. 2013. Fibroblasts remodeling of type IV collagen at a biomaterials interface. Biomaterials Science 1: 494-502.

Coelho NM, Gonzalez-Garcia C, Salmeron-Sanchez M, Altankov G. 2011a. Arrangement of type IV collagen on NH(2) and COOH functionalized surfaces. Biotechnol Bioeng 108: 3009-3018.

—. 2011b. Arrangement of type IV collagen and laminin on substrates with controlled density of -OH groups. Tissue Eng Part A 17: 2245-2257.

Coelho NM, Llopis-Hernández V, Salmerón-Sánchez M, Altankov G. 2016. Dynamic Reorganization and Enzymatic Remodeling of Type IV Collagen at Cell–Biomaterial Interface. Advances in Protein Chemistry and Structural Biology 105: 81-104.

Coelho NM, Gonzalez-Garcia C, Planell J, Salmerón-Sánchez M, Altankov G. 2010. Different assembly of type IV collagen on hydrophilic and hydrophobic substrata alters endothelial cells interaction. Eur Cell Mater 19: 262-272.

Cortiella J, Niles J, Cantu A, Brettler A, Pham A, Vargas G, Winston S, Wang J, Walls S, Nichols JE. 2010. Influence of Acellular Natural Lung Matrix on Murine Embryonic Stem Cell Differentiation and Tissue Formation. Tissue Engineering Part A 16: 2565-2580.

Cosgrove D, Liu S. 2016. Collagen IV diseases: A focus on the glomerular basement membrane in Alport syndrome. Matrix Biol.

Costell M, Gustafsson E, Aszodi A, Morgelin M, Bloch W, Hunziker E, Addicks K, Timpl R, Fassler R. 1999. Perlecan maintains the integrity of cartilage and some basement membranes. J Cell Biol 147: 1109-1122.

Cox TR, Erler JT. 2011. Remodeling and homeostasis of the extracellular matrix: implications for fibrotic diseases and cancer. Dis Model Mech 4: 165-178.

Dafforn TR, Della M, Miller AD. 2001. The molecular interactions of heat shock protein 47 (Hsp47) and their implications for collagen biosynthesis. J Biol Chem 276: 49310-49319.

Dalby MJ, Gadegaard N, Tare R, Andar A, Riehle MO, Herzyk P, Wilkinson CDW, Oreffo ROC. 2007. The control of human mesenchymal cell differentiation using nanoscale symmetry and disorder. Nat Mater 6: 997-1003.

Darenfed H, Dayanandan B, Zhang T, Hsieh SH, Fournier AE, Mandato CA. 2007. Molecular characterization of the effects of Y-27632. Cell Motil Cytoskeleton 64: 97-109.

de Clerck YA, Jones PA. 1980. The effect of ascorbic acid on the nature and production of collagen and elastin by rat smooth-muscle cells. Biochem J 186: 217-225.

Deligianni D, Korovessis P, Porte-Derrieu MC, Amedee J. 2005. Fibronectin preadsorbed on hydroxyapatite together with rough surface structure increases osteoblasts' adhesion "in vitro": the theoretical usefulness of fibronectin preadsorption on hydroxyapatite to increase permanent stability and longevity in spine implants. J Spinal Disord Tech 18: 257-262.

Deligianni DD, Katsala N, Ladas S, Sotiropoulou D, Amedee J, Missirlis YF. 2001. Effect of surface roughness of the titanium alloy Ti-6Al-4V on human bone marrow cell response and on protein adsorption. Biomaterials 22: 1241-1251.

Desai LP, White SR, Waters CM. 2009. Mechanical stretch decreases FAK phosphorylation and reduces cell migration through loss of JIP3-induced JNK phosphorylation in airway epithelial cells. American Journal of Physiology - Lung Cellular and Molecular Physiology 297: L520-L529.

Disatnik MH, Rando TA. 1999. Integrin-mediated muscle cell spreading. The role of protein kinase c in outside-in and inside-out signaling and evidence of integrin cross-talk. J Biol Chem 274.

Discher DE, Janmey P, Wang YL. 2005. Tissue cells feel and respond to the stiffness of their substrate. Science 310: 1139-1143.

Domogatskaya A, Rodin S, Boutaud A, Tryggvason K. 2008. Laminin-511 but not -332, -111, or -411 enables mouse embryonic stem cell self-renewal in vitro. Stem Cells 26: 2800-2809.

Dumbauld DW, Shin H, Gallant ND, Michael KE, Radhakrishna H, García AJ. 2010. Contractility Modulates Cell Adhesion Strengthening Through Focal Adhesion Kinase and Assembly of Vinculin-Containing Focal Adhesions. Journal of cellular physiology 223: 746-756.

Dupont-Gillain CC, Pamula E, Denis F, De Cupere V, Dufrene Y, Rouxhet P. 2004. Controlling the supramolecular organisation of adsorbed collagen layers. Journal of Materials Science: Materials in Medicine 15: 347-353.

Durbeej M. 2010. Laminins. Cell Tissue Res 339: 259-268.

Emch R, Clivaz X, Taylor-Denes C, Vaudaux P, Descouts P. 1990. Scanning tunneling microscopy for studying the biomaterial–biological tissue interface. Journal of Vacuum Science & Technology A: Vacuum, Surfaces, and Films 8: 655-658.

Emch R, Zenhausern F, Jobin M, Taborelli M, Descouts P. 1992. Morphological difference between fibronectin sprayed on mica and on PMMA. Ultramicroscopy 42: 1155-1160.

Engler AJ, Carag-Krieger C, Johnson CP, Raab M, Tang HY, Speicher DW, Sanger JW, Sanger JM, Discher DE. 2008. Embryonic cardiomyocytes beat best on a matrix with heart-like elasticity: scar-like rigidity inhibits beating. J Cell Sci 121: 3794-3802.

Erler JT, Weaver VM. 2009. Three-dimensional context regulation of metastasis. Clin Exp Metastasis 26: 35-49.

Favor J, Gloeckner CJ, Janik D, Klempt M, Neuhauser-Klaus A, Pretsch W, Schmahl W, Quintanilla-Fend L. 2007. Type IV procollagen missense mutations associated with defects of the eye, vascular stability, the brain, kidney function and embryonic or postnatal viability in the mouse, Mus musculus: an extension of the Col4a1 allelic series and the identification of the first two Col4a2 mutant alleles. Genetics 175: 725-736.

Foster MH. 2017. Basement membranes and autoimmune diseases. Matrix Biology 57–58: 149-168.

Frantz C, Stewart KM, Weaver VM. 2010. The extracellular matrix at a glance. J Cell Sci 123: 4195-4200.

Gale DP, Oygar DD, Lin F, Oygar PD, Khan N, Connor TMF, Lapsley M, Maxwell PH, Neild GH. 2016. A novel COL4A1 frameshift mutation in familial kidney disease: The importance of the C-terminal NC1 domain of type IV collagen. Nephrology Dialysis Transplantation 31: 1908-1914.

Gallant ND, Michael KE, Garcia AJ. 2005. Cell adhesion strengthening: contributions of adhesive area, integrin binding, and focal adhesion assembly. Mol Biol Cell 16: 4329-4340.

Garcia AJ. 2005. Get a grip: integrins in cell-biomaterial interactions. Biomaterials 26: 7525-7529.

Garcia AJ, Gallant ND. 2003. Stick and grip: measurement systems and quantitative analyses of integrin-mediated cell adhesion strength. Cell Biochem Biophys 39: 61-73.

Garcia AJ, Takagi J, Boettiger D. 1998a. Two-stage activation for alpha5beta1 integrin binding to surface-adsorbed fibronectin. J Biol Chem 273: 34710-34715.

Garcia AJ, Huber F, Boettiger D. 1998b. Force required to break alpha5beta1 integrin-fibronectin bonds in intact adherent cells is sensitive to integrin activation state. J Biol Chem 273: 10988-10993.

García AJ. 2006. Interfaces to Control Cell-Biomaterial Adhesive Interactions. Pages 171-190 in Werner C, ed. Polymers for Regenerative Medicine. Berlin, Heidelberg: Springer Berlin Heidelberg.

García AJ, Ducheyne P, Boettiger D. 1997. Quantification of cell adhesion using a spinning disc device and application to surface-reactive materials. Biomaterials 18: 1091-1098.

Geesin JC, Darr D, Kaufman R, Murad S, Pinnell SR. 1988. Ascorbic acid specifically increases type I and type III procollagen messenger RNA levels in human skin fibroblast. J Invest Dermatol 90: 420-424.

Geiger B, Spatz JP, Bershadsky AD. 2009. Environmental sensing through focal adhesions. Nat Rev Mol Cell Biol 10: 21-33.

Geiger B, Bershadsky A, Pankov R, Yamada KM. 2001. Transmembrane crosstalk between the extracellular matrix--cytoskeleton crosstalk. Nat Rev Mol Cell Biol 2: 793-805.

Gonzalez-Garcia C, Sousa SR, Moratal D, Rico P, Salmeron-Sanchez M. 2010. Effect of nanoscale topography on fibronectin adsorption, focal adhesion size and matrix organisation. Colloids Surf B Biointerfaces 77: 181-190.

Gonzalez-Garcia C, Moratal D, Oreffo RO, Dalby MJ, Salmeron-Sanchez M. 2012. Surface mobility regulates skeletal stem cell differentiation. Integr Biol (Camb) 4: 531-539.

González-García C, Salmerón-Sánchez M, García AJ. 2015. Focal Adhesion Kinase in Cell–Material Interactions. Polymers in Regenerative Medicine: Biomedical Applications from Nano-to Macro-Structures: 147-176.

Gordon MK, Hahn RA. 2010. Collagens. Cell Tissue Res 339: 247-257.

Gould DB, Marchant JK, Savinova OV, Smith RS, John SW. 2007. Col4a1 mutation causes endoplasmic reticulum stress and genetically modifiable ocular dysgenesis. Hum Mol Genet 16: 798-807.

Gould DB, Phalan FC, Breedveld GJ, van Mil SE, Smith RS, Schimenti JC, Aguglia U, van der Knaap MS, Heutink P, John SW. 2005. Mutations in Col4a1 cause perinatal cerebral hemorrhage and porencephaly. Science 308: 1167-1171.

Gould DB, et al. 2006. Role of COL4A1 in small-vessel disease and hemorrhagic stroke. N Engl J Med 354: 1489-1496.

Grinnell F. 1986. Focal adhesion sites and the removal of substratum-bound fibronectin. J Cell Biol 103: 2697-2706.

Grinnell F, Feld M. 1982. Fibronectin adsorption on hydrophilic and hydrophobic surfaces detected by antibody binding and analyzed during cell adhesion in serum-containing medium. J Biol Chem 257: 4888-4893.

Gross O, et al. 2004. DDR1-deficient mice show localized subepithelial GBM thickening with focal loss of slit diaphragms and proteinuria. Kidney Int 66: 102-111.

Gubbiotti MA, Iozzo RV. 2015. Proteoglycans regulate autophagy via outside-in signaling: an emerging new concept. Matrix Biology 48: 6-13.

Gugutkov D, Gonzalez-Garcia C, Rodriguez Hernandez JC, Altankov G, Salmeron-Sanchez M. 2009. Biological activity of the substrate-induced fibronectin network: insight into the third dimension through electrospun fibers. Langmuir 25: 10893-10900.

Gumbiner BM. 1996. Cell adhesion: the molecular basis of tissue architecture and morphogenesis. Cell 84: 345-357.

Gunda B, Mine M, Kovacs T, Hornyak C, Bereczki D, Varallyay G, Rudas G, Audrezet MP, Tournier-Lasserve E. 2014. COL4A2 mutation causing adult onset recurrent intracerebral hemorrhage and leukoencephalopathy. J Neurol 261: 500-503.

Gupta MC, Graham PL, Kramer JM. 1997. Characterization of alpha1(IV) collagen mutations in Caenorhabditis elegans and the effects of alpha1 and alpha2(IV) mutations on type IV collagen distribution. J Cell Biol 137: 1185-1196.

Ha TLB, Quan TM, Vu DN, Si DM. 2013. Naturally Derived Biomaterials: Preparation and Application. Pages Ch. 11 in Andrades JA, ed. Regenerative Medicine and Tissue Engineering. Rijeka: InTech.

Ha TT, Sadleir LG, Mandelstam SA, Paterson SJ, Scheffer IE, Gecz J, Corbett MA. 2016. A mutation in COL4A2 causes autosomal dominant porencephaly with cataracts. Am J Med Genet A 170a: 1059-1063.

Hadjipanayi E, Mudera V, Brown RA. 2009. Guiding cell migration in 3D: a collagen matrix with graded directional stiffness. Cell Motil Cytoskeleton 66: 121-128.

Hall PE, Lathia JD, Caldwell MA, Ffrench-Constant C. 2008. Laminin enhances the growth of human neural stem cells in defined culture media. BMC Neurosci 9: 71.

Hammer DA, Lauffenburger DA. 1987. A dynamical model for receptor-mediated cell adhesion to surfaces. Biophysical Journal 52: 475-487.

Han DC, Rodriguez LG, Guan JL. 2001. Identification of a novel interaction between integrin beta1 and 14-3-3beta. Oncogene 20: 346-357.

Hanein D, Horwitz AR. 2012. The structure of cell-matrix adhesions: the new frontier. Curr Opin Cell Biol 24: 134-140.

Hanks SK, Calalb MB, Harper MC, Patel SK. 1992. Focal adhesion protein-tyrosine kinase phosphorylated in response to cell attachment to fibronectin. Proc Natl Acad Sci U S A 89: 8487-8491.

Harding HP, Zhang Y, Ron D. 1999. Protein translation and folding are coupled by an endoplasmic-reticulum-resident kinase. Nature 397: 271-274.

Harvey SJ, Perry J, Zheng K, Chen D, Sado Y, Jefferson B, Ninomiya Y, Jacobs R, Hudson BG, Thorner PS. 2006. Sequential expression of type IV collagen networks: testis as a model and relevance to spermatogenesis. Am J Pathol 168: 1587-1597.

Haze K, Yoshida H, Yanagi H, Yura T, Mori K. 1999. Mammalian transcription factor ATF6 is synthesized as a transmembrane protein and activated by proteolysis in response to endoplasmic reticulum stress. Mol Biol Cell 10: 3787-3799.

Helbling-Leclerc A, et al. 1995. Mutations in the laminin alpha 2-chain gene (LAMA2) cause merosin-deficient congenital muscular dystrophy. Nat Genet 11: 216-218.

Hernández JCR, Sánchez MS, Soria JM, Ribelles JLG, Pradas MM. 2007. Substrate chemistry-dependent conformations of single laminin molecules on polymer surfaces are revealed by the phase signal of atomic force microscopy. Biophysical journal 93: 202-207.

Hochman-Mendez C, Cantini M, Moratal D, Salmeron-Sanchez M, Coelho-Sampaio T. 2014. A fractal nature for polymerized laminin. PLoS One 9: e109388.

Hohenester E, Yurchenco PD. 2013a. Laminins in basement membrane assembly. Cell Adh Migr 7: 56-63.

Hohenester E, Yurchenco PD. 2013b. Laminins in basement membrane assembly. Cell Adhesion & Migration 7: 56-63.

Horton ER, et al. 2015. Definition of a consensus integrin adhesome and its dynamics during adhesion complex assembly and disassembly. Nat Cell Biol 17: 1577-1587.

Huang J, Grater SV, Corbellini F, Rinck S, Bock E, Kemkemer R, Kessler H, Ding J, Spatz JP. 2009. Impact of order and disorder in RGD nanopatterns on cell adhesion. Nano Lett 9: 1111-1116.

Hubbell JA. 2003. Materials as morphogenetic guides in tissue engineering. Curr Opin Biotechnol 14: 551-558.

Hudson BG, Reeders ST, Tryggvason K. 1993. Type IV collagen: structure, gene organization, and role in human diseases. Molecular basis of Goodpasture and Alport syndromes and diffuse leiomyomatosis. J Biol Chem 268: 26033-26036.

Hudson BG, Tryggvason K, Sundaramoorthy M, Neilson EG. 2003. Alport's syndrome, Goodpasture's syndrome, and type IV collagen. N Engl J Med 348: 2543-2556.

Humphries MJ. 2009. Cell adhesion assays. Methods Mol Biol 522: 203-210.

Hunziker EB, Quinn TM, Hauselmann HJ. 2002. Quantitative structural organization of normal adult human articular cartilage. Osteoarthritis Cartilage 10: 564-572.

Hynes RO. 2002. Integrins: bidirectional, allosteric signaling machines. Cell 110: 673-687.

—. 2009. The extracellular matrix: not just pretty fibrils. Science 326: 1216-1219.

Ilic D, et al. 2004. FAK promotes organization of fibronectin matrix and fibrillar adhesions. J Cell Sci 117: 177-187.

Iozzo RV. 1994. Perlecan: A gem of a proteoglycan. Matrix Biology 14: 203-208.

Ishikawa Y, Ito S, Nagata K, Sakai LY, Bachinger HP. 2016. Intracellular mechanisms of molecular recognition and sorting for transport of large extracellular matrix molecules. Proc Natl Acad Sci U S A 113: E6036-e6044.

Jansen KA, Atherton P, Ballestrem C. 2017. Mechanotransduction at the cell-matrix interface. Seminars in Cell & Developmental Biology.

Jarvelainen H, Sainio A, Koulu M, Wight TN, Penttinen R. 2009. Extracellular matrix molecules: potential targets in pharmacotherapy. Pharmacol Rev 61: 198-223.

Järveläinen H, Sainio A, Koulu M, Wight TN, Penttinen R. 2009. Extracellular matrix molecules: potential targets in pharmacotherapy. Pharmacological reviews 61: 198-223.

Jeanne M, Gould DB. 2016. Genotype-phenotype correlations in pathology caused by collagen type IV alpha 1 and 2 mutations. Matrix Biology.

Jeanne M, Gould DB. 2017. Genotype-phenotype correlations in pathology caused by collagen type IV alpha 1 and 2 mutations. Matrix Biol 57-58: 29-44.

Jeanne M, Jorgensen J, Gould DB. 2015. Molecular and Genetic Analyses of Collagen Type IV Mutant Mouse Models of Spontaneous Intracerebral Hemorrhage Identify Mechanisms for Stroke Prevention. Circulation 131: 1555-1565.

Jeanne M, Labelle-Dumais C, Jorgensen J, Kauffman WB, Mancini Grazia M, Favor J, Valant V, Greenberg Steven M, Rosand J, Gould Douglas B. 2012. COL4A2 Mutations Impair COL4A1 and COL4A2 Secretion and Cause Hemorrhagic Stroke. The American Journal of Human Genetics 90: 91-101.

Jin H, Varner J. 2004. Integrins: roles in cancer development and as treatment targets. Br J Cancer 90: 561-565.

Jones FE, et al. 2016. ER stress and basement membrane defects combine to cause glomerular and tubular renal disease resulting from Col4a1 mutations in mice. Dis Model Mech 9: 165-176.

Kalluri R. 2002. Discovery of type IV collagen non-collagenous domains as novel integrin ligands and endogenous inhibitors of angiogenesis. Cold Spring Harb Symp Quant Biol 67: 255-266.

—. 2003. Basement membranes: structure, assembly and role in tumour angiogenesis. Nat Rev Cancer 3: 422-433.

Karperien A. 2013. FracLac for ImageJ. http://rsb.info.nih.gov/ij/plugins/fraclac/FLHelp/Introduction.htm.

Kern A, Eble J, Golbik R, Kuhn K. 1993. Interaction of type IV collagen with the isolated integrins alpha 1 beta 1 and alpha 2 beta 1. Eur J Biochem 215: 151-159.

Keselowsky BG, Collard DM, Garcia AJ. 2003. Surface chemistry modulates fibronectin conformation and directs integrin binding and specificity to control cell adhesion. J Biomed Mater Res A 66: 247-259.

—. 2004. Surface chemistry modulates focal adhesion composition and signaling through changes in integrin binding. Biomaterials 25: 5947-5954.

Khoshnoodi J, Pedchenko V, Hudson BG. 2008. Mammalian collagen IV. Microsc Res Tech 71: 357-370.

Klotzsch E, Smith ML, Kubow KE, Muntwyler S, Little WC, Beyeler F, Gourdon D, Nelson BJ, Vogel V. 2009. Fibronectin forms the most extensible biological fibers displaying switchable force-exposed cryptic binding sites. Proceedings of the National Academy of Sciences of the United States of America 106: 18267-18272.

Knight CG, Morton LF, Peachey AR, Tuckwell DS, Farndale RW, Barnes MJ. 2000. The collagen-binding A-domains of integrins alpha(1)beta(1) and alpha(2)beta(1) recognize the same specific amino acid sequence, GFOGER, in native (triple-helical) collagens. J Biol Chem 275: 35-40.

Koch M, Schulze J, Hansen U, Ashwodt T, Keene DR, Brunken WJ, Burgeson RE, Bruckner P, Bruckner-Tuderman L. 2004. A novel marker of tissue junctions, collagen XXII. J Biol Chem 279: 22514-22521.

Kowalczyńska HM, Nowak-Wyrzykowska M, Kołos R, Dobkowski J, Kamiński J. 2005. Fibronectin adsorption and arrangement on copolymer surfaces and their significance in cell adhesion. Journal of Biomedical Materials Research Part A 72: 228-236.

Kundu AK, Khatiwala CB, Putnam AJ. 2009. Extracellular matrix remodeling, integrin expression, and downstream signaling pathways influence the osteogenic differentiation of mesenchymal stem cells on poly(lactide-co-glycolide) substrates. Tissue Eng Part A 15: 273-283.

Kuo DS, Labelle-Dumais C, Gould DB. 2012. COL4A1 and COL4A2 mutations and disease: insights into pathogenic mechanisms and potential therapeutic targets. Hum Mol Genet 21: R97-110.

Labelle-Dumais C, et al. 2011. COL4A1 mutations cause ocular dysgenesis, neuronal localization defects, and myopathy in mice and Walker-Warburg syndrome in humans. PLoS Genet 7: e1002062.

Larsen M, Artym VV, Green JA, Yamada KM. 2006. The matrix reorganized: extracellular matrix remodeling and integrin signaling. Current Opinion in Cell Biology 18: 463-471.

Laurie GW, Bing JT, Kleinman HK, Hassell JR, Aumailley M, Martin GR, Feldmann RJ. 1986. Localization of binding sites for laminin, heparan sulfate proteoglycan and fibronectin on basement membrane (type IV) collagen. J Mol Biol 189: 205-216.

LeBleu VS, Macdonald B, Kalluri R. 2007. Structure and function of basement membranes. Exp Biol Med (Maywood) 232: 1121-1129.

Leitinger B, Hohenester E. 2007. Mammalian collagen receptors. Matrix Biol 26: 146-155.

Linsenmayer TF, Chen QA, Gibney E, Gordon MK, Marchant JK, Mayne R, Schmid TM. 1991. Collagen types IX and X in the developing chick tibiotarsus: analyses of mRNAs and proteins. Development 111: 191-196.

Liu Z, van Grunsven LA, Van Rossen E, Schroyen B, Timmermans J-P, Geerts A, Reynaert H. 2010. Blebbistatin inhibits contraction and accelerates migration in mouse hepatic stellate cells. British Journal of Pharmacology 159: 304-315.

Liu ZX, Yu CF, Nickel C, Thomas S, Cantley LG. 2002. Hepatocyte growth factor induces ERK-dependent paxillin phosphorylation and regulates paxillin-focal adhesion kinase association. J Biol Chem 277: 10452-10458.

Llopis-Hernandez V, Rico P, Ballester-Beltran J, Moratal D, Salmeron-Sanchez M. 2011. Role of surface chemistry in protein remodeling at the cell-material interface. PLoS One 6: e19610.

Llopis-Hernandez V, Cantini M, Gonzalez-Garcia C, Cheng ZA, Yang J, Tsimbouri PM, Garcia AJ, Dalby MJ, Salmeron-Sanchez M. 2016. Material-driven fibronectin assembly for high-efficiency presentation of growth factors. Sci Adv 2: e1600188.

Llopis-Hernández V, Rico P, Moratal D, Altankov G, Salmerón-Sánchez M. 2013. Role of material-driven fibronectin fibrillogenesis in protein remodeling. BioResearch open access 2: 364-373.

Lotz MM, Burdsal CA, Erickson HP, McClay DR. 1989. Cell adhesion to fibronectin and tenascin: quantitative measurements of initial binding and subsequent strengthening response. J Cell Biol 109: 1795-1805.

Lu H, Hoshiba T, Kawazoe N, Chen G. 2012. Comparison of decellularization techniques for preparation of extracellular matrix scaffolds derived from three-dimensional cell culture. J Biomed Mater Res A 100: 2507-2516.

MacDonald D, Markovic B, Allen M, Somasundaran P, Boskey A. 1998. Surface analysis of human plasma fibronectin adsorbed to commercially pure titanium materials. Journal of biomedical materials research 41: 120-130.

Maneva-Radicheva L, Ebert U, Dimoudis N, Altankov G. 2008. Fibroblast remodeling of adsorbed collagen type IV is altered in contact with cancer cells. Histol Histopathol 23: 833-842.

Manning G, Whyte DB, Martinez R, Hunter T, Sudarsanam S. 2002. The protein kinase complement of the human genome. Science 298: 1912-1934.

Mao Y, Schwarzbauer JE. 2005. Fibronectin fibrillogenesis, a cell-mediated matrix assembly process. Matrix Biol 24: 389-399.

Mecham RP, Hinek A, Griffin GL, Senior RM, Liotta LA. 1989. The elastin receptor shows structural and functional similarities to the 67-kDa tumor cell laminin receptor. J Biol Chem 264: 16652-16657.

Merna N. 2014. Impact of Extracellular Matrix Structure and Integrin Expression on Human Fibroblast Phenotype.

Meuwissen MEC, et al. 2015. The expanding phenotype of COL4A1 and COL4A2 mutations: clinical data on 13 newly identified families and a review of the literature. Genet Med 17: 843-853.

Michael KE, Dumbauld DW, Burns KL, Hanks SK, Garcia AJ. 2009. Focal adhesion kinase modulates cell adhesion strengthening via integrin activation. Mol Biol Cell 20: 2508-2519.

Miller T, Boettiger D. 2003. Control of Intracellular Signaling by Modulation of Fibronectin Conformation at the Cell−Materials Interface. Langmuir 19: 1723-1729.

Miner JH, Li C, Mudd JL, Go G, Sutherland AE. 2004. Compositional and structural requirements for laminin and basement membranes during mouse embryo implantation and gastrulation. Development 131: 2247-2256.

Mitra SK, Hanson DA, Schlaepfer DD. 2005. Focal adhesion kinase: in command and control of cell motility. Nat Rev Mol Cell Biol 6: 56-68.

Miyazaki T, Futaki S, Hasegawa K, Kawasaki M, Sanzen N, Hayashi M, Kawase E, Sekiguchi K, Nakatsuji N, Suemori H. 2008. Recombinant human laminin isoforms can support the undifferentiated growth of human embryonic stem cells. Biochem Biophys Res Commun 375: 27-32.

Moulisová V, Gonzalez-García C, Cantini M, Rodrigo-Navarro A, Weaver J, Costell M, Sabater i Serra R, Dalby MJ, García AJ, Salmerón-Sánchez M. 2017. Engineered microenvironments for synergistic VEGF – Integrin signalling during vascularization. Biomaterials 126: 61-74.

Mouw JK, Ou G, Weaver VM. 2014. Extracellular matrix assembly: a multiscale deconstruction. Nat Rev Mol Cell Biol 15: 771-785.

Murray LS, Lu Y, Taggart A, Van Regemorter N, Vilain C, Abramowicz M, Kadler KE, Van Agtmael T. 2014. Chemical chaperone treatment reduces intracellular accumulation of mutant collagen IV and ameliorates the cellular phenotype of a COL4A2 mutation that causes haemorrhagic stroke. Hum Mol Genet 23: 283-292.

Myllyharju J, Kivirikko KI. 2004. Collagens, modifying enzymes and their mutations in humans, flies and worms. Trends Genet 20: 33-43.

Nakanishi K, Sakiyama T, Imamura K. 2001. On the adsorption of proteins on solid surfaces, a common but very complicated phenomenon. J Biosci Bioeng 91: 233-244.

Ngandu Mpoyi E, Cantini M, Reynolds PM, Gadegaard N, Dalby MJ, Salmeron-Sanchez M. 2016. Protein Adsorption as a Key Mediator in the Nanotopographical Control of Cell Behavior. ACS Nano 10: 6638-6647.

Nomizu M, Kim WH, Yamamura K, Utani A, Song S-Y, Otaka A, Roller PP, Kleinman HK, Yamada Y. 1995. Identification of cell binding sites in the laminin α1 chain carboxyl-terminal globular

domain by systematic screening of synthetic peptides. Journal of Biological Chemistry 270: 20583-20590.

Noonan DM, Fulle A, Valente P, Cai S, Horigan E, Sasaki M, Yamada Y, Hassell JR. 1991. The complete sequence of perlecan, a basement membrane heparan sulfate proteoglycan, reveals extensive similarity with laminin A chain, low density lipoprotein-receptor, and the neural cell adhesion molecule. J Biol Chem 266: 22939-22947.

Nystrom A, Bornert O, Kuhl T. 2017. Cell therapy for basement membrane-linked diseases. Matrix Biol 57-58: 124-139.

Olsson A-K, Dimberg A, Kreuger J, Claesson-Welsh L. 2006. VEGF receptor signalling ? in control of vascular function. Nat Rev Mol Cell Biol 7: 359-371.

Paralkar VM, Weeks BS, Yu YM, Kleinman HK, Reddi AH. 1992. Recombinant human bone morphogenetic protein 2B stimulates PC12 cell differentiation: potentiation and binding to type IV collagen. J Cell Biol 119: 1721-1728.

Parsons JT. 2003. Focal adhesion kinase: the first ten years. J Cell Sci 116: 1409-1416.

Pastor-Pareja José C, Xu T. 2011. Shaping Cells and Organs in Drosophila by Opposing Roles of Fat Body-Secreted Collagen IV and Perlecan. Developmental Cell 21: 245-256.

Paulsson M. 1992. Basement membrane proteins: structure, assembly, and cellular interactions. Crit Rev Biochem Mol Biol 27: 93-127.

Plaisier E, et al. 2007. COL4A1 mutations and hereditary angiopathy, nephropathy, aneurysms, and muscle cramps. N Engl J Med 357: 2687-2695.

Polishchuk RS, Polishchuk EV, Marra P, Alberti S, Buccione R, Luini A, Mironov AA. 2000. Correlative light-electron microscopy reveals the tubular-saccular ultrastructure of carriers operating between Golgi apparatus and plasma membrane. J Cell Biol 148: 45-58.

Pompe T, Markowski M, Werner C. 2004. Modulated fibronectin anchorage at polymer substrates controls angiogenesis. Tissue Eng 10: 841-848.

Poschl E, Schlotzer-Schrehardt U, Brachvogel B, Saito K, Ninomiya Y, Mayer U. 2004. Collagen IV is essential for basement membrane stability but dispensable for initiation of its assembly during early development. Development 131: 1619-1628.

Pozzi A, Yurchenco PD, Iozzo RV. 2016. The nature and biology of basement membranes. Matrix Biology.

Prewitz MC, Stißel A, Friedrichs J, Träber N, Vogler S, Bornhäuser M, Werner C. 2015. Extracellular matrix deposition of bone marrow stroma enhanced by macromolecular crowding. Biomaterials 73: 60-69.

Prockop DJ. 1992. Seminars in medicine of the Beth Israel Hospital, Boston. Mutations in collagen genes as a cause of connective-tissue diseases. N Engl J Med 326: 540-546.

Provenzano PP, Inman DR, Eliceiri KW, Keely PJ. 2009. Matrix density-induced mechanoregulation of breast cell phenotype, signaling and gene expression through a FAK-ERK linkage. Oncogene 28: 4326-4343.

Rabe M, Verdes D, Seeger S. 2011. Understanding protein adsorption phenomena at solid surfaces. Adv Colloid Interface Sci 162: 87-106.

Rannikmae K, et al. 2015. Common variation in COL4A1/COL4A2 is associated with sporadic cerebral small vessel disease. Neurology 84: 918-926.

Reddig PJ, Juliano RL. 2005. Clinging to life: cell to matrix adhesion and cell survival. Cancer Metastasis Rev 24: 425-439.

Reilly GC, Engler AJ. 2010. Intrinsic extracellular matrix properties regulate stem cell differentiation. J Biomech 43: 55-62.

Reiske HR, Kao SC, Cary LA, Guan JL, Lai JF, Chen HC. 1999. Requirement of phosphatidylinositol 3-kinase in focal adhesion kinase-promoted cell migration. J Biol Chem 274: 12361-12366.

Rezania A, Healy KE. 1999. Biomimetic peptide surfaces that regulate adhesion, spreading, cytoskeletal organization, and mineralization of the matrix deposited by osteoblast-like cells. Biotechnol Prog 15: 19-32.

Ricard-Blum S. 2011. The Collagen Family. Cold Spring Harbor Perspectives in Biology 3: a004978.

Rico P, Cantini M, Altankov G, Salmerón-Sánchez M. 2014. Matrix Protein Interactions with Synthetic Surfaces. Pages 91-146. Polymers in Regenerative Medicine, John Wiley & Sons, Inc.

Rico P, Hernández JCR, Moratal D, Altankov G, Pradas MM, Salmerón-Sánchez M. 2009. Substrate-induced assembly of fibronectin into networks: influence of surface chemistry and effect on osteoblast adhesion. Tissue Engineering Part A 15: 3271-3281.

Riveline D, Zamir E, Balaban NQ, Schwarz US, Ishizaki T, Narumiya S, Kam Z, Geiger B, Bershadsky AD. 2001. Focal contacts as mechanosensors: externally applied local mechanical force induces growth of focal contacts by an mDia1-dependent and ROCK-independent mechanism. J Cell Biol 153: 1175-1186.

Robinson J, Gospodarowicz D. 1984. Effect of p-nitrophenyl-beta-D-xyloside on proteoglycan synthesis and extracellular matrix formation by bovine corneal endothelial cell cultures. J Biol Chem 259: 3818-3824.

Rodgers KD, Sasaki T, Aszodi A, Jacenko O. 2007. Reduced perlecan in mice results in chondrodysplasia resembling Schwartz-Jampel syndrome. Hum Mol Genet 16: 515-528.

Rodin S, Domogatskaya A, Strom S, Hansson EM, Chien KR, Inzunza J, Hovatta O, Tryggvason K. 2010. Long-term self-renewal of human pluripotent stem cells on human recombinant laminin-511. Nat Biotechnol 28: 611-615.

Rodriguez Hernandez JC, Salmeron Sanchez M, Soria JM, Gomez Ribelles JL, Monleon Pradas M. 2007. Substrate chemistry-dependent conformations of single laminin molecules on polymer surfaces are revealed by the phase signal of atomic force microscopy. Biophys J 93: 202-207.

Roskoski R, Jr. 2010. RAF protein-serine/threonine kinases: structure and regulation. Biochem Biophys Res Commun 399: 313-317.

—. 2012. ERK1/2 MAP kinases: structure, function, and regulation. Pharmacol Res 66: 105-143.

Rozario T, DeSimone DW. 2010. The extracellular matrix in development and morphogenesis: a dynamic view. Dev Biol 341: 126-140.

Rubin J, Rubin C, Jacobs CR. 2006. Molecular pathways mediating mechanical signaling in bone. Gene 367: 1-16.

Russell DA, Hanson JD, Ott E. 1980. Dimension of Strange Attractors. Physical Review Letters 45: 1175-1178.

Rutkowski DT, Arnold SM, Miller CN, Wu J, Li J, Gunnison KM, Mori K, Sadighi Akha AA, Raden D, Kaufman RJ. 2006. Adaptation to ER stress is mediated by differential stabilities of pro-survival and pro-apoptotic mRNAs and proteins. PLoS Biol 4: e374.

Salmeron-Sanchez M, Rico P, Moratal D, Lee TT, Schwarzbauer JE, Garcia AJ. 2011. Role of material-driven fibronectin fibrillogenesis in cell differentiation. Biomaterials 32: 2099-2105.

Salmerón-Sánchez M, Altankov G. 2010. Cell-protein-material interaction in tissue engineering: Citeseer.

Sastry SK, Burridge K. 2000. Focal adhesions: a nexus for intracellular signaling and cytoskeletal dynamics. Exp Cell Res 261: 25-36.

Sawada Y, Tamada M, Dubin-Thaler BJ, Cherniavskaya O, Sakai R, Tanaka S, Sheetz MP. 2006. Force sensing by mechanical extension of the Src family kinase substrate p130Cas. Cell 127: 1015-26.

Schaffner F, Ray AM, Dontenwill M. 2013. Integrin α5β1, the Fibronectin Receptor, as a Pertinent Therapeutic Target in Solid Tumors. Cancers 5: 27-47.

Schaller MD. 2001. Biochemical signals and biological responses elicited by the focal adhesion kinase. Biochim Biophys Acta 1540: 1-21.

Schaller MD, Hildebrand JD, Shannon JD, Fox JW, Vines RR, Parsons JT. 1994. Autophosphorylation of the focal adhesion kinase, pp125FAK, directs SH2-dependent binding of pp60src. Mol Cell Biol 14: 1680-1688.

Schiller HB, Fassler R. 2013. Mechanosensitivity and compositional dynamics of cell-matrix adhesions. EMBO Rep 14: 509-519.

Schwarzbauer JE, DeSimone DW. 2011. Fibronectins, their fibrillogenesis, and in vivo functions. Cold Spring Harb Perspect Biol 3.

Selinummi J, Seppala J, Yli-Harja O, Puhakka JA. 2005. Software for quantification of labeled bacteria from digital microscope images by automated image analysis. Biotechniques 39: 859-863.

Shattil SJ, Kim C, Ginsberg MH. 2010. The final steps of integrin activation: the end game. Nat Rev Mol Cell Biol 11: 288-300.

Sillat T, Saat R, Pollanen R, Hukkanen M, Takagi M, Konttinen YT. 2012. Basement membrane collagen type IV expression by human mesenchymal stem cells during adipogenic differentiation. J Cell Mol Med 16: 1485-1495.

Singh P, Carraher C, Schwarzbauer JE. 2010. Assembly of fibronectin extracellular matrix. Annu Rev Cell Dev Biol 26: 397-419.

Sipe JD. 2002. Tissue engineering and reparative medicine. Ann N Y Acad Sci 961: 1-9.

Smith ML, Gourdon D, Little WC, Kubow KE, Eguiluz RA, Luna-Morris S, Vogel V. 2007. Force-induced unfolding of fibronectin in the extracellular matrix of living cells. PLoS Biol 5: e268.

Smith T, Lange G, Marks W. 1996a. Fractal methods and results in cellular morphology—dimensions, lacunarity and multifractals. Journal of neuroscience methods 69: 123-136.

Smith TG, Jr., Lange GD, Marks WB. 1996b. Fractal methods and results in cellular morphology--dimensions, lacunarity and multifractals. J Neurosci Methods 69: 123-136.

Soderhall C, et al. 2007. Variants in a novel epidermal collagen gene (COL29A1) are associated with atopic dermatitis. PLoS Biol 5: e242.

Soille P, Rivest J-F. 1996. On the validity of fractal dimension measurements in image analysis. Journal of visual communication and image representation 7: 217-229.

Soria JM, et al. 2007. Influence of the substrate's hydrophilicity on the in vitro Schwann cells viability. J Biomed Mater Res A 83: 463-470.

Sottile J, Hocking DC. 2002. Fibronectin polymerization regulates the composition and stability of extracellular matrix fibrils and cell-matrix adhesions. Mol Biol Cell 13: 3546-3559.

Sun Z, Guo SS, Fässler R. 2016. Integrin-mediated mechanotransduction. Journal of Cell Biology 215: 445-456.

Tabas I, Ron D. 2011. Integrating the mechanisms of apoptosis induced by endoplasmic reticulum stress. Nat Cell Biol 13: 184-190.

Takahashi S, Kasemura T, Asano K. 1997. Surface molecular mobility for copolymers having perfluorooctyl and/or polyether side chains via dynamic contact angle. Polymer 38: 2107-2111.

Tamada Y, Ikada Y. 1994. Fibroblast growth on polymer surfaces and biosynthesis of collagen. J Biomed Mater Res 28: 783-789.

Theiler J. 1990. Estimating fractal dimension. JOSA A 7: 1055-1073.

Thomas G, Burnham NA, Camesano TA, Wen Q. 2013. Measuring the mechanical properties of living cells using atomic force microscopy. J Vis Exp.

Timpl R, Aumailley M. 1989. Biochemistry of basement membranes. Adv Nephrol Necker Hosp 18: 59-76.

Timpl R, Brown JC. 1994. The laminins. Matrix Biol 14: 275-281.

—. 1996. Supramolecular assembly of basement membranes. Bioessays 18: 123-132.

Timpl R, Oberbaumer I, von der Mark H, Bode W, Wick G, Weber S, Engel J. 1985. Structure and biology of the globular domain of basement membrane type IV collagen. Ann N Y Acad Sci 460: 58-72.

To WS, Midwood KS. 2011. Plasma and cellular fibronectin: distinct and independent functions during tissue repair. Fibrogenesis Tissue Repair 4: 21.

Tong Y, Xu Y, Scearce-Levie K, Ptacek LJ, Fu YH. 2010. COL25A1 triggers and promotes Alzheimer's disease-like pathology in vivo. Neurogenetics 11: 41-52.

Traylor M, et al. 2016. Genome-wide meta-analysis of cerebral white matter hyperintensities in patients with stroke. Neurology 86: 146-153.

Tsang KY, Cheung MC, Chan D, Cheah KS. 2010. The developmental roles of the extracellular matrix: beyond structure to regulation. Cell Tissue Res 339: 93-110.

Tzu J, Marinkovich MP. 2008. Bridging structure with function: structural, regulatory, and developmental role of laminins. Int J Biochem Cell Biol 40: 199-214.

Vahedi K, Alamowitch S. 2011. Clinical spectrum of type IV collagen (COL4A1) mutations: a novel genetic multisystem disease. Curr Opin Neurol 24: 63-68.

Van Agtmael T, Bruckner-Tuderman L. 2010. Basement membranes and human disease. Cell Tissue Res 339: 167-188.

Van Agtmael T, Bailey MA, Schlotzer-Schrehardt U, Craigie E, Jackson IJ, Brownstein DG, Megson IL, Mullins JJ. 2010. Col4a1 mutation in mice causes defects in vascular function and low blood pressure associated with reduced red blood cell volume. Hum Mol Genet 19: 1119-1128.

Van Agtmael T, Schlotzer-Schrehardt U, McKie L, Brownstein DG, Lee AW, Cross SH, Sado Y, Mullins JJ, Poschl E, Jackson IJ. 2005. Dominant mutations of Col4a1 result in basement membrane defects which lead to anterior segment dysgenesis and glomerulopathy. Hum Mol Genet 14: 3161-3168.

Van Damme H, Hogt A, Feijen J. 1986. Surface mobility and structural transitions of poly (n-alkyl methacrylates) probed by dynamic contact angle measurements. Journal of colloid and interface science 114: 167-172.

Vanacore R, Ham AJ, Voehler M, Sanders CR, Conrads TP, Veenstra TD, Sharpless KB, Dawson PE, Hudson BG. 2009. A sulfilimine bond identified in collagen IV. Science 325: 1230-1234.

Vanterpool FA, Cantini M, Seib FP, Salmeron-Sanchez M. 2014. A material-based platform to modulate fibronectin activity and focal adhesion assembly. Biores Open Access 3: 286-296.

Vasudevan A, Ho MS, Weiergraber M, Nischt R, Schneider T, Lie A, Smyth N, Kohling R. 2010. Basement membrane protein nidogen-1 shapes hippocampal synaptic plasticity and excitability. Hippocampus 20: 608-620.

Velling T, Risteli J, Wennerberg K, Mosher DF, Johansson S. 2002. Polymerization of type I and III collagens is dependent on fibronectin and enhanced by integrins alpha 11beta 1 and alpha 2beta 1. J Biol Chem 277: 37377-37381.

Verbeek E, et al. 2012. COL4A2 mutation associated with familial porencephaly and small-vessel disease. Eur J Hum Genet 20: 844-851.

Vogel W, Gish GD, Alves F, Pawson T. 1997. The discoidin domain receptor tyrosine kinases are activated by collagen. Mol Cell 1: 13-23.

Vranka JA, Sakai LY, Bachinger HP. 2004. Prolyl 3-hydroxylase 1, enzyme characterization and identification of a novel family of enzymes. J Biol Chem 279: 23615-23621.

Wang HB, Dembo M, Hanks SK, Wang Y. 2001. Focal adhesion kinase is involved in mechanosensing during fibroblast migration. Proc Natl Acad Sci U S A 98: 11295-11300.

Wang N, Tolic-Norrelykke IM, Chen J, Mijailovich SM, Butler JP, Fredberg JJ, Stamenovic D. 2002. Cell prestress. I. Stiffness and prestress are closely associated in adherent contractile cells. Am J Physiol Cell Physiol 282: C606-616.

Wehrle-Haller B. 2012a. Structure and function of focal adhesions. Curr Opin Cell Biol 24: 116-124.

—. 2012b. Assembly and disassembly of cell matrix adhesions. Curr Opin Cell Biol 24: 569-581.
Wehrle-Haller B, Imhof BA. 2003. Integrin-dependent pathologies. J Pathol 200: 481-487.
Weinberg SH, Mair DB, Lemmon CA. 2017. Mechanotransduction Dynamics at the Cell-Matrix Interface. Biophys J 112: 1962-1974.
Werb Z, Tremble PM, Behrendtsen O, Crowley E, Damsky CH. 1989. Signal transduction through the fibronectin receptor induces collagenase and stromelysin gene expression. The Journal of Cell Biology 109: 877-889.
Willem M, Miosge N, Halfter W, Smyth N, Jannetti I, Burghart E, Timpl R, Mayer U. 2002. Specific ablation of the nidogen-binding site in the laminin gamma1 chain interferes with kidney and lung development. Development 129: 2711-2722.
Wilson CJ, Clegg RE, Leavesley DI, Pearcy MJ. 2005. Mediation of Biomaterial–Cell Interactions by Adsorbed Proteins: A Review. Tissue Engineering 11: 1-18.
Wipff P-J, Rifkin DB, Meister J-J, Hinz B. 2007. Myofibroblast contraction activates latent TGF-β1 from the extracellular matrix. The Journal of Cell Biology 179: 1311-1323.
Xu L-C, Siedlecki C. 2017. Comprehensive Biomaterials II: Elsevier 1: 25-45.
Yamada Y, et al. 2007. Genetic risk for myocardial infarction determined by polymorphisms of candidate genes in Japanese individuals. Journal of Medical Genetics.
Yoon S, Seger R. 2006. The extracellular signal-regulated kinase: multiple substrates regulate diverse cellular functions. Growth Factors 24: 21-44.
Yurchenco PD, Schittny JC. 1990. Molecular architecture of basement membranes. Faseb j 4: 1577-1590.
Yurchenco PD, O'Rear JJ. 1994. Basal lamina assembly. Curr Opin Cell Biol 6: 674-681.
Yurchenco PD, Patton BL. 2009. Developmental and pathogenic mechanisms of basement membrane assembly. Curr Pharm Des 15: 1277-1294.
Yurchenco PD, Cheng YS, Colognato H. 1992. Laminin forms an independent network in basement membranes. J Cell Biol 117: 1119-1133.
Yurchenco PD, Smirnov S, Mathus T. 2002. Analysis of basement membrane self-assembly and cellular interactions with native and recombinant glycoproteins. Methods Cell Biol 69: 111-144.
Yurchenco PD, Tsilibary EC, Charonis AS, Furthmayr H. 1985. Laminin polymerization in vitro. Evidence for a two-step assembly with domain specificity. J Biol Chem 260: 7636-7644.
Zenker M, et al. 2004. Human laminin beta2 deficiency causes congenital nephrosis with mesangial sclerosis and distinct eye abnormalities. Hum Mol Genet 13: 2625-2632.
Zoppi N, Gardella R, De Paepe A, Barlati S, Colombi M. 2004. Human fibroblasts with mutations in COL5A1 and COL3A1 genes do not organize collagens and fibronectin in the extracellular matrix, down-regulate alpha2beta1 integrin, and recruit alphavbeta3 Instead of alpha5beta1 integrin. J Biol Chem 279: 18157-18168.
Zouein FA, Kurdi M, Booz GW, Fuseler JW. 2014. Applying fractal dimension and image analysis to quantify fibrotic collagen deposition and organization in the normal and hypertensive heart. Microsc Microanal 20: 1134-1144.
Zouq NK, Keeble JA, Lindsay J, Valentijn AJ, Zhang L, Mills D, Turner CE, Streuli CH, Gilmore AP. 2009. FAK engages multiple pathways to maintain survival of fibroblasts and epithelia: differential roles for paxillin and p130Cas. J Cell Sci 122: 357-367.
Zuyderhoff EM, Dupont-Gillain CC. 2011. Nano-organized collagen layers obtained by adsorption on phase-separated polymer thin films. Langmuir 28: 2007-2014.